NISTIR 5280

1993 ANNUAL CONFERENCE ON FIRE RESEARCH: BOOK OF ABSTRACTS

Wanda J. Duffin, Editor

Building and Fire Research Laboratory
Gaithersburg, Maryland 20899

United States Department of Commerce
Technology Administration
National Institute of Standards and Technology

NISTIR 5280

1993 ANNUAL CONFERENCE ON FIRE RESEARCH: BOOK OF ABSTRACTS

Wanda J. Duffin, Editor

October, 1993
Building and Fire Research Laboratory
National Institute of Standards and Technology
Gaithersburg, MD 20899

U.S. Department of Commerce
Ronald H. Brown, *Secretary*
Technology Administration
Mary L. Good, *Under Secretary for Technology*
National Institute of Standards and Technology
Arati Prabhakar, *Director*

TABLE OF CONTENTS

SESSION X Fire Risk and Hazard Analysis

POSTERS

INTRODUCTION

The NIST Annual Conference on Fire Research has long been a prime forum for presentation and discussion of the latest advances in fire science and engineering. The conference includes mostly fire research performed within Federal laboratories, or sponsored by Federal agencies. However, some private sector and foreign fire research is also included.

This year's conference focuses on the development, verification of fire safety engineering tools, and their application to building fires, transportation fires, underground fires, and large fires. This will enable scientists and engineers to describe recent work on fire models and measurement methods and users to describe experiences and limitations in the use of these tools. There are ten technical sessions, single sessions on the opening day, and double sessions on the second and third days.

The topic for the ten technical sessions are:

- Fire modeling; burning rate/flame spread
- Fire modeling; plumes
- Large fires
- Real scale fire tests
- Advanced measurement
- Fire detection
- Suppression; water
- Suppression; halon
- Smoke production
- Fire risk and hazard analysis

In addition to the 73 papers presented at the technical sessions, there are 21 posters focusing on aspects of fire research not directly within the primary focus of the technical sessions. This booklet contains abstracts of technical papers and posters presented at the NIST Annual Conference on Fire Research held on October 18-20, 1993, at the Holiday Inn Crowne Plaza Hotel in Rockville, MD.

Andrew J. Fowell, Conference Chair
Chief, Fire Safety Engineering Division
Building and Fire Research Laboratory
National Institute of Standards and Technology

A MODEL FOR THE BURNING OF A HORIZONTAL SLAB OF PMMA

K. Steckler, A. Hamins, and T. Kashiwagi
Building and Fire Research Laboratory
National Institute of Standards and Technology

The combustion of a horizontal slab of polymethylmethacrylate (PMMA), exposed to an external radiant source, was modeled in terms of two coupled submodels which simulate gas and condensed phase processes. A simple analytic steady-state global model [1] was used to describe the gas phase processes while the condensed phase processes were modeled using one-dimensional transient numerical computations which assume that the solid is opaque, has finite thickness, and that the heat of vaporization, the vaporization temperature, and piloted-ignition temperature can be specified and are constant. The condensed-phase models -- one for the preheating period, the other for the gasification period -- are heat conduction equations without and with a moving boundary, respectively [2]. They are expressed as partial differential equations which, in the current work, were solved with the MOL1D (Method Of Lines, 1 Dimension) [3] software package.

These particular condensed-phase models are limited in that they permit either a fixed surface boundary with a rising surface temperature (preheating) or a moving surface with a constant surface temperature (gasification/burning). **These models do not allow simultaneous gasification and surface-temperature rise.**

Figure 1 shows the experimental surface-temperature history of a 0.30 m diameter, 12.7 mm thick, horizontal slab of PMMA as it was heated beneath radiant heating panels in the presence of a small ignitor. Note the rapid increase in temperature from the piloted-ignition temperature (about 565 K) to the vaporization temperature (673 K) in the brief period following piloted ignition. **Clearly simultaneous gasification and rapid temperature change occurred during this transition period.** Although the transition could not be modeled accurately by either of the condensed-phase options cited above, an approximate solution was obtained by continuing the preheating calculation (without gasification) using a higher absorbed heat flux that includes an approximate contribution from the flame that appears after piloted ignition. For the case at hand, the absorbed external flux of 21.4 kW/m^2 (the product of the incident external flux and the surface absorptivity) was increased by 15.5 kW/m^2 to account for the presence of a flame fueled at the rate of 0.01 $kg/s\text{-}m^2$. This gasification rate was judged to be the average mass-loss rate observed during the experiment during the transition period. Given this gasification rate, the gas-phase model predicted that the resulting flame would add 15.5 kW/m^2 to the absorbed flux.

When the calculated surface temperature reached the vaporization temperature, the condensed-phase simulation was switched to the moving-surface constant-surface-temperature model, which then interacted with the analytic gas-phase sub-model to simulate the burning process.

Figures 1 and 2 present the experimental and calculated surface temperatures and gasification rates, respectively. The theoretical curve in Fig. 2 shows the onset of gasification/burning at 176.5 seconds. The solution was unstable during the first few seconds but stabilized quickly thereafter. The rapid increase of the theoretical curve after about 600 seconds is the result of a decrease of conduction from the surface as the slab becomes thinner. The calculation

terminated at 790 seconds when surface regression reduced the total number of computational nodes below 5, the minimum required for solution by MOL1D.

References

1. Hamins, A., Yang, J.C., and Kashiwagi, T., 1993, A Simple Global Model Predicting the Burning Rate of Liquid Pool Fires, submitted to Fire Safety Journal.

2. Stecklx K.D. Kashiwagi, T., Baum, H.R., and Kanemaru, K., Analytical Model for Transient Gasification of Noncharring Thermoplastic Materials, Fire Safety Science -- Proceedings of the Third International Symposium, 1991, pp.895-904.

3. Hyman, J.M., The NYU Report - The Method of Lines Solution of Partial Differential Equations, October, 1976, Los Alamos Scientific Laboratory, Los Alamos, NM, (computer code Revision No. 1, October 1978).

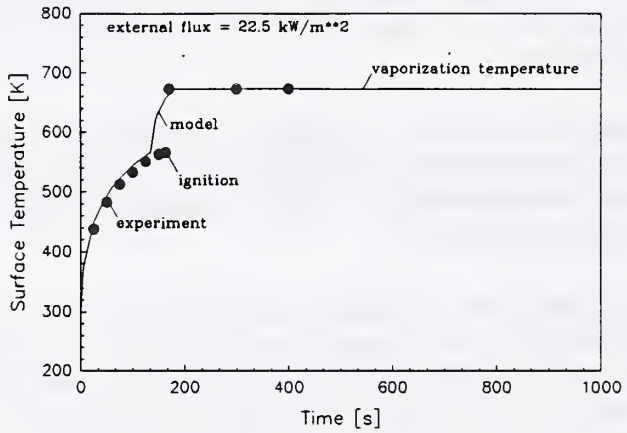

Figure 1. Surface temperature of PMMA while preheating and burning under 22.5 kW/m_2 incident external heat flux.

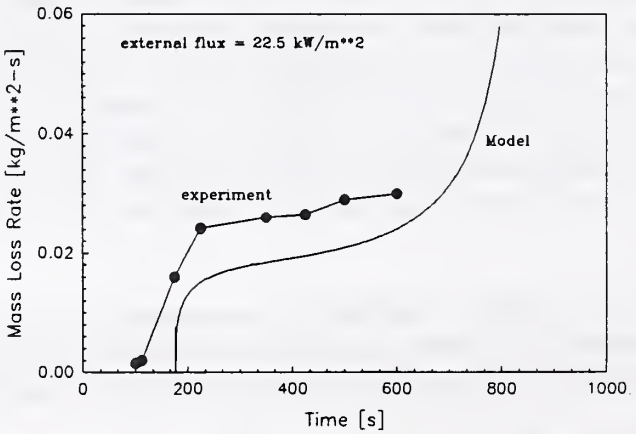

Figure 2. Burning rate of PMMA under 22.5 kW/m^2 incident external radiative heat flux.

AN APPROXIMATE TRANSIENT BURNING RATE MODEL

N. IQBAL, B. RHODES and J. QUINTIERE
Department of Fire Protection Engineering
College of Engineering
University of Maryland College Park
College Park, MD 20742, USA

ABSTRACT

An approximate one dimensional model has been developed for the transient burning of non-charring thermoplastic materials [1]. The model includes conduction, convection and radiation effects at the surface for non-flaming and flaming materials. The approximate solution is compared with existing experimental and numerical results to assess its validity. Ultimately it is hoped that such a model may provide an engineering solution to predict the burning rate of a wide range of materials.

For the pure pyrolysis case (non-flaming), the approximate solution is compared with Steckler's [2] numerical solution and the experimental results of Kashiwagi and Ohlemiller [3] for PMMA exposed to a constant external heat flux. Figure 1 shows the preheating period of the PMMA during which no pyrolysis occurs. When the surface reaches a specified vaporization temperature, Tv, pyrolysis begins and the surface temperature remains constant. Figure 2 compares the burning for the present model with the results of Steckler and Kashiwagi and Ohlemiller. The present model shows good agreement with both numerical and experimental results for the pure pyrolysis case.

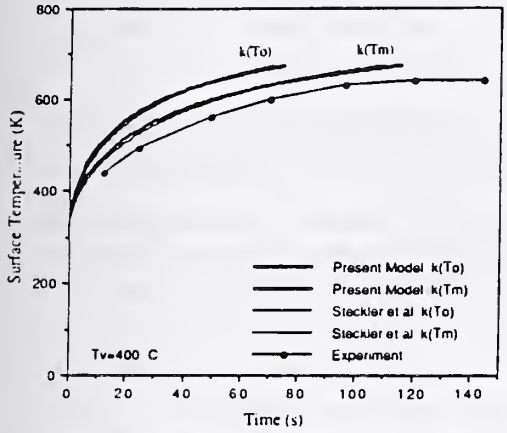

Figure - 1 Surface temperature of PMMA exposed to 40 kW/m^2 incident heat flux

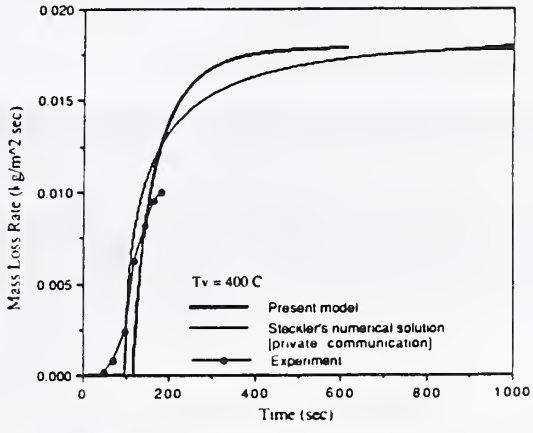

Figure - 2 Mass loss rate of PMMA exposed to 40 kW/m^2 incident heat flux

An exact solution can be written for the burning rate model where $\dot{q}''$ is the constant net heat flux to the surface [1].

$$\dot{m}'' = \frac{\dot{q}'' - \frac{2k(T_V - T_O)}{\delta}}{\Delta H_V}$$

$$\ln\left(\frac{x}{x_O}\right) = \frac{(x - x_O) - \beta(\tau - \tau_V)}{2}$$

where,

$$x = 2\left(1 - \frac{\delta}{\delta_S}\right), \quad \delta_S = \frac{2kL_g}{c\dot{q}''},$$

$$\beta = \frac{3L_g}{\Delta H_V}, \quad \tau = \frac{4\alpha t}{\delta_S^2}.$$

δ - thermal penetration depth
δ_s - steady state δ
L_g - heat of gasification
ΔH_v - heat of vaporization
α - thermal diffusivity
c - specific heat
k - thermal conductivity
t - time

Determining the flame radiation to the surface presents a problem in predicting the burning rate of materials. Currently, a general model to predict the flame radiation does not exist. The present model is used to determine flame radiation from experimental burning rate data and is compared to an empirical radiation model. Figure 3 shows computations for conduction, re-radiation, convection, fuel gasification and flame radiation based on the experimental burning rate results of Modak and Croce [4]. The flame radiation is inferred using the present model by using the experimental burning rates. Modak and Croce did not include the re-radiation term shown in Figure 3 in their analysis of flame radiation; hence their results have been corrected here. Orloff and De Ris [5] present an empirical solution for the flame radiation as a function of the burning rate. Figure 4 compares the flame radiation determined from the present model using experimental data and the flame radiation predicted by Orloff and De Ris.

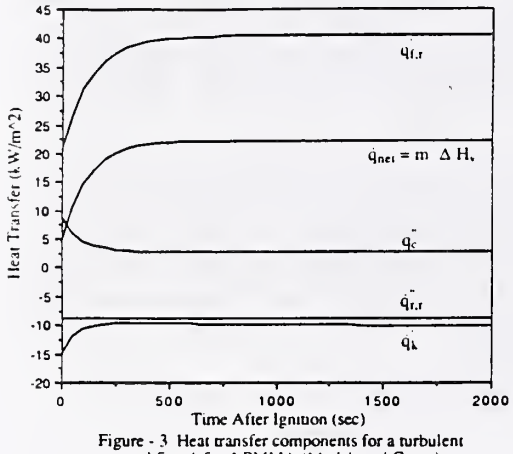

Figure - 3 Heat transfer components for a turbulent pool fire, 1.5 m^ PMMA (Modak and Croce)

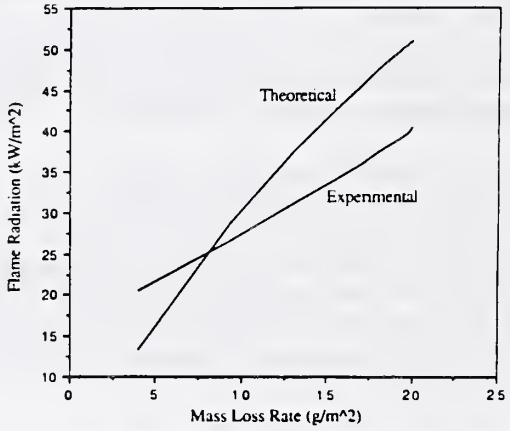

Figure - 4 Experimental and theoretical flame radiation vs mass loss rate of turbulent PMMA pool fire

Where the prediction of Orloff and De Ris fall below the inferred experimental value in Figure 4, the transient burning rate model has no solution. This shows the sensitivity of the model to flame radiation.

Experimental flame radiation data is being collected using a cone-heater apparatus. These data shall be used to provide further insight as to how flame heat transfer controls burning rate in the Cone Calorimeter. Without the inclusion of flame heat transfer, it will not be possible to extrapolate small scale test data.

REFERENCES

1. Iqbal, N., "Burning Rate Model for Thermoplastic Materials", Master's Thesis, Fire Protection Engineering Department, College of Engineering, University of Maryland, College Park, MD, 1993.

2. Steckler, K., Private Communications.

3. Kashiwagi, T. and Ohlemiller, T.J., "A Study of Oxygen Effects on Nonflaming Transient Gasification of PMMA and PE During Thermal Irradiation", Nineteenth Symposium (International) on Combustion, pp. 815-823, The Combustion Institute, Pittsburgh, PA, 1982.

4. Modak, A. and Croce P., "Plastic Pool Fires", Combustion and Flames, Volume 30, 1977 pp. 251-265.

5. Orloff, L. and De Ris, J., "Froude Modeling of Pool Fires", Nineteenth Symposium (International) on Combustion, pp. 885-895, The Combustion Institute, Pittsburgh, PA, 1982.

Upward Fire Spread Over PMMA Walls - A Model/Experiment Comparison

by
P. K. Wu, M. M. Delichatsios, and J. de Ris
Factory Mutual Research Corporation
Norwood, MA 02062

The way to develop a rational, scientifically based approach to the control and investigation of fire hazards is to combine theory and experiment, as suggested by Howard Emmons, Ref.1. Along these lines, Factory Mutual Research Corporation (FMRC) has recently developed a Fire Spread and Growth (FSG) computer model, Ref.2, based on: (1) scientific concepts; (2) available material flammability properties; and (3) empirical data from a previous 5 foot high PMMA upward fire spread experiment, Ref.3. The problem of upward fire spread has been studied by many investigators, Ref.2-8. To validate the model, we are comparing its predictions against: (1) small scale tests in the FMRC Flammability Apparatus , and (2) a 5 m large-scale fire test. In both cases, predictions were made prior to the tests.

Bench-Scale Experiments - Two small-scale upward fire spread experiments were performed using the FMRC Flammability Apparatus burning a PMMA panel which had a width of 0.2 m and a height of 0.9 m. The sides were taped with aluminum foil to minimize edge effects. The ignition at the bottom of the panel was accomplished by 20 ml of methanol and cotton balls in an aluminum dish (0.025 m x 0.2 m x 0.01 m high). The tests were run under atmospheric conditions. The measurements included mass loss, chemical heat release history, and visual observations of flame height and pyrolysis locations at selected times.

Pre-test predictions were made with the FSG model and baseline flame properties which included: (1) a radiant fraction Xr = 0.3, (2) a flame height correlation given by $Zf = a*\dot{Q}ch^{**}b$ (a and b are constants, Zf is the flame height, and $\dot{Q}ch$ is the chemical heat release rate), and (3) a triangular distribution of flame radiation, truncated at 60 kW/m2, an optically thick limit. For the values of the flame height correlation constants (i.e., a and b), Delichatsios (Ref.4) recommends a = 0.52 and b = 2/3 by considering purely convective wall fires. More recent radiation data by Markstein and de Ris (Ref.6) suggest a = 0.14 and b = 1/2. For the wall height of about 0.9 m, both these correlations give virtually the same results. The difference between the two correlations becomes more obvious in the full-scale experiment discussed in the next section.

Since the ignition process is very difficult to be numerically simulated, time scales are referenced to the time when the pyrolysis zone reaches the top of the panel. For both bench-scale experiments, the flame took off at approximately 500 seconds and the pyrolysis height reached the top of the panel at about 950 seconds. The tests were

terminated at 1300 seconds. At the end of the experiment, the model predicted a 700 g mass loss. From the experiments, the mass loss was measured at 715 g and 702 g. For the chemical heat release rate, the model prediction/data comparison is fairly good, Fig 1.This is from the first experiment. The dark squares are the experimental data while the solid line is the model prediction. Similar results were obtained from the second test.

Full-Scale Experiment - An upward fire spread experiment was carried out under the Fire Products Collector at the FMRC Test Center, West Glocester, Rhode Island with a 0.025 m thick PMMA slab, 0.58 m wide x 5 m high. No burnout was observed. As shown in Fig.2, the PMMA wall was extended another 0.3 m on each side by Marinite panels. At the outer edge of the Marinite panels, a perpendicular 0.6 m flow barrier (24 gauge steel) is used to minimize the effects of room drafts. On top of the wall, a 3 m extension (24 gauge steel) provided a background for measuring the flame heights.

The ignition at the bottom of the wall was accomplished by 35 ml of heptane in a copper dish (0.025 m x 0.6 m x 0.025 m high) which was half-filled with water. Besides the standard measurements of chemical heat release rate, mass loss, and radiation (with wide angle radiometer), there were six thermocouples and six heat flux gauges at various locations on the PMMA panel surface. For simplicity, only the results for the pyrolysis height, the mass loss, and the chemical heat release rate are presented in this abstract.

Pre-test predictions were again made with the FSG model and the baseline properties. Due to the difficulty of simulating the ignition process, time scales were synchronized by matching the pyrolysis height at the first thermocouple location (i.e., at about 0.9 m). As shown in Fig.3, the model prediction/data comparison for the pyrolysis height is good up to approximately 1.5 m. The diamonds represent the pyrolysis height derived from the thermocouple temperature traces, the solid line is the visual observation, and the dashed lines are the calculations with the previously mentioned flame height correlations. The visual data are fairly consistent with the thermocouple data. Above a height of about 1.5 m, both model calculations predict a faster pyrolysis front velocity (i.e., approaching about 0.04 m/s at about 5 m) than that from the data.

The model calculation provides a two dimensional solution (i.e., a wall with an infinite width). For the 0.58 m wide PMMA wall, the data diverge from the predictions at approximately 1.5 m, Fig.3. Above 1.5 m, the data show a slower pyrolysis front velocity, which asymptotically approaches a steady 0.01 m/s at the top of the panel. The model prediction/data comparisons for the mass loss and the chemical heat release rate are shown in Fig.4 and Fig.5. Again, both the mass loss and the chemical heat release rate data show good agreement up to a pyrolysis height of about 1.5 m, and then, the data fall below the model prediction. This disagreement beyond a pyrolysis height of 1.5 m may well be due to the absence of side walls in the present experiment, the assumed heat flux distribution, and/or the width effects. The model is being extended to include the effects of width and a full-scale experiment with 0.4 m and 0.2 m wide is planned for the near future to further validate our model.

References:

1. Thomas, P.H., "Fire, Flames and Dimensional Analysis ", Fire Safety Science - Proceedings of the Third International Symposium, Scotland, July 1991, pp.3-26.
2. Delichatsios, M.M., Mathews, M.K., and Delichatsios, M.A.," Upward Fire Spread Simulation Code: Version I: Noncharring Fuels ", FMRC Report No. J.I. 0R0J2.BU, November 1990.
3. Orloff, L., de Ris, J., and Markstein, G.H.," Upward Turbulent Fire Spread And Burning of Fuel Surface ", Presented at the 15th International Symposium On Combustion, Tokyo, Japan, August 1974.
4. Delichatsios, M.A., "Flame Heights in Turbulent Wall Fires With Significant Flame Radiation", Combustion Science and Technology, 34, 195, 1984.
5. Saito, K., Quintiere, J.G., and Williams, F.A.," Upward Turbulent Flame Spread ", International Symposium on Fire Safety Science, Gaithersburg, 1985, p.75.
6. Markstein, G.H., and de Ris, J.," Wall-Fire Radiant Emission, Part 1: Slot-Burner Flames, Comparison With Jet Flames ",Presented at The 23rd International Symposium On Combustion, Orleans, France, July 1990.
7. Hasemi, Y., Yoshida, M., and Nohara, A., Building Research Institute, Tsukento, Japan 1990.
8. Thomas, P.H., and Karlsson, B., " On Upward Flame Spread ",SELUTVDG/TVBB 3058, Dept. of Fire Safety Engineering, Lund University, December 1990.

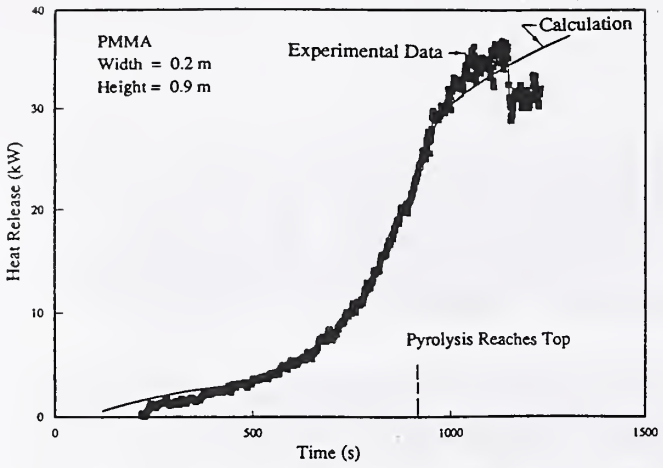

Figure 1 Chemical Heat Release Rate (Small scale)

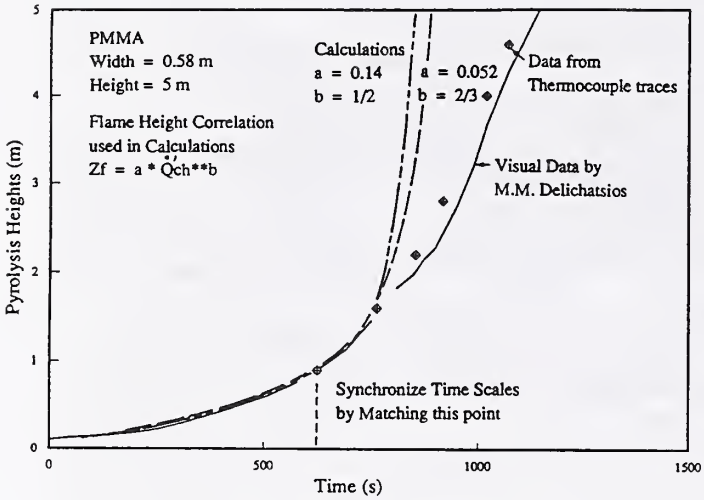

Figure 3 Pyrolysis Height (Full Scale)

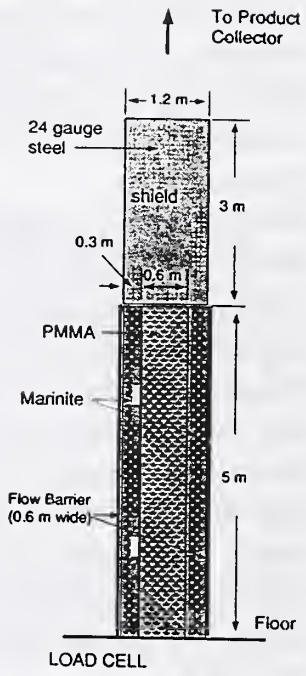

Figure 2 Full Scale Test

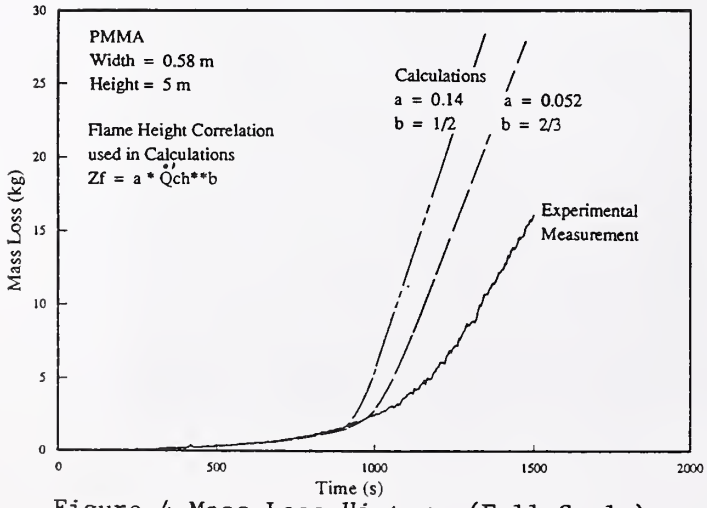

Figure 4 Mass Loss History (Full Scale)

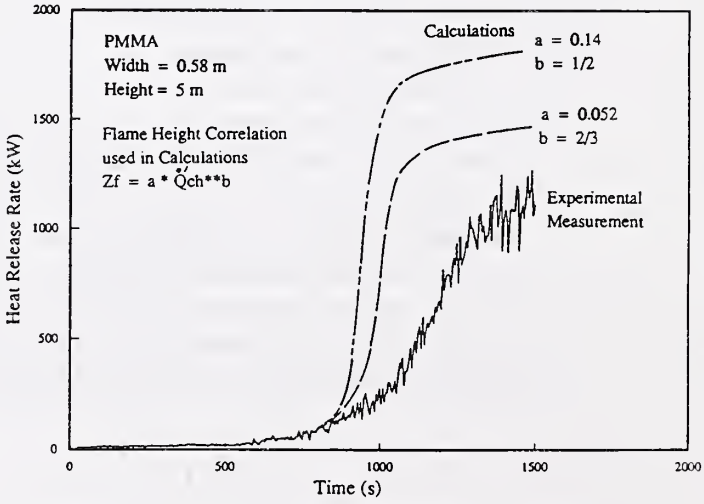

Figure 5 Chemical Heat Release Rate (Full Scale)

Flame Spread Over Thin Solid Fuels in Vitiated Atmospheres*

P. D. Ronney, J. B. Greenberg,† Y. Zhang and E. V. Roegner
Department of Mechanical and Aerospace Engineering
Princeton University, Princeton, NJ 08544 USA

Abstract

Flame spread over thin fuels is a useful paradigm for studying the behavior of more complex two-phase nonpremixed flames, such as those found in building fires. One aspect of flame spread which has not received much attention is flame spread in vitiated atmospheres, i.e. atmospheres which have been partially depleted of oxygen and contain some products of combustion. Information on this aspect of flame spread is of practical value because in building fires, combustion frequently occurs under very oxygen-deficient conditions. In such cases oxygen is partially depleted from the air and is replaced with vaporized but uncombusted or partially combusted material such as fuel or CO. This atmosphere may later come in contact with other fuel surfaces and under such conditions flame spread will occur with a vitiated atmosphere.

Consequently, the goal of this work was to study the effect of vitiated atmospheres on flame spread over thin solid fuels, in particular its effect on the spread rate (S_f). The experimental apparatus used was the same as that employed previously [1]. Simulated vitiated atmospheres were created by employing gas mixtures with varying amounts of gaseous fuels, oxygen, and N_2. CO, H_2, CH_4, C_3H_8 and NH_3 fuels were employed. The heat release per mole of O_2 consumed is similar for these fuels but their premixed laminar burning velocities (S_L) at a given adiabatic flame temperature vary substantially. The latter point indicates that the characteristic chemical reaction rates (RR) are very different for these fuels, since RR ~ S_L^2. Thus, any differences in flame spread between different fuels at the same gas-phase equivalence ratio (ϕ) is probably due mostly to finite-rate kinetic effects rather than thermal effects. Values of ϕ between zero and the lean flammability limit for the gas-phase mixture were tested.

Figure 1 shows the effect of mole fraction of O_2 (X_{ox}) and CO (X_{CO}) on S_f. S_f is plotted as a function of $X_{ox} + 1/2\ X_{CO}$ - i.e. the total oxygen atom mole fraction as O_2 equivalent. Figure 1 shows a remarkable result: the spread rate is *always greater* when a given number of oxygen atoms are present in the gas phase in the form of CO rather than O_2. Also, Fig. 1 shows that flame spread is possible with about 13% fewer O atoms in the atmospheres when the oxygen is present as O_2 + CO rather than 1.5 O_2. Hence, vitiated atmospheres containing CO as the product of partial oxidation provide higher spread rates and lower minimum oxygen indices than

---

*Presented at the Annual Conference on Fire Research, Rockville, MD, Oct. 18-22, 1993. This work was supported by the National Science Foundation under a Presidential Young Investigator Award to PDR.

†Faculty of Aerospace Engineering, Technion, Israel Institute of Technology, Haifa 32000, Israel

non-vitiated atmospheres - and this does not even consider that in practical fires the vitiated air will be hotter than ambient due to the heat release associated with the partial oxidation.

Figure 2 shows S_f as a function of ϕ, with the O_2 mole fraction fixed at 18%, for all five gaseous fuels tested. Here ϕ is increased by replacing the N_2 diluent with gaseous fuel. There is a dramatic effect of fuel type on the increase in S_f over the value with no fuel. The most to least effective fuels are, in order, H_2, CO, hydrocarbons, and NH_3. This order is nearly the same as the order of their S_L at fixed T_{ad}. Also note that the ranking does not correlate at all with the (relatively small) differences in heat release per mole of O_2 consumed or the Lewis numbers of the different fuels. These results lead us to a somewhat surprising conclusion: the characteristic reaction rates of the gaseous fuel have a strong effect on S_f, *even far from extinction, where the reaction rate of the solid fuel vapors with* O_2 *does not affect the spread rate* [2,3].

We conclude that for the purposes of modelling building fires in which vitiated air may be present, results on spread rates and extinction conditions obtained in pure air should not be used without consideration of the constituents of the vitiated atmosphere - at least in the case of downward flame spread over thermally thin fuels. It is not currently known whether this behavior would also apply for upward flame spread and/or thermally thick fuels.

References

1. Zhang, Y., Ronney, P., Roegner, E., Greenberg, J., *Combust. Flame* 91, 71 (1992).
2. Fernandez-Pello, A., Ray, S., Glassman, I., *18th Symposium (International) on Combustion*, The Combustion Institute, Pittsburgh, p. 579, 1981.
3. Wichman, I., Williams, F., *Combust. Sci. Tech.* 33, 207 (1983).

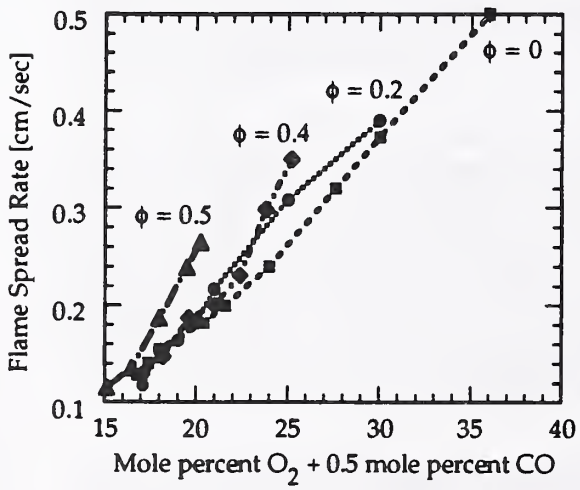

Figure 1. Downward flame spread rate O_2-CO-N_2 atmospheres with fuel bed thickness 0.0065".

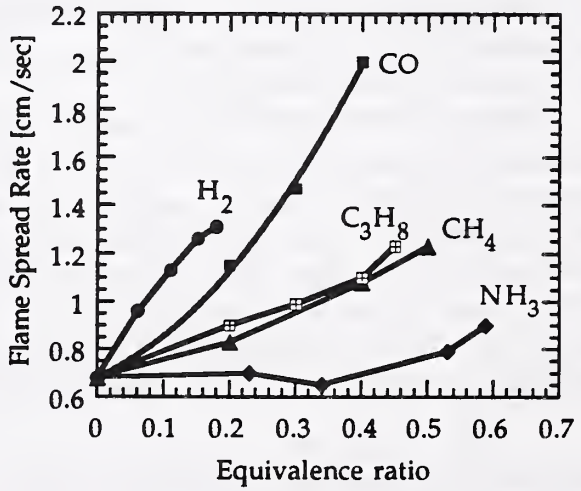

Figure 2. Effect of gaseous fuels on downward flame spread rate with fuel bed thickness 0.002".

A NUMERICAL MODEL FOR UPWARD FLAME SPREAD UNDER EXTERNAL RADIATION

E. G. Brehob and A. K. Kulkarni
Pennsylvania State University
University Park, PA 16802

The overall objective of the present project is to understand the upward flame spread phenomenon under simulated surrounding fire conditions. This is achieved by conducting experiments on upward flame spread under external radiation, developing a mathematical model, measuring the relevant basic material properties needed, and checking the validity of the model by comparing predictions with the data. In the current phase of the project, a numerical model of the upward flame spread process is being developed.

The physical situation being modeled is shown in Figure 1. A slab of material is subjected to a known, transient heat flux on its face, and the back has a convective heat transfer boundary condition. The top and bottom surfaces are assumed to be insulated. The two-dimensional transient heat conduction equation with the following boundary conditions is the starting point for the model.

$$\frac{\partial^2 T}{\partial x^2} + \frac{\partial^2 T}{\partial y^2} = \frac{1}{\alpha}\frac{\partial T}{\partial t} \qquad (1)$$

Initial Condition: $T(x,y,0) = T_o$

Boundary Conditions: $T(x,0,t) = T_{ign}$ for $x < x_p$

$$-k\left|\frac{\partial T}{\partial y}\right|_{y=0} = \dot{q}''_w(x,t) \quad \text{for } x > x_p$$

$$-k\left|\frac{\partial T}{\partial y}\right|_{y=D} = h(T-T_o)$$

$$-k\left|\frac{\partial T}{\partial x}\right|_{x=0} = -k\left|\frac{\partial T}{\partial x}\right|_{x=H} = 0$$

where T is temperature, α and k are thermal diffusivity and conductivity, t is time, and the other symbols are shown in Figure 1. The effect of external radiation comes into play in modeling of the forward wall heat flux term. It is modeled as,

$$\dot{q}''_w(x,t) = \dot{q}''_{wo}\exp\left[C_o\left(\frac{x-x_p}{x_f-x_p}\right)\right] + \dot{q}''_{er} - \dot{q}''_{rerad} \qquad (2)$$

where $\dot{q}''_{wo}$ is the maximum forward heat flux measured for a specific material and C_o is a constant applicable for all materials, equal to -1.37. The justification for using the above form of equation and the constants are available from our work on experimental measurements. $\dot{q}''_{rerad}$ is external radiation and $\dot{q}''_{wo}$ is reradiation of the wall to the surroundings. To close the upward flame spread model, a consideration of pyrolysis height (x_p), burn-out edge (x_b), and flame front (x_f) is necessary. They are given by

$$x_p = x \text{ when } T_{surface}(x) = T_{ign} \qquad (3)$$

$$x_b(t) = x_p(t-t_b) \tag{4}$$

$$x_f(t) - x_b(t) = K\left[\dot{Q}' + h_c\int_{x_b(t)}^{x_p(t)} \dot{m}''dx\right]^n \tag{5}$$

where t_b is the burn-out time (the amount of time between when a particular element first reaches pyrolysis temperature until the combustible part of material has been consumed), the K and n have been experimentally determined, Q' is the line burner strength, and $\dot{m}''$ is the mass loss rate. The $\dot{m}''$ term in the equation is the experimentally determined mass loss rate and takes into account the effect of external radiation in addition to the material characteristics such as thickness and charring. Equations 1 through 5 make up the governing equations for the flame spread model. The five unknowns are T, $\dot{q}''_w$, x_b, x_p, and x_f. Other variables are known properties for the material or are obtainable from experimental data from this work or previous work.

Some preliminary results of the numerical model have been made for 3.2 thick mm hardboard and are shown in Figure 2. Flame height and pyrolysis front histories at two levels of external radiation are compared in the figure. The convergence of the flame and pyrolysis height for the unradiated case is indicative of extinguishment of the upward flame spread prior to reaching the top of the sample. The experimental measurement for hardboard also confirmed this result. For the case with an average external flux of 2.2 kW/m^2 applied, the flame and pyrolysis front spread is faster and the sample sustained flame spread to the top. Further work on comparison of predicted data with experimental results and predictions for other materials is in progress.

This work was supported by the National Institute of Standards and Technology under grant no. 60NANB8D0849.

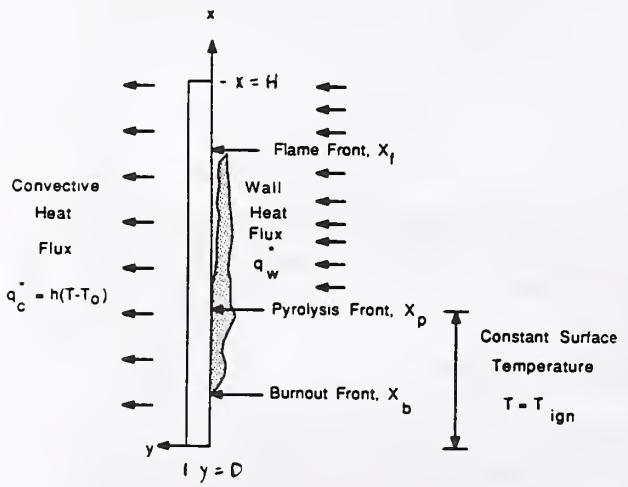

Figure 1. Boundary Conditions for the Burning Wall

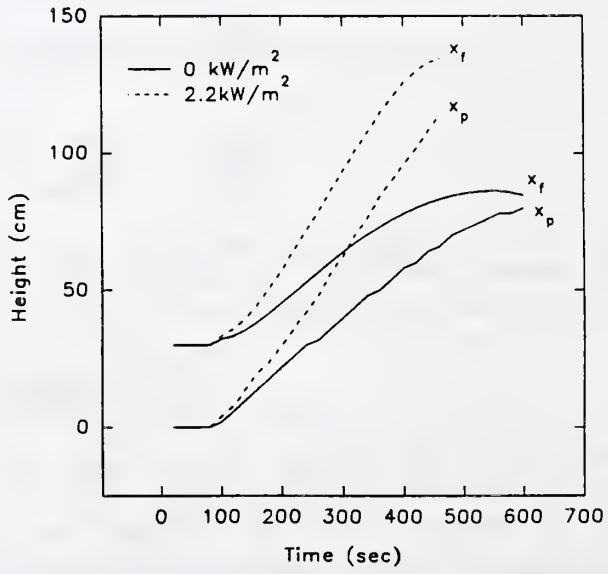

Figure 2. Flame Height and Pyrolysis Front Histories for 3.2 mm Hardboard at Two Levels of External Radiation

RESULTS ON MODELING ROOM CORNER TESTS

J. G. QUINTIERE
Department of Fire Protection Engineering
University of Maryland
College Park, MD

ABSTRACT

Several studies have been completed using a simulation model for a room corner tests. The model contains approximate mathematical formulations for the primary fire phenomena associated with the room corner test. The model also uses data obtainable from standard test methods to describe properties of the material or product tested. It uses derived material property data from the Cone Calorimeter to calculate the needed information at the heat flux experienced by the material in the room-corner test, and also uses data from the LIFT apparatus (ASTM E 1321-90, "Standard Method for Determining Material Ignition and Flame Spread Properties"). The model is in its early development and can be improved in many aspects, but it has been reasonably successful in its accuracy. Moreover it appears to illustrate and reveal the sensitive aspects of fire growth related to the material properties and the configuration of the test. In particular, the operation of the burner in terms of its energy release rate and position appears to be a significant factor in determining fire growth. These results will be reviewed.

The model simulates the ignition by the burner, flame spread, burn-out, and burning rate of wall and ceiling materials.

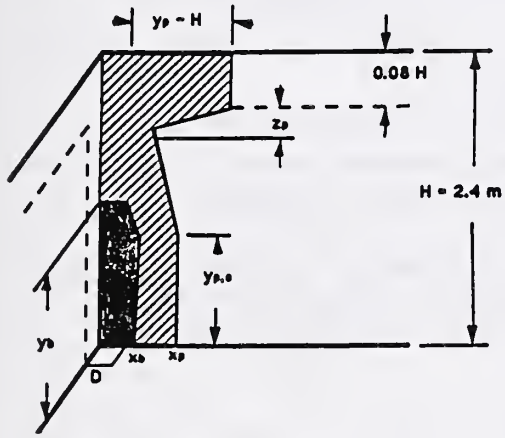

Fig. 1 Simulation model.

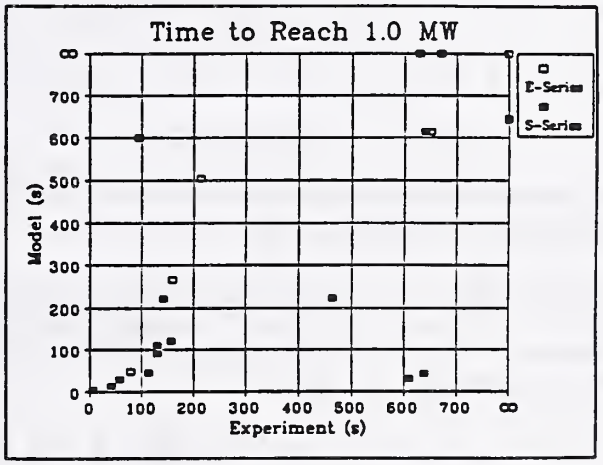

Fig. 2 Flashover predictions

The flame pyrolysis and burn-out fronts are computed with respect to two modes of flame spread. One mode includes upward spread, spread along the ceiling, and spread along the wall-ceiling jet region. This is shown in Figure 1 where the dashed lines enclose the region of wind-aided flame spread due to the burner, and the ceiling jet. At this time, no distinction for wall and ceiling wind-aided flame spread is made in the model and they are universally treated as governed by upward flame spread.

The second mode of spread is composed of lateral spread along the wall and subsequent downward spread from the ceiling jet. Again, the same relationship will be considered for both. In this fashion, the pyrolysis and burn-out areas are computed. An illustration of the pyrolysis (y_p, x_p, and z_p) and burn-out (y_b and x_b) fronts is also shown in Figure 1. Ceiling combustion is not illustrated in that Figure, but can be included as desired.

The energy release rate per unit area is computed from the net heat flux in the pyrolysis region. It is considered constant over the pyrolysis area which is computed from the front configuration as a function of time. The energy release rate per unit area is governed by both the flame heat flux and the radiative

feedback from the heated room.

Flame heat flux is considered constant over the pyrolysis area, and constant over the extended flame length. Two values are selected: one over the pyrolysis area and for the square burner corner ignition flame which governs burning rate and ignition, respectively; and the other for the extended flame region beyond the pyrolysis region which governs upward flame spread. The latter value has been selected as 30 kW/m^2 indicative of wall flame heat transfer.

The room thermal feedback controls both the rate of spread through a computation of the material surface temperature ahead of the flame, and the rate of energy release per unit area through radiative heat transfer from the gas layer in the room. Global models are considered for average room surface and gas layer temperatures. The radiative effects are considered to be maximized to give an upper limit for its effect.

Figure 2 summarizes the results in predicting flashover or the time to attain 1 MW in the Swedish and EUREFIC ISO room corner test results.

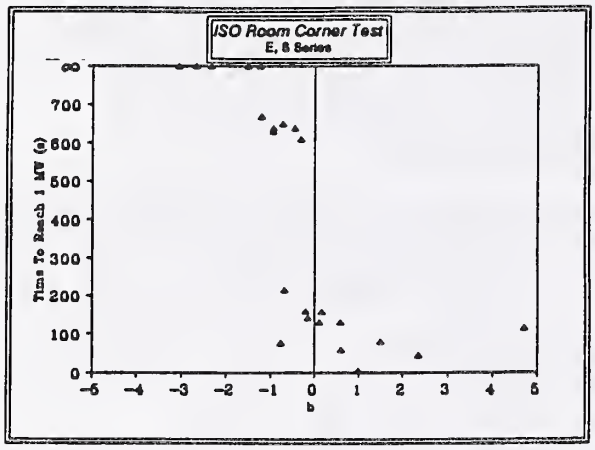

Fig. 3 Correlation for flashover times

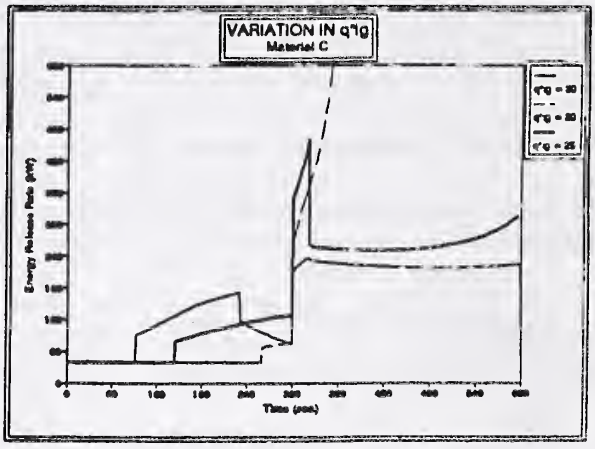

Fig. 4 Burner effect on simulation

It has been found that in some cases small changes in the input properties have a pronounced effect on the outcome. This an be explained to some extent by Figure 3 which shows a correlation of the experimental flashover time plotted against a significant parameter of the simulation model, b. The b parameter is given by

$$b = k_f \dot{Q}'' - 1 - t_{ig}/t_b$$

where $\dot{Q}''$ is the energy release per unit area, t_{ig} is the ignition time, and t_b is the burn-out time. These quantities are computed in the context of the model which attempts to simulate the fire conditions in the particular room corner test.

Figure 4 illustrates the effect of varying the burner heat flux in the simulation during the first level application of a two-step burner ignition energy release rate. The simulation is based on the Uniform Building Code standard for textile wall coverings (UBC Standard No. 42-2) where the corner burner is varied from 40 kW to 150 kW after 5 minutes. Figure 4 considers the burner heat flux varying from 20 to 30 kW/m^2. The simulated results show a marked difference in the outcome with the lowest burner heat flux giving the worst outcome. The variation in burner heat flux can simulate the variation in the distance the ignition burner is from the corner.

The simulation model has had reasonable success at predicting room corner tests, but the results can be sensitive to small changes in the input parameters in some cases. Thin materials appear to be more sensitive due to burn-out. The burner settings and their durations can also be significant factors. Simulation models, even with limited accuracy, can illustrate these factors which can be very important in the design and interpretation of the room corner test method.

UPWARD FLAME SPREAD ALONG THE VERTICAL CORNER WALLS

Cheng Qian, Hiroki Ishida and Kozo Saito
Department of Mechanical Engineering
University of Kentucky
Lexington, KY 40506

BACKGROUND

Upward flame spread is an important subject in fire safety engineering because of its rapid growth rate and intense emission from the fire. In our recent studies on corner fires, it has been proved that the behavior of flame and the spread pattern of pyrolysis front were affected by the initial mode of ignition at the bottom of corner walls. Fire-induced flow along the corner wall is transient three dimensional causing complex convective and radiative heat transfer to the unburned corner wall. Furthermore, under some conditions, a fire-induced vortex was formed along the corner; it might enhance the upward spread rate significantly.

Based on these findings, the flame spread behavior and the pyrolysis region spread characteristics along the vertical corner wall was studied in detail through the experiments using an automated infrared imaging system (IR system). The IR system was developed at the Combustion and Fire Research Laboratory at the University of Kentucky, and it has been proved to be very useful for the measurement of the flame spread rate through the obtaied transient temperature mapping. An interesting finding through the IR system is that the formation of M-shape pyrolysis front along the vertical corner wall. This means the flame does not spread along the corner but does spread a few centimeters away from the corner with the maximum rate. To predict the upward flame spread rate, therefore, it is important to understand the mechanism of the M-shape pyrolysis front formation. Four different mechanisms were thought and the significance of each mechanism on the M-shape formation was experimentally studied. Among them, the flame displacement effect was found to be the principal reason.

In addtion to the above, our current studies include:
(1) Experimental findings in characteristics of spreading flame behavior and pyrolysis front shape on the corner wall fires.
(2) Assessment of the applicability for the one-dimensional thermal prediction model to the corner spread rate.

Two-Dimensional Numerical Modeling of Laminar Flame Spread over a Porous Solid Fuel

M. Karim Moallemi, and Hui Zhang

Department of Mechanical Engineering
Polytechnic University
Six MetroTech Center, Brooklyn, NY 11201

Abstract

Due to their critical contribution to the fire hazard, flame spread and wind-assisted flame spread over a solid fuel have been extensively studied both experimentally and theoretically over the last few decades [1-3]. However, more work is needed to establish a comprehensive and predictive knowledge base that can be used to characterize the behavior of different materials under different fire conditions. At present, a realistic analytical or numerical model capable of using the intrinsic thermo-chemical properties of materials to predict different aspects of their fire performance (flammability, heat release, mass loss rate, etc.) is not available even for the simplest and most commonly encountered material (*i.e.*, wood). The majority of the available theoretical models are attempts to rate and characterize performance of different materials by using standard flammability test measurements (*i.e.*, mass loss and surface temperature histories) as inputs [2-4]. The *effective* or *equivalent* fire properties that are defined and used by these so called *thermal* models, however, are not only functions of the intrinsic properties of the materials, but depend on the fire conditions as well. This has led to the development of different models for various fire modes (*e.g.*, ignition, smoldering, flaming, and flame spreading) [1-4]. These models have limited application for assessment of fire hazards, mainly because *i)* realistic fire scenarios involve more than a single fire mode, and *ii)* similarity between the standard tests and actual fire conditions is not easy to fulfill [5, 6] due to the multiplicity of transport processes with different length scales and scaling relationships.

The present paper is concerned with the formulation of a phenomenological model and the development of a two-dimensional numerical solution procedure to relate the intrinsic thermophysical properties a solid fuel to its behavior under flaming condition. The chemical mechanisms are simplified by assuming:

$$\textit{virgin solid} \longrightarrow \alpha_c\ \textit{char} + (1 - \alpha_c)\ \textit{volatiles}$$

$$\textit{char} + \alpha_{co}\ O_2 \longrightarrow \alpha_a\ \textit{ash} + (1 + \alpha_{co} - \alpha_a)\ \textit{gases}$$

$$\textit{volatiles} + \alpha_{vo}\ O_2 \longrightarrow (1 + \alpha_{vo})\ \textit{gases}$$

Using the of apparent kinetic parameters of these reactions (determined typically by thermal analysis, *i.e.*, DSC and TGA), various chemical and thermal mechanisms involved in the combustion of a porous solid and their contribution to heat and mass transfer processes in the three phases are considered. The problem is formulated via conservation equations of mass, species, linear momentum, and energy. The continuum solid/gas description of the media [2] and local thermodynamic equilibrium assumption are employed, so that one set of conservation equations for the entire domain may be developed by volume averaging the microscopic conservation equations of the constituent phases (*i.e.*, gaseous mixture, solid fuel, and porous char and ash). Transient laminar flow, and heat and mass transfer are considered. The thermophysical properties of the condensed phases and fluid are homogeneous and isotropic, but may depend on temperature. Radiation

exchange between the combustion gases and the solid surfaces in their view are accounted for, but the gases are taken to be non-participating (transparent). Included in this formulation are the effects of transport processes such as heat-up, degradation and smoldering of the solid fuel and its char; diffusion and mixing of gaseous reactants, oxidant, and combustion products; motion of the charring and burning front, and volatile flaming combustion.

The transient two-dimensional governing equations of the problem, in terms of primitive variables, are discretized over non-uniform control-volumes and solved by an iterative numerical procedure. Detailed description of the model and numerical procedure may be found in [7,8]. As a test problem, the flaming combustion of a flat PMMA surface is modeled. The physical situation modeled and some of the boundary conditions used are presented in Figure 1, along with a sample of temperature distribution in the gas and solid. The physical model and numerical procedure are validated by performing simulations of laminar flame spread over horizontal and vertical flat surfaces of PMMA, and comparing the results with the available experimental data [9]. The detailed results of the simulations will be presented in terms of the field variations of velocity, composition, and temperature of the gas; the temperature distribution in the solid, char and ash; and the temporal position and velocity of the smoldering/burning front.

References

1. Ohlemiller, T. J., *Prog. Energy Combust. Sci.*, 11:277-310 (1985).
2. Thomas, P. H., *Fire Safety J.*, 19:125-140 (1992).
3. Wichman, I. S., *Prog. Energy Combust. Sci.*, 18:553-593 (1992).
4. Bhattacharjee, S., *Combust. Flame*, 93:434-444 (1993).
5. Quintiere, J. G., *J. Res. Natl. Bur. Stand.*, 93:61-70 (1988).
6. Babrauskas, V., *Fire Safety J.*, 17:13-26 (1991).
7. Moallemi, M. K., Zhang, H., Kumar, S., *Combust. Flame*, 1993 (in print).
8. Zhang, H., and Moallemi, M. K., *Combust. Flame*, 1993 (to be submitted).
9. Fernandez-Pello, A., and Williams, F. A., *Combust. Flame*, 28:251-277 (1977).

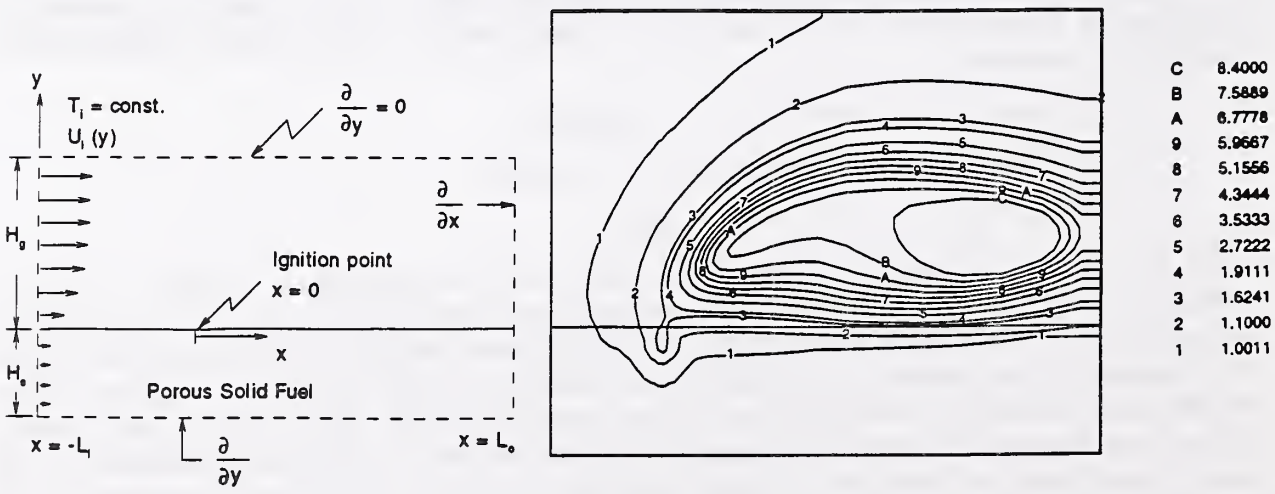

Figure 1. Schematic of problem domain and boundary conditions (left), and solid- and gas-phase temperature contours in a concurrent forced flow.

EFFECT OF RADIATIVE HEAT LOSS ON DIFFUSION FLAMES IN QUIESCENT MICROGRAVITY ATMOSPHERE

ARVIND ATREYA AND SANJAY AGRAWAL

Combustion and Heat Transfer Laboratory
Department of Mechanical Engineering and Applied Mechanics
The University of Michigan, Ann Arbor, MI 48109-2125
(Supported by NASA, GRI and NSF)

Abstract In this paper we present the results of a theoretical calculation for radiation-induced extinction of a one-dimensional unsteady diffusion flame in a quiescent microgravity environment. The model formulation includes both gas and soot radiation. Soot volume fraction is not a priori assumed, instead it is produced and oxidized according to temperature and species dependent formation and oxidation rates. Thus, soot volume fraction and the resulting flame radiation varies with space and time. Three cases are considered (i) a non-radiating flame, (ii) a scarcely sooty flame, and (iii) a very sooty flame. For a non-radiating flame, the maximum flame temperature remains constant and it does not extinguish. However, the reaction rate decreases as $t^{-1/2}$ making the flame "weaker." For radiating flames, the flame temperature decreases due to radiative heat loss for both cases resulting in extinction. The decrease in the reaction rate for radiating flames is also much faster than $t^{-1/2}$. Surprisingly, gas radiation has a larger effect on the flame temperature in this configuration. This is because combustion products accumulate in the high temperature reaction zone. This accumulation of combustion products also reduces the soot concentration via oxidation by OH radicals. At early times, before a significant increase in the concentration of combustion products, large amount of soot is formed and radiation from soot is also very large. However, this radiative heat loss does not cause a local depression in the temperature profile because it is offset by the heat release due to soot oxidation (see Fig. 3). These results are consistent with the experiments and provide considerable insight into radiative cooling of sooty flames. This work clearly shows that radiative-extinction of diffusion flames can occur in a microgravity environment.

Introduction The absence of buoyancy-induced flows in a microgravity environment and the resulting increase in the reactant residence time significantly alters the fundamentals of many combustion processes. Substantial differences between normal gravity and microgravity flames have been reported during droplet combustion, flame spread over solids, candle flames and others. These differences are more basic than just in the visible flame shape. Longer residence time and higher concentration of combustion products create a thermochemical environment which changes the flame chemistry. Processes such as soot formation and oxidation and ensuing flame radiation, which are often ignored under normal gravity, become very important and sometimes controlling. As an example, consider the droplet burning problem. The visible flame shape is spherical under microgravity versus a teardrop shape under normal gravity. Since most models of droplet combustion utilize spherical symmetry, excellent agreement with experiments is anticipated. However, microgravity experiments show that a soot shell is formed between the flame and the evaporating droplet of a sooty fuel. This soot shell alters the heat and mass transfer between the droplet and its flame resulting in significant changes in the burning rate and the propensity for flame extinction. This change in the nature of the process seems to have occurred because of two reasons: (i) soot formed could not be swept out of the flame due to the absence of buoyant flows, and (ii) soot formation was enhanced due to an increase in the residence time.

Recently, some very interesting observations of candle flames under various atmospheres in microgravity have been reported. It was found that for the same atmosphere, the burning rate per unit wick surface area and the flame temperature were considerably reduced in microgravity as compared with normal gravity. Also, the flame (spherical in microgravity) was much thicker and further removed from the wick. It thus appears that the flame becomes "weaker" in microgravity due to the absence of buoyancy generated flow which serves to transport the oxidizer to the combustion zone and remove the hot combustion products from it. The buoyant flow, which may be characterized by the strain rate, assists the diffusion process to execute these essential functions for the survival of the flame. Thus, the diffusion flame is "weak" at very low strain rates and as the strain rate increases the flame is initially "strengthened" and eventually it may be "blown out." The computed flammability boundaries show that such a reversal in material flammability occurs at strain rates around 5 sec^{-1}.

The above experimental observations suggest that flame radiation will substantially influence diffusion flames under microgravity conditions, particularly the conditions at extinction. This is because, flame radiation at very low or zero strain rates is enhanced due to: (i) high concentration of combustion products in the flame zone which increases the gas radiation, and (ii) low strain rates provide sufficient residence time for substantial amounts of soot to form which is usually responsible for most of the radiative heat loss. This radiative heat loss may extinguish the already "weak"

diffusion flame. Thus, the objective of this work is to theoretically investigate the reason why the diffusion flame becomes "weak" under microgravity conditions and determine the effect of flame radiation on this "weak" diffusion flame. This will lead to radiation-induced extinction limits. This work is important for spacecraft fire safety.

The Model Problem and Results We note that the problem at hand is inherently transient and to study the effect of flame radiation we must focus on the reaction zone. Also, since the reaction zone is usually thin compared with other characteristic dimensions of the flame, its basic structure is essentially independent of the flame shape. Thus, we consider a simple model problem consisting of an unsteady one-dimensional diffusion flame (*with flame radiation*) initiated at the interface of two quiescent half spaces of fuel and oxidizer at time t=0. Zero gravity, constant properties, one-step irreversible reaction and unity Lewis number are assumed. A novel feature of the formulation presented below is that soot volume fraction is not a priori specified to determine the ensuing flame radiation. Instead, soot is produced and oxidized according to the temperature and species concentration dependent formation and oxidation rates. Thus, the soot volume fraction and its location within the flame evolve as a function of space and time. The soot formation and oxidation rates used here are obtained from our counterflow diffusion flame experiments and models. A schematic of the physical problem along with the imposed boundary conditions is presented in Fig. 1. The equations were numerically integrated by using a finite difference Crank-Nickolson method. Predictor-corrector method was used to evaluate the nonlinear reaction terms.

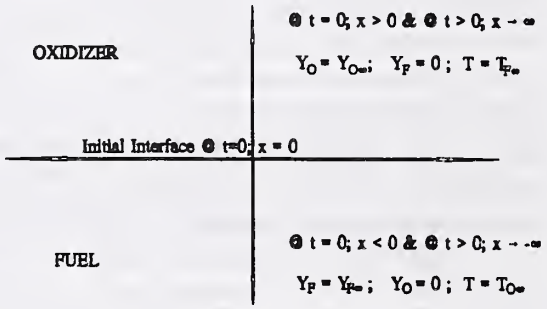

Figure 1 : Schematic of the Model Problem

It was that in the absence of external flow (i.e., zero strain rate) it was found that the flame temperature decreases due to flame radiation and the flame thickness increases because of diffusion *(radiation-induced extinction)*. It was found that the soot volume fraction for Case 1 was two orders of magnitude smaller than for Case 2 (Fig. 2). Physically, Case 1 represents a barely sooting blue flame and Case 2 represents a fairly sooty blue-yellow-orange flame. However, despite the differences in the magnitude of the soot volume fraction for the two cases, it first increases and later decreases with time and its spatial distribution shifts toward the fuel side for both cases.This decrease in the soot volume fraction occurs because of two reasons: (i) A reduction in the flame temperature due to radiation reduces the soot formation rate, and (ii) A buildup in the concentration of CO_2 and H_2O near the high-temperature reaction zone, increases the OH radical concentration which reduces the formation of soot precursors and assists in soot oxidation. This increased OH radical concentration is also responsible for shifting the soot profile toward the fuel side. Figure 3 shows that the temperature profiles are essentially symmetrical. This implies that the heat lost via soot radiation approximately equals the heat produced via soot oxidation. Since both occur at the same location, a discernible local depression in the temperature profile is not observed. This fact is experimentally substantiated by our low strain rate counterflow diffusion flame experiments. It is also consistent with the observation that radiation from a soot particle at these high temperatures will quickly quench the particle unless its temperature is maintained via some local heat release. In the present case, this heat release is due to soot oxidation. Thus, a portion of the fuel that is converted into soot oxidizes at a location different from the main reaction zone and nearly all the heat released during this process is radiated away. The remaining fuel is oxidized at the main reaction zone resulting in a lower heat release and hence a reduced peak flame temperature.

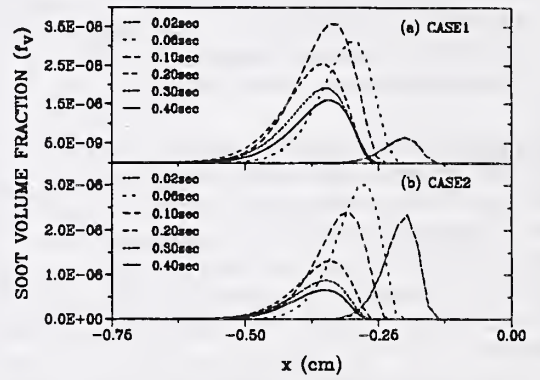

Figure 2 : Soot volume fraction vs distance at various instants

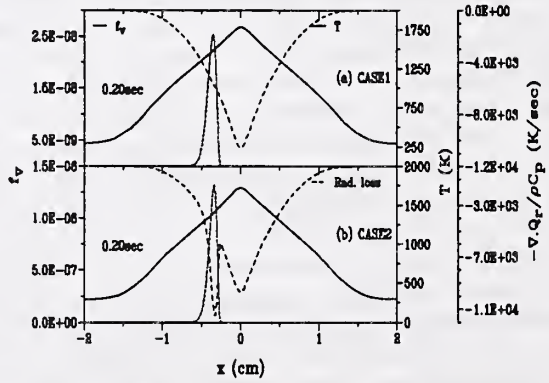

Figure 3 : Spatial Distribution of temperature, soot volume fraction and radiative heat loss

ON BURNING ZONE DURING UNSTEADY WIND-AIDED FLAME SPREAD

SANJAY AGRAWAL AND ARVIND ATREYA

Combustion and Heat Transfer Laboratory
Department of Mechanical Engineering and Applied Mechanics
The University of Michigan, Ann Arbor, MI 48109-2125

(Supported by USDA and NSF)

This study presents a numerical model of wind-aided flame spread over thick vaporizing solids like PMMA. Model predictions are limited to burning zone behavior and compare favorably with the experiments conducted in the ceiling configuration. The model assumes steady gas-phase and transient solid-phase. Effects of surface radiative heat loss and influence of flame radiation on total fuel production is analyzed. It is found that even small flame radiation (0.5 W/cm^2) has a big impact on total fuel production, flame length and in turn spread rates. Inclusion of flame radiation is essential to predict transient spread rates observed during flame spread experiments. It is found that 75% of the fuel produced is consumed in the burning zone and the flame lies close to the solid surface as observed during the experiments. Results suggest that further studies should be conducted over a steadily vaporizing solid so that local measurements can be obtained which could form basis for the development of better models and comparisons.

Wind-aided flame spread is the most hazardous type of flame spread in building fires, and has been the most difficult to understand and quantify. An improved understanding of wind-aided flame spread will result in better material hazard classification and greater fire safety. From the point-of-view of fire safety, the knowledge of the burning rate as a function of time is very important because it controls the flame size or the flame length and the flame radiation associated with it. The analysis of the burning zone is also important for determining the rate of species production and consumption. During wind-aided flame spread, the overall burning rate depends upon the local burning rate and the burning area (or length in the 2-D ceiling configuration) which is changing with time. Previous studies of wind-aided flame spread have primarily focussed on determining the length of the burning (or pyrolyzing) zone and have assumed the local pyrolysis rate to be steady. Thus, bypassing the transient analysis of the pyrolyzing zone. As a result, the pyrolysis front location and its speed (which primarily depends on the ease of ignition of the as-yet-unburned material) have been extensively analyzed in the presence of a hypothetical flame length. Most of the emphasis has been on determining the effects of free stream velocity and oxygen mass fraction on the pyrolysis front speed. In all of these analyses, re-radiation from and flame radiation to the burning solid were neglected. These assumptions are often made because they lead to similarity and enable the three independent variable system in the preheat zone (x,y,t) to be reduced to a two independent variable system (x/t, y/√x). However, this forces the pyrolysis front speed to be a constant. Our flame spread experiments on a vaporizing solid (PMMA) show that the pyrolysis front speed is not constant. For some cases it accelerates and for others it decelerates and even becomes zero (see Fig. 1). As will be shown below, the first scenario can be attributed to flame radiation and the second to radiative surface heat losses. Inclusion of these phenomena in the analysis results in the loss of similarity and the subsequent problem can only be solved numerically. Our previous experimental investigation has shown that during wind-aided flame spread over a vaporizing solid (PMMA), the solid-phase undergoes transient pyrolysis while the gas-phase remains quasi-steady. Moreover, the flame length and the flame tip speed are controlled by unsteady pyrolysis of the solid in the burning zone and the rate of progress of the pyrolysis front is controlled by heat transfer from the flame and hot gases to the solid ahead of the pyrolysis front. Recent models have also predicted quantitatively the effects of transient pyrolysis on spread rates. These studies include the effect of surface re-radiation, however, they do not discuss the role of flame radiation on the spread rates. In our recent paper, we developed a model to predict the total oxygen consumption rate as a function of the pyrolysis front location and time. Based on our experimental observation, we assumed that the flame lies on the solid surface and used integral methods to solve for steady gas-phase and transient solid-phase equations. In the present study we relax the assumption of the

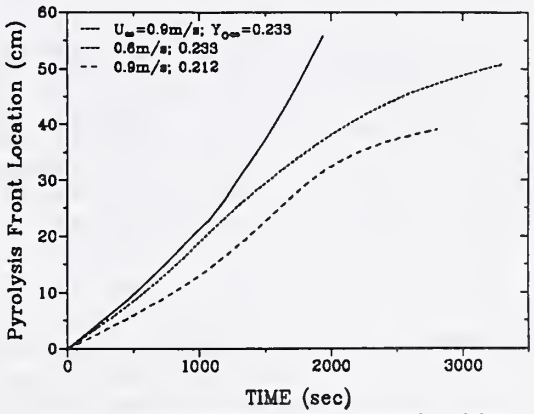

Figure 1 : Pyrolysis front location as a function of time

flame lying adjacent to the sample surface and solve the governing equations numerically. This is done both to understand the reasons why the experimentally observed flame lies so close to the sample surface and to evaluate the effect of the previous assumption on the model predictions. Although flame radiation is not included in the governing equations, its effect and importance is studied with the help of experimental and numerical results. Thus, the objectives of this study are: (i) To develop a steady laminar gas-phase model and a transient solid-phase model for wind-aided flame spread; (ii) To couple them with appropriate boundary conditions at the solid-gas interface to predict the total fuel produced, regressed surface location and the flame length as a function of the pyrolysis front location and time; (iii) Study the effect of flame radiation on the flame spread process, and (iv) To provide a physical understanding which could serve as a basis for material hazard evaluation and future model developments.

The schematic of this problem is shown in Fig. 2. After ignition, the tip of the surface-pyrolysis zone (x_p) propogates downstream with velocity V_p, while the flame front (x_f) propagates downstream at a higher velocity V_f, burning the "excess" fuel produced from the pyrolyzing solid. In the schematic shown in Fig. 2 there are two distinct zones to be considered. First is the burning (pyrolysis) zone ($0 < x < x_p$), where there is fuel efflux from the surface. For vaporizing solids pyrolysis occurs only after the surface has been heated to the "vaporization temperature", T_v. The second is the preheat zone ($x > x_p$) in which excess fuel is burned and the virgin solid is heated by the "excess fuel" flame and the hot combustion products. The rate of pyrolysis front speed is determined by the rate at which the solid fuel can be heated to T_v, while the rate of flame spread depends on the transient behavior of solid, gas-phase mixing and reaction rates. This requires a complete analysis of the burning zone which has been missing in the literature. In this paper we analyze the burning zone which produces the fuel, its effect on flame length and its rate of spread. In a complete contrast to previous analyses, which essentially solved for the rate of propagation of the pyrolysis front we will use the experimental results for the pyrolysis front location as a function of time (see Fig. 1) and focus on the burning zone problem. Once the burning zone solution is obtained and understood it can be easily coupled to the preheat zone solution to provide both x_p and x_f as a function of time.

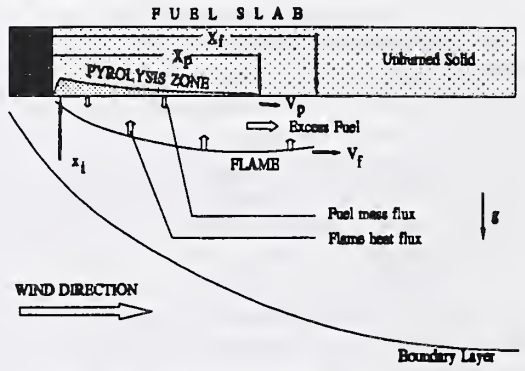

Figure 2 : Schematic of the wind-aided spread model problem

The gas-phase equations, although steady, have to be solved at every time step because solid and the boundary conditions are unsteady. A growing boundary layer poses further numerical difficulties of grid resolution and false diffusion making standard central difference schemes unsuitable. GENMIX was used to solve governing equations. GENMIX, however, was developed for solving steady boundary layer equations with predefined boundary conditions. For application of GENMIX to our problem, where the heat flux and mass flux are coupled at the solid-gas interface, the solutions need to be iterated at each streamwise location and at any instant. The code was modified to do this. The model predictions were in good agreement with the experimental results. It was found that flame radiation can have significant effect on flame length, total fuel production and consequently flame spread. Inclusion of it can only result it transient spread rates as observed during experiments. Figure 3 presents the regressed solid surface location as a function of the streamwise distance. Numerical results are obtained by integrating the evolved mass flux at a given location from start of vaporization to the end of experiment, and then multiplying with the solid density. Experimental results are obtained by cutting the sample and measuring the difference in between the burned and unburned thickness. Note that the comparison is satisfactory for streamwise distance > 3cm and very poor for distance < 3cm. This zone is dominated by streamwise diffusion in both the solid and gas rendering the present governing equations inapplicable.

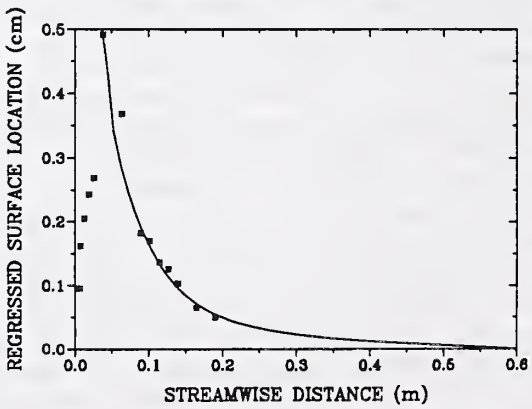

Figure 3 : Regressed Surface location vs distance

PROGRESS with the CEILING JET

Howard W. Emmons
Harvard University
Prediction of Fire Dynamics
Task 1; Prediction of Fire in Buildings
Factory Mutual Research

It has been known for some time (1) that the one dimensional theory of ceiling jet flow with or without suitable density and velocity profiles fails to be able to meet appropriate boundary conditions if heat transfer to the ceiling and or ambient are included - as they always must be for fire gases. Current theories and data of which there are many papers starting with that of Alpert (2) satisfy conditions at their source but ignore conditions at the far end.

Transient solutions have been obtained with and without friction which clarifies what boundary conditions can and cannot be satisfied. These solutions are compared with the ceiling jet that would occur if its progress were a succession of steady states. Although it appears that all fire ceiling jets are in tranquil flow (froude Number < 1, Richardson Number > 1) the corresponding shooting flow with hydraulic jumps are also examined.

Figure 1 shows the transient ceiling jet without friction. As it arrives at the corridor end it is already in its steady state. Figure 2 shows that the transient ceiling jet with friction (friction factor = .01) advances in about the same way as the frictionless case and reaches the corridor end in 11 seconds but then continues to develop during the next several minutes before the steady state is reached. The transient if it were a succession of steady states would appear as in Figure 3 which is far from the correct transient.

Since the initial transient is very different from the final steady state ceiling jet, the effect of adding heat transfer will also be different and will be discussed. It is anticipated that the initial transient with heat transfer will develop without difficulty but will fail as the solution approaches steady state.

The importance of adding the effect of the ceiling jet fluid accelerations normal to the ceiling to the horizontal momentum equation will be presented.

References:

1. H. Emmons, "The Ceiling Jet in Fire", 3rd International Symposium on IAFSS, pg. 24, 1991.

2. R. Alpert, "Turbulent Ceiling Jet Induced by Large Scale Fires", Comb. Sci. and Tech., 11, pg. 197, 1975.

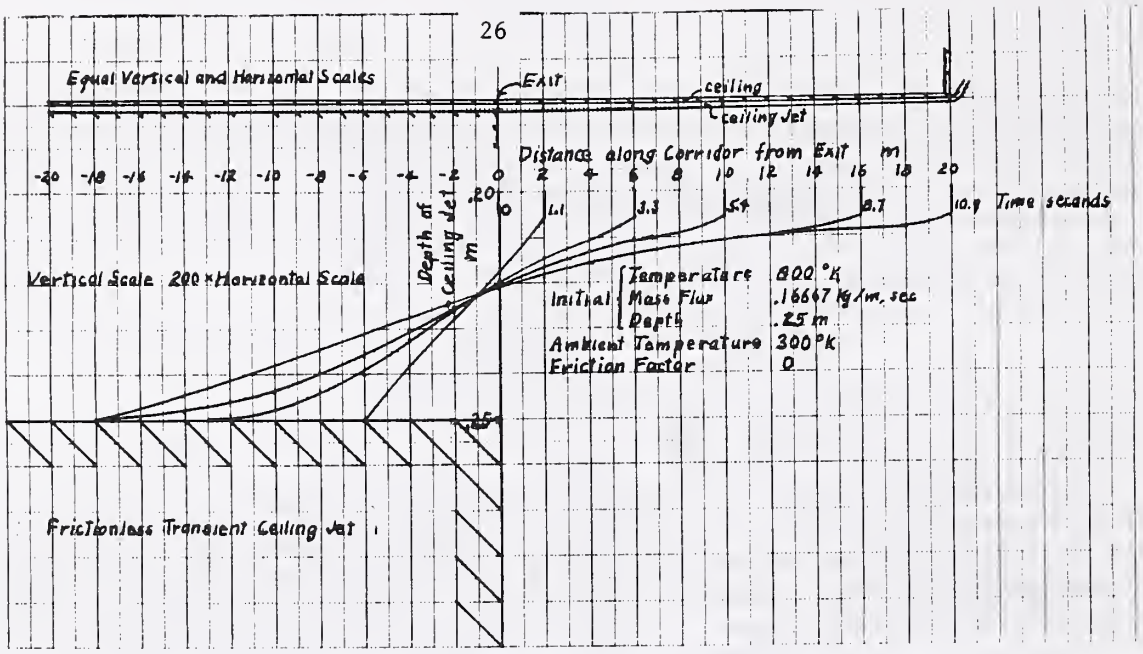
Equal Vertical and Horizontal Scales
Exit
ceiling
ceiling Jet
Distance along Corridor from Exit m
Depth of Ceiling Jet m
Time seconds
Vertical Scale 200 × Horizontal Scale
Initial Temperature 800 °K
Mass Flux .16667 kg/m. sec
Depth .25 m
Ambient Temperature 300 °K
Friction Factor 0
Frictionless Transient Ceiling Jet

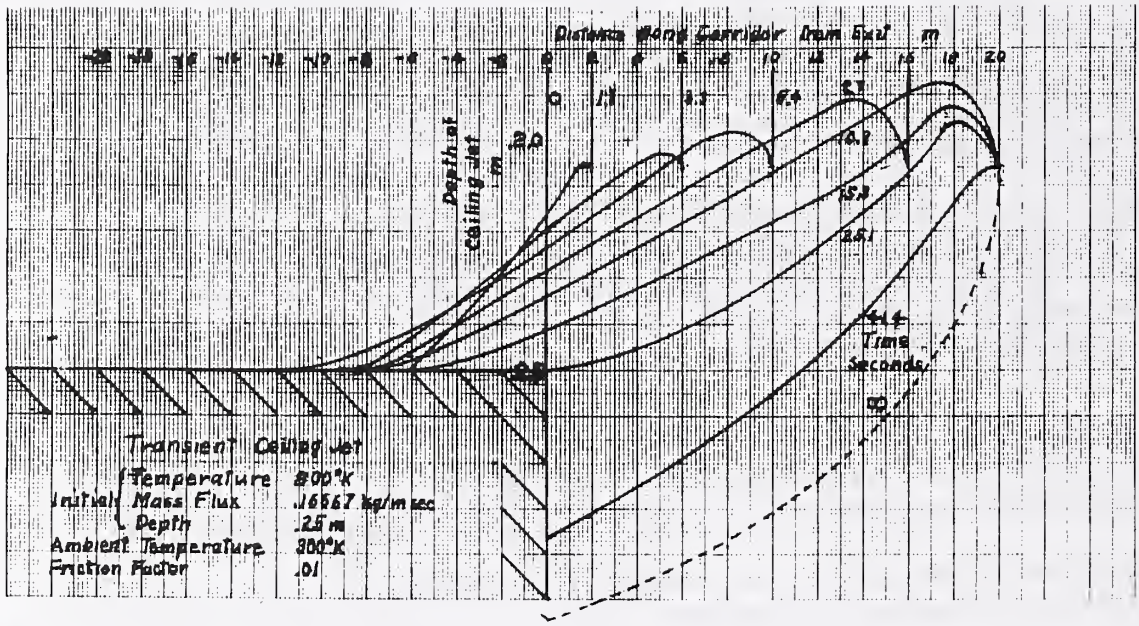
Distance along Corridor from Exit m
Depth of Ceiling Jet m
Time Seconds
Transient Ceiling Jet
Initial Temperature 800°K
Mass Flux .16667 kg/m sec
Depth .25 m
Ambient Temperature 300°K
Friction Factor .01

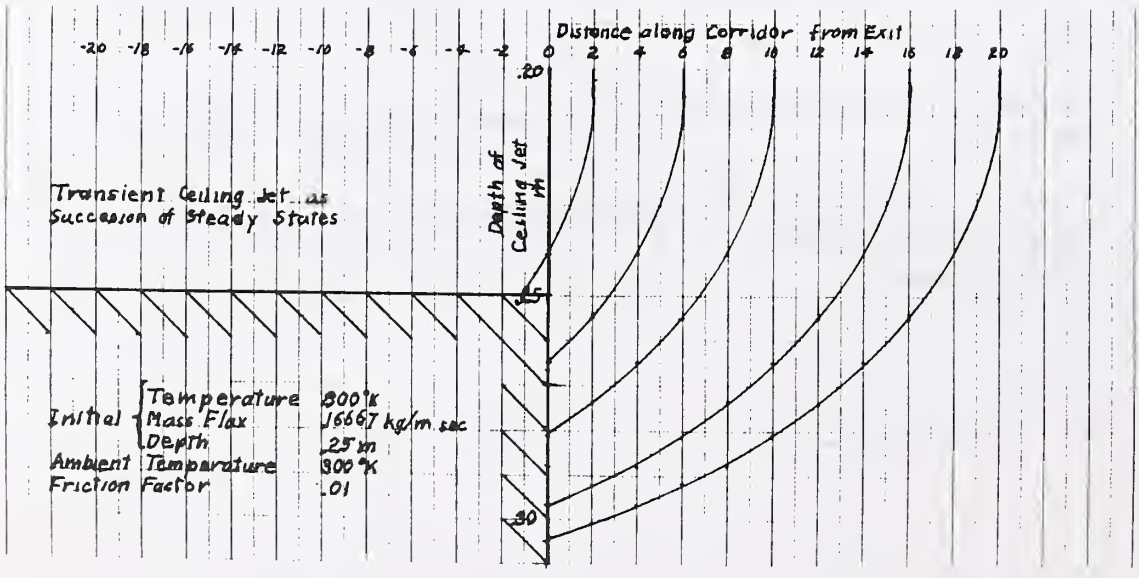
Distance along Corridor from Exit
Depth of Ceiling Jet m
Transient Ceiling Jet as Succession of Steady States
Initial Temperature 800°K
Mass Flux .16667 kg/m sec
Depth .25 m
Ambient Temperature 300°K
Friction Factor .01

A NUMERICAL MODEL OF BUOYANT PLUMES IN ROOM FIRES WITH TWO-LAYER STRATIFIED ATMOSPHERE

J. T. Costa and A. K. Kulkarni
Department of Mechanical Engineering
The Pennsylvania State University
University Park, PA 16802

Pool fire in a room is often studied as a plume interacting with a two-layer stably stratified atmosphere[1]. Small scale hot air jet experiments and salt-water analog experiments have been conducted to simulate the flow, and also zone models of this type of flow have been attempted previously[2,3,4]. The overall objective of the present project is to study the flow using a comprehensive computational fluid dynamics model. This paper presents the results of the first phase of the project which deals with the flow simulation of salt-water experiments that were completed and reported recently[4].

The domain of flow computations is nearly identical to what was used in our experiments. It is axisymmetric, 0.2m high and 0.4 m diameter, consisting of two layers of water initially at rest. (See Figure 1) Buoyancy forces due to density differences are modeled using different temperatures of water (similar to actual room fire situation). The lower layer has an initial temperature of 7° C and it linearly increases through a thin (10 mm) interfacial layer to 50° C in the upper layer. A narrow uniform jet of either 50° C or 82° C water enters the center of the lower layer through a 6.3 mm diameter nozzle at a speed of 0.04 m/s. The model consists of the Navier-Stokes and energy equations with Boussinesq approximation for buoyancy.

The region of interest was divided into a mesh with 59 radial and 37 axial nonuniform divisions having a total of 522 elements and 2183 nodes. A commercially available finite element software package called Fluid Dynamics Analysis Package (FIDAP) was used to numerically solve the governing equations. Computations were performed on a Cray Y-MP computer at the National Center for Supercomputing Applications, Urbana-Champaign, Illinois.

Figures 2 and 3 show the temperature contour and streamline plots at 7 s after injection for the plume injection temperature of 50° C. Only half the flow region is shown because of symmetry. The buoyancy is much stronger in the lower layer and also there is initial upward momentum in the plume. As the flow moves into the upper layer, the buoyancy decreases because of the higher surrounding temperature and the entrainment of surrounding liquid into the plume. Penetration is impeded in the upper layer and the plume spreads out laterally. Figure 4 shows a temperature contour plot for a case with the same conditions except that the plume injection temperature is 82° C. Here the injected plume penetrates further into the upper layer as compared to the previous case. A video movie of the developing flow pattern will be made for easier flow visualization. Such flow simulations of single or multiroom fires and plume spread can be very useful in hazard prediction, smoke movement, sprinkler location studies, and other aspects of fire research.

Support for computing was obtained through a grant from the National Science Foundation.

References

1. Evans, D. D., Plume Flow in a Two-Layer Environment, *Fire Dynamics and Heat Transfer*, ASME HTD Vol. 25, 1983, pg 89 - 95.
2. Zukoski, E. E., Development of a Stratified Ceiling Layer in the Early Stages of a Closed Room Fire, *Fire and Materials*, Vol. 2 , 1978, pg. 54.
3. Cooper, L. Y. , Harkelroad, M., Quintiere, J., and Rinkinen, W., An Experimental Study of Upper Hot Layer Stratification In Full-Scale Multiroom Fire Scenario, *J. of Heat Transfer*, Vol. 104, 1982, pg. 741.
4. Kulkarni, A. K., Murphy, F., Manohar, S. S. , Interaction of Buoyant Plumes with Two-Layer Stably Stratified Media, *Experimental Thermal and Fluid Science,* to be published.

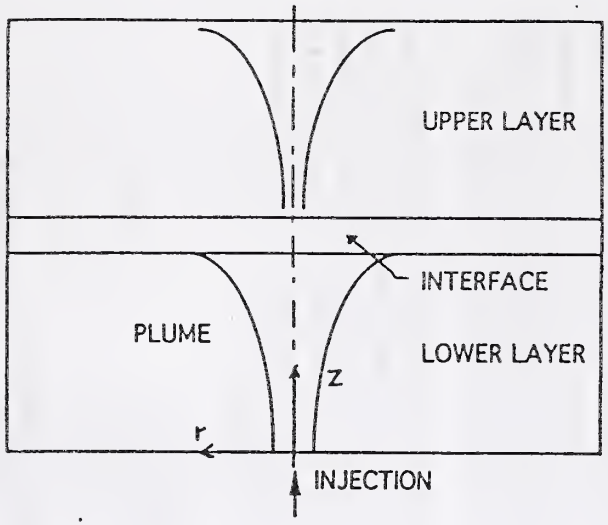

Figure 1. A schematic of the plume flow.

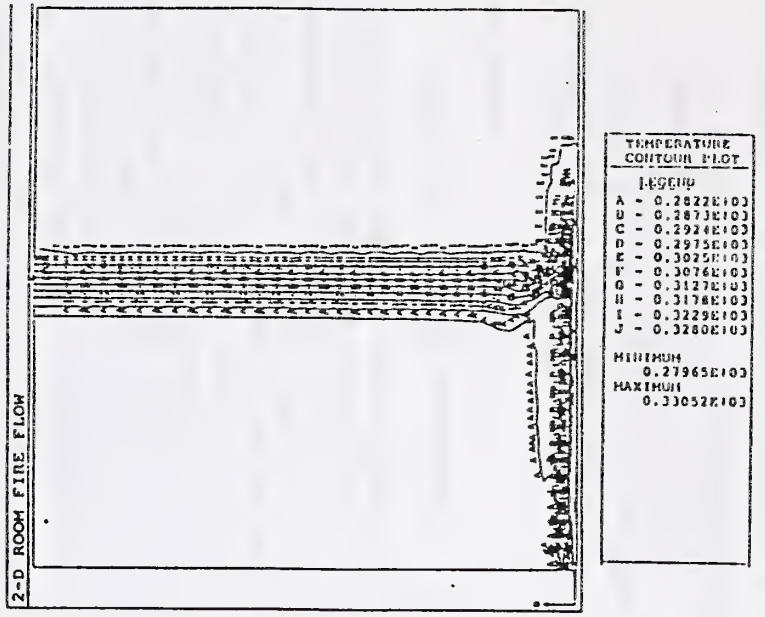

Figure 2. Temperature contour plot; $T_{injection}=50^{o}$ C; t = 7 s

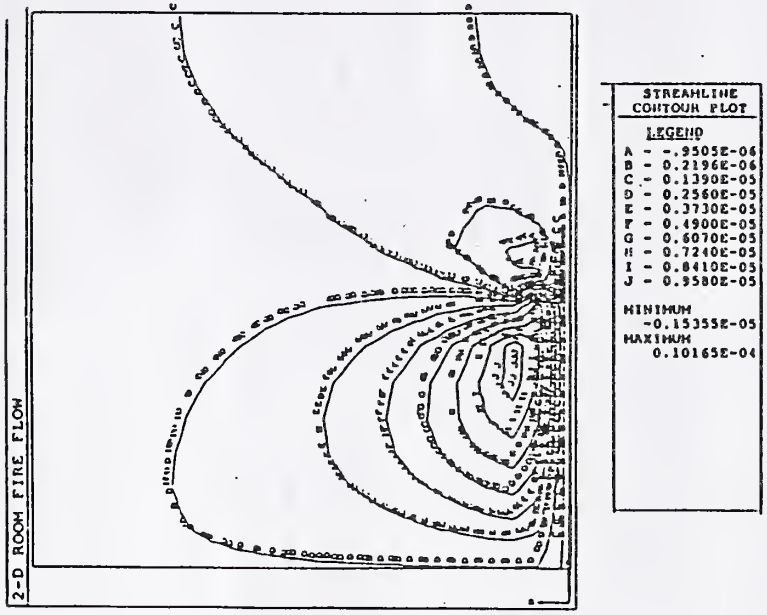

Figure 3. Streamline plot; $T_{injection}=50^{o}$ C; t = 7 s

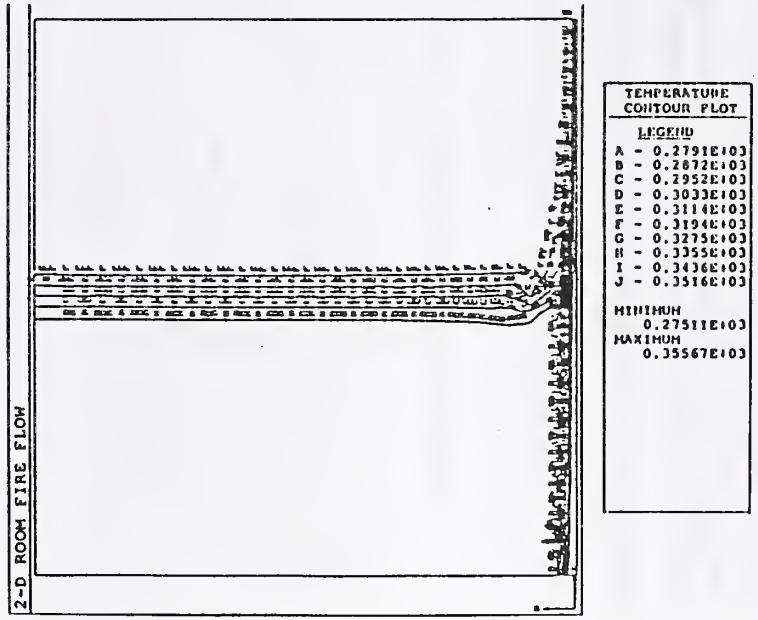

Figure 4. Temperature contour plot; $T_{injection}=82^{o}$ C; t = 7 s

TURBULENT TRANSPORT IN BUOYANT PLUMES AND MEDIUM SIZED POOL FIRES

M.A. Pivovarov, H. Zhang and D.E. Ramaker
Chemistry Department, George Washington University,
Washington, DC 20052

P.A. Tatem and F.W. Williams
Chemistry Division, Naval Research Laboratory,
Washington, DC 20375-500

Buoyant plumes

Vertical axisymmetric turbulent buoyant plumes in quiescent surroundings have been extensively investigated [1 - 6]. These plumes establish a similarity behavior starting at a particular elevation above the origin, usually for the mean characteristics of the flow at $z = 5\ l_m$, and for the turbulence properties at $z = 14\ l_m$. All experimental data support the general notion that in the similarity region the following universal laws are observed:

(a) the dimensionless profiles, $u/u_c = f_U(r/r_{1/2U})$ and $t/t_c = f_T(r/r_{1/2T})$, are universal;
(b) the centerline values scale with z^{-n}, $u_c = A_U B_0^{1/3} z^{-1/3}$ and $t_c = A_T(\beta g)^{-1} B_0^{2/3} z^{-5/3}$; and
(c) the local half-radii linearly depend on the axial coordinate: $r_{1/2U} = K_U z$ and $r_{1/2T} = K_T z$.

The dimensionless parameters A_U, A_T, K_U, and K_T and functions f_U and f_T are fundamentally unknown but are expected to be universal. There is excellent agreement on the specific forms for the functions f_U and f_T. However, we find a significant disagreement between different sets of experimental data on the values of the parameters A_U, A_T, K_U, and K_T. We attribute this disagreement to differences in the experimental setup. If fewer precautions are taken against plume perturbations, both the velocity and temperature radial profiles are widened. This means that the experimentally observed values for A_U and A_T increase and the values for K_U and K_T decrease for well protected plumes.

Utilizing our similarity solution [7] for the standard k-ϵ model for turbulence, we find that adjustment of only one parameter, $C_\mu = \nu_T \epsilon / k^2$, provides excellent agreement with the experimentally observed functions for f_U and f_T, and the parameters, A_U, A_T, K_U, and K_T. The specific values for C_μ which give the best agreement with experimental data are: 0.15 - 0.17 for experiments without a surrounding mesh about the orifice [2 - 4]; 0.09 for experiments with a surrounding mesh [6]; and 0.12 for other data [1 and 5]. Since the parameter C_μ may be a measure of the intensity of turbulent transport, our estimates suggest that the well protected plumes demonstrate less radial turbulent transport.

There is no correlation between the value of C_μ and the type of fluid (air [1, 2, 4 and 6] and water [3, 5] have been utilized). However, there is a strong correlation between the value of C_μ and the geometry of a relatively small mesh around the orifice [4]. We attribute this effect to a strong influence of the source conditions on the whole flow, which was considered in a more general context previously [8], utilizing a similarity approach different from this analysis.

Comparing our similarity theoretical profiles with experimental data [5 and 6] obtained in the

region $z < 5\ l_m$ where the similarity is not yet developed, we find excellent agreement can be obtained by further increasing C_μ up to 0.3. Although the mathematical validity of this comparison is not clear, we consider this result as supporting evidence for additional increase in turbulent transport at the region of the developing plume ($z < 5\ l_m$).

Considering the similarity formulation in the context of the algebraic stress model [9], we find that the parameter C_μ is not a constant parameter but a function of the radial coordinate. However, we find that variation of this parameter across the plume does not influence significantly the radial profiles for the mean variables. We are able to predict properly the turbulence properties utilizing the algebraic relations between them [9], along with the similarity profiles for u, t, k and ϵ which are calculated from the k-ϵ model.

Medium Sized Pool Fires

We utilize a modified version of our previously reported fire model [10] for numerical computations on 0.3 m diameter ethanol and heptane pool fires. Based upon our results for plumes, we consider the parameter, C_μ, as a step-function of the vertical coordinate: 0.30 for $z < D$ and 0.15 for $z > D$. Utilization of the step-function approximation gives excellent agreement with experimental data [11] for the ethanol fire. It also provides good agreement with experimental data [12] for the heptane fire; however, the agreement is not as good as for ethanol. We conclude that utilization of the "standard" value, 0.09, for C_μ in previous numerical models is probably the main reason for the shortcoming of these models in predicting the fire width and entrainment levels.

Acknowledgement: Three of the authors (M. A. P., H. Z., and D. E. R.) acknowledge the partial support of this work by the Naval Research Laboratory.

Nomenclature: B_0 and M_0 - initial buoyancy and momentum of the plume; D - pool diameter; g - acceleration of gravity; k - kinetic energy of turbulence; $l_m = M_0^{3/4}B_0^{-1/2}$ - Morton length scale; r and z - radial and axial coordinates; $r_{1/2T}(z)$, $r_{1/2U}(z)$ - local half-radii for the temperature and velocity; t - mean temperature excess with surroundings; u - axial component of mean velocity; ß - coefficient of thermal expansion; ϵ - turbulent dissipation; ν_T - turbulent viscosity. Index "c" means the centerline value.

References: 1. Rouse, H., Yih, C.-S., and Humphreys, H.W., *Tellus*, 8:201 (1952).
2. George, K.G., Alpert, R.I., and Tamanini, F., *Int. J. Heat Mass Transfer*, 20:1145 (1977).
3. Kotsovinos, N.E., *Int. J. Heat Mass Transfer*, 28:771 (1985).
4. Shabbir, A., Ph. D. thesis, SUNY (1987).
5. Papanicolaou, P.N., and List, E.J., *Int. J. Heat Mass Transfer*, 30:2059 (1987).
6. Dai, Z., Tseng, L.-K., and Faeth, G.M., 1992 Annual Conf. Fire Research, p. 47 (1992).
7. Pivovarov, M.A., Zhang, H., Ramaker, D.E., Tatem, P.A., and Williams, F.A., *Comb. Flame*,92:308 (1993).
8. George, W.K., at: Advances in Turbulence, (W.K. George and R. Arndt, Eds.), p.39 (1989).
9. Tamanini, F., *J. Heat Transfer*, 100:659 (1977).
10. Adiga, K.G., Ramaker, D.E., Tatem, P.A., Williams, F.A., *Fire Safety J.*, 16:443 (1990).
11. Fisher, S.J., Ph.D. thesis, Washington State University (1988).
12. Klassen, M., Ph.D. thesis, Purdue University (1992).

Annual Conference on Fire Research
National Institute of Standards and Technology

An Integral Combustion Model for Buoyant Diffusion Flames

Yonggang Chen and Vahid Motevalli
Worcester Polytechnic Institute
Worcester, Massachusetts

Michael. A. Delichatsios
Factory Mutual Research Corp.
Norwood, Massachusetts

Introduction

The primary motivation for the development of the combustion model presented here is to predict flame behavior from burning of a solid surface. This model can be coupled with other phenomenon such as flame spread or used as a key component of enclosure fire models. These time dependent coupled phenomena would require large computation times and thus any combustion model used must be computationally efficient. Before solving the buoyant diffusion problem (i.e. pool fire) a more defined problem of a turbulent jet diffusion flame was addressed[1,2]. The model predictions for a jet flame were compared to data from two different investigators with different degrees of success[1]. The comparisons included heat release rate as a function of height, CO generation and radiation fraction.

Approach

The integral combustion model includes calculation of the flame radiation and its relation to flame turbulence and the sooting tendency of the fuel. The soot generated by the fuel has been characterized by the laminar smoke-point height[3]. This model relies both on previous integral models and more detailed k-ϵ-g models. The key characteristics of this integral model are the use of a dimensionless correlation for the entrainment spanning the range from momentum to buoyant turbulent jet flames and use of a direct relationship for the fluctuation of a conserved scaler. Such entrainment correlations can be extended to a pool fire or a horizontal burning solid surface. The entrainment correlations have been used instead of an entrainment equation for computational expediency. The model has been tested numerically and compared with results from a turbulent jet diffusion flame previously[1]. These results include CO and CO_2 species concentration, flame temperature as well as the radiation fraction. The combustion model has been described in more details by Motevalli et al.[1,4]. The extension and application to a pool fire condition involves not only altering the entrainment relations (developed by Delichatsios[5]), but also developing a methodology to deal with the flow near the source. This is being evaluated since the complexities may require computations that will negate the robustness of the integral approach. The fluid mechanics near the flame base can play an important role in that they affect the mixture fraction relations.

Among the predictions from the model, the average species concentration and temperature can be obtained by integrating the local laminar quantity weighted by the probability distribution function (PDF) which is based on the approximation of the turbulent diffusion flame as an ensemble of luminous flamelets along with known state relationship (i.e. species concentration as a function of mixture fraction) for various products of combustion (i.e., N_2, O_2, fuel {e.g. CH_4}, CO_2, H_2O, CO and H_2), has been applied to develop the combustion model[6,7]. These state relationships (some of which are available in chemical libraries) can be obtained by experiments in laminar flames[8] or by detailed chemical kinetics calculations. Radial profiles for the mixture fraction and velocity are derived in order to preserve the strong non-linearity of the combustion process[9]. The radiation distribution can be related with enthalpy

loss by the flame using the control volume analysis. Radiation is treated here in the optically thin limit as a first attempt and with approximations stated previously[4].

Comparison of numerical and experimental results

The results from the integral model has been compared to data obtained by Tamanini[10] and Jeng et al.[11] for a turbulent buoyant jet flame and has been presented before[1]. The heat release rate, temperature, CO production rate and radiant fraction have been compared with a promising agreement for the jet flame. Some preliminary results have been obtained for the pool fire scenario by simply replacing the entrainment equation. This obviously ignores the flow effect near the fire base. The results indicate that indeed this is an important effect that the numerical prediction and experimental results of Tamanini[10] (for a large propane burner, 38 cm in diameter, which nearly simulate a pool fire) almost match at the far field and are not acceptable near the flame base and for most of the flame height (Figure 1). Further evaluation of this problem is underway.

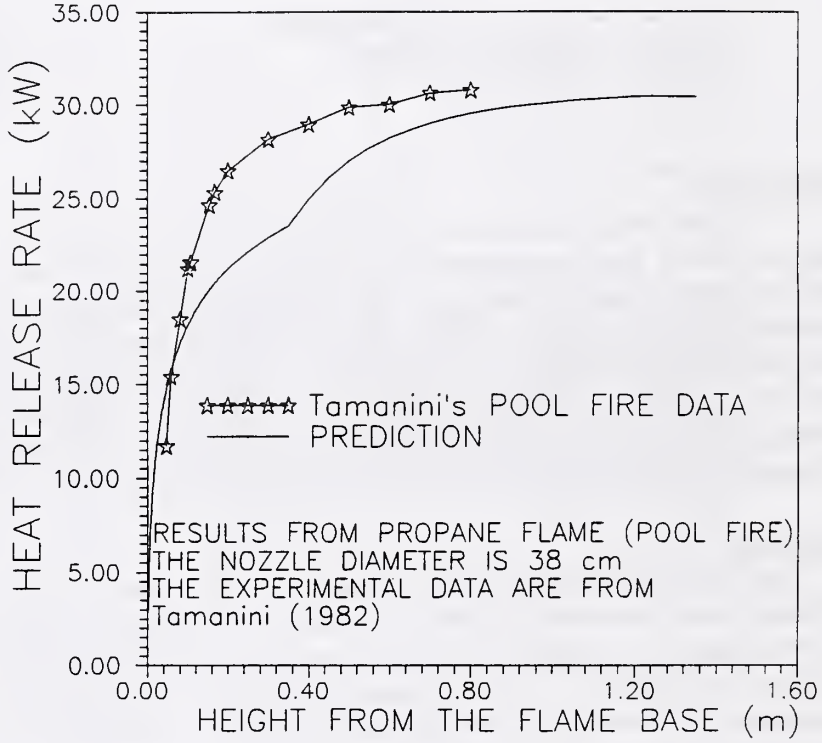

Figure 1 Heat release rates at different height along a turbulent buoyant flame (close to a pool fire): comparison of theory with experiment.

Acknowledgement

The authors would like to acknowledge the grant from Naval Research Laboratory (N00014-91-J-2023).

References

1. Motevalli, V., Chen, Y. and Delichatsios, M.A., Int'l Congress on Computational Methods in Engineering, Shiraz, Iran, May 3-6, 1993.
2. Chen, Y., Motevalli, V. and Delichatsios, M.A., Proc. of the Eastern Section of the Comb. Inst., New Orleans, March 1993.
3. Markstein, G.H., 21st(Int'l) Symp. on Combustion, The Comb. Inst., 1986.
4. Motevalli, V., Chen, Y. and Delichatsios, M.A., Annual Rpt. to Naval Res. Lab., Sept. 1992.
5. Delichatsios, M.A., SFPE Handbook of Fire Protection Eng., p. 1-306, 1988.
6. Gore, J.P. & Faeth, G.M., 21st Int'l Symp. (Int'l) on Comb., p. 1521, 1986.
7. Sivathanu, Y.R., Kounalakis, M.E. and Faeth, G.M., NIST-GCR-90-570, 1990.
8. Sivathanu, Y.R. and Faeth, G.M., Comb. Flame, 82, pp. 211-230, 1990.
9. Delichatsios, M.A. & Mathews, M.K., 2nd Int'l Fire Safety Sci. Symp., p. 149, 1989.
10. Tamanini, F., FMRC Technical Report No. J.I. OF0N4.BU, 1982.
11. Jeng, S-M, Lai, M-C and Faeth, G.M., NBS-GCR-84-458, Nat'l Bureau of Stds., 1984.

FLOW OF FIRE-INDUCED BUOYANT GASES ACROSS HORIZONTAL VENTS AND IN OPEN VERTICAL SHAFTS

Y. Jaluria, S.H.-K. Lee and G.P. Mercier
Mechanical and Aerospace Engineering Department
Rutgers University, New Brunswick, NJ 08903

Introduction

Buoyancy induced flows generated by fires in enclosures such as rooms have received considerable attention in the literature. However, not much work has been done on the flow through openings or vents such as those between containment areas in nuclear power systems, connecting rooms in buildings and between decks in ships. Flows in open vertical shafts in multi-leveled buildings have also received very little attention. The flow rate through horizontal vents can be estimated, as done for vertical vents, by using Bernoulli's equation (Emmons,1988; Heskestad and Spaulding, 1989). However, this model breaks down for problems where both density and pressure differences, $\Delta\rho$ and Δp, respectively, exist across the vent giving rise to significant buoyancy effects in addition to the pressure effect (Cooper, 1990). Some experimental work has been done on the buoyancy driven flow through horizontal vents for the circumstance of zero pressure difference across the vent (Epstein, 1988). In this case, the flow is bidirectional with the flow rates in the two directions being equal due to continuity.

The standard vent-flow model, based on Bernoulli's equation, assumes unidirectional flow and breaks down if a bidirectional flow exchange occurs under the combined effects of buoyancy and pressure. This model predicts zero flow when $\Delta p = 0$. This is obviously incorrect since flow arises due to the buoyancy effects, as mentioned above. With increasing pressure difference Δp, the bidirectional flow is replaced by unidirectional flow. The conditions under which this transition in the flow regime occurs is termed as purging or flooding. Thus, at purging, the pressure difference is large enough to overcome the buoyancy effects. If $|\Delta p|$ exceeds some critical value, $|\Delta p_c|$, then the flow becomes unidirectional and the flow in the direction opposite to the exerted pressure becomes zero. For vent aspect ratio $L/D \approx 0$, the correlation equation for the discharge coefficient C_D, which is the ratio of the upward flow rate to that given by Bernoulli's equation, was obtained as $C_D = 0.61 - 0.379\ B^{0.31}$ by Tan and Jaluria (1992) with a water/brine experiment, where $B = g\Delta\rho D/\Delta p$. Here, the work done on air as the fluid, with the density difference obtained due to the temperature, is presented. Also, work has recently been initiated on the flow of hot gases in vertical shafts in the presence of natural or forced ventilation. The experimental system for this problem, along with some preliminary results, are also presented.

Experimental Arrangement and Results

The experimental set-up for the horizontal vent study is shown in Fig. 1. The temperature within the glass enclosure is monitored by thermocouples mounted vertically along the wall. On the top of the inlet side, a pressure tap is placed. A low-pressure transducer (Omega), with a range of 0-2.5 mm of water and an accuracy of 0.5%, was employed for the pressure measurements. A stagnation chamber was used to pressurize the glass enclosure. A rotameter type flow meter was connected upstream of this chamber to measure the mean flow rate. Smoke was introduced into the stagnation chamber by burning incense. To visualize the flow in the duct, a vertical laser sheet was passed through the center of the exit duct, and the resulting scattering off the smoke particles was recorded (Jaluria et al., 1993).

The flow pattern was also found to exhibit many different variations, depending on the value of the buoyancy parameter B and the L/D ratio (Jaluria et al., 1993). Different flow regimes were found to arise and the flow was found to be much more complex than that observed for water. The flow was videotaped and the results were analyzed for the inflow and outflow characteristics. The time between inflows for a range of net upward mass flow rate was obtained. Even when the net upward flow rate was positive, there was a fair amount of reverse flow and this reversal was found to occur periodically with frequencies in the same range as those observed in earlier studies on fires in vented compartments (Takeda, 1990). The corresponding fraction of the net outflow across the vent that occurs as inflow was also plotted against the net flow. With increasing pressure difference, the net flow increases and the inflow decreases as expected, till finally there is no inflow at all. This is treated as purging.

The purging, or flooding, pressure for a very thin vent, L/D ≈ 0, is shown in Fig. 2. As expected, the flooding pressure increases as the density difference $\Delta\rho$, due to the temperature difference ΔT, increases. The pressure differences obtained are very small and are of the same order as the buoyancy effect. Figure 3 shows typical results on the measured net mass flow rate across the vent as a function of the pressure difference for two values of the temperature difference. The flow rate is seen to increase with the pressure difference and to decrease with an increase in the temperature difference. Therefore, the trends are similar to those observed in water. However, the scatter in the data is much more for air than for water due to the even smaller pressure differences of interest in air and the large transient variations that arise in the flow.

Figure 4 shows the experimental system for the study of the spread of smoke and hot gases in open vertical shafts with natural or forced ventilation. A wide range of venting conditions can be obtained with this system. Work has been done on smoke spread using a smoke generator and on the flow of hot gases for the natural venting case. Aiding forced ventilation has also been investigated.

Acknowledgements

The authors acknowledge the financial support provided by the National Institute of Standards and Technology, under Grant No. 60NANB1H1171, for this work and the several discussions with Dr. Leonard Y. Cooper on this problem.

References

Cooper, L.Y., 1990,"Calculation of the Flow Through a Horizontal Ceiling/Floor Vent," NIST Tech. Report, Rep. No. NISTIR-89-4052 (1989). Also, *Ann. Conf. Fire Res.*, Gaithersburg, MD (1990).

Emmons, H., 1988,"Vent Flows," *SFPE Handbook of Fire Protection Engg.*, Soc. Fire Protection Engg., Boston, Sec. 1, Ch.8.

Epstein, M., 1988,"Buoyancy-Driven Exchange Flow Through Small Openings in Horizontal Partitions," *J. Heat Transfer*, Vol.110, pp.885-893 .

Heskestad, G. and Spaulding, R.D., 1989,"Inflow of Air Required at Wall and Ceiling Apertures to Prevent Escape of Fire Smoke," Tech. Rep., Factory Mutual Res., Norwood, MA.

Takeda, H., 1990,"Model Experiments of Ship Fire," *22nd Int. Symp. Combust.*, pp.1311-1317.

Tan, Q. and Jaluria, Y., 1992, "Flow Through a Horizontal Vent in an Enclosure Fire," ASME Heat Transfer Div. HTD-Vol. 199, pp. 115-122.

Jaluria, Y., Lee, S.H.-K., Mercier, G.P. and Tan, Q., 1993, "Visualization of Transport Across a Horizontal Vent due to Density and Pressure Differences," ASME Nat. Heat Transfer Conf., Aug. 1993.

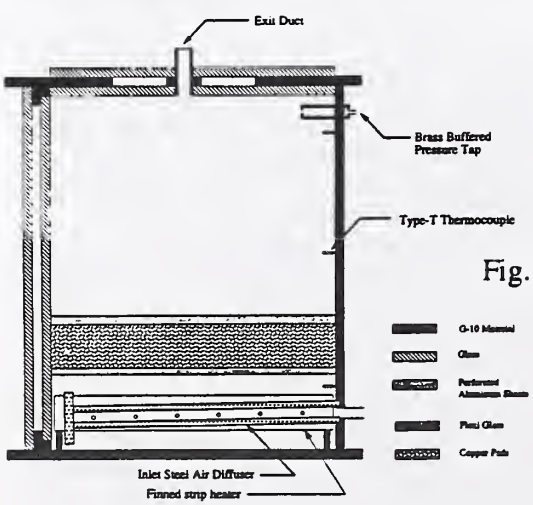

Fig. 1

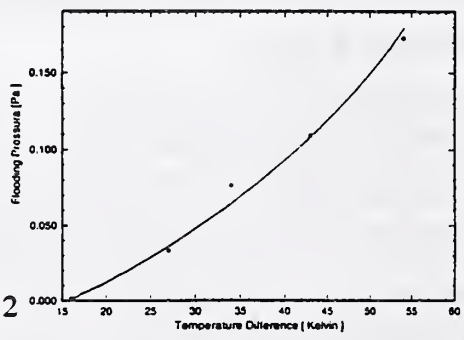

Fig. 2

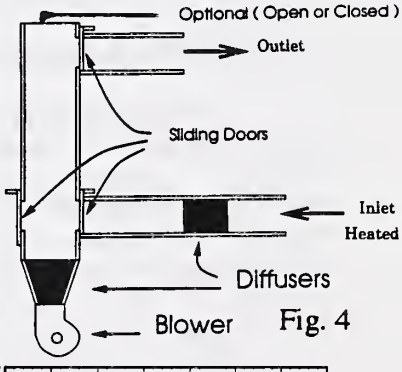

Fig. 4

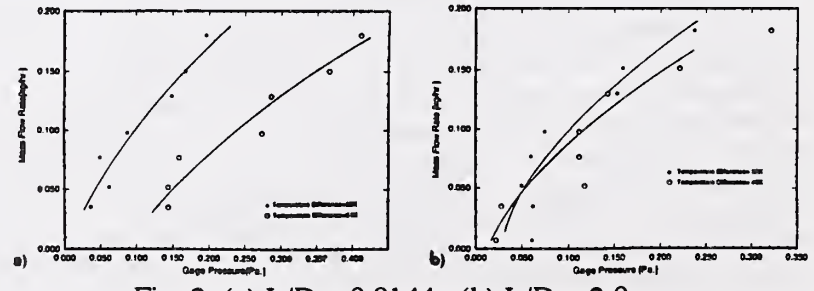

Fig. 3 (a) L/D = 0.0144; (b) L/D = 2.0

THE VORTICITY FIELD IN MEDIUM-SCALE POOL FIRES [1]

R. Kaazempur-Mofrad[2], E.J. Weckman and A.B Strong
Department of Mechanical Engineering
University of Waterloo, Waterloo, Ontario, Canada, N2L 3G1

Introduction

Mixing and entrainment phenomena in free burning fires are thought to be driven by the formation and shedding of large-scale structures from the continuous flaming region of the fire. These are postulated to be large ring shaped vortical structures which are formed and shed with a well-defined frequency dependent on the fire source diameter [1]. However, more detailed explanations of their behaviour which are critical to the incorporation of mixing and entrainment phenomena into mathematical models of fire behaviour are only in their formative stages. One of the reasons for this is that only a limited number of detailed measurements of local velocities, temperatures and species concentration have been reported due to difficulties in making measurements near the base of the fire. Determinations of local correlations between parameters, the key to understanding mixing and entrainment, have been limited to some autocorrelations [2] and only a few Reynolds stress and axial velocity and temperature correlations [1-4]. Most of the data has not been detailed enough to calculate any macroscopic properties, such as vorticity, which would directly relate to the formation and shedding of the large scale structures in the fire flow field.

In this study, a full set of velocity measurements were made in the continuous flaming region of a 0.31 m diameter methanol pool fire. Mean values of both axial and radial velocity were calculated at each measurement point and velocity profiles were constructed. Because of scatter in the velocity data, the measured velocity profiles were curve fit over sequential ranges using different low order polynomial line segments, so as to obtain a consistent determination of the appropriate derivatives for each velocity component. From these, the mean local azimuthal vorticity was determined. The resulting profiles of mean vorticity further describe the development of the large scale structures responsible for mixing and entrainment in the fire.

The Experiment

The fires were established in the existing University of Waterloo pool fire test facility [1]. Axial and radial components of velocity were measured using two component LDA operated in the forward scatter configuration. The data acquisition system allowed simultaneous sampling of the two channels of velocity data. Time series of data consisting of 40,000 measurements were analysed to provide mean and rms values of both radial and axial velocity [5]. Data was measured at 2 cm intervals from the centreline out to the edge of the fire and from the liquid fuel surface up to 30 cm (1 pool diameter) above the surface of the fuel. 150 measurement points were used to obtain the vorticity field in the continuous flame region of the fire.

Results and Conclusions

Distributions of mean azimuthal vorticity determined as described above are shown in Figure 1. In this figure, the radial position of 0 cm signifies the central axis of the fire, while 16 cm is the outer edge of the pool burner. The two curves shown are for heights $z = 12$ and $z = 24$ cm above the surface of the fuel. These results were obtained in the region well above the pool surface wherein the entrainment process is reasonably well established in the temporal sense. Results not shown here, obtained near the base of the fire, are quantitatively not as reliable due to scatter in the velocity data as well as to the very unsteady nature of the entrainment processes.

[1] Research supported through individual NSERC Operating Grants to E.J. Weckman and A.B. Strong
[2] Research Assistant

Nevertheless, overall, the results confirm the existence of a ring of strong localized vorticity near the bottom edge of the pool fire. This ring is observed to increase in strength as it moves up the fire axis, while the region of maximum intensity also moves towards the central axis of the fire. Finally, it is apparent that the overall width of the region of strong vorticity decreases with height above the surface of the fuel.

These qualitative results tend to confirm experimental observations of the development of large scale structures in pool fires [1, 6]. Strictly quantitative results, however, will require data which is processed with the time dependent large scale structures resolved in a temporal manner, presumably using conditional sampling (or other) techniques.

References

1. Weckman, E.J.: Ph.D. Thesis, University of Waterloo (1987).
2. Gengembre, E.: Ph.D. Thesis, E.N.S.M.A., University of Poitiers (1983).
3. Crauford, N.L.: Ph.D. Thesis, University of Southhampton (1984).
4. Annaruma, M., Most, J.M. and Joulain, P.: *12th ICDERS*, Michigan (1989).
5. Weckman, E.J., and Strong, A.B.: NIST Fire Research Conference, Maryland (1992).
6. Venkatesh, S., Ito, A. and Saito, K.: Nist Fire Research Conference, Maryland (1992)

Comparison of KAMELEON Fire Model to Experimental Data

V. F. Nicolette
Thermal & Fluid Engineering
Sandia National Laboratories
Albuquerque, NM 87185

J. H. Holen and B. F. Magnussen
Division Thermodynamics
SINTEF/Norwegian Technical Institute
Trondheim, Norway N-7034

Abstract

The KAMELEON Fire model is a state-of-the-art computer code for the modeling of fire and combustion problems. Recently, KAMELEON Fire has been applied to simulate jet fires and pool fires (with and without wind, and with and without objects). The results of the simulations show good agreement with experimental data for models of this type, and are very encouraging.

The KAMELEON Fire model [1] has been developed at the Norwegian Technical Institute and is based on a more general heat and mass transfer model known as KAMELEON. KAMELEON Fire solves the governing elliptic partial differential equations for heat, mass, and momentum transfer in three-dimensions using a finite difference technique. A standard κ-ε turbulence model is employed to solve the fluid flow. The KAMELEON Fire model has several unique features, including: 1) the Eddy Dissipation Concept combustion model, 2) the Magnussen soot model, and 3) a fast-running gas radiation model based on the Shah-Lockwood technique.

Jet Fire Calculations

Calculations were performed with KAMELEON Fire to simulate a jet of 80% ethylene/20% nitrogen that mixes with the ambient air and is ignited. For these calculations, the jet velocity was varied in order to determine if the model could calculate the flame lift-off height and the blow-out point. The experimental data used for comparison was generated at Sandia National Laboratories by D. Stamps and S. Tieszen [2]. A mass source in the vertical direction was used to introduce fuel into the computational domain at the nozzle exit. A non-uniform grid of 26 x 15 x 26 cells was used to model a 1.5 m x 0.75 m x 1.5 m volume. A symmetry plane was used through the center of the jet/nozzle, normal to the shortest (0.75 m) axis.

For low jet velocities (~60 m/s), the results were very good, indicating that the flame was attached to the nozzle (in agreement with the experimental data). A cross-sectional view of the calculated flame showed the hollow structure of the flame, also in good agreement with the experimental data. At intermediate velocities (~120 m/s), the calculations indicated that the visible portion of the flame would be lifted off of the nozzle by about 20-30 cm. This was determined by examining the calculated soot and temperature profiles, and is in excellent agreement with the experimental results. At high velocities (~150 m/s), the calculated flames became very cold (1200 K), whereas in the experiments the flame extinguished completely. This particular result can be directly attributed to the irreversible combustion model employed in KAMELEON Fire. In general, the results of the KAMELEON Fire model for jet flames were very good qualitatively and quantitatively when compared to data.

Pool Fire Calculations (No Objects, No Wind)

Calculations were performed with KAMELEON Fire for circular, open pool fires without any objects in them, and with no wind. A 15 m diameter pool of JP-4 jet fuel (aviation-grade kerosene), approximately

35 mm in depth, was used in the calculation. The data used for comparison for the circular pool fires was obtained from J. Mansfield [3]. For these tests, there was virtually zero wind. These tests were selected because of the size of the pool and the amount of instrumentation present within the flame volume. A 30 x 20 x 35 non-uniform grid was used to model a 50 m x 25 m x 70 m volume, with a symmetry plane through the center of the pool normal to the shortest (25 m) axis. The fuel evaporation rate from the pool was calculated by KAMELEON Fire for this simulation, and was not specified *a priori*.

The calculated flame height for this simulation was 57 m (arbitrarily taken to be the maximum height of the 1100 K isotherm). This is 27% higher than the visual estimate of a 45 m flame height for the test. The calculated results indicated good agreement with the experimental temperatures. The calculated results were about 200 C higher than the measured temperatures. Heat fluxes back to the pool surface were about a factor of 2 higher than measured. These higher heat fluxes are consistent with the higher temperatures calculated by the model, using a simple T^4 relationship, and are also consistent with the larger flame height calculated (due to more fuel evaporation). This agreement is quite reasonable considering the nature of the problem. Efforts are planned that are expected to improve this agreement.

Pool Fire Calculations (With Objects, With Wind)

Pool fire calculations including objects in the fire and wind were also performed. These calculations simulated a 9 m x 18 m pool of JP-4 fuel, and were compared to experimental data given in [4]. In these simulations, a large 10 tonne shipping cask was included in the fire. An average wind velocity and direction were input to the model to represent the tests, along with a specified fuel evaporation rate. Once again, the flame temperatures were approximately 200 C higher than measured experimentally. Calculated heat fluxes to the calorimeter were again higher by a factor of 2 compared to the experimental results, consistent with the higher calculated temperatures. The variation in heat flux around the circumference of the calorimeter predicted by the model was in reasonable agreement with the data.

Summary

KAMELEON Fire is a very powerful tool for calculating the heat fluxes and temperatures in a wide variety of very complex combustion environments. In general, the agreement with experimental data is very good for models of this type. Further development is expected to improve this agreement, and enhance its applicability to a wider range of problems.

References

1. J. Holen, M. Brostrom, and B. F. Magnussen, "Finite Difference Calculation of Pool Fires," Twenty-Third Symposium on Combustion, pp. 1677-1683, 1990.

2. D. Stamps and S. R. Tieszen, Sandia National Laboratories, Albuquerque, New Mexico, private communication, 1993.

3. J. Mansfield, China Lake NAWC, private communication, 1992.

4. J. J. Gregory, N. R. Keltner, R. Mata, "Thermal Measurements in a Series of Large Pool Fires," Journal of Heat Transfer, vol. 111, no. 2, pp. 446-454, May 1989.

Smoke Plume Trajectory Modeling

K.B. McGrattan and H.R. Baum
Building and Fire Research Laboratory
R.G. Rehm
Computing and Applied Mathematics Laboratory
National Institute of Standards and Technology

A principal concern in the decision to use *in situ* burning as an oil spill mitigation technique is the anticipated trajectory of the plume and the settling out of particulates. We have implemented a Large Eddy Simulation (LES) model of smoke transport which may be used to predict the concentration of combustion products downwind of the fire. We assume that the plume may be described in terms of steady-state convective transport by a uniform ambient wind of heated gases and particulate matter introduced into the atmosphere by a continuously burning fire. The plume trajectory may be broken down into three regions — the first lies in the immediate vicinity of the fire, the second extends several tens of kilometers downwind of the fire, and the third, which can be described as the far field, extends hundreds of kilometers further downwind. The first region is characterized by large temperature gradients, significant radiation effects, and a velocity field dominated by the rising of the combustion products. The second region is characterized by small temperature gradients, minimal radiation effects, and a velocity field dominated by the prevailing wind. In this region the plume gases ascend to a point in the atmosphere of neutral buoyancy, and then slowly descend as the heat from the fire dissipates. In the third region, or far field, the descent, dispersion, and deposition of the combustion products is governed by the regional meteorological conditions rather than the fire.

The Large Eddy Simulation of the smoke plume trajectory is appropriate for the second and third regions. For this reason it is not necessary to describe the fire in detail, provided that the overall rate of heat release and the fraction of the fuel converted to particulate matter are known. The subsequent location of the plume as it is carried downwind is determined by the ambient wind and the atmospheric stratification and turbulence along the plume trajectory. Since it is not our objective to calculate the local meteorology, it is assumed that this information is available. The wind is taken as uniform, but the temperature may vary with height according to a prescribed profile. The atmospheric turbulence effects mixing on a wide range of scales, extending to scales which are smaller than the resolution of the calculations performed here. There are two mechanisms by which we introduce turbulent atmospheric motions into the simulation. First, the small scale mixing is represented by a constant eddy viscosity, which is taken to be several orders of magnitude greater than the viscosity of air. For the resolution of the calculations reported here, this translates to Reynolds numbers on the order of 10^4. Larger scale atmospheric motion, which may be thought of as the variation of the prevailing wind, is a directly measurable quantity and can be introduced into the model through random perturbations to the velocity field.

Figure 1 compares the "centerline" plume trajectory with the observed centerline of the plume from mesoscale burn 5/30 of Reference [1]. Figure 2 shows the development of the plume in the first few thousand meters downwind of the source. Of particular interest in this figure are the two main vortices which entrain a large amount of the particulate and surrounding air. The ambient stratification introduces a natural frequency into the problem which results in a damped oscillation

of the plume about the level of neutral buoyancy as its contents mix and disperse. Of concern to emergency response professionals is the level of particulate concentration in the plume, especially those parts of the plume extending to the ground.

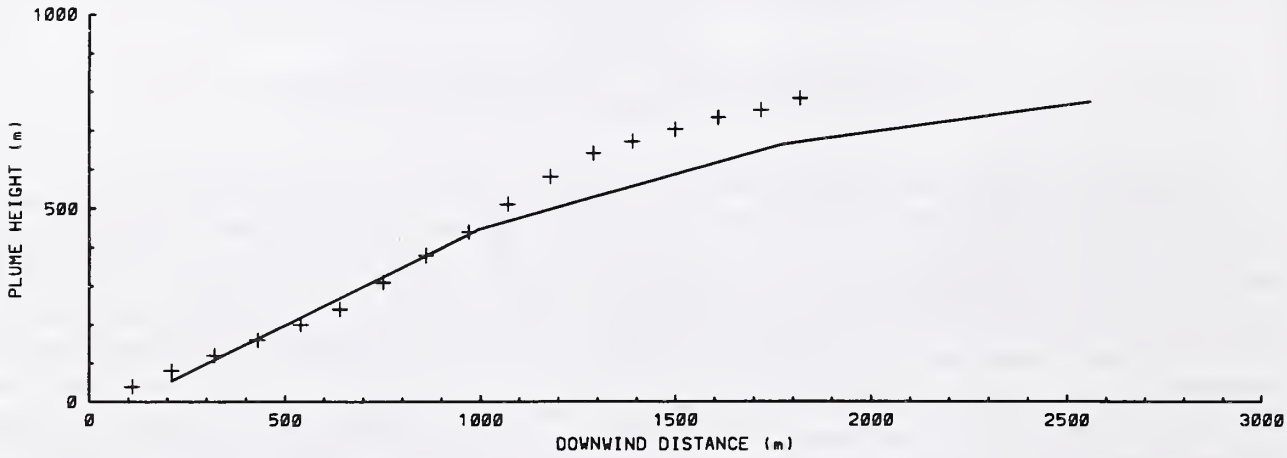

Figure 1: Centerline plume height for mesoscale burn 5/30. The computational trajectory is denoted by a solid line, the observed trajectory by stars.

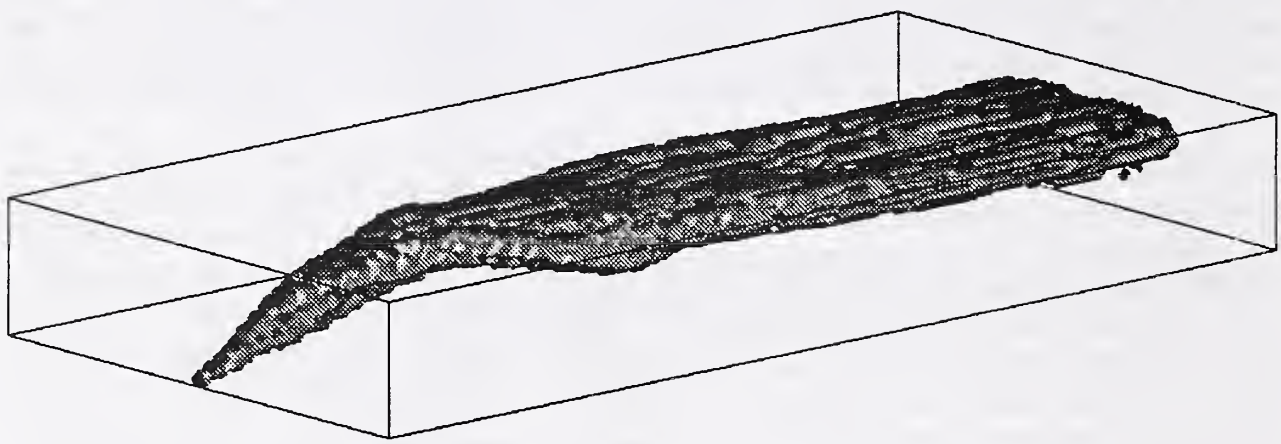

Figure 2: Three dimensional view of smoke plume from a 150 MW mesoscale burn. The height of the viewing area is approximately 1,100 meters, the length 8,800 m, and the width 4,400 m. The prevailing wind speed is 3 m/s.

References

[1] Evans, D.D. *et al.*, *In-Situ Burning of Oil Spills: Mesoscale Experiments,* in Proceedings of the Fifteenth Arctic and Marine Oil Spill Program, Technical Seminar, June 10–12, 1993, Edmonton, Alberta, pp. 593–657.

Computer Simulation of the Environmental Impact of Large Fires: Plume Rise and Dispersion

Ahmed F. Ghoniem and Xiaoming Zhang
Massachusetts Institute of Technology
Cambridge, MA 02139

ABSTRACT

The rise, dispersion, physical and chemical transformations, and deposition of plumes generated from large fires are responsible for distributing hazardous materials in the atmosphere and on the ground [1]. The objective of this work is to develop an efficient and accurate computational tool for predicting plume trajectory, dispersion pattern, and ground deposition as a function of fire parameters, wind, atmospheric conditions, and ground terrain. We have formulated a moving plane model to describe the plume cross sections in the wind direction. Numerical solutions are obtained using the Lagrangian transport element method and compared with experimental measurements. During the past year, we focused on: (1) validating the model, especially the dispersion pattern, against laboratory and field observations; (2) investigating plume rise and dispersion in a linearly stratified atmosphere; (3) performing parametric studies on plume penetration through low-level atmospheric inversion; (4) extending the computational capability to capture phenomena, such as soot formation and dispersion, radiative heat transfer, and combustion, which occur close to fire zone.

The evolution of the plume cross section, in terms of the density contours in the plume cross sections downwind the source, in a neutrally stratified atmosphere is compared with water plume experiments in Fig.1. . The numerical [2] and laboratory results [3], almost identical, exhibit the generation and evolution of a kidney-shaped pattern which, as shown by our investigations, is associated with two buoyancy-generated vortices that govern the dynamics and the entrainment process. In the case of a linearly stratified atmosphere, the predicted plume trajectories are shown in Fig.2 for different Richardson numbers, defined as the ratio between the plume buoyancy and the background stratification [4]. As expected, the stronger the stratification, the shorter of the vertical rise of the plume. We have extended the conventional two-thirds power law for the trajectory to describe this case, and found that the added mass coefficient and the entrainment rate are 0.7 and 0.49, respectively.

The trapping of buoyant plumes below low-level inversion is a strong function of plume buoyancy, the height, strength, and thickness of the inversion. The higher the inversion layer, the more difficult for the plume to penetrate through, thus, the larger the trapping fraction. The trapping fraction also increases as the inversion strength increases, or the inversion thickness decreases. The asymptotic trapping ratio as a function of the dimensionless buoyancy flux, which incorporates the effects of both initial inversion height and strength, is shown in Fig. 3, where the numerical results are shown to be indistinguishable from those obtained from laboratory experiments [5].

In the coming year, we plan to focus on the study of the burning fire zone, where fluid mechanics, radiative heat transfer, combustion physics and chemistry play important and interrelated roles. Results of this study should provide the initial conditions of the plume dispersion.

References:

1. Ghoniem, A.F., Zhang, X., Knio, O.M., Baum, H., and Rehm, R. *J. Haz. Mat.*, **33**, 275-293, 1993.
2. Zhang X. and Ghoniem A. F. A computational model for the rise and dispersion of wind-blown, buoyancy-driven plumes, Part 1, Neutrally stratified atmosphere. *Atmos. Environ.* (In press), 1993
3. Alton, B. W., Davidson, G. A. and Slawson, P. R. *Atmos. Environ.*, **27A**, 589-598, 1993.
4. Zhang X. and Ghoniem A. F. A computational model for the rise and dispersion of wind-blown, buoyancy driven plumes, Part 2, Linearly stratified atmosphere. *Atmos. Environ.* (To be submitted),1993.
5. Zhang X. and Ghoniem A. F. A computational model for the rise and dispersion of wind-blown, buoyancy driven plumes, Part 3, Atmosphere with inversion layer. *Atmos. Environ.* (In preparation), 1993.

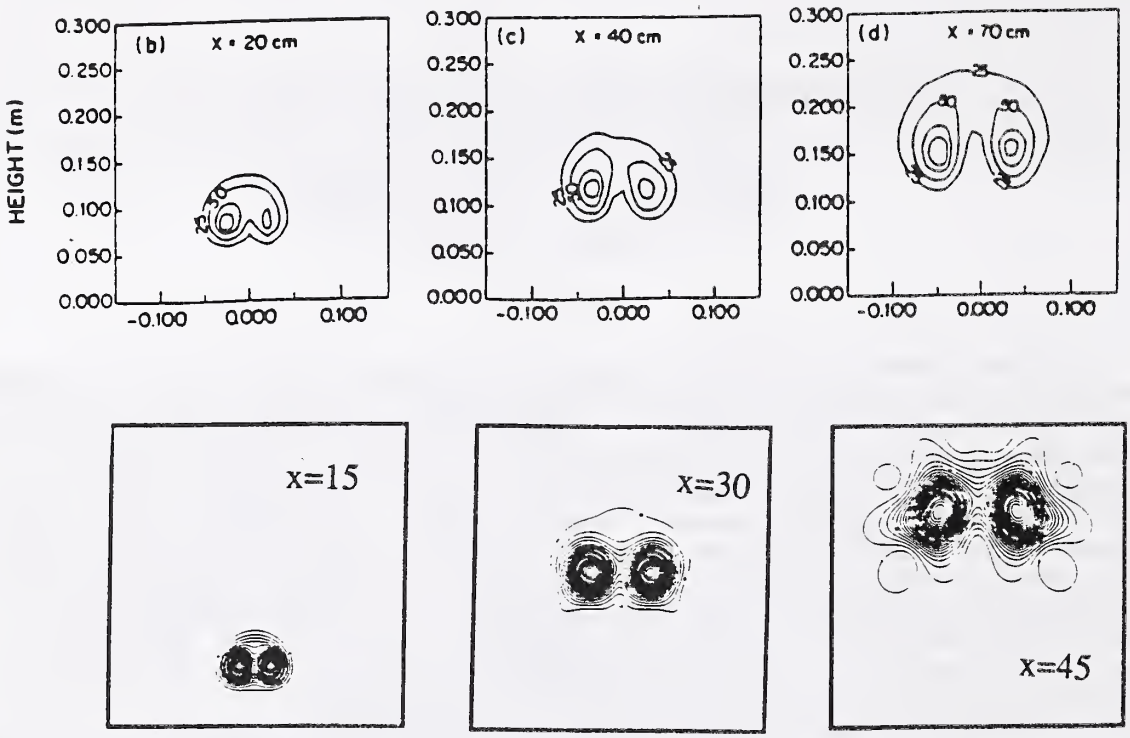

Figure 1. A comparison between laboratory measurements (top) of Alton et al., and our numerical simulation results (bottom) of the density contours in the plume cross sections.

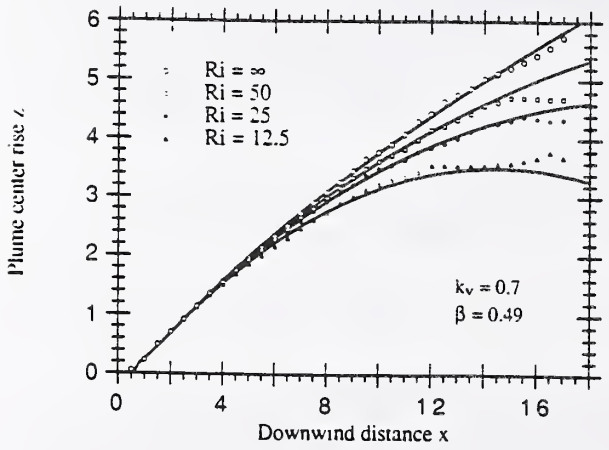

Figure 2. A comparison between the numerically predicted plume trajectory in a linearly stratified atmosphere, shown in open symbols, and the two-thids power law model. Note that the latter cannot capture the level-off part of the trajectory.

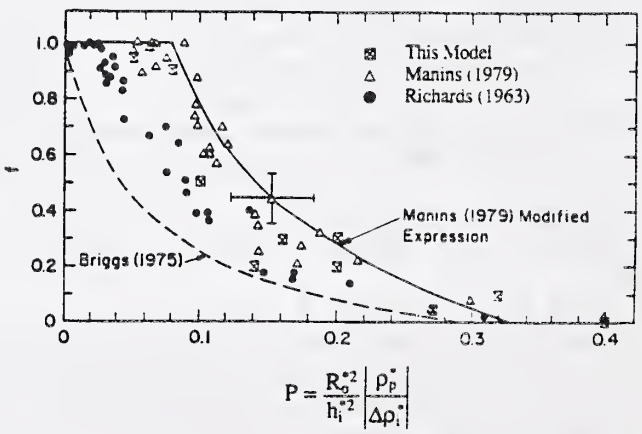

Figure 3. A comparison between the numerical predictions and the experimental measurements of the trapping fraction as a function of dimensionless buoyant flux.

AIR FLOW, VORTICITY AND CONVERGENCE IN STREETS IN A LARGE EXPERIMENTAL FIRE

Thomas Y. Palmer
(619) 728-4567
P.O. 278, Fallbrook, CA
92088

The Project Flambeau experimental fires were conducted between 20 to 25 years ago. The in-fire measurements still represent most of the large scale, free-burning outdoor experimental data. The experiments were particularly unique because of their size and the uniformity of the fuels. This paper presents the results of the continuing analysis of the data.

One of the experimental fires designed to study air flows, vorticity and convergence in the streets of the 4.8 hectare, simulated apartment complex as illustrated in Figure 1.

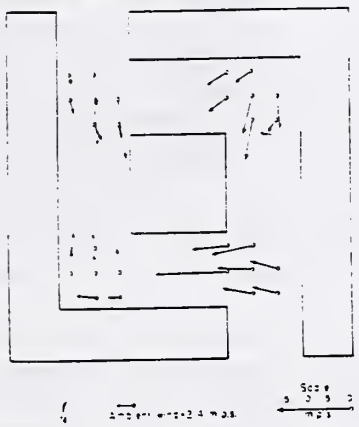

Fig. 1. The plan of Project Flambeau Fire 6. Twenty eight instrument sites were spaced as illustrated inside the burning area (enclosed boxes.) Wind vectors for five minutes after ignition are shown. Winds as great as 20 meters per second were observed. Total area was 4.8 hectare, total fuel was slightly over 6000 tonnes.

X-Y-Z wind components were measured at the 28 sites indicated in Fig. 1. Each instrument was individually wind tunnel calibrated. They were mounted at the two meter level on guyed steel towers, and were seperate by approximately fifteen meters (the distances were accurately surveyed. Output data was in the form of ten second summations of the number of rotations. The electic pulses was conveyed to an instrument trailer by buried wires. There it was recorded on punched paper tape (state-of-the-art at that time.) The temperature-resistant wind instruments and punched paper tape recoding system have been described elsewhere.

There was extensive camera coverage, both cine and 35mm still photos of the exterior of the fire. Unfortunately some of the most striking cine picture were lost in transit shortly after the experiment.

These instrument arrays were designed to measure partial derivatives as described in Abramowitz (Handbook of Mathematical Functions, p.883 et seq). From these values, local and total area vorticity and convergence have been calculated using the standard two dimensional form of the equations. No attempt was made to

measure temperature and other fire related variables because of the limited number of recorder channels.

A sample of the vorticity calculations for the south-east set of anemometers is shown in Figure 2. This region was near the "entrance" to the non-burning area. Cine photos designed to depict the flow of air about the periphery of the burning area at altitude showed the air flow was around the fire, then decending into the interior of the fire near this point. Attempts to launch radiosonde balloons in this area repeatedly failed because the balloons were forced to the ground by the descending air. Spectral analysis of the vorticity fluctuations in this data (and from other sets of observations in this experiment) have a peak at about 120 seconds. This is consistent with analysis of oscillations in exterior flow about other Project Flambeau fires (Palmer, et al., 1991.)

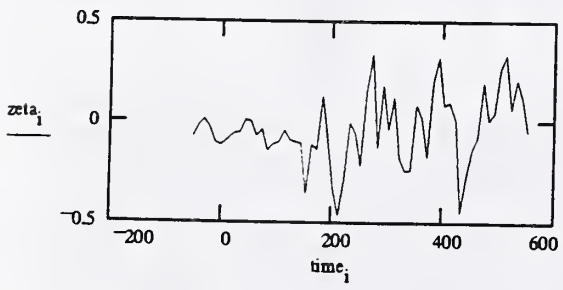

Figure 2. Measured vorticity zeta as a function of time at towers 22 to 28 in the southeast corner of experimental Fire 6. Data has not been smoothed. Ignition was at time zero.

Conclusions: These experimental results show that large fire models, based either on similarity of computer simulations must incorporate the effects of fire generated vortices which probably occur as vortex pairs. It is also apparent that the extreme winds that have been reported in and about large fires result from vortex flows generated by the fire. It is not necessary to have strong ambient vorticity to generate these winds, since the vortices are in a paired configuration. The integral of the vorticity taken in the horizontal about a large fire is thus near zero.

The observed rate of fire pulsation (at a rate of about one per 120 seconds) in this large fires depended upon the structure of the environmental boundary layer. This result is congruent with the results from similar fires in this series. It follows that the structure of the convection column is related to the boundary layer.

References: Abramowitz, M. and I.A. Stegun, Handbook of Mathematical Functions. Supt. Doc. Washington, D.C., 1964.

Palmer, T. Y., T. C. Goodale and S.B. Martin, Layer Replacement in Wildland Fire. In 11th Conf. Fire and Forest Meteorology, SAF, Bethesda, Md., 1991.

JET FIRE TESTING FOR OFFSHORE OIL PLATFORMS

Arthur J. Parker
James R. Griffith
Alex B. Wenzel
Department of Fire Technology
Southwest Research Institute
San Antonio, TX

ABSTRACT

Offshore oil platforms pose a potentially unique fire protection problem due to their remote locations and the type of flammable liquids and gases which are processed and stored. One of the most severe fires that an oil platform must be protected from is a jet fire. This type of fire occurs when high pressure a gas handling line breaks and the flammable liquid or gas is ignited forming a torch. The jet fire presents a much more severe fire than a hydrocarbon pool fire because in addition to high temperature and flux levels, a jet fire has direct flame impingement from gases stream exiting approaching sonic velocities. These speeds produce severe erosive effects on impinged steel members and combined with the high temperatures can erode a hole in a bare piece of steel in a matter of seconds. Passive fire protection systems such as spray-applied fire protective coatings must be capable of preventing the underlying structural steel, bulkheads or critical safety systems from failing. This paper describes the test facility and instrumentation to generate adequate thermal and radiative profiles as well as erosive effects to simulate large-scale fires.

COMPUTATIONAL FLUID DYNAMICS MODELING OF LARGE-SCALE HORIZONTALLY RELEASED NATURAL-GAS JET FIRES

by

A.D. Johnson and P. Peccard

Shell Research Limited, Thornton Research Centre, P.O. Box 1, Chester CH1 3SH

Large-scale accidental jet fires, involving flammable, pressurised hydrocarbons, pose a substantial hazard to personnel and property and can lead to escalation of an accident, particularly in congested areas. Quantification of the hazard is essential if process plants and storage areas are to be designed and operated safely.

One approach to obtaining tools for predicting the hazards is to derive scaling laws so that potential large-scale accidents can be modelled by small-scale experiments. Unfortunately, the complex interaction of the turbulent flowfield and thermo-chemical processes make such scaling extremely difficult and often unreliable.

The approach adopted at Shell Research has been to carry out experiments at a scale large enough to be representative of potential accidents. Examples of such experiments are listed in Table 1. These tests were carried out as part of a comprehensive set of horizontally released LPG and natural-gas jet fires, performed in collaboration with British Gas plc, and co-sponsored in part by the CEC (the STEP project) [1].

The predictive tools we have developed are created from physically based models and correlations fitted to the experimental measurements. Unfortunately, such models become unreliable for predicting the hazards from fires outside the range of the experiments from which they were derived. For example, a model for predicting thermal fluxes to objects outside free natural-gas jet fires cannot be used to give accurate predictions of thermal fluxes when the fire is confined and distorted within a compartment, or when fuelled, say by oil.

This presentation describes our first attempts at using a more fundamental, computational fluid dynamics (CFD) approach to modeling large-scale jet fires, in which the equations describing the basic physics and chemistry of a turbulent reacting flow are solved numerically in space and time. However, it is not our objective to develop a CFD computer program for safety engineers to use in designing process plant. Such models have very complex input and output and runtimes are still measured in hundreds of hours. We intend to use CFD models as an adjunct to experiments, to help us understand and interpret the small number of measurements that can be made at large-scale, and as an aid to developing new, simple safety design tools. CFD models also offer the opportunity to incorporate knowledge of combustion and heat transfer processes in turbulent diffusion flames obtained from detailed laboratory-scale measurements and complex chemical kinetics modeling.

We are using the commercially available CFD program HARWELL-FLOW3D as the basis for our model. In this presentation, we illustrate some of the capabilities and limitations of the current physical sub-models within this program, by comparison with measurements from some of the experiments listed in Table 1. The models for high-pressure gas source, the numerical grid and

boundary conditions and the combustion and radiative heat transfer models will be described. Comparison will be made between predictions and measurements of flame shape and trajectory (as shown for example in Figure 1), temperatures and velocities within the flame and radiation heat fluxes to external radiometers.

Table 1

Experimental conditions for horizontally released free natural gas jet fires

Orifice diameter, mm	Stagnation pressure, bar gauge	Mass flow, kg/s	Approximate flame length, m	Number of tests	Wind speed, m/s
152	0.02	2.7	20	2	3
152	2.1	8.5	31	2	0.3-4
75	11.5	8.5	32	2	4
20	64	3.6	20	2	3-9

REFERENCES

1. J.N. Davenport, J.F. Bennett, L.T. Cowley and J.J. Rowson, "Large-scale natural gas and LPG jet fires. Final report to the CEC", TNER.91.022, publ. Shell Research Ltd, 1991.

ACKNOWLEDGEMENTS

The large-scale experimental work described in this presentation required a great deal of effort. The authors wish to thank all those within Shell Research who gave practical help or guidance, those within Shell International and the CEC who sponsored the work, and the staff of British Gas plc who participated in the tests.

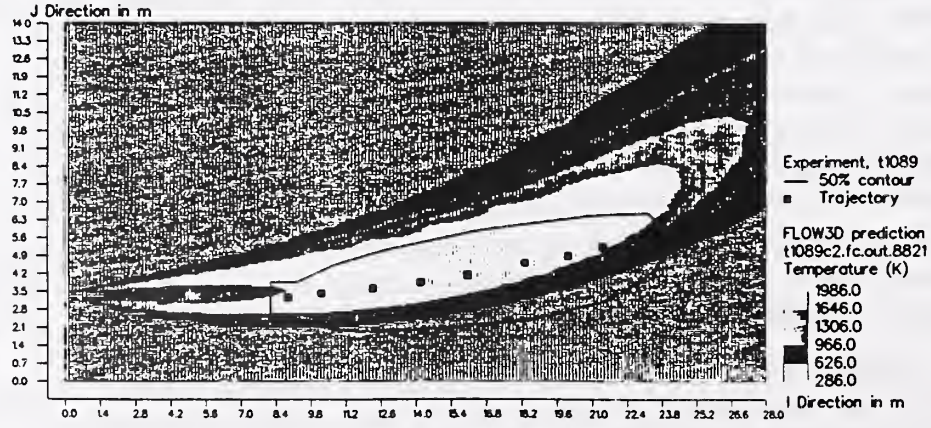

FIG. 1 - Natural-gas jet flame, 3.8 kg/s, released horizontally, 3 m above ground from a 20 mm diameter orifice under a stagnation pressure of 66 bar gauge and a co-flowing wind of 9 m/s. Comparison between predicted temperatures on a vertical plane containing the release axis and the measured visible flame shape and trajectory.

Large Scale Heat Release Tests With Electrical Cables

Marcelo M. Hirschler
Safety Engineering Laboratories
38 Oak Road
Rocky River, OH, 44116

The performance of electrical cables in fire tests depends upon both the materials and the constructions (type and designation) used to make the cables. The initial set of fire tests for electrical cables used were all small scale tests addressing individual types of materials. They were designed primarily to give a degree of quality assurance in terms of physical and electrical properties rather than to ensure fire safety. Subsequently, some tests were developed which used small flames (e.g. a Bunsen or a Tirrill burner) on single lengths of wires or cables. These tests have been severely criticized, correctly, for failing to address the issues of radiation and of bunching of cables. This led to the development of the most common type of fire tests for cables today: those that measure the fire propagation characteristics of bunched cables, either by determining the extent of travel of the luminous flame along the sample or by determining the extent of fire damage to the cable coating material, which is normally investigated after the test. These tests involve burning in vertical or horizontal cable trays: IEC 332 part 3 (internationally), UL 1581, IEEE 1202, UL 1666 or UL 910 (in the USA) and CSA FT-4 or CSA FT-6 (in Canada).

The study of fire hazard has led in recent times to the realization that heat release rate is the single most important measurement indicative of overall fire hazard. Standard measurements of this property are made in bench scale, with the cone calorimeter (ASTM E1354, ISO 5660) or the Ohio State University calorimeter (ASTM E906, FAR 25.853), and in large scale, with the room corner burn test (NFPA 265, ISO 9705, UBC 42-2) or the furniture fire test (ASTM E1537).

It is now possible, thus, to add heat release rate measurements to those cable tray tests mentioned. Moreover, the same cables can also be tested in the bench-scale tests, and correlations between both can be attempted, involving both heat release and flame spread.

In this study, a total of 21 electrical cables were made, all with identical construction, but differing in the chemical composition of the plastic components, both jacket and insulation. All the materials used were commercially available, and included a total of ten polymers: five halogenated and five non-halogenated ones. All cables were tested in three tests: (1) a large scale cable tray test, ASTM D5424, as based on IEEE 1202 or CSA FT-4, with measurements of heat and smoke release in the duct and a total length of 2.44 m, (2) the cone calorimeter and (3) the IEC 332-3 cable tray test (at a length of 3.5 m). Some major results are shown in Table 1.

Peak and average heat release rate values, measured either in the large scale or in the small scale test, were excellent criteria for distinguishing between cables passing or failing the traditional char length pass/fail criterion. Moreover cables passing the test tended to release less smoke than those failing the test. The IEC 332-3 test is much less severe than the North American one, which means that different heat release criteria are needed to make distinctions addressing "passes".

Table 1. Results of Full Scale and Cone Calorimeter (20 kW/m^2) Cable Tests

Cable Full	Pk RHR kW	Avg RHR kW	THR@20 MJ	Pk RSR m^2/s	TSR@20 m^2	Mass loss % combust	Ht Comb MJ/kg	Char m	Flam Ht m
9 H/NH	510	101	100	0.86	233	74.52	35.9	2.44	3.30
13 NH/H	368	117	115	0.22	87	67.12	45.4	2.44	3.30
10 H/NH	325	82	84	0.82	360	67.75	32.7	2.44	3.30
12 NH/NH	280	106	105	0.23	74	69.22	39.6	2.44	3.10
3 NH/H	232	72	64	0.40	166	56.16	26.5	2.44	3.10
16 NH/NH	206	31	105	0.13	77	48.69	42.4	2.44	3.00
11 H/NH	184	82	74	0.56	310	65.27	30.4	2.44	3.00
14 H/NH	67	30	33	0.37	184	19.37	34.8	1.43	1.19
15 H/NH	66	30	27	0.35	146	16.57	32.7	1.28	1.23
18 NH/H	66	34	13	0.14	36	15.80	22.6	1.14	1.28
1 H/H	59	33	10	0.74	187	16.54	13.6	1.11	1.25
4 H/H	55	32	13	0.70	185	16.58	15.7	1.06	1.25
20 NH/NH	54	33	15	0.06	27	10.25	42.6	1.02	1.13
2 H/H	52	27	8	0.64	168	14.45	12.5	1.12	1.30
7 NH/H	52	30	12	0.14	54	15.33	16.0	0.99	1.23
8 NH/H	46	30	12	0.20	61	13.37	16.6	0.97	1.10
5 H/H	38	25	5	0.67	179	12.49	8.3	0.91	1.00
6 H/H	33	25	6	0.38	115	13.36	8.4	1.00	0.98
19 H/NH	29	22	2	0.08	27	8.84	8.5	0.77	0.80
21 H/H	28	25	5	0.02	10	5.89	23.5	0.76	0.75
17 H/H	26	23	3	0.05	27	9.75	7.1	0.80	0.75

Cable Cone20	Pk RHR kW/m^2	TTI s	THR@20 MJ/m^2	Pk RSR 1/s	TSR@20 (-)	Mass loss % combust	Ht Comb MJ/kg	TTI/RHR s m^2/kW	SmkFct MW/m^2
9 H/NH	416	287	137	9.0	3128	74.86	27.83	0.688	95
13 NH/NH	296	606	162	3.6	1497	71.56	34.36	2.059	3
10 H/NH	406	338	131	8.4	3053	74.05	26.55	0.850	82
12 NH/NH	270	276	150	4.0	1648	68.74	32.57	1.022	18
3 NH/H	227	285	89	9.7	2394	59.02	19.85	1.263	16
16 NH/NH	391	1116	99	5.3	1722	52.14	22.51	2.853	26
11 H/NH	217	605	95	7.5	2563	68.58	21.52	2.833	17
14 H/NH	226	360	56	5.1	2634	53.36	12.58	1.595	88
15 H/NH	266	383	58	7.1	2819	53.52	12.82	1.439	95
18 NH/H	247	254	51	11.4	1442	66.22	10.61	1.031	15
1 H/H	174	275	60	12.0	2720	59.05	12.47	1.583	44
4 H/H	157	239	68	10.3	2856	58.33	13.93	1.519	78
20 NH/NH	112	297	60	1.2	604	43.65	20.88	2.666	12
2 H/H	177	265	60	12.9	2986	60.17	12.49	1.496	62
7 NH/H	99	267	59	2.5	1037	50.11	14.33	2.696	5
8 NH/H	132	444	24	4.0	906	27.83	9.13	3.392	2
5 H/H	156	272	56	10.0	2644	56.64	11.95	1.749	46
6 H/H	85	473	14	3.2	666	38.38	4.41	5.637	5
19 H/NH	1	10000	0.1	1.4	310	25.25	0.10	11379	0.1
21 H/H	1	10000	0.1	0.5	198	3.22	0.79	9165	0.05
17 H/H	3	10000	3	2.1	514	22.65	1.78	4038	0.3

Note: H and NH in the table refers to whether the jacket (first) or the insulation (second) are halogenated or non halogenated.

The results of these tests indicate two things: (1) heat release rate measurements are very adequate full scale and small scale cable test measurements for predicting fire hazard from cables, in terms of flame spread and (2) cables with excellent fire performance can be made by using a variety of materials, both halogenated and non-halogenated. Finally, if enough research can be done, heat release techniques and calculations may eventually lead directly to cable listing.

AIRPLANE CLASS B CARGO COMPARTMENT FIRE PROTECTION

DAVID BLAKE

FAA TECHNICAL CENTER
FIRE SAFETY BRANCH
ATLANTIC CITY, NJ 08405

The Fire Safety Branch of the FAA Technical Center conducted a fire test program to determine the hazards generated during a fire in a main deck cargo compartment and to determine the effectiveness of various detection and containment options. The FAA classifies a cargo compartment on the main deck of an airplane that also carries passengers on the main deck as a Class B cargo compartment. This type of compartment was required to have a smoke detection system to alert the flight crew of the presence of a fire and was required to have sufficient access to the cargo to enable a crew member to effectively reach any part of the compartment with the contents of a hand held fire extinguisher. In addition, no hazardous quantities of smoke, flames or extinguishing agent were permitted to enter any compartment occupied by the crew or passengers. Airplanes configured with Class B cargo compartments are generally referred to as "combis".

This fire test program was undertaken following the crash of a South African Airways 747-200 in the Indian Ocean. The flight was operating from Taipei to Mauritius with 159 people onboard. With less than one hour left in the over ten hour flight, the main deck smoke detector alarmed. The cockpit voice recorder , located in the cargo compartment, stopped recording approximately one minute 20 seconds after the smoke alarm when the fire damaged the wiring to the recorder. The airplane continued to fly for approximately 20 minutes after the smoke alarm before it crashed into the ocean killing all aboard. Most of the wreckage was photographed on the ocean floor at a depth of 14000 feet and some of it was retrieved. The fire was determined to have started in the forward right pallet just behind the partition separating the cargo compartment from the passenger section. No evidence of explosives, hazardous materials or sabotage was found and the ignition source was never determined. Combis have been operating throughout the world for approximately 25 years. This was the only incident of a fire in a Class B cargo compartment and the only crash of a combi in that time frame.

The test program consisted of sixteen fire tests conducted in a 707 test article, a DC-10 test article and on pallets in the Full Scale Fire Test Facility. The test articles were instrumented with thermocouples, heat flux transducers, smoke meters and oxygen, carbon monoxide, carbon dioxide and Halon 1301 gas analyzers. The fire load for most tests was cardboard boxes filled with shredded newspaper. For some tests, an accelerant (alcohol) was added to the fire load and in other tests, hazardous material (aerosol cans with hydrocarbon propellant) was added. The 707 tests and some of the pallet tests were used to determine the effectiveness of fire containment covers over pallets. These covers were constructed of fire resistant material and were meant to control a fire in a pallet through oxygen starvation. The build up of hazards in the cargo compartment and the adjacent passenger cabin were measured for unprotected pallet fires versus fires ignited in pallets covered with a fire containment cover. The DC-10 tests were conducted to determine the effectiveness of a total flood Halon 1301 suppression system in a large (9000 cubic foot) cargo compartment. The system was designed to give an initial discharge of Halon that provided a 5 percent concentration of agent in an empty compartment and a metered system that leaked a controlled amount of agent into the compartment to maintain a 3 percent concentration for an additional 30 minutes. The tests were conducted with different delay times

between smoke detector activation and Halon discharge. This was done to determine the consequences of using a crew member to verify the presence of a fire compared to discharging the Halon system immediately upon smoke detector alarm. Manual verification of a fire is desirable because there are approximately 10 times more instances of false alarms than actual fires in airplane cargo compartments. While verification would save the time and expense of diverting the airplane to the nearest airport and the unnecessary release of Halon into the atmosphere, the cargo compartment must be able to withstand the effects of the fire until the Halon system becomes effective. Some of the other factors that the testing examined were: the threat to the airplane in terms of ceiling temperatures and heat flux prior to and just after smoke detector alarm.; comparison of alarm times between smoke detectors and Infrared detectors for different ignition locations; the effectiveness of fire containment covers with simulated in service damage such as rips and tears; the ability of a trained firefighter to extinguish a pallet fire with hand held extinguishers; and the difference in fire intensity and flame spread rate for pallet fires using low density fire load versus higher density loads.

The main conclusions from this fire test program were that: the fire containment covers effectively contained but did not extinguish the pallet fires even with some simulated in service damage and with accelerants and hazardous materials added to the fire load; the Halon system suppressed but did not extinguish the pallet fires; a firefighter with hand held extinguishers would not be effective on these types of fires; the fire intensity and flame spread rate that resulted from a pallet fire using an 8 pound per cubic foot fire load appeared to be the same as that which resulted from a fire using a 2.5 pound per cubic foot fire load; in all but one case, the smoke detectors alarmed when the compartment ceiling temperatures were still at or near ambient; and that infrared detectors did not show a significant improvement in alarm times when compared to smoke detectors.

An FAA Airworthiness Directive dealing with Class B cargo compartments has been issued, based in part on the results of this program. The main requirement of the AD is that operators must either cover all pallets in Class B cargo compartments with fire containment covers or install a Halon suppression system that is effective for 90 minutes.

THE THERMAL SEVERITY OF FIRE RESISTANCE FURNACES : GETTING BETTER AGREEMENT USING PLATE THERMOMETER CONTROL?

Dr Gordon M E Cooke, Fire Safety Specialist, Fire Research Station (FRS), Building Research Establishment, United Kingdom

Background

When a fire resistance test is conducted according to ISO 834, the combustion gas temperatures are measured by conventional thermocouples at several positions in the furnace, and their average temperature is made to follow a standard temperature-time curve by adjusting the fuel supply. The primary modes of heat transfer are by radiation and convection, the former being affected inter alia by the emissivity of the furnace gases and the emissivity and temperature of the furnace linings. Unfortunately the heat transfer to a specimen, such as a floor or wall, may be different in different furnaces depending upon the design of the furnace (eg size and shape of furnace, number and location of burners, and the thermal insulation of the furnace linings) and the fuel used (eg oil or gas), and this can markedly affect the fire resistance attributed to the test specimen, which has commercial implications.

It has been argued by Babrauskas (USA) and, more recently, Wickström (Sweden) that an improved design of thermocouple for furnace control, which senses a higher ratio of radiative to convective heat transfer than is possible with the conventional thermocouple, should incorporate a thin inconel 'plate' roughly 100 mm square with a fast response conventional thermocouple attached to the centre of the unexposed face. Details of the Swedish plate thermometer are given elsewhere[1]. A number of fire test laboratories have gained experienced with the so-called plate thermometer, and its efficacy, when used in European (UK, German, French and Italian) wall furnaces, has been evaluated in BCR-funded research[2]. The author proposed that an evaluation of heat transfer rates in floor furnaces was needed and the Construction Directorate of the UK Department of the Environment agreed to sponsor tests in two gas-fired UK furnaces and one oil-fired German furnace.

The Experiments

A programme of eleven tests was undertaken - 4 in the Warrington Fire Research Centre (WFRC) furnace, 2 in the Loss Prevention Council (LPC) furnace, and 5 in the Institut für Baustoffe, Massivbau und Brandschutz (IBMB) furnace in Braunschweig, FRG - using a purpose made well insulated furnace roof rig which contained five 350 mm square calibration plate elements kindly loaned by the Swedish National Testing and Research Institute, Borås, Sweden and several other FRS-manufactured unprotected stainless steel elements of different size and shape located at different positions within the furnace. The purpose of the calibration elements was to measure their heating rates in at least two identical tests in each furnace - one using conventional thermocouple control, and the other using plate thermometer control. Seven tests were made using the ISO 834 'cellulosic' heating exposure and four (without the calibration plate elements) using the NPD 'hydrocarbon' heating exposure.

Although more than 40 calibration elements were used only some of the results for the exposed plate of the centrally placed calibration plate element in the ISO 834 exposures are presented here. The calibration plate element consists of a 5 mm thick exposed stainless steel plate, an unexposed steel plate, and a core of ceramic fibre insulation roughly 50 mm thick.

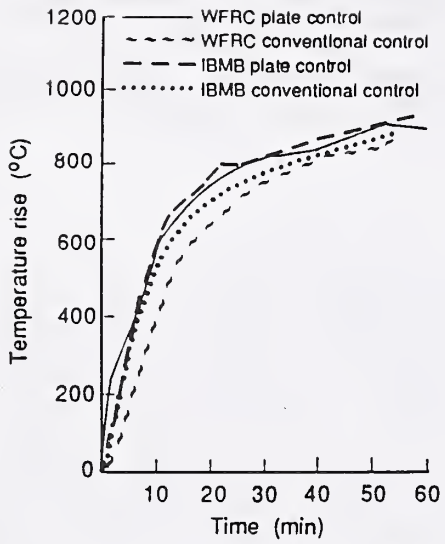

Figure 1 Heating rates of calibration element in WFRC and IBMB furnaces

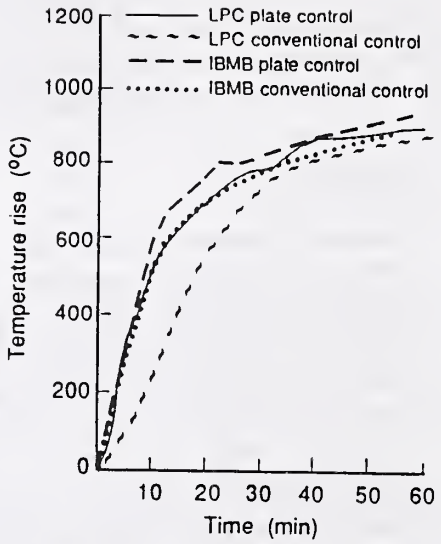

Figure 2 Heating rates of calibration element in LPC and IBMB furnaces

Conclusions

1. Figures 1 and 2 show the heating rates for the central 350 mm square calibration plate element achieved in the three furnaces when the furnace was controlled either with plate thermometers or conventional thermocouples. Both figures show that better agreement in heating rates is achieved with plate thermometer control, especially within the first 30 minutes.

2. Accuracy of manual furnace control was similar for all six tests illustrated in figures 1 and 2, although it was found to be more difficult to follow the standard curve using plate thermometers because of their slower thermal response.

3. Further testing of plate thermometers is needed. First to show that the improved agreement in heating rates witnessed in the present tests, which used a highly insulating roof construction, is also achieved with floor and roof specimens representative of building practice, including constructions of high heat transfer (eg an uninsulated roller steel shutter) and constructions which, because of their combustible nature, produce flames during a test (eg a timber floor). Secondly the durability and ease of use of plate thermometers needs to be evaluated - aspects which are being addressed by a number of laboratories on an ad hoc basis.

4. Further improvements might be achieved by insulating the refractory lining of a furnace using a low density highly insulating layer of ceramic fibre insulating blanket, as is the practice in some North American furnaces, but further test data are needed to quantify the improvements.

References

1. Wickström U. The Plate Thermometer - A simple instrumment for reaching harmonised fire resistance tests, SP-Report 1989:03, Swedish National Testing and Research Institute, Borås 1989.

2. Olsson S. Calibration of fire resistance furnaces with plate thermometers, Commission of the European Communities Report EUR 14555EN, 1993.

THE SEVERITY OF FIRES IN LARGE COMPARTMENTS : THEORY AND EXPERIMENT

Dr Gordon M E Cooke, Fire Safety Specialist, Fire Research Station (FRS),
Building Research Establishment, United Kingdom

Background

As part of the harmonised European package of Codes and Standards, the proposed Structural Eurocodes include an empirical equation which enables the amount of fire resistance required to resist a burn-out of the contents of a compartment to be calculated. The equation does not include any factor of safety which might be required under life safety regulations. The equation (usually termed the equation for equivalent time of exposure) is defined as $t_e = qc'W$ where t_e is the equivalent time of exposure (mins), q is the fire load density (MJ/m^2), c′ is a conversion factor to allow for the thermal properties of the enclosure, and W is a ventilation factor. More details are given elsewhere[1]. Following the author's observation that the equation had only been validated for 'small' compartments (ie $\geq$ 60 m^2 floor area), the Construction Directorate of the Government's Department of the Environment agreed to sponsor tests in a larger compartment. British Steel were also interested in the use of the equation for the fire engineering design of steel structures and became a co-sponsor.

A programme of 6 tests was originally envisaged in which the effect on fire severity of varying the fire load density and ventilation could be measured. The tests would also quantify the effect of fire which spreads naturally, as in a real fire, through the 23 m depth of compartment from rear to front (open end). Earlier tests had involved simultaneous ignition of all of the fire load.

A recognised way of determining t_e is to measure the maximum temperature, θ_m, reached by a steel member in the experimental fire and find, by reference to a standard fire resistance test report for an identical member, the time when the steel member reached θ_m in the furnace. This time is the equivalent time of exposure and was obtained in the present tests using temperature data for a number of 1 metre long unprotected and protected steel I-section beams and columns with thermocouples embedded in them which were suspended below the roof of the compartment at 3 positions.

The Experiments

A compartment was built in the unique FRS facility at Cardington - a laboratory 245 m long by 80 m wide by 55 m high - in which controlled environmental conditions could be provided.

The concrete compartment was 23 m deep x 6 m wide x 3 m high and was lined internally with a 50 mm layer of highly insulating ceramic fibre. The concrete floor was insulated with 100 mm thick layer of dry sand. The fire load was in the form of 33 cribs arranged in 11 rows of 3. Each crib was 1 m square, formed from kiln-dried 50 mm square sticks of Hemlock spaced 50 mm apart. For reasons of safety the cribs were ignited from outside the compartment using fuse cord and incendiary devices. Six of the cribs in the central row were supported on load cell platforms so that weight loss could be measured.

Conclusions

1. Measured and calculated values of t_e agreed well for all the tests (except Test 1 and Test 2 for which the measured value was greater than the predicted value by 20% and 40% respectively) when using $c' = 0.09$. However the Eurocode recommends $c' = 0.06$ where no detailed assessment of the thermal properties of the enclosure is possible and this would result in

PARAMETER	NOTE	TEST					
		1	2	3	4	5	6
Fire load density (MJ/m^2)	i	760	380	380	760	380	380
Ventilation (%)	ii	100	100	50	50	25	12.5
t_e measured (mins)	iii	119	71	80	143	99	111
t_e predicted (mins)	iv	101	50	79	158	100	112

Notes:

(i) All cribs uniformly spaced nominally 1 m apart
(ii) Eg 100% means all of the front wall (6m x 3 m high) open
(iii) Data are for members insulated with exfoliated vermiculite board (20mm on beams, 30 mm on columns)
(iv) Using a c′ value of 0.09

non-conservative values for t_e for all six tests. Referring to the CIB design guide[2], which is known to be the basis of this aspect of the Eurocode, three values of c′ (0.09 for well insulated enclosures, 0.07 and 0.05 for poorly insulated enclosures) are recommended for the majority of applications. Adopting a value of 0.09 as in the present analysis, does not, however, differentiate between a practical lining material such as plasterboard and the highly insulating ceramic fibre adopted in the present tests, so that use of c′ = 0.09 may be too conservative for plasterboard - a point that will be examined in a future test in the large compartment.

2. The Eurocode equation for t_e appears inappropriate for long duration, poorly ventilated fires, as in Test 6 which lasted more than 8 hours and which gave measured t_e values ranging from 30 minutes for unprotected steel to more than 3 hours for steel protected with 70 mm of exfoliated vermiculite board.

3. The mode of fire spread was similar in all tests. Following ignition of the 3 cribs at the rear of the compartment, fire spread to the front of the compartment via the tops of the cribs, assisted by radiation from the layer of hot gases under the ceiling. The front row of cribs then burnt downwards and then the next row similarly while burning in the rear of the compartment had stopped. Full depth burning of the cribs then proceeded towards the rear of the compartment. It is planned to conduct a further test which will involve simultaneous ignition of the 33 cribs to see if the fire severity is unaffected, as it is likely to be.

References

1. Eurocode on Actions on Structures, Part 10 - Actions on Structures Exposed to Fire, September 17, 1992.

2. Design Guide, Structural Fire Safety Workshop, CIB W14, Fire Safety J., 10(2) (1986).

THE FIREFIGHTING PERFORMANCE OF LOW EXPANSION FOAMS DURING LARGE SCALE FIRE TESTS AND ISO/CEN STANDARD FIRE TESTS

Bryan P. Johnson
Home Office Fire Experimental Unit
c/o Fire Service College, Moreton-in-Marsh
Gloucestershire, United Kingdom

For several years, members of the Fire Experimental Unit (FEU) have been involved in the formulation of European (CEN) and International (ISO) Standards for firefighting foam concentrates. Standards for low, medium and high expansion foams are due to be issued shortly. The Fire Experimental Units' main concern is that the quality of the foam concentrates currently being used by the UK fire service should not be adversely affected by the introduction of these standards.

FEU has concentrated on the 'low expansion foam for immiscible fuels' standards because this is the area of most concern for UK fire brigades. In particular we have tried out the standard pool fire tests which are intended as the main fire test methods for low expansion foam concentrates. These medium scale fire tests are essentially the same for both the International and European Standards.

The standard fire test consists of applying foam at 11.4 litres per minute through a standard branchpipe into a 4.5m^2 fire tray containing burning heptane. For each test, foam application commences one minute after ignition of the fuel. Two application methods are used, "forceful" which involves plunging the foam stream directly into the fuel, and "gentle" which involves applying the foam gently on to the fuel by the use of a backplate. Five minutes after the cessation of foam application, a burnback test is performed.

The foam concentrate types that are generally available to the UK fire service were used: in all 15 different foam concentrates were tested. All of these foam concentrates were used at the concentration recommended by the manufacturer for hydrocarbon liquid fires. In addition, the effects of using weak foam concentrates were investigated with the film forming foam concentrates being used at two-thirds and half strength.

The results of the standard fire tests showed some peculiar trends. In particular, FFFP foam concentrates which had performed well during previous FEU large scale fire tests, often failed to extinguish the gentle application test and consequently failed to meet the standard. In contrast, a good quality AFFF foam concentrate, whose performance had matched that of FFFP on large scale tests, passed the standard fire test very easily. This concentrate, when used during a large scale fire test at half the recommended concentration did not perform as well; in fact it took twice as long to extinguish the fire, but it still passed the standard test very easily.

These results were obviously of concern to the UK fire service and contradicted much of the advice given on foams in the past. It was therefore decided to carry out some large scale fire tests which simulated a situation in which the UK fire service are often involved

and where low expansion foam is used: a petrol (gasoline) spill fire. It was thought that the results of these large scale tests could be used to gauge how realistic the standard foam test results were.

The FEU large scale tests involved fires of petrol in a 56 square metre circular fire tray. To make these large scale fire tests as near to an operational incident as possible, the same foams as used during the standard tests were applied forcefully to the burning fuel surface by a fire service officer at the minimum recommended UK fire service application rates and using standard UK fire service low expansion foam equipment. For each test, the petrol was ignited and allowed to burn for 1 minute before the foam stream was applied. Five minutes after the fire had been extinguished, a burnback test was performed on the foam blanket to assess its resistance to flame.

The large scale tests showed that the doubts concerning the International and European foam standards were well founded. When used at their recommended concentrations, the FFFP foam concentrates that failed the standard fire test were performing as well as the AFFF foam concentrates. When used at below their recommended concentrations, the firefighting performances of the AFFF foam concentrates degraded significantly while those of FFFP were only slightly affected. The standards were favouring AFFF foam concentrates while heavily penalising FFFP.

In addition, some of the foam concentrates, when diluted to half of their normal usage concentration, passed the standard fire test even though their extinction performance significantly degraded with dilution during the large fire tests. These results indicate that safety factors can exist in the quality of foam concentrates. These safety factors ensure that, under severe firefighting conditions, the ability of foam concentrates to extinguish hydrocarbon fires is not seriously diminished. In general, the safety factor can be expected to be higher for better quality foam concentrates. It is these safety factors that are not explored in the International and European Standards. Consequently, foams that just pass these standards will be of a greatly inferior quality to those currently used by the UK fire service and are unlikely to allow for any margin of error when in use. Although they will be much cheaper to purchase, they would not be cheap to use. This is due to the increased resources, such as extra concentrate and equipment, needed to cope with their inferior firefighting performance.

As a consequence of these results, work is continuing at FEU to produce a new small scale fire tests to augment the existing standards. This new test will help to ensure that the high quality of foam concentrates used by the UK fire Service is maintained.

ADVANCES IN POSITIVE PRESSURE VENTILATION: LIVE FIRE TESTS AND LABORATORY SIMULATION

by
P. S. Ziesler and F. S. Gunnerson
University of Central Florida
College of Engineering
Orlando, FL 32816
and
S. K. Williams
Orange County Fire Rescue Division
4700 Lake Underhill Rd.
Orlando, FL 32807

Since Fall 1992, the University of Central Florida (UCF) and the Orange County Fire Rescue Division (OCFRD) have been conducting a joint research program to evaluate the effectiveness of Positive Pressure Ventilation (PPV) as a fire fighting technique. The objectives of the research program are to quantitatively measure temperatures, air quality and visibility during actual live fire exercises. Using the data from three (3) residential fires, a novel technique was developed to conduct underwater, scale model PPV simulation.

PPV is a technique where fans with high volumetric flow rates are used to create a slight positive gage pressure within a structure to force heat and combustion products from a structure through strategically selected exhaust openings. This rapidly reduces temperatures and retards the combustion process by hindering pyrolysis (conversion of solid fuel to gaseous, combustible fuel). Visibility is improved inside the structure by the removal of smoke and the survivability potential for victims is increased by removing toxic gases, lowering temperatures and introducing fresh air.

Results suggest PPV to be an effective technique that can be of significant value when properly applied. Results, specific to this program, which exemplify advantages of PPV include:

1. **Reduced temperatures for fire fighters and victims.**
   For example: At key fire fighting positions, PPV contributed to temperature reductions from 860°F to 140°F within one minute.
2. **Improved air quality for fire fighters.**
   PPV was shown to contribute to oxygen addition and carbon monoxide removal.
3. **Smoke was removed and visibility restored faster with PPV.**
   Six minutes after the start of a residential fire (with PPV), fire fighters had water on the fire and were walking upright within a cool, high-visibility environment. In contrast, eight minutes after the start of a second fire (without PPV) fire fighters were still crawling within a hot, smoke-filled environment.
4. **PPV reversed the direction of flames away from the fire fighting location.**
   For example, flashover flames that entered a hallway were pushed back into the burning bedroom soon after the start of PPV.
5. **PPV was shown not to spread heat damage.**
   Examination of lateral extent and depth of char on pine 2x4's placed in the path of the flames for PPV and Non-PPV fires showed no spreading of heat or flame damage caused by PPV.

Full scale PPV research and training can be expensive. During the course of this project, a technique was developed to conduct scale model PPV simulation. The simulations are conducted underwater with transparent scale models of the residences. The thermodynamics of the fire and the fluid mechanics of PPV are simulated by injecting colored water dyes at rates determined from actual fire measurements. Results from the residential fires colorfully illustrate that the spread of heat and the effects of PPV can be accurately and safely simulated within the laboratory.

Support for this continuing research is being provided by OCFRD and the UCF Institute for Simulation and Training.

USING SMOKE RELEASE RATE DATA FOR PREDICTING SMOKE OBSCURATION IN ROOMS

BY
DR. PRAVINRAY D. GANDHI
SENIOR STAFF ENGINEER
UNDERWRITERS LABORATORIES INC, NORTHBROOK, IL 60062

ABSTRACT

Fires in a room often start small with the ignition of a combustible item such as a waste paper basket. As the fire grows, a smoke layer develops at the ceiling. The smoke, as it descends, obscures signs and egress routes. This makes it difficult to escape from the fire affected room.

The smoke obscuration from a fire may be measured during a fire test using light source and detector system in the fire test room. However, in many instances, data are obtained using a smoke hood and a calorimeter as smokereiease rate. In these instances, it would be beneficial if the smoke release data may used in a fire model to estimate the obscuration of light in a room.

In this paper, a brief discussion is given on the measurement of smoke and the importance of various smoke measurement parameters. A model is then developed for predicting smoke obscuration in a fire-affected room using calorimeter data and concepts of zone modeling. The model shows that smoke release rate (measured in calorimeter tests) is an important driving function for determining smoke obscuration. The model also reveals that the ratio of smoke extinction cross-section area and heat of combustion (σ/h_c) is an important smoke parameter for flaming fires.

Three fire room corner tests were conducted using the proposed ASTM test procedure. The tests were conducted in a 2.44m x 3.66m x 2.44m high room with one 0.76m wide by 2.03m high doorway. In each of the fire tests, a wall lining material was installed on the three walls not including the doorway. The wall lining materials used were (i) polyurethane foam; (ii) polystyrene foam; and (iii) composite material. The floor and the ceiling of the room were lined with gypsum wall boards. The test room was instrumented to measure the obscuration of light in the hot gas layer, as well as temperature at various locations. A propane gas sand burner was used as an ignition source placed in a corner facing the doorway. A smoke hood was placed at the doorway to collect the combustion products. The combustion products were analyzed to calculate heat and smoke release rates in an instrumented duct attached to the smoke hood.

The temperature data were used to estimate the hot gas layer thickness and the average temperature. The temperature and the gas layer thickness obtained from the fire tests along with the smoke release rate data were used in the fire model to predict the smoke obscuration in the room.

The results were compared with the smoke obscuration measured in the test room during the fire tests. The predictions using the fire model were in reasonable agreement with the test data for the polyurethane foam, and the composite wall lining materials. The model however, under predicted the smoke obscuration for the polystyrene foam when compared with the test data. The lower estimates for the polystyrene foam is suspected to be due to deposition of the soot on duct surfaces during the transport of smoke from the fire-test room doorway to the measuring instruments.

Laser Doppler Velocimetry and Particle Imaging Velocimetry Based Measurements of Air Entrainment into Pool Fires

X. C. Zhou and J. P. Gore
School of Mechanical Engineering
Purdue University, West Lafayette, IN 47907

Entrainment rate of ambient air into a fire determines its height, shape and size. The rate of entrainment is defined as the rate of increase in the mass flow rate in the axial direction. Some of the past studies of average entrainment into pool fires have used a technique analogous to that of Ricou and Spalding in which the mass flow rate through a porous or imaginary enclosure is measured by establishing a balance between the inflow and the outflow under steady state conditions. Other studies have measured the rate of change in axial mass flux by measuring this quantity at two stations. The rate of change in axial flux can also be obtained from the measurement of inflow of ambient material at a boundary. This approach has been sparsely used in the past. For free flows such as fires, this is the only technique that results in a clear definition of the boundary and is therefore capable of resolving the conflicting measurements of the past.

In the present work, inflow velocity was measured at many points over the area of an imaginary enclosure shown schematically in Fig. 1. A 0.07 meter diameter pool fire was studied in a 1.2x1.2x2.5 meters enclosure seeded with smoke particles but not vitiated. The smoke particles served as scattering objects for a single component, dual beam, forward scattered, laser Doppler velocimeter (LDV). A frequency shifter was used to avoid directional ambiguity and measure relatively low velocities. The technique was examined by comparison with the Ricou and Spalding correlation of entrainment for a constant density jet as shown in Fig. 2. Since the jet exit is located above the floor the axial mass flux is greater than the jet mass flux at X/D=0. The correlation is applicable to locations far away from the jet. A secondary advantage of the present technique is that entrainment near the source can be measured as shown in Fig. 2.

The technique is applied to a 7.1 cm toluene pool flame next. The resulting data are compared with an existing correlation in Fig. 4. The correlation and measurements agree in the far field. At the fuel surface, the measurements show that the total axial mass flow rate at the fuel surface is greater than the burning rate since the floor is located below the liquid surface. The correlation assumes that the floor is located flush with fuel surface, hence the data and the correlation are expected to differ in the near field. Measurements with a floor flush with the fuel surface are in progress.

Since LDV provides transient measurements, the fluctuations in entrainment can also be studied from the resulting data. Particle imaging velocimetry (PIV), which is capable of revealing the physics of the entrainment process in much greater detail is currently being applied to pool fires. Figure 4 shows a sample PIV double image of particles with overlaid velocity vectors.

Acknowledgement: The work is supported by NIST Grant 60NANB2D1291 with Drs. Kashiwagi and Hamins serving as Scientific Officers.

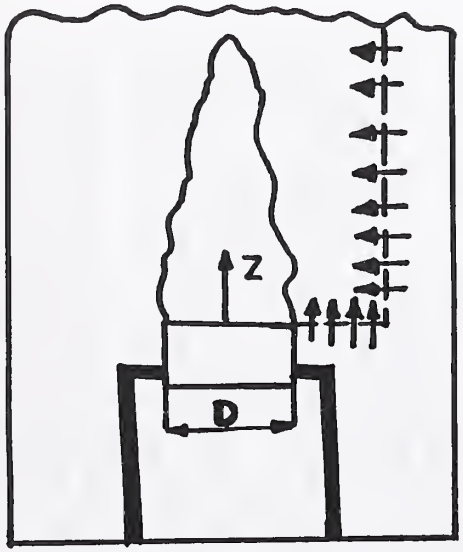

Figure 1 A schematic diagram of the entrainment measurement.

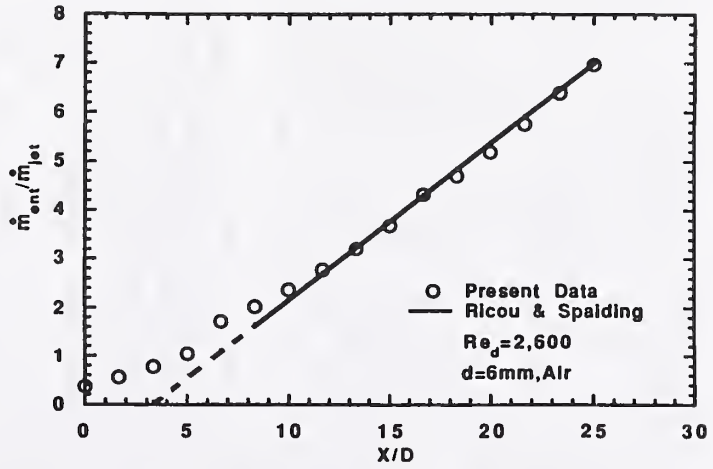

Figure 2 Comparison of the present entrainment mass flow for air jet measurements with the correlation of Ricou and Spalding.

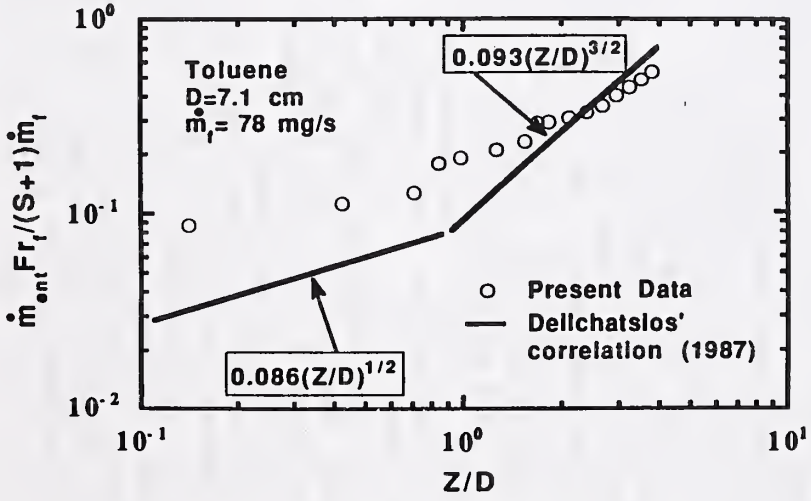

Figure 3 Entrainment mass flow into a toluene fire.

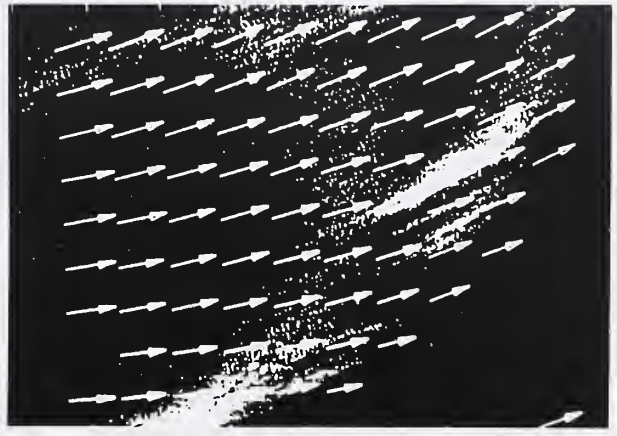

Figure 4 A sample double image of smoke seed flowing into a fire obtained with the Particle Imaging Velocimetry (PIV) instrument.

FTIR Remote Sensing Measurements of Benzene Released During the Evaporation and Burning of Oil

Marc R. Nyden, William Grosshandler, Darren Lowe, Richard Harris and Emil Braun
Building and Fire Research Laboratory
National Institute of Standards and Technology
Gaithersburg, MD 20899

Combustion is being explored as a method to remediate the environmental impact of oil spills on the open-seas. Upto now, researchers have relied on gas chromatography and other point sampling techniques to monitor atmospheric releases from burning oil. The capabilities of the present generation of FTIR remote sensing spectrometers, which include high resolution and fast scanning over extended optical paths, have the potential to make continuous measurements of atmospheric pollutants along a line-of-sight. This possibility could open a new dimension to research directed at assessing the environmental impact of oil and other large-scale fires.

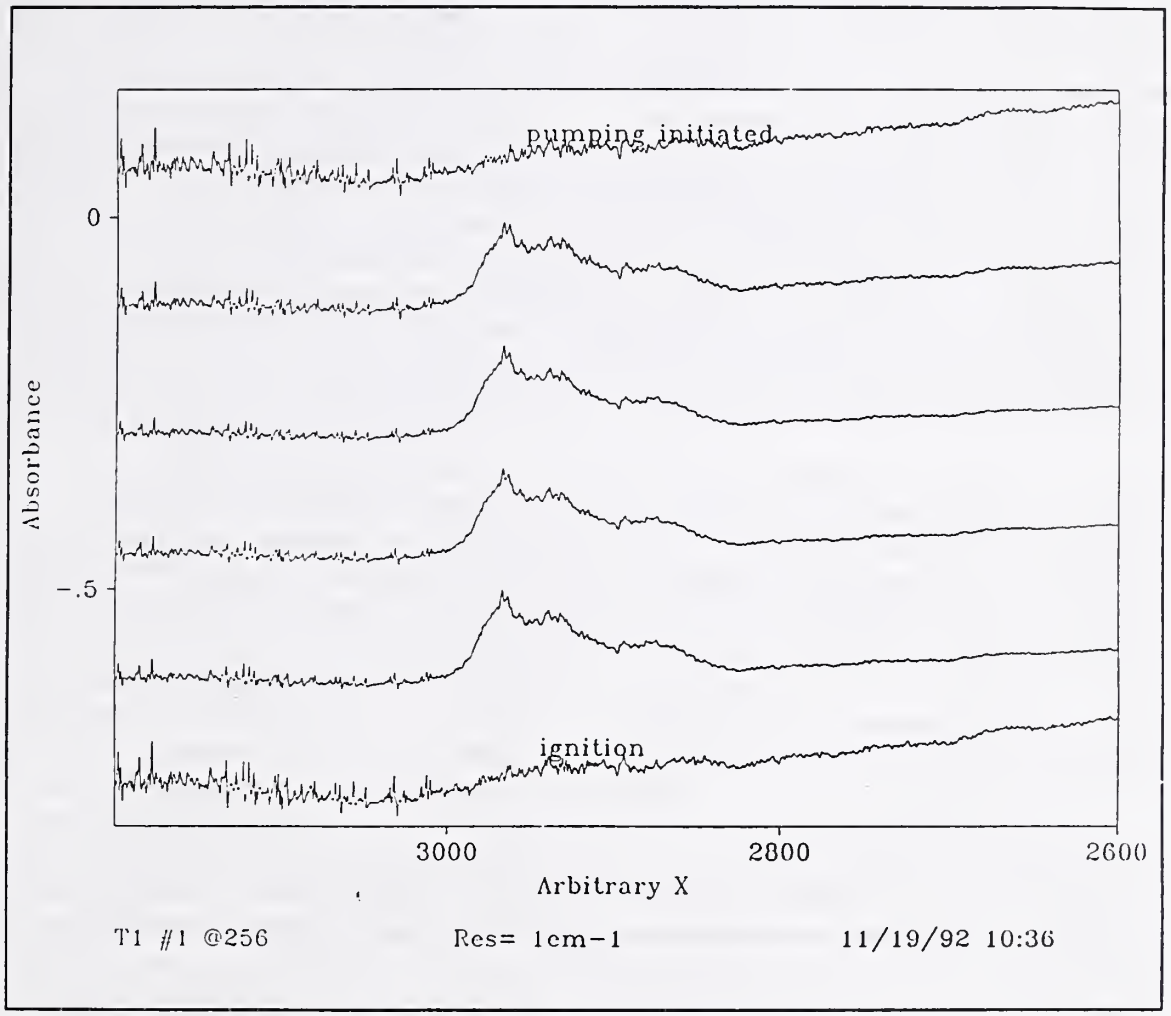

Figure 1. Time series showing the absorbance due to the presence of hydrocarbons from the onset of pumping (top) to ignition (bottom) of the oil.

The spectra displayed in Figures 1 and 2 were collected during a series of oil evaporation and burn experiments conducted in a 230 m^2 square pan located on Little Sand Island in Mobile, Alabama. The time sequence displayed in Figure 1 indicates that the absorbance in the C-H stretching region disappears as soon

as the oil is ignited. This suggests that the non-aromatic hydrocarbons present in the original crude oil are effectively destroyed by the fire. The objective of this study is to determine if the more stable aromatics, which would otherwise be released into the atmosphere during evaporation on the open-seas, are also destroyed.

A series of bench-scale experiments were conducted onsite. Spectra were collected during both evaporation and burning at various heights above a circular pan ($1.13m^2$) containing a layer of Louisiana Sweet crude oil floating on water. Benzene is difficult to measure over an open path through the atmosphere. This is particularly true in the vicinity of a fire. The most intense feature in the spectrum of benzene (674 cm^{-1}) is obscurred by the absorbance of the CO_2 bending mode at 667 cm^{-1}. The benzene concentrations reported in this study were determined by integration of a much weaker band centered at 1037 cm^{-1} (Figure 2).

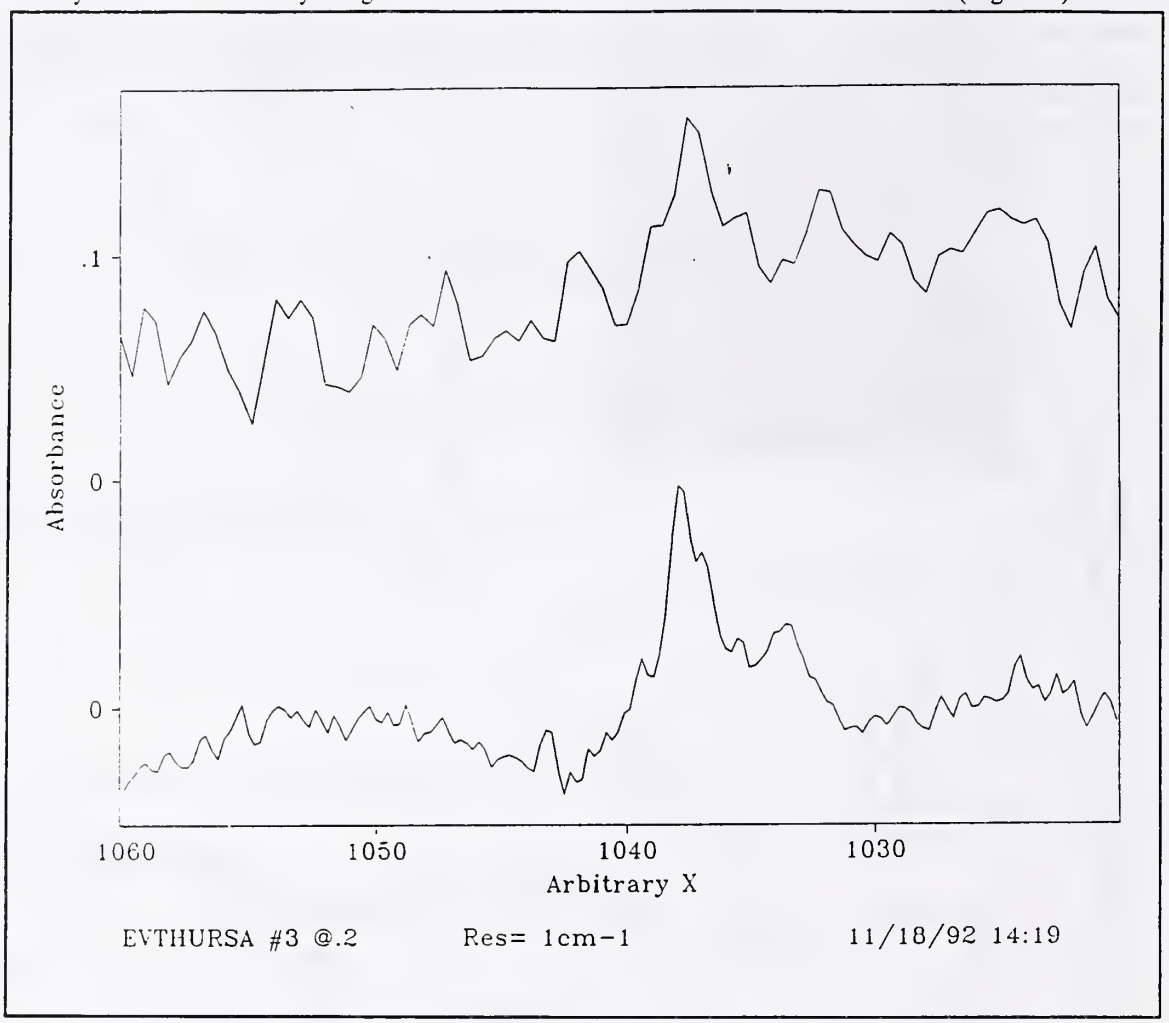

Figure 2. A spectrum measured during evaporation (top) is compared to a library spectrum of benzene(bottom). The presence of benzene is indicated by the peak centered at 1037 cm^{-1}.

The destruction efficiency of benzene by the fire was estimated using this data in conjunction with the results of chromatographic analyses of the liquid oil taken before ignition and after the fire was extinguished by covering the pan with a marinite slab.

SIMULTANEOUS OPTICAL MEASUREMENT OF SOOT VOLUME FRACTION AND TEMPERATURE

M.Y. Choi, A. Hamins, G.W. Mulholland and T. Kashiwagi
Building And Fire Research Laboratory
National Institute Of Standards And Technology
Gaithersburg, MD 20899

In large pool fires radiative heat transfer governs the burning and flame spread rates and therefore is a key factor in assessing potential fire hazards. The radiative heat feedback from the flame to the fuel surface is controlled by the temperature and soot distribution inside the fire. Early attempts at modeling this process involved several limiting assumptions including the use of average flame emissivity and constant flame temperatures or mean temperatures and absorption/emission coefficients as a function of height and effective flame shapes. Due to the turbulent nature of these fires, the use of mean radiative properties can lead to significant differences between the predicted and measured fuel burning rates **[1]**. **Markstein [2]** investigated spatial and temporal variations of the emission intensity for pool fires and suggested the importance of turbulent fluctuations of temperatures and soot volume fractions on the heat transfer mechanism. In an attempt to characterize turbulence-radiation interactions, **Gore et al [3,4]** estimated the heat feedback by consolidating the radiation (calculated with uncorrelated local temperature and soot volume fraction measurements) from discrete locations **[3]** for toluene.

In this study, the performance of a three-line optical probe technique for measuring soot volume fraction and temperature (similar to the system used by **Gore et al**) was assessed by conducting experiments in the path-invariant region of a premixed flame. Thus, a rigorous test of the measurement technique can be accomplished prior to its eventual use in large pool fires burning heptane. Using a premixed ethylene/air flame, the temperature and soot volume fractions (f_{va}, based on absorption measurements at 632.8 nm and f_{ve}, based on emission measurements at 900 nm and 1000 nm) were compared to previously reported results. Although, the temperatures and mean soot volume fractions compared favorably, the discrepancy between f_{va} and f_{ve} prompted new measurements to evaluate the importance of source wavelength on the f_{va} measurements, scattering by soot particles, light absorption by 'large' molecules and the use of different indices of refraction reported in the literature.

Soot scattering experiments and the experiments assessing the degree of absorption by 'large' molecules confirmed that the common practice of using the absorption coefficients (instead of the extinction coefficient) of soot for optical measurements is valid for the conditions of the present study. However, the agreement between f_{va} and f_{ve} is dependent on the choice of refractive indices used to calculate the absorption coefficients. For all sets of absorption coefficients used in this study, the agreement in the soot volume fractions improved as the extinction source wavelength increased from 488 nm to 1550 nm. This is due to the reduced uncertainties in the measurement of the refractive indices and the validity of the use of Rayleigh-limit formulation to calculate the absorption coefficients. Thus, future

soot extinction measurements in the authors' laboratory will be performed using a 1523 nm He-Ne laser.

Iso-kinetic soot sampling experiments were also performed to compare with the optically-measured soot volume fractions. This technique advantageous because it does not rely on the refractive indices of soot and therefore provides an independent measure of the soot volume fraction. The soot volume fractions measured using this method and optical techniques were of comparable magnitude.

In previous studies, it was believed that the reduced degree of sooting in the heptane fire (relative to toluene) would produce insufficient emission signals. However, preliminary experiments indicate that the higher flame temperatures for heptane produce emission signals that are of comparable magnitude to the toluene fires. In this study, the radiative heat feedback in heptane pool fires will be analyzed for different pool diameters. The temperature and soot volume fraction measurements will be incorporated in multi-ray radiation models for comparisons with the experimentally measured burning rates. Multiple ionization detectors will also be used to determine the motion of the flame as it traverses the optical probe volume. This information is necessary for determining the correlation for the temperature and soot volume fraction measurements at different locations in the fire. For measurements made near the top of the flame, the degree of agglomeration of the soot particles can be substantial due to the long residence times in the fuel-rich region. Under these conditions, scattering (relative to absorption) cannot be neglected. In order to account for the degree of scattering, soot will be sampled at various heights above the burner surface using thermophoretic probes and the structure will be analyzed from the TEM images. Using the primary size and radius of gyration information, the ratio of scattering to absorption cross-section will be estimated [5].

ACKNOWLEDGEMENTS

The authors would like to acknowledge the helpful discussions provided by Drs. K.C. Smyth, C. Shaddix, J. Harrington and W. Grosshandler of NIST, Dr. G.H. Markstein of FMC, Professor J. Gore and Dr. M. Klassen of Purdue University and Professor I.K. Puri of the University of Illinois at Chicago.

REFERENCES

1. Fischer, S.J., Hardouin-Duparc, B. and Grosshandler, W.L., Comb. Flame, 70:291 (1987).
2. Markstein, G.H., Eleventh Symposium (Int'l) On Combustion, The Combustion Institute, Pittsburgh, 1981, p. 1055.
3. Klassen, M., Gore, J.P., Hamins, A. and Kashiwagi, T., Twenty-Fourth (International) Symposium on Combustion, The Combustion Institute, Pittsburgh, 1992.
4. Klassen, M., Sivathanu, Y.R. and Gore, J.P., Comb. Flame, 90:34 (1992).
5. Dobbins, R.A., Mulholland, G.W. and Bryner, N.P., "Comparison of a Fractal Smoke Optics Model With Light Extinction Measurements". Atmospheric Environment, in press, 1993.

Measurements of Spray Characteristics of Selected ESFR Sprinklers

Tak-Sang Chan

Factory Mutual Research Corporation

Norwood, Massachusetts 02062, USA

Characteristics of single sprinkler sprays for two Early Suppression Fast Response (ESFR) sprinklers, designated as models CPK and ESFR-1, were investigated. The water density, drop size and velocity distributions were measured at an elevation 2.84 m below the sprinkler deflectors, 1.37 m above the floor. Two water discharge pressures, 1.72 and 3.45 bars, were used for the CPK sprinkler model. For the ESFR-1 model, measurements were conducted at 3.45 bar. Measurements began at 0.61 m from the sprinkler axis and extended to near spray boundary. The farthest radial locations were 3.66 m from sprinklers when discharging at 1.72 bar and 3.05 m at 3.45 bar, respectively. For every 0.61 m increment, the measurements were performed for 10 azimuthal angles with 45 degree intervals, except near the sprinkler pipe, where the interval was 25 degree.

The drop size and velocity distributions were measured with the FRMC PMS (Particle Measuring Systems Inc.) Drop Size Measuring System[1], which is composed of an optical imaging probe and a high speed data processor. The system can measure drop size ranging from 0.1 to 6.2 mm with a resolution of 0.1 mm.

Figure 1 shows typical results of water density distribution measurements. The corresponding drop size distributions are shown in Figure 2. While the sprinklers tend to project larger drops to outer area than near the sprinkler axis, the water densities are diminishing with increasing radial distance. Figure 3 shows the comparison between the measured droplet velocities, averaged over the entire sprinkler sprays, and the experimental terminal velocities[2] for a single water drop traveling through air.

Based on the local water density and drop size measurements, the gross drop size distributions for the entire sprinkler sprays can be derived[3]. Figure 4 presents the derived gross drop size distributions for all the measurement conditions. The gross drop size distribution curves for the two sprinkler models discharging at 3.45 bar were found similar, with one model being uniformly smaller than the other one. Each gross drop size distribution can be expressed as a combination of the log-normal equation and the Rosin-Rammler equation.

References

1) You, H-Z. and Symonds, A. P., "Sprinkler Drop-Size Measurements, Part I: An

Investigation of the FMRC PMS Drop-Size Measuring System," FMRC Technical Report, J. I. 0G1E7.RA, 1982.

2) Blanchard, D. C., "From Raindrops to Volcanoes," Doubleday, Garden City, N.Y., 1967.

3) Chan, T-S., "Water Density and Drop Size Distribution Measurements For Selected ESFR Sprinklers," FMRC Technical Report, J. I. 0Q3E9.RA, 1992.

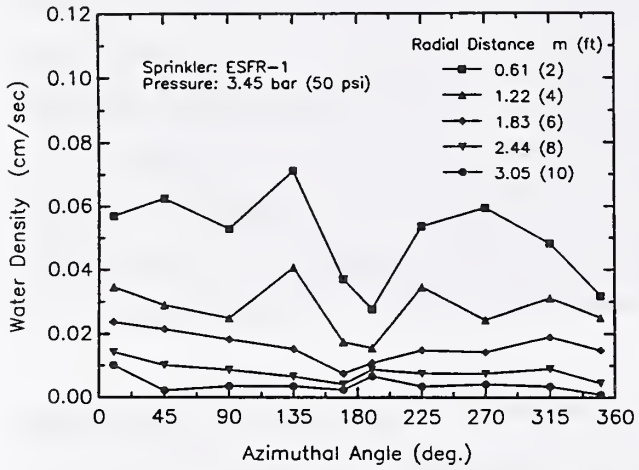

Figure 1. Azimuthal water density variation as a function of radial distance from the sprinkler centerline.

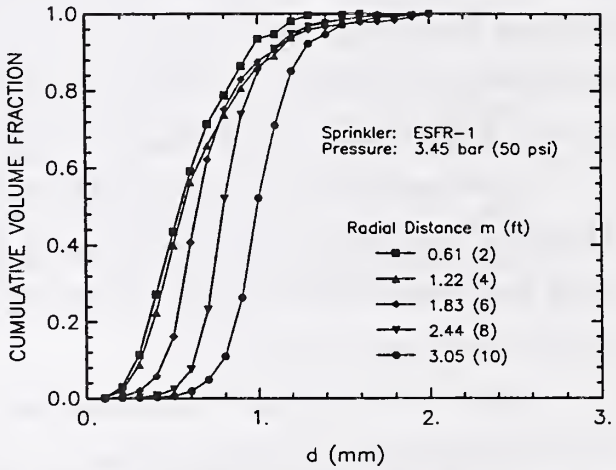

Figure 2. Drop size distribution as a function of radial distance from the sprinkler centerline.

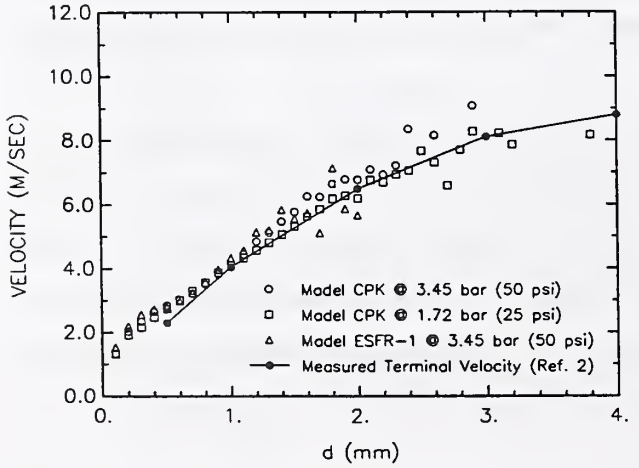

Figure 3. Water droplet velocities in comparison with experimental terminal velocities.

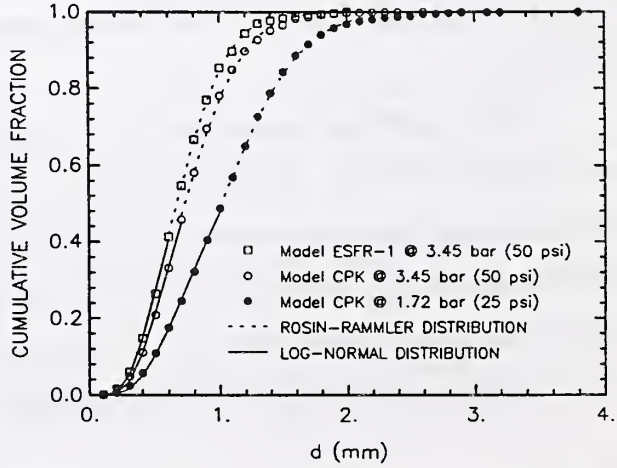

Figure 4. Gross Drop Size Distribution Fitted with Rosin-Rommler and Log-Normal Distributions.

MEASUREMENT OF SPECTRAL HEMISPHERICAL REFLECTANCE OF MATERIALS

by R. B. Nair, A. K. Kulkarni and S . T. Thynell
Department of Mechanical Engineering
The Pennsylvania State University
University Park, PA 16802

The overall objective of this project is to determine the spectral variation of the radiation properties of nonburning as well as burning materials. A practical problem where these properties are required is in analysis of flame spread over semi-transparent or opaque solid fuels, such as a burning wall or floor in presence of a surrounding fire. In case of large fires, the emitted radiation from the surroundings to burning objects is significant, so it is necessary to know how much of the incident radiation is absorbed by the material and how much is reflected.

The spectral reflectance properties are measured using a Fourier Transform Infrared spectrometer (FTIR) and a modified version of heated cavity reflectometer previously employed by Dunkle et. al. [1]. A schematic of the apparatus is shown in Figure 1. The reflectometer consists of a cavity formed by twelve flat plate heating elements that are heated to approximately 650 deg. C. Power supplied to each heating element is individually regulated by a variac to ensure uniform heating of the cavity. The material sample is mounted on a water-cooled sample holder. The sample holder is rotated to provide a variation in the polar angle. Provision is made for igniting the sample and purging the cavity of exhaust gases. The FTIR acquires and processes the thermal radiation energy reflected by the sample. Relative directional spectral reflectance is obtained by subtracting the background emission from the reflected signal and the blackbody emission signal, and then taking the ratios of the two.

Results of measurements for various materials are shown in Figure 2. Measurements for commercial finish aluminum were made to check validity of experimental data. The results for black PMMA reveal an increase in reflectance with increase in the polar angle while that for clear PMMA does not. Commercial cotton paper exhibits diffuse behavior. The principal source of error in the measurement of properties by this method is the difficulty in making the entire cavity reasonably isothermal, so that the reference signal can be made proportional to that from a blackbody at the cavity-wall temperature. Also, if the sample heats up during the period of measurement, then emission from the sample is no longer negligible and contributes to the error in measurement. Properties of samples *while they are burning* will be measured in the next phase of this project.

The reflectance property data can be useful, for example, in the analysis of a combustible wall or floor subjected to strong radiation. For certain materials, a significant fraction of the radiation may be simply reflected off the surface, not contributing to the ignition, combustion or flame spread process. Also, the properties may change significantly once the wall or floor starts burning. Analytical models may yield misleading results unless these properties are adequately taken into account.

This work was partially supported by the National Institute of Standards and Technology under grant no. 60NANB8D0849.

REFERENCES

1. Dunkle, R. V., Edwards, D. K., Gier, J. T., Nelson, K. E., and Roddick, R. D., "Heated Cavity Reflectometer for Angular Reflectance Measurements", *Progress in International Research on Thermodynamic and Transport Properties*, Am. Soc. of Mech. Engrs., New York, 1962, pp. 541-562.

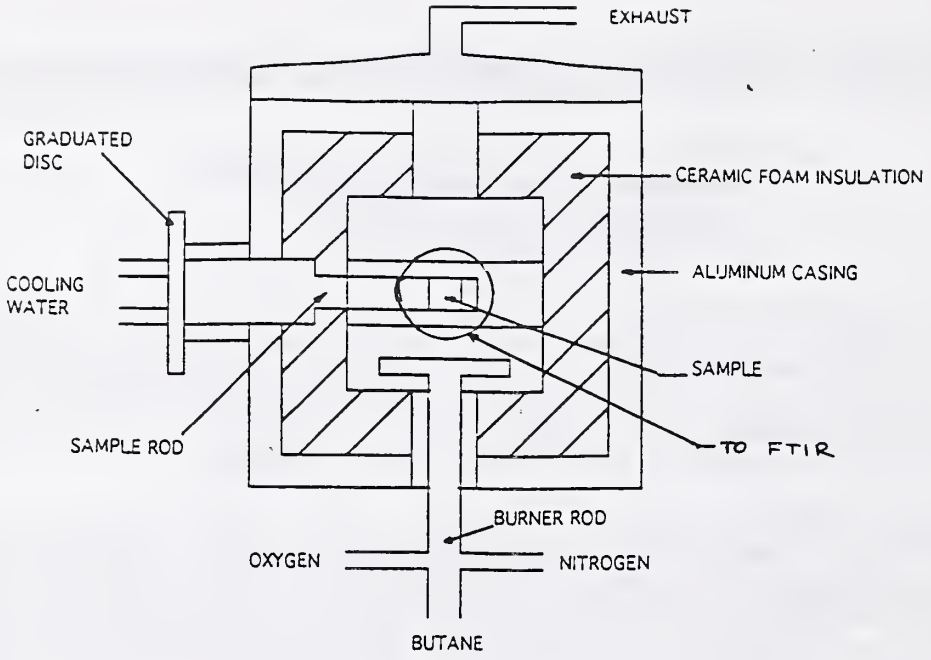

Fig. 1 Heated Cavity Reflectometer

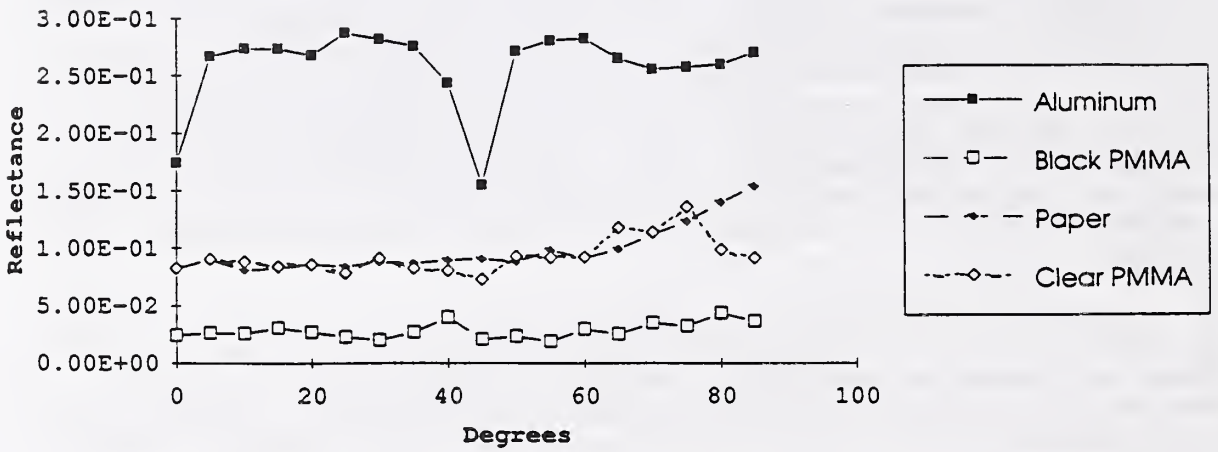

Fig. 2 Relative Directional Hemispherical Reflectance of Various Materials

LARGE SCALE, HIGH RATE OXYGEN CONSUMPTION CALORIMETER

N. R. Keltner and J. L. Moya
Sandia National Laboratories, Albuquerque, NM

The development of oxygen consumption calorimetry in the 1980's was a significant factor in advancing fire safety research. It is based on the observation that the amount of heat released from burning materials is nearly constant per unit of oxygen consumed. Work at National Institute of Standards and Technology (NIST) and other organizations has led to the Cone Calorimeter; this device exposes small samples (approximately 100mm x 100mm) to steady state heat fluxes that are representative of enclosure (i.e., building) fire conditions.

It has been recognized that some aspects of material response and fire growth cannot be obtained by extrapolating Cone Calorimeter and other small scale results to larger scales. Fiberglas Reinforced Plastic (FRP) ventilation duct is an example of a material that has passed standardized, small scale, fire response tests, such as those developed by ASTM, and yet failed catastrophically when pushed beyond some undefined limit. A study by the Bureau of Mines once showed that five out of six FRP duct materials which had passed small scale tests and were labeled as non-propagating actually produced rapidly growing fires when tested in larger scale.

The importance of these undefined limits has lead to the development of larger scale calorimeters using gas-fired radiant panels. However, all of these systems have significant limitations in either the type of test item or the heat flux levels that can be produced without adverse interactions between the heater and the test unit. The fire environments that Sandia uses to evaluate the integrity of radioactive material shipping containers, expose materials to high heat fluxes with very fast rise times. Like the scale effects, rate effects can produce significant differences in the fire response of decomposing materials.

The heat flux level, scale, and rate problems described above affect the uncertainty of risk assessments for hazardous material shipping containers. As a result, an internal proposal was developed to combine the detailed mass loss and smoke/gas measurement capabilities typical in a Cone Calorimeter with a large scale, high rate, simulated fire test system in use at Sandia National Laboratories. Because this combination has potential application in different areas of fire safety research, this presentation is an attempt to communicate with other organizations.

PROPOSED TEST FACILITY

For regulatory testing of small radioactive material shipping containers, a test fixture has been developed at Sandia's Radiant Heat Facility to simulate the severe thermal environment of a hydrocarbon pool fire. It is unique because it simulates both the heat fluxes and temperatures found in these fires, it is programmable, and it is very fast. This dial-a-fire capability allows the simulation of a given fire scenario or regulatory environment. An example would be simulation of an enclosure fire, the system could be programmed to follow a fire growth scenario and at the time predicted for flashover ramp up to the post-flashover heat flux levels in less than a minute.

The simulated fire test fixture uses modular lamp arrays to heat either a stainless steel or Inconel shroud which radiates to the test assembly. Each 1.2 m x 0.3 m module contains up to 62 halogen lamps. The maximum electrical power dissipation is 372 kW per module; this provides a maximum heat flux capability of approximately 1 MW/m^2. This configuration provides the fastest rise time; the startup of a hydrocarbon spill/pool fire is simulated by heating the shroud from ambient to 1000 C in less than a minute. The speed of the system provides the capability to reproduce the initial fire transients and the thermomechanical stresses they produce or to repeatedly generate a particular fire scenario. If such a fast rise is not required, the maximum power per module can be reduced and the number of modules can be increased to provide for a larger test item. At the Radiant Heat Facility, the largest simulated fire test to date used 12 independent power control channels to operate 24 modules with a total heater size of 2.4 m x 3.6 m. The independent controls allow tailored heat flux profiles over the surface of the test unit.

Both sides of a shroud are painted with a high emissivity, high temperature paint. Controlling the temperature of the shroud limits the maximum source temperature exposure of the test item; simultaneously, it produces an approximately gray body heat flux level and spectral distribution corresponding to that temperature. The proper thermal radiation spectrum is necessary to produce the proper fire response in non-opaque materials. The emissivity/absorptivity of a flat shroud is typically in the range of 0.85 to 0.9. For a cylindrical shroud, the effective emissivity is approximately 0.95; as a result, the heat flux level is approximately 95% of the blackbody heat flux corresponding to the control temperature. A stainless steel shroud can operate at temperatures up to 1100 C; this provides a heat flux of up to 200 kW/m^2 depending upon the configuration. An Inconel shroud can operate up to 1200 C with a maximum heat flux of approximately 250 kW/m^2.

The proposed system would use the detailed mass loss and smoke/gas measurement capabilities typical in a Cone Calorimeter with a scaled up smoke collection and flow system. Instrumentation for oxygen consumption calorimetry would be similar to that in a Cone Calorimeter (Ref. 1). The flow system would be sized similar to the Furniture Calorimeter at NIST or the Room Burn Calorimeter at Weyerhauser Corporation which can handle a heat release rate of approximately 15 MW.

DEVELOPMENT AND USE

To develop and use this unique facility will require research in several areas: a) The scaling laws between small scale tests and large scale tests need to be developed to help understand the fire response of materials. The smallest tests to be run should be large enough to produce one-dimensional response in the test object. The largest, which are limited by the size of the heater arrays, would attempt to define two-dimensional effects such as feedback to the test unit surface due to combustion of the pyrolysis products. b) To differentiate between the material response (devolatization) and the effects of combustion of the pyrolysis products, the technique of running these thermal response tests in an inert (vitiated) atmosphere needs to be developed. c) The heat flux levels and the rise times are important in producing the proper rate effects. Models of high-rate devolatization reactions need to be developed to allow proper interpretation of the data.

The combination of oxygen consumption calorimetry with large scale, simulated fire environments would result in a unique test capability for providing the data necessary to develop models of the response of decomposing materials to severe fire exposures. The system could simulate the thermal environments typical of the post-flashover conditions in building fires, severe transportation accident fire simulations such as post-crash aircraft fires, or offshore oil platform fires. The ability to provide detailed fire response data will aid efforts to optimize the design of shipping containers for radioactive and hazardous materials and to understand how decomposing materials, such as urethane foams, affect their integrity during an accident . The ability to evaluate the fire response of large composite structures would aid initiatives in transportation safety and advanced transportation systems. For example, an aircraft fuselage cross-section could be tested as part of a fire safety assessment to improve the survivability of post-crash fires. The system would provide a unique tool for evaluating fire protection materials used in energy production facilities such as offshore oil platforms, pipeline junctions, and refineries; in these applications, improved materials would help protect both the personnel and the environment.

If the proposal is accepted, the facility would be available in approximately one year to support fire safety research efforts to protect people and reduce damage from severe fires.

REFERENCES

1. Heat Release in Fires, Edited By V. Babrauskas and S. J. Grayson, Elsevier Science Publishing, New York, 1992.

ACKNOWLEDGMENT

Sandia National Laboratories is operated by AT&T for the United States Department of Energy.

Towards an Artificial Nose for Fire Detection

by

D. Pan
T. Mc Avoy
Department of Chemical Engineering
and
Institute of Systems Research

and
J. Milke
Department of Fire Protection Engineering

University of Maryland
College Park, MD, 20742

A recent paper by Okayama [1] illustrates the ability of two tin oxide detectors to discriminate between smoke from smoldering fires and ordinary odors from organic compounds, when the sensors were coupled with a neural network. Okayama used a standard backpropagation type neural network. The purpose of this paper is to discuss alternative neural network architectures, based upon modeling the neural network associated with the olfactory system, that can be coupled with modern sensors to enhance fire detection.

The problem of detecting fires by coupling sensors and neural networks is one of pattern recognition. In recent times two broad approaches to pattern recognition have been taken. The first, involves the development of mathemically based computer methods for the task. Statistical methods, such as Bayesian classifiers, as well as the standard neural networks used by Okayama have been used. The second broad approach involves studying in detail how living orgasims carry out pattern recognition. Over the last 20 or so years, a number of papers on olfactory neural networks have appeared [2,3]. This research holds great promise as a method to process data from sensors in order to detect fires more effectively. The nose has a truly remarkable ability to detect and then accurately classify an odor based upon being exposed to minute amounts of a chemical. Olfactory neural network models have been developed which beginning to explain how the nose achieves its results. In particular Freeman [2] has developed detailed olfactory models which were initially based on animal experiments. His simulations show that the olfactory system acts as a chaotic oscillator. The overall behavior is that of an associative memory in which an input triggers the recall of a pre-

stored output. Complete recall from a partial input is possible, and the model is immune to background noise. The chaos and the fact that the system is close to instability give rise to high speed performance, in a way similar to modern high speed fighter aircraft that are open loop unstable. When even a trace of a new odor is sensed, Freeman's olfactory model very quickly jumps to a new attractor. Indeed, research such as Freeman's is showing the way toward how the nose's ability to recognize odors can be duplicated artifically.

Table 1 is taken from one of Freeman's papers [2] and it gives results for the problem of classifying good and bad screws based upon an acoustical measurement as the screws pass by. As can be seen, the best method of classifying defective parts was achieved by a neural network based upon the real olfactory system. While this result is very encouraging, it should be noted that testing of such olfactory neural network models on practical problems, such as fire detection, has been very limited to date. The Freeman model also has a limitation in that it assumes that sensor signals have been transformed into a crisp, binary input. The issue of how to get from an array of non-specific sensors to this binary input is not explicitly addressed. The model is slow to run on a computer because of its size. In spite of these limitations, the thought of an "Artificial Nose" for use in fire detection is an exciting possibility that may be achievable in the not too distant future.

Table 1: Comparison of different classification methods

Classification Approach Comparison	Classification Rates	
	Unacceptable Parts	Acceptable Parts
Direct classification by distance (G)	80%	50%
Direct classification by distance (S)	70%	50%
Olfactory KII model (G)	50%	50%
Olfactory KII model (S)	50%	70%
Olfactory KIII model (G)	100%	80%
Olfactory KIII model (S)	60%	50%
Hopfield model (G)	80%	50%
Hopfield model (S)	80%	50%
Backpropagation network (G)	80%	37.5%
Backpropagation network (S)	40%	62.5%

G, S: involve two different data preprocessing approaches

1. Okayama, Y. (1991) in Third International Symposium of Fire Safety Science, pp. 955-964.
2. Yao, Y., Freeman, W., Burke, B., and Qing, Y. (1991), Neural Networks, 4, pp103-121.
3. Hopfield, J. (1991), Proceedings of National Academy of Science, 88, pp6462-6466.

INITIAL APPLICATION OF NEURAL NETWORKS TO DISCRIMINATE BETWEEN FIRE AND NON-FIRE ODORS

James A. Milke and Samuel A. Denny
Department of Fire Protection Engineering

Thomas J. McAvoy and D. Pan
Department of Chemical Engineering

University of Maryland at College Park
College Park, MD 20742

Preliminary research was conducted toward the development of a smart fire detector. In part, the intent of this research was to repeat work conducted by Okayama (1) involving small-scale experiments with gas sensors and a neural network. The combination of the gas sensors and neural network was successful in discriminating between odors from fire and non-fire sources.

At the University of Maryland, the initial research was conducted by teams in the Department of Fire Protection Engineering and the Department of Chemical Engineering. The fire protection engineering team concentrated on identifying signatures from fire and non-fire sources. The chemical engineering team investigated the applicability of various neural networks for fire detection.

Small-scale tests were conducted to characterize the signatures from fire and non-fire sources. The experiments were designed to be conceptually similar to those by Okayama (1). Modifications were incorporated to provide a greater range of measurements for describing the signature.

The experimental apparatus illustrated in Figure 1 includes means for generating odors, measurement equipment and sensors. The apparatus is adapted from the "smoke-box" specified in UL 217 (2). The principal modification consists of the straight configuration rather than the U-shaped configuration in UL 217 for smoke flow. For this experimental program, the straight configuration is preferred to limit smoke and odor deposition on the interior surfaces of the enclosure and alleviate concerns for the characteristics of the fluid flow near any turns.

The overall length of the apparatus is approximately 150 cm. The cross-sectional area of the flow stream is approximately 0.09 m^2. Measurements of light obscuration, temperature, presence of oxidizable gas and gas species concentrations (CO, CO_2 and O_2) are provided. Several of the instruments are placed near the center of the box, *i.e.* approximately 75 cm from the inlet. Consideration was given to placing the instruments to minimize any adverse effects of one instrument shadowing other instruments downstream.

Temperature is recorded by Type K thermocouples, placed in the middle of the flow stream near the inlet and discharge positions of the apparatus. Light obscuration is measured by a vertical light beam traversing the centerline of the flow stream at the mid-point of the box. The light beam source is a 0.95 mW laser, with a photocell used to monitor the amount of light transmitted across the flow stream. A gas sampling tube is also located near the midpoint of the box at the center of the cross-section. This gas sampling tube is manifolded to three gas monitors: CO, CO_2 and O_2. The metal oxide gas sensor is placed slightly off-center of the flow stream cross-section near the mid-point of the box. A variable-speed fan (maximum capacity of 0.5 m^3/s) is placed at the discharge end of the box to draw smoke or odors into the box.

Sources of the smoke or odor are placed under a hood at the inlet end of the apparatus. Smoke and odors are produced from a wide range of conditions: samples with flaming and smoldering combustion, heated samples and samples maintained at ambient conditions where the odor is introduced into the box via an atomizer. Examples of fuels include cellulosic and polymeric solids, such as paper, cotton, wood, thermoplastic polymers and thermoset

polymers. Examples of environmental sources include alcohol, perfume, dust, aerosol sprays, tobacco smoke, hot cooking oil and cooked food.

Data from these experiments is supplied to the chemical engineering group. The data is arbitrarily divided into two categories, one for learning by the neural network and one for testing of the predictive capability of the neural network. Six neural network methods are applied in this analysis.

This work is ongoing. Trial testing of the six neural networks has been conducted on an assortment of non-fire-related data. Collection of experimental data and the analysis by neural networks has been recently initiated.

Selected References

(1) Okayama, Y., "Approach to Detection of Fires in Their Very Early Stage by Odor Sensors and Neural Net", Proceedings of the Third International Symposium of Fire Safety Science, 1991, p. 955-964.

(2) Underwriters Laboratories, "Single and Multiple Station Smoke Detectors," UL 217, Northbrook, IL: UL, 1985.

Figure 1. Experimental Apparatus

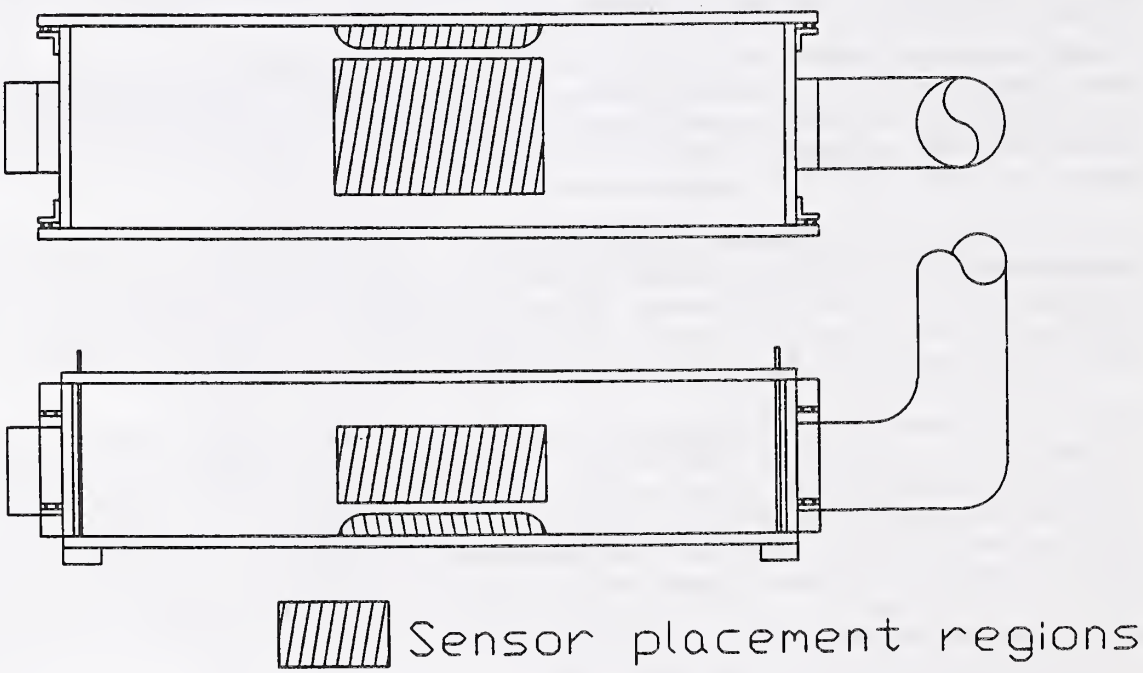

MACHINE VISION FIRE DETECTION SYSTEM [MVFDS]

Douglas F. Nelson

Air Base Fire Protection and Crash Rescue System Section
Wright Laboratories, WL/FIVCF, Tyndall AFB, Florida 32403-5323

Development is continuing of a Machine Vision Fire Detection System [MVFDS] which can "see" fires, analyze spectral and "flicker" flame characteristics, and make a rapid and reliable decision to sound an alarm or activate extinguishing systems. Prototype equipment has been tested. Final evaluations will be discussed of MVFDS capabilities to provide fire detection and extinguishing actuation for Air Force hangar facilities.

Prominent spectral features for fires include band regions around 0.18 - 0.24 microns (UV) and 4.4 microns (IR). Previous optical fire detectors [OFDs] were tuned to either or both of these frequencies. However, many sources other than fire (arc welding; sunlight; lightning; propane torches; and hot exhaust manifolds) also have rich spectral contributions in these same wavelengths. Early OFDs typically operated as single band UV or IR detectors and were thus very prone to respond to many false alarm IR or UV sources. Even with the recent multispectral detectors, false alarms still result from multiple sources of IR or UV radiation which are often found in complex environments.

In 1989 we began work on the MVFDS which identifies not only IR and UV flame signatures, but also "flicker" effects common to flames but not to steady radiations from false alarm sources. Flames are characterized by rapid color changes, highly variable edges, and outward growth from starting points. To identify such effects, a charge-coupled solid-state video camera is used with a grid of 260,000 picture elements (pixels), 512 on a side. Intensities of red, green and blue light impacting each pixel are sequentially input into computer memory, forming virtual image frames analyzed and compared every 0.03 second for changes in flame color, edge geometries, and growth rate. Flame size is computed by counting all pixels meeting "fire" criteria. Fixed installation range is computed by comparison with calibrated standard fire criteria.

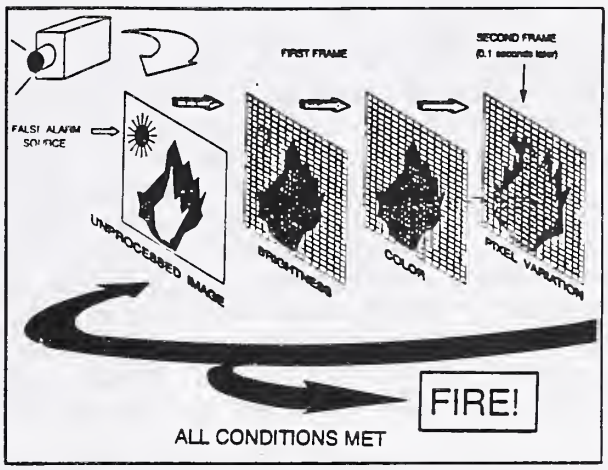

Fire Decision Criteria

The degree of fire threat can be determined, knowing fire size and growth rate. This allows selection of responses ranging from sounding an alarm to alert area personnel and firefighters for small fires, to actuation of automatic full-scale fire suppressing systems for fully developed fires. MVFDS cameras can identify

one-square-foot fires as far away as 100 feet, with response of 0.1second or less. Unlike previous OFD systems, detection speed is unrelated to accuracy; faster microprocessors enable faster times. (OFDs need 3 to 30 seconds to respond to a fire, and cannot discern fire magnitudes since a close small fire has the same signal as a large fire further away.) With OFDs, a small fire can trigger massive discharge of firefighting foam, requiring costly cleanup for what could have been extinguished easily by hand. The advanced MVFDS can activate directional nozzles for localized response, avoiding unnecessary cleanup and, for very large fires, getting more agent on the fire. Subsequent MVFDS applications may include fire detection and ranging for automatic turret operations for crash rescue vehicles, aircraft dry bay and munitions fire/explosion detection, aircraft engine bay fire detection, and aircraft cargo bay and facility overheat and fire detection.

Machine Vision Hardware

Component elements of the MVFDS test program included: detectability of small fires at 100 foot distances; ability to discern sizes of fires, and to actuate automatic release of fire suppressant at programmed fire sizes; time to detect; ability to serve singly or together in a multiple detector system, and to provide video images of the field of view on a remote CRT; compatibility with existing fire protection system units; and immunity to false alarms from heated surfaces. False alarm sources included arc welding, lit matches, cigarettes, sunlight, lightning, and electrical discharges, with modulated radiations by chopping effects provided by fans, rapid interruptions of power, people passing between the camera and radiation, and videotaped images of fires and lights. Also tested was MVFDS ability to detect fires in the presence of false alarm sources.

Hardware components of the MVFD System, including the video camera, are all "off the shelf", with concomitant reductions in cost and technical risk. Current cost of all components is about $2,500 and is expected to drop, following the general trend of hardware costs in the computer industry. A new image processing board has already been incorporated which has eliminated the need for a separate controlling microprocessor. The final prototype consists of a camera, power supply, two circuit boards containing a microprocessor, memory, and all the protocols for fire detection and decision making. Time for the prototype to recognize a fire and make a fire/no fire decision is 0.1 second.

RESIDENTIAL SMOKE DETECTOR PERFORMANCE IN THE UNITED STATES

Margaret L. Neily*
U.S. Consumer Product Safety Commission

The National Smoke Detector Project is a large public/private partnership sponsored by the Consumer Product Safety Commission (CPSC), the United States Fire Administration, National Fire Protection Association, and the Congressional Fire Services Institute. The major goal of the Project is to decrease the number of residential fire deaths in the U.S. by increasing the number of **working** smoke detectors in homes.

In support of this effort, the Consumer Product Safety Commission conducted a national survey of the operability of smoke detectors in homes. The purpose of the Smoke Detector Operability Survey was to determine the extent of and reasons for non-working detectors in the general population of households. Detectors that did not respond to a test with standard aerosol smoke (initially or after power was restored) and those with which consumers experienced problems were collected and analyzed further in the Engineering Laboratory.

The survey presents substantial information about the condition of residential smoke detectors in the U.S.: the number that exist, types in use, the number that are working, consumer perceptions about operability status, results of field operability tests, and consumer problems with detectors (such as nuisance alarms). Demographic data from surveyed households suggests additional factors related to smoke detector operability. Laboratory analysis of inoperable detectors collected by the survey provides invaluable information regarding the technical reasons for smoke detector failures and operating problems.

The data gathered from this survey (and another similar study conducted on homes experiencing fires) will define smoke detector inoperability problems so that solutions can be developed and implemented in the form of updated consumer safety messages, changes in smoke detector performance standards or design, and improvements in code requirements.

*Acknowledgements:
Charles L. Smith, CPSC, Directorate for Economic Analysis
Julie I. Shapiro, CPSC, Directorate for Engineering Sciences

AN ANALYSIS OF DELAY IN STAFF RESPONSE TO FIRE ALARM SIGNALS

IN

HEALTH CARE OCCUPANCIES

Master of Science Thesis
Worcester Polytechnic Institute
and
Prepared for
U.S. Department of Veterans Affairs

by

EUGENE A. CABLE
Regional Safety and Fire Protection Engineer
U.S. Department of Veterans Affairs
Regional Division Office, Albany, New York
January 1993

Abstract

The U.S. Department of Veterans Affairs (VA) has a strong interest in modernizing its "guide specifications" for fire alarm systems. There has been much confusion as Architects/Engineers propose fire alarm system designs which do not match the VA's requirement for a coded signal, summoning alarm, and evacuation alarm.

By VA suggestion and with their total cooperation, 238 unannounced "special" fire drills were conducted in VA facilities across the United States to examine staff response to fire alarm signals. An experiment procedure and participant survey form were developed based on available literature concerning human behavior. This procedure measured staff response delay and enabled study into the important features of a fire alarm system and it's performance which significantly influence human response TIME.

In 75% of the drills a delay in response greater than 6 seconds was observed, the average delay was 27.2 seconds. This represents the FASTEST response among all staff on the ward where the fire alarm was secretly activated.

The Statistical Package for the Social Sciences (SPSS) computer program was utilized to analyze correlations, and conduct multiple regression between any one or all of the 48 survey factors and the dependent variable "TIME to action". Several complications involving differences in health care staff response procedures may have hampered statistical results (for example other staff arriving on the ward to help). The analysis yielded

based on these results must be of a suggestive nature. However, data correlations did agree with accepted psychological theories concerning the false alarm effect or "cry wolf" syndrome.

The factors found most dominant (relative to others) in explaining variation in TIME to action or response TIME (in this order):

FLOORSPACE: Larger fire alarm systems correlated with longer staff response delays.

SYSTEM CONFIDENCE: Lower confidence in the fire alarm system correlated with longer response delays.

The following factors were significantly correlated but explained only a very small percentage of the variance in response delay. They also varied slightly in order of importance depending on staff "response category":

INITIAL: Initial type signal heard, coded signal systems showed longer response delay.

ZONEQUIP: Type of fire protection equipment and/or alarm early warning features in zone; more fire protection equipment correlated with longer response delays.

TOTAL ALARMS: Total number of alarms - over past 6 months, more alarms correlated with longer response delays.

NUMBER FALSE: Number of false alarms over past 6 months, more false alarms correlated with longer response delays.

LOCATION: Staff person's location when alarm sounded, if involved in direct patient care correlated with longer response delays.

This same type study and test procedure conducted in a different, less complicated occupancy would likely produce correlations with higher confidence.

Based on this study the VA has adopted procedural changes and is seriously considering several major conceptual changes to it's fire alarm system guide specifications. Among them are the following:

1. Do not sound fire alarm signals during system tests;

2. Within the zone initiating an alarm, a non-coded distinct signal will be utilized, signal is distinct from that given in remainder of building or facility complex.

3. All other zones will receive a summoning alarm, preferably automatic voice.

FIRE DETECTION IN A FULL-SCALE ROOM USING ACOUSTIC EMISSION SENSORS

William Grosshandler and Emil Braun
Building and Fire Research Laboratory
National Institute of Standards and Technology
Technology Administration, U.S. Department of Commerce
Gaithersburg, MD 20899

ABSTRACT

The use of acoustic emission (AE) as an early indicator of a hidden structural fire was previously investigated[1] and found to be a viable, but undeveloped, concept. Piezoelectric transducers were mounted directly on beams of different structural materials, and the ultrasonic events resulting from a small flame placed under the beam were recorded. The number of AE events in a minute and the cumulative energy released during the heating cycle were found to provide a good measure of the overheated state of some of these materials before a significant temperature increase was indicated. The measured signals varied in energy and number with the type of material, the thickness of the specimen and heat flux. Wood was particularly susceptible to acoustic emission, producing more than 1000 events per minute in a solid fir board and 30/min in 13 mm thick plywood when the flame exceeded 1.0 kW. A gypsum board produced 16 events in a minute. The differences in cumulative energy were equally striking, with the plywood being four times more energetic than the gypsum board even though the heating period for the wood was half as long, and 30 times more energetic than aluminum.

The general behavior of the materials studied could be explained qualitatively by comparison to the simplified theory developed by Clough[2] which predicts acoustic emission during laser heating of a surface. In particular the following trends were found to be consistent with most of the limited amount of data collected:

- the energy detected increases about quadratically with increasing heat flux
- the energy detected increases directly with the square of the thermal expansion and specific volume, and indirectly with the thermal conductivity and specific heat
- the energy detected decreases with increasing sample thickness

The number of emissions/minute varies for a given material in a manner similar to the energy. However, the absolute number of emissions can not be predicted *a priori* because the number of defects and the moisture content are highly variable for heterogeneous materials.

---

[1]Grosshandler, W., and Jackson, M., "Acoustic Emission of Structural Materials Exposed to Open Flames," submitted to *Fire Safety Journal*, December, 1992.

[2]Clough, R.B., "The Energetics of Acoustic Emission Source Characterization," *Materials Evaluation 45*, 556-563 (1987).

The heat source was 0.3 m removed from the sensor for the previous tests. Since the acoustic wave for materials with high internal damping loses energy in proportion to distance, one could extrapolate that at a distance of 3 m the signal would decrease to the level of the noise. Complex geometries and the number of interfaces between the source and the transducer would certainly affect this estimate. An issue which remains to be determined, then, is the size of the area which one AE transducer can monitor.

Additional experiments have been performed in a 3x3x2.5 m high room, constructed of gypsum board nailed to 37x88 mm (2x4) fir beams, with an open door located on one wall. Two AE transducers were mounted on top of the ceiling joists, one above the center of the room and the other where the joist met the wall. A third transducer was mounted behind the center wall panel on a vertical beam, one meter above the floor. Thermocouples were mounted adjacent to each AE sensor and at several points on the wall and ceiling. An ionization-type smoke detector was attached to the ceiling near the door opening. Two distinct fire types were examined: (a) an open flaming fire, and (b) a hidden smoldering fire. The flaming fire was a 150 mm diameter pan fed with methane which produced a thermal load of between 12 and 125 kW. Smoldering was achieved by attaching a 500 W electrical charcoal lighter to a vertical wooden beam located behind the gypsum board.

The acoustic events were monitored for several hours to determine the background level. For the smoldering situation, the power level of the electric heater was set at 500 W. Acoustic emission from the sensor mounted on the heated vertical beam was evident within 30 seconds. A signal discernable above the background was recorded by the corner mounted AE sensor but not from the sensor furthest from the heat source. The maximum temperature measured 30 minutes into the test next to the heating element was about 650 °C. Adjacent to the AE sensors, the temperature was less than 45 °C. The smoke detector was not triggered during the entire heating period.

The vertical wooden beam and wall panels were replaced before the open flame experiment was performed. The gas burner was located 0.6 m from the wall along the centerline of the room, and the flow was initially set to produce a 12 kW flame. The flame was increased every five minutes until a maximum of 125 kW was reached thirty minutes into the test. The AE activity was less than in the previous experiment, but exceeded the background level on the two ceiling mounted AE sensors about ten minutes after the flame was ignited. The smoke detector failed after 34 minutes because the electrical insulation melted; the smoke detector had not sensed the fire up to that point in time.

The conclusion is that AE emission appears to be sufficiently sensitive to detect two distinct fire situations, and that an overheated condition in a wall or ceiling can be detected if it is not much more than 2.0 m from the transducer. Additional experiments are required to determine the type of interfering AE signals that are likely to complicate the differentiation between a false and a true fire event.

EVALUATION OF A VIDEO FIRE DETECTION SYSTEM

B.N. Munk, R.F. Richards, and O.A. Plumb
Department of Mechanical and Materials Engineering
Washington State University
Pullman, WA 99163-2920

In order to gain commercial acceptance a system to detect accidental fires in industrial environments such as warehouse and factory floors must be both flexible and inexpensive. In addition, the system must respond to fire threats quickly with a low incidence of false alarms. A candidate fire detection system intended to meet these needs, employing one or more video cameras to monitor thermochromic, liquid-crystal, temperature sensors, is described and evaluated.

The proposed system uses a video camera in conjunction with a personal computer to continuously evaluate the temperature field around an industrial workspace by monitoring the color changes of thermochromic liquid crystal sensors. Thermochromic liquid crystals change color in response to temperature changes in a precise and repeatable manner. Reliable and inexpensive temperature sensors can be made of thermochromic liquid crystals by encapsulating the material and printing it on adhesive labels. In the proposed system these inexpensive temperature sensors are pasted over large areas of an industrial workspace. A video camera is used to monitor the color changes of many sensors simultaneously. In this way the temperature field of a large fraction of the workspace can be continuously tracked. A personal computer using digitized images transferred from the video camera translates sensor colors into workspace temperatures and determines if a fire hazard exists.

The performance of the proposed video fire detection system is simulated with a modified version of the compartment fire zone model LAVENT, developed by L.Y. Cooper. LAVENT calculates ceiling heat fluxes and temperatures in rectangular parallelepipedal compartments accounting for convective heat transfer from the fire plume and radiative heat transfer from the fire reaction zone. Modifications made to LAVENT enhance the calculation of heat fluxes and surface temperatures in regions where liquid crystal temperature sensors are to be applied in the proposed detection system. These modifications include addition of convective heat transfer from the ceiling jet of hot combustion gases to the upper sidewalls of the compartment, gas radiation from hot combustion gases and surface-to-surface radiation between compartment ceiling, sidewalls, and floor. The presence of the radiatively participating combustion products is accounted for using a mean-beam-length formulation. Features of the modified code which permit rapid calculation of compartment temperatures will be pointed out.

Performance of the video fire detection system for simulated compartment fires under the idealized condition of steady heat release and the more realistic condition of exponential growth, is demonstrated. Evaluation of the proposed system is presented through a side-by-side comparison of the video system with a standard fusible link sprinkler system. Comparison of the two systems will focus on the effectiveness of fire suppression and economy of operation. In particular the time to detection, and the ability to match suppression measures to the location and size of the fire threat will be compared for the two systems. An estimate of the cost of deployment of the proposed system will be presented.

USE OF COMPUTER MODELS TO PREDICT THE RESPONSE OF SPRINKLERS AND DETECTORS IN LARGE SPACES

Kathy A. Notarianni, P.E. and William D. Davis, Ph.D.
National Institute of Standards and Technology
Gaithersburg, MD 20899

Large spaces, such as those found in warehouses, historical buildings, atriums, and aircraft hangars, represent some of the most difficult fire protection challenges since they are frequently of historical significance, contain large quantities of fuel, and/or present special life safety problems. Accurate activation predictions are important in these large spaces, as timely detection of a fire is more difficult due to the distance heat and products of combustion must travel to reach sprinklers and detectors. An increased time to detection results in larger fires at the time of detection and larger fires to be suppressed by, e.g., an automatic sprinkler system. Since fires frequently grow at an exponential rate, even a modest uncertainty in the prediction of the activation time may lead to a large uncertainty in the fire size used to predict the hazard.

Model verification is important since it is the responsibility of the user of a model to determine the suitability of a particular fire model for a given situation. A successful comparison of the model predictions with real-scale fire results helps the user make that decision. There has been substantial effort to verify activation predictions in small and medium sized rooms, but little in large spaces *1. Conducting verification experiments for large spaces is difficult due to the lack of availability of adequate facilities for live fire tests.

The Building and Fire Research Laboratory (BFRL) was given the opportunity to make measurements during fire calibration tests of the heat detection system in an aircraft hangar with a 30.4 m ceiling height near Dallas, TX. The aircraft hangar measured approximately 389 m long by 115 m deep (81 m to a firewall). The hangar had seven bays approximately 12.5 m in length. The bays were separated by 3.7 m deep draft curtains.

The test fire was a 7.5 m^2 isopropyl alcohol pan fire with a heat release rate of approximately 8250 kW. The fire was located on the floor in the center of bay #4, the center bay. At 6 seconds after ignition of one pan, all pans were fully involved. Steady burning was maintained for approximately three minutes and 30 seconds. After 3 1/2 minutes, the flame height started to decrease. The fire was allowed to burn out.

---

*Walton, W.D., and Notarianni, K.A., A Comparison of Ceiling Jet Temperatures Measured in an Aircraft Hanger Test Fire with Temperatures Predicted by the DETACT-QS and LAVENT Computer Models, NISTIR 4947, National Institute of Standards and Technology, Gaithersburg, MD, 1992.

Fire gas temperatures and disk temperatures were measured above the fire and along the ceiling to: 1) measure the temperature and velocity of the ceiling jet 2) measure smoke filling in the fire test bay 3) measure the centerline plume temperatures, and 4) to track the flow of smoke.

Instrument locations were determined utilizing the computer fire models FPETOOL, DETACT-QS, and LAVENT. The results of the fire experiments were then compared to the predictions from the computer models in order to determine the limits of applicability of the models and to develop recommendations for use in large spaces.

Comparisons were made of the measured ceiling jet temperatures with the predictions of DETACT-QS, LAVENT, and FPETOOL, inside and outside of the plume region. Inside the plume region, both the FPETOOL and DETACT-QS computer programs underpredict the ceiling jet temperatures, thereby providing a conservative estimate of the time to activation of a sprinkler or detector. LAVENT predicts a greater temperature gradient in the vertical direction in ceiling jet than was measured. The predictions of LAVENT for the positions nearer to the ceiling are closer to the measured values, and thus more accurate than the DETACT-QS or FPETOOL predictions. For the positions further from the ceiling, the predictions of DETACT-QS and FPETOOL are closer to the measured values.

Outside of the plume region, the comparison of the measured and predicted ceiling jet temperatures is more accurate than inside the plume region. These measurement positions are on the other side of the main bay draft curtain. Flow around the draft curtain provides for some mixing and cooling, and the predictions more closely match the measurements. It should be noted, however, that none of the computer programs account for the draft curtains.

Simulations, using the field model, have been done using both two and three dimensional grids and initial comparison between calculation and experiment for the center line plume temperature give reasonable agreement. Additional work remains to be done since the fire plume exhibits some asymmetric behavior. This effect and the noise introduced in the experimental measurements due to the time variations of the pan fires need to be addressed before a valid comparison between the experiment and the field model can be completed.

Application of CFD models to optimum siting of fire sensors in spaces with complex ceiling geometries

Richard W. Bukowski Glenn P. Forney William D. Davis

1 Introduction

Nationally recognized codes which include guidelines for the placement of fire sensors in buildings are void of specific guidance for situations other than for smooth ceilings of limited height, without physical obstructions nor significant air movement. This project utilizes a state-of-the-art CFD code to perform parametric studies of the influence of exposed beams, joists and obstructions on the optimum placement of thermal and smoke sensing detectors. The model is used to predict the distribution of temperature and flow velocity in the plane below the ceiling in which the sensors would be placed. These data are then analyzed to identify the most effective locations and are reduced to engineering design parameters for inclusion into the codes.

The first task was to confirm that fire detector response can be evaluated using computational data obtained from numerical simulations. A field model was verified for this application by showing that its temperature predictions match experimental results obtained earlier by Heskestad and Delichatsios. The second task consisted of performing a parameter study to show the effect of smoke flow under beamed ceilings for various geometries and fire sizes. One question that is addressed is under what conditions can sensors be located under beams rather than in beam pockets. Time to sensor activation contour plots are presented that address this question. Twenty cases were run for various fire sizes, beam depths, beam spacings and ceiling heights.

Release 2.3.2 of Harwell-FLOW3D[1] was used to perform the numerical simulations. It solves the three dimensional, fully compressible version of the conservation equations for mass, momentum and energy.

The presentation will review the results obtained in the first year as well as the innovative visualization technique developed to analyze the data from the model.

2 Model Suitability

Six beam configurations were investigated experimentally in [2, 3]. Three configurations consisted of beams with dimensions 0.305 m (1 ft) by 0.152 m (6 in) with 0.61, 1.22 and 1.83 m (2, 4 and 6 ft) center to center spacing. The other three configurations consisted of beams with dimensions 0.61 m (2 ft) by 0.305 m (1 ft) with 1.22, 2.44 and 3.66 m (4, 8 and 12 ft) center to center spacing. Each of these six configurations consisted of a suspended beamed ceiling with no walls and a solid floor. Three experiments were performed for each configuration. An additional three experiments were performed with draft curtains in addition to the beams.

Figure 1 shows a schematic of the top view of the experimental configuration for experiment 16. The beams are spaced 2.44 m (8 ft) apart. Due to the wide spacing, the temperature comparisons are made in adjacent channels rather than every third channel. The numbers denote the temperature sensor locations. The sensors are located 0.152 m (6 in) below the ceiling (or beam) and the fire

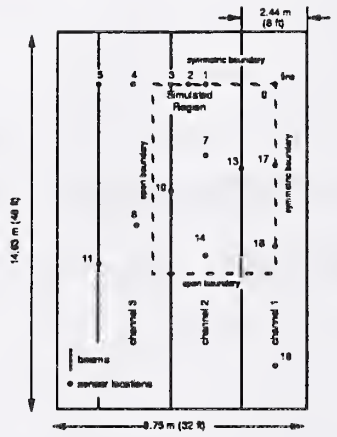

Figure 1: Physical Configuration for 2.44 m (8 ft) Beam Spaced Experiment

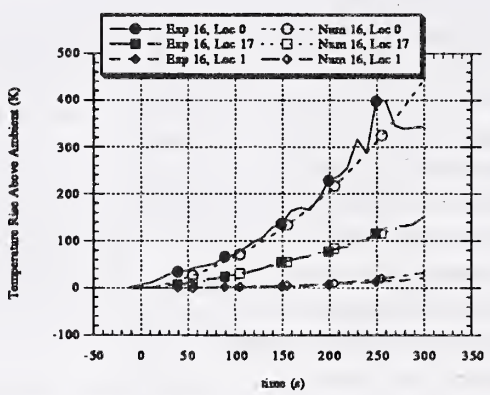

Figure 2: Comparison of Numerical and Experimental Temperature Data for a 2.44 m (8 ft) Beam Spaced Scenario

source is located at position 0. The thick solid line denotes the beams and the dashed inner rectangle indicates the portion of the physical experiment that was simulated numerically. Temperature comparisons made at location 0 (over the fire), 17 (in the first channel near the fire) and 1 (in the second channel) are shown in Figure 2. Data for the comparison was obtained from [2]. Comparisons were also made at locations 18, 7, 14 and 2 with comparable results.

The model does a good job of predicting the experimental temperatures even though the grid is coarse and the fire is modeled as a heat source.

3 Data Reduction

The following steps were performed in order to reduce the data produced by the field model into a form where decisions about detector siting could be made.

1. Record temperature and velocity field values calculated by the field model for each control volume every 5 seconds

2. Solve the heat detector temperature differential equation,

$$\frac{dT}{dt} = \sqrt{S(t)}(T_g(t) - T(t))/RTI$$

where T is the temperature of the detector link, $S(t)$ and $T_g(t)$ are the speed and temperature of the gas flowing past the link and RTI is a parameter specifying the sensitivity of the detector. at every control volume

3. Record the time when either the gas temperature (smoke detector) or detector link temperature (heat detector) exceeds a trigger temperature.

4. Generate contour plots with shades, white, light grey and dark grey where

   white indicates where the detector has not activated when fire has reached 1.0 MW,

   light grey indicates where the detector has activated when fire has reached 1.0 MW,

   dark grey indicates where the detector has activated when fire has reached 100KW.

5. Construct a table showing beam spacing requirements for cases in parameter study

4 Analysis

Contour plots showing smoke detector activation times for various beam depths are presented in Figure 3. A given contour shade represents a constant response surface for the detector being analyzed. From this information detector placement strategies can be suggested. In particular, plots such as these can be used to predict whether a detector can be placed in a pocket or under a beam.

References

[1] CFD Department, AEA Industrial Technology, Harwell Laboratory, Oxfordshire, United Kingdom. *HARWELL-FLOW3D Release 2.3: User Manual*, July 1990.

[2] G. Heskestad and M. A. Delichatsios. Environments of Fire Detectors - Phase II: Effect of Ceiling Configuration. Volume I. Measurements. NBS-GCR-78-128, National Institute of Standards and Technology, 1978.

[3] G. Heskestad and M. A. Delichatsios. Environments of Fire Detectors - Phase II: Effect of Ceiling Configuration. Volume I. Analysis. NBS-GCR-78-129, National Institute of Standards and Technology, 1978.

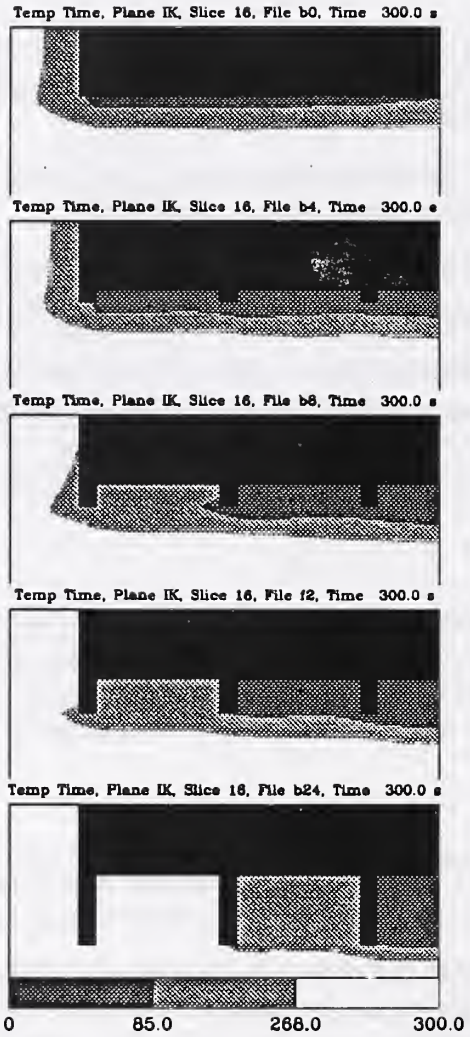

Figure 3: Shaded contour plot of smoke detector activation locations for various beam depths: 0.0 m (0 in), 0.10 m (4 in), 0.20 m (8 in), 0.30 (12 in), 0.61 m (24 in). Dark and light grey denotes where a sensor activates before the fire reaches 100 kW and 1.0 MW respectively. White denotes where the sensor would not activate. Activation criteria: when the gas temperature rises 13°C above ambient.

The Effect of Ventilation on the Use of Automatic Sprinkler Systems in Underground Coal Mines

By M. W. Ryan, A. C. Smith, and C. P. Lazzara

U.S. Department of Interior, Bureau of Mines
Pittsburgh Research Center, P.O. Box 18070
Pittsburgh, Pennsylvania 15236

ABSTRACT

The demonstrated effectiveness of automatic sprinkler systems in aboveground applications, along with their reliability and low maintenance, has led to their increased use in underground mines. However, automatic sprinklers were not designed to operate in ventilated conditions and the standards that apply to their installation do not consider the effect of ventilation on their performance. In an underground coal mine automatic sprinkler systems are installed in an environment where ventilation flows are necessary. Data on the performance of automatic sprinkler systems under ventilated conditions are lacking. Information on the how ventilation will effect the performance of an automatic sprinkler system is of utmost importance in designing sprinkler systems in order to maximize their effectiveness in extinguishing a mine fire.

The U.S. Bureau of Mines conducted a study to evaluate automatic sprinkler performance under ventilated conditions typical in underground coal mines. Experiments were conducted in a large-scale rectangular tunnel to examine the effect of ventilation on the water distribution patterns of commercial sprinklers at airflows from 0 to 4.1 m/s. Experiments were also conducted to evaluate the effect of ventilation on the performance of automatic sprinklers in extinguishing small wood crib fires.

To evaluate the effect of ventilation on the water spray patterns of automatic sprinklers, experiments were conducted in a 9.8 m long, 2.3 m wide, 1.8 m high tunnel with pendent, upright, pendent sidewall, and horizontal sidewall sprinklers at air velocities of 0, 0.76, 1.5, 2.5, and 4.1 m/s. As the air velocities were increased, there were significant shifts in the total water coverage areas and in the water density distribution patterns, as well as in the maximum coverage densities, for all types of sprinklers. The pendent and upright sprinklers exhibited upstream shifts in total coverage in the direction of the airflow ranging from 1.2 to 1.8 m, while the downstream coverage distances were extended up to 3.7 m at the 4.1 m/s airflow. The shift in upstream coverage distance for the sidewall sprinklers ranged from 1.8 m to 3.7 m, while the downstream coverage was extended up to 6.7 m at 4.1 m/s (1).

Extinguishment experiments were also conducted in the same tunnel to determine the effect of ventilation on the performance of automatic sprinkler systems in extinguishing small wood crib fires. The wood cribs were constructed of pieces of Douglas fir, weighed approximately 18.1 kg, and measured 30.5- by 30.5- by 80.1- cm. Experiments were conducted at airflows of 0, 0.76, 1.5, 2.5, and 4.1 m/s. Two experiments were conducted at each airflow, using 74° C fast response, pendent sprinklers in one experiment and 74° C fast response, horizontal sidewall sprinklers in the other experiment. In the experiments at 0 and 0.76 m/s, sprinklers were located directly above the fire and 2.4 m upstream and downstream of the fire. The sprinkler directly above the fire was the only sprinkler to operate with no discernible difference in the suppression capability of the pendent and horizontal sidewall sprinklers. The average response time of the sprinklers in the experiments at 0 and 0.76 m/s were 4 minutes and 30 seconds and 16 minutes and 30 seconds, respectively. In the experiments at airflows 1.5 and 2.5 m/s, sprinklers were located directly above the fire and 2.4 and 4.8 m downstream of the fire. The sprinkler located 2.4 m downstream was the only sprinkler to operate with the

horizontal sidewall sprinkler being more effective in extinguishing the wood crib fire. The average response times of the sprinklers at airflows of 1.5 and 2.5 m/s were 17 minutes and 30 seconds and 18 minutes and 35 seconds, respectively. In the experiment at 4.1 m/s, a fire size of 230 kW was not large enough to activate the sprinkler system.

These results showed that the ventilation caused the sprinkler downstream to operate and that the response time was also affected. At airflows as low as 0.76 m/s, the average response time was more than 3-1/2 times the average response time at 0 m/s. It is interesting to note that the response times of the sprinklers at airflows of 0.76 m/s were similar to the response times at airflows of 1.5 and 2.5 m/s. The average response time of the sprinkler for the experiments at airflows of 0.76 m/s is 11% less than the average response time of the experiments at airflows of 2.5 m/s, while still 3-1/2 times larger than the average response time at 0 m/s. The sprinklers used in these experiments were 74° C rated, fast response sprinklers. Most sprinklers installed in underground coal mines are either 74° C or 100° C rated standard response sprinklers. They would take longer to respond to the fires used in this study and would consequently allow a fire to grow larger before they activated.

The growth rate of the fire was also affected by the ventilation in these experiments. The average fire size when the sprinkler activated increased as the ventilation was increased in these experiments. At 0 m/s, the average fire size after 300 s was approximately 28 kW. At airflows of 0.76, 1.5, 2.5, and 4.1 m/s, the average fire sizes approximately 1,000 s after ignition of the wood crib were 78, 130, 180, and 230 kW, respectively. Although the fire size was larger at the higher airflows, the downstream roof temperatures when the sprinkler operated were lower. The increased airflow, due to increased cooling and dilution capacity, may reduce the hazards of the fire downstream in its early stages (2).

From these experiments it can be seen that ventilation has a significant effect on the performance of automatic sprinkler systems. The results from these experiments clearly illustrate the effect of ventilation on water distribution patterns, response times and extinguishing effectiveness. Consideration should be given to using horizontal sidewall sprinklers when airflows of 1.5 m/s or greater are present.

REFERENCES

1. Smith, A.C., M.W. Ryan, R.W. Pro, and C.P. Lazzara. The Effect of Ventilation on the Water Spray Pattern of Automatic Sprinkler Heads. BuMines RI 9459, 1993, 14 pp.

2. Ryan, M.W., A.C. Smith, and C.P. Lazzara. The Effect of Ventilation on the Performance of Automatic Sprinkler Systems. Published in Proceedings of 6th U.S. Mine Ventilation Symposium, Salt Lake City, UT, 1993, 6 pp.

Modelling of Dropwise Evaporation in a Radiant Heat Field

G. White, S. Tinker, M. di Marzo
Mechanical Engineering Department
University of Maryland at College Park

The modelling of the heat and mass transfer phenomena associated with the evaporation of a water droplet gently deposited on a glass-like material (Macor) surface is discussed. Previous validated computations for the case of heat input by conduction from below the solid have shown that a one dimensional model for the transient conduction in the liquid provides a reasonable representation of the phenomena in a thin water layer (*diMarzo et al., 1993*). Three aspects of the modelling effort are outlined here: a) the effect of direct radiation from above on the droplet evaporation; b) the evolution of the droplet shape during the evaporative transient; and c) the three sub-models used for the liquid layer during the various phases of the transient.

The geometry of the radiant heat source has been described in Fig. 1 where the three electric radiant panels located above the surface are identified in terms of their respective fractional surface area coverage at various polar angles. Note the cumulative effect of the two truncated conical panels on either side of the surface and the third, lower-aspect-ratio panel located around the whole surface around its perimeter.

Figure 2 shows the heat flux transmitted in a liquid layer at various depths. For high temperature of the source, the heat flux is significant at depths which are comparable to the heights of deposited droplets (i.e. about 2 millimeters). In the specific experimental conditions (*Dawson and diMarzo, 1993*), the heaters are at 1000 K or less. Figure 3 illustrates the volumetric heat generation due to the direct radiant heat flux. For low temperature sources, most of the direct radiant heat flux contribution to the evaporative process is limited to a very thin layer at the liquid vapor interface.

The modeling of the transient heat conduction in the liquid region is one dimensional and it is subdivided in three sub-models: a) initial contact close form solution; b) full transient diffusion equation; and b) quasi-steady state conduction equation. The radiant heat input is treated as a boundary condition at the liquid-vapor interface for this case. This model provides the necessary input for the code simulating the cooling effect of a water spray (*Tartarini et al. 1992*).

The droplet shape is rather complex because, initially, the liquid layer exhibits a low-aspect-ratio disk-like shape which then regresses to a spherical cap with shrinking base. Figure 4 depicts the transient droplet shape as computed by the proposed model.

Acknowledgements The authors are indebted to Drs. Evans and Baum (BFRL-NIST) for their guidance and to the Building and Fire Research Laboratory for the support of this research.

References

M. di Marzo, P. Tartarini, Y. Liao, D. Evans, H. Baum, "Evaporative Cooling Due to a Gently deposited Droplet" *International Journal of Heat and Mass Transfer*, in press (1993)

P. Tartarini, Y. Liao, M. di Marzo, "Numerical Simulation of Multi-Droplet Evaporative Cooling" *Proceedings of the X UIT National Heat Transfer Conference*, Genova, Italy, pp. 123-132 (1992) also to appear in *Heat and Technology*

H. Dawson, M. di Marzo, "Multi-Droplet Evaporative Cooling: Experimental Results" *Proceedings of the 29th ASME/AIChE/ANS National Heat Transfer Conference*, Atlanta, GA, (1993)

FIGURE 1 - Fractional radiant source coverege as a function of the polar angle

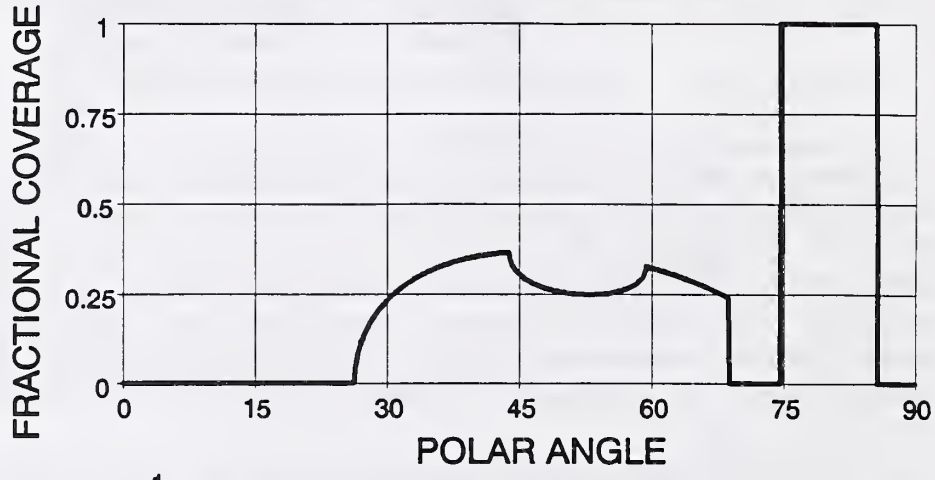

FIGURE 2 - Normalized radiative heat flux versus liquid depth

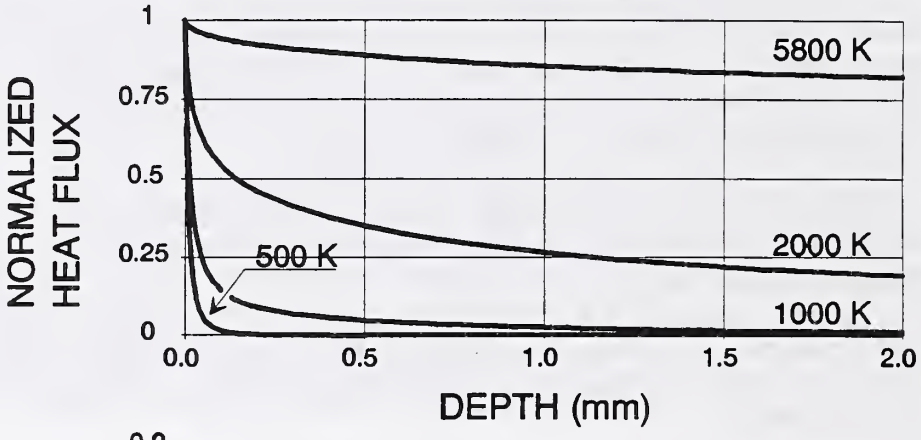

FIGURE 3 - Normalized volumetric heat generation due to the radiant heat flux versus liquid depth

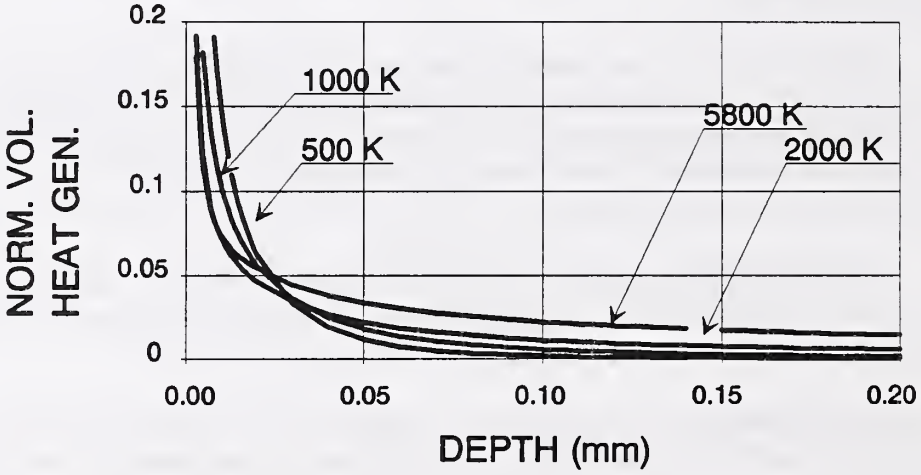

FIGURE 4 - Normalized droplet shape during the evaporative transient

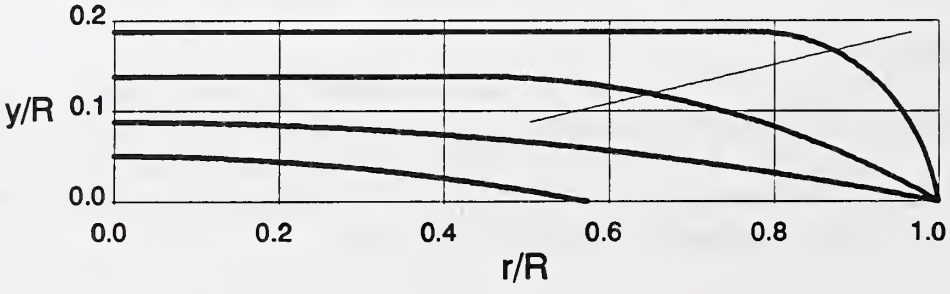

EFFECTIVENESS OF AN ON-BOARD WATER SPRAY FIRE SUPPRESSION SYSTEM IN AIRCRAFT

Constantine P. Sarkos
Richard G. Hill
Timothy R. Marker

Federal Aviation Administration Technical Center

This paper describes a series of full-scale fire tests to evaluate and optimize an aircraft cabin water spray system, designed to improve passenger survivability during a postcrash fire. The initial system consisted of a large number of ceiling nozzles which continuously discharged water throughout the cabin for a period of 3 minutes. Several scenarios, each initiated by a jet fuel pool fire, were examined in both narrow-body and wide-body test articles.

Figures 1-3 present the benefits of the "continuous" water spray system in the narrow-body test article when flames from an external fuel fire are drawn into a fuselage opening by a moderate wind condition. The water spray caused significant reductions in cabin air temperatures and toxic gas concentrations, and delayed the onset of flashover. On the basis of a fractional effective dose (FED) model, the survivability was improved by 215 seconds. Based on additional narrow body tests under other postcrash fire scenarios, and similar tests in the wide body article, it was concluded that under all but the most unusually severe fire condition, the continuous spray system was highly effective, providing a 2-3 minute increase in survival time. Although the continuous spray system requires far less water than a building sprinkler system, the weight penalty is still excessive by aircraft standards. Therefore, a "zoned" water spray system was conceptualized, designed, and tested. Discharge of water within each zone is independent of the other zones and triggered by a sensor within the zone. In this manner the quantity of water discharged is dictated by the presence and spread of fire, eliminating the ineffectual and wasteful discharge of water spray away from the fire as in the continuous spray system.

The goal of the zoned system was to minimize the quantity of water while retaining the effectiveness of the continuous spray system. In order to develop an optimized zone system design, two important parameters were evaluated - total weight of available water and nozzle flow rate. Figure 4 compares the FED calculations for zoned system tests at 4, 8 and 24 gallons, using medium flow rate nozzles, with the baseline test without water and with the continuous system test (denoted as SAVE system). It is evident that relatively small quantities of water in a zoned system provide a significant improvement in survival time compared to a system that discharges water throughout the cabin. For example,a zoned system utilizing 8 gallons of water and medium flow rate nozzles provided a 55-second longer survival time than the continuous spray (SAVE) system, which requires 72 gallons of water.

Improved visibility is another advantage of a zoned water spray system since continuously discharging water throughout the airplane tends to lower the ceiling smoke layer. With the zoned system the disruption of the smoke layer is primarily confined to the spray zones. Visibility during the zoned system tests improved by approximately 40-50 seconds

compared to the continuous system test (figure 5).

The efficiency of a water spray system may be defined as the ratio of the additional available escape time (seconds) to the quantity of water discharged (gallons), or seconds per gallons (SPG). Figure 6 compares SPG for the various water spray configurations on the basis of nozzle flow rate. It is evident that the zoned system utilizes a medium flow rate nozzle (0.35 gpm) and a water quantity of 8 gallons. The optimum zoned water spray system (SPG = 20.4) is a factor of 13.6 more efficient than the continuous water spray system (SPG = 1.5). It is significant that as much as 20 seconds of additional available escape time per gallon of water discharged may be achieved by a water spray system, operating effectively in a postcrash fire environment, where each second of available escape time is critical.

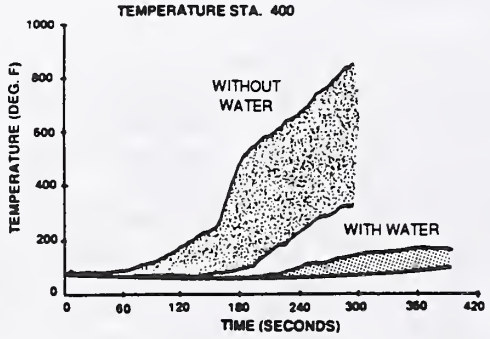

FIGURE 1
CONTINUOUS SYSTEM TEMPERATURE IMPROVEMENT
NARROW BODY/MODERATE WIND

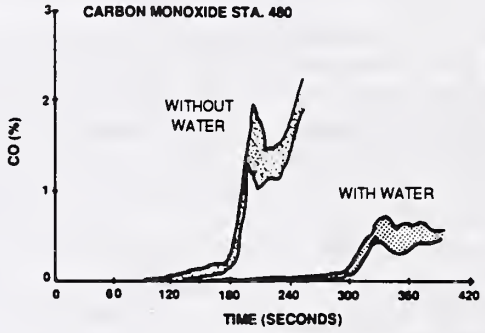

FIGURE 2
CONTINUOUS SYSTEM CO IMPROVEMENT
NARROW BODY/MODERATE WIND

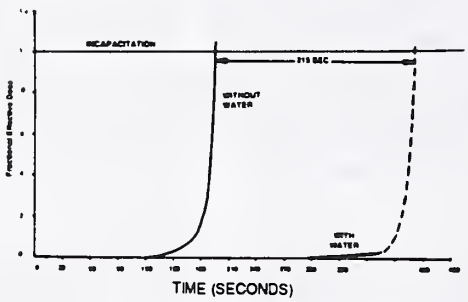

FIGURE 3
CONTINUOUS SYSTEM FED IMPROVEMENT
NARROW BODY/MODERATE WIND

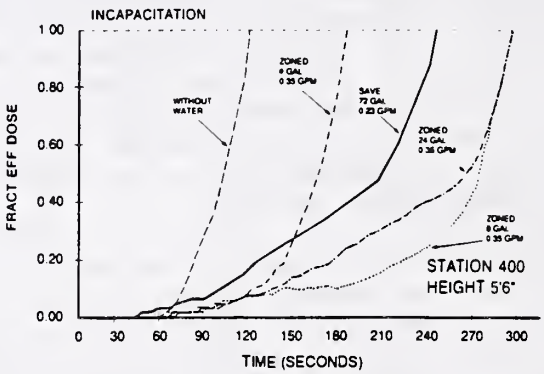

FIGURE 4
ZONED SYSTEM SURVIVAL TIME
IMPROVEMENT/4, 8 AND 24 GALLONS

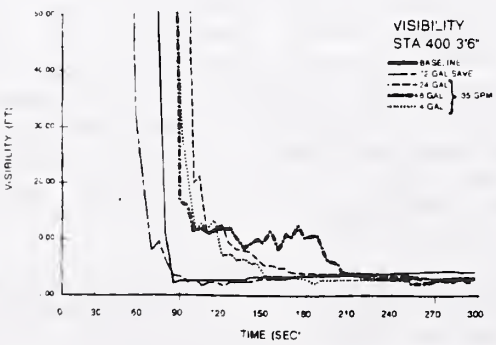

FIGURE 5
ZONED SYSTEM VISIBILITY IMPROVEMENT

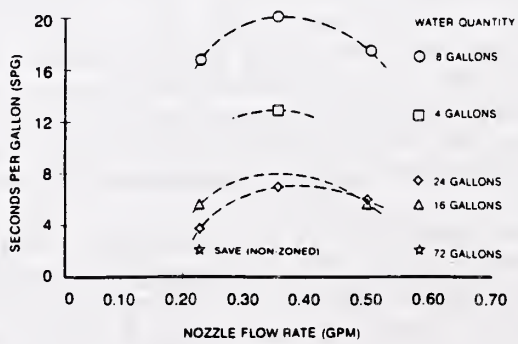

FIGURE 6
ZONED SYSTEM OPTIMIZATION

Numerical Simulation of Sprinkler Spray and Interaction with Fire

Soonil Nam

Factory Mutual Research Corporation

Norwood, Massachusetts 02062, USA

Water spray from an Early Suppression Fast Response (ESFR) sprinkler and its interaction with a fire were numerically simulated, and the simulations were compared with experimental results. Since early work[1] with a residential sprinklers indicated that precise simulation of a sprinkler spray would be a critical factor in the success of simulating interaction between fire and spray, extensive measurement of the water spray was carried out to validate the numerical simulation. The water drop size, speed, and density distribution at different locations for an ESFR sprinkler were measured[2] at 70 and 99 gpm discharge rates. The thrust force of water spray at several axial and radial locations was also measured at 30, 50 , 70, and 99 gpm discharge rates.

The water density measurements at 70 and 99 gpm show a remarkable similarity (see the experimental data in Figure 2) when the nondimensional water density, δ_r/δ_R, is plotted against the nondimensional radius, r/R, where r is the radius; R is the maximum radius of a circle which a sprinkler spray covers; δ_r is the average water density over an annulus whose radii are $r + \Delta r$ and $r - \Delta r$ (here Δr is 0.5 ft); δ_R is the average water density over the circle whose radius is R. This similarity strongly suggests that a universal water spray pattern, independent of flow rate, may exist. All the numerical simulations of sprinkler spray followed that assumption. For the computation associated with the water spray, a numerical code GENTRA, which was provided by CHAM of North America and subsequently revised extensively by FMRC[1], was used in conjunction with the gas flow calculations performed using PHOENICS code, which was also modified by FMRC[3] to provide an adequate simulation of fire plumes.

The thrust force of water spray obtained by the computation shows excellent agreement with the measurement at the different axial locations along the central axis as shown in Figure 1. The comparisons along the different radial locations also match well. The median drop size and the drop velocity computed through the simulation also agree well with the measurements. The nondimensional water density distribution obtained by the computation matches well with the correlation shown by the measurement as shown in Figure 2, which provides a significant tool for the spray modelling. Thermal plumes mimicking 500, 1000, 1500 kW fires generated by a 9.5 m/s air blower surrounded by 9 heptane spray nozzles, which simulate the FMRC-Standard-Class-II-Commodity Rack-Storage fire, were numerically created. The comparisons with the measurements in terms of the axial velocities and the radial-directional temperature profiles at several locations were reasonably good. After the plume reached a steady state, the spray was turned on and iteration was continued until both the plume and the spray reached a steady state for the simulation of the interaction between spray and fire. Figure 3 shows the interaction between the 500 kW fire and the water spray of 30 gpm.

The Actual Delivered Density (ADD)* was measured by collecting water over 20 collecting pans which were placed under the fire source. The center of the twenty-pan-arrangement coincides with that of the sprinkler which is directly above the center of the fire. The densities were computed over two areas: the smaller one covering only the central region, Area I (16 ft^2); and the larger one covering all the pans, Area II (56 ft^2). The results in Figure 4 show a good agreement, considering the complexity of the problem, between the numerical simulation and the measurement.

REFERENCES

1. Nam, S. and Bill, R.G.Jr., "Calculation of Actual Delivered Density Using PHOENICS with GENTRA," FMRC Technical Report, J.I.0R0J2.RA(3), Factory Mutual Research Corporation, Norwood, MA, 1992.
2. Chan, T.S., "Water Density and Drop Size Distribution Measurements for Selected ESFR Sprinklers," FMRC Technical Report, J.I.0Q3E9.RA, Factory Mutual Research Corporation, Norwood, MA, 1992.
3. Nam, S. and Bill, R.G.Jr., "Numerical Simulation of Thermal Plumes," To appear in Fire Safety Journal, 1993.

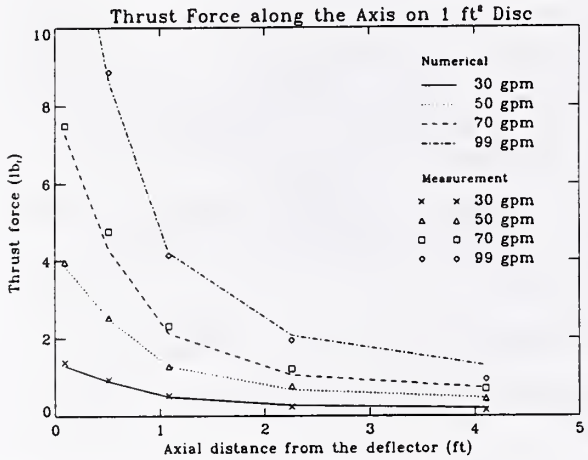

Figure 1. Comparison between numerical computation and experiment of sprinkler thrust force exerted over 1 ft^2 disc along the center-axis.

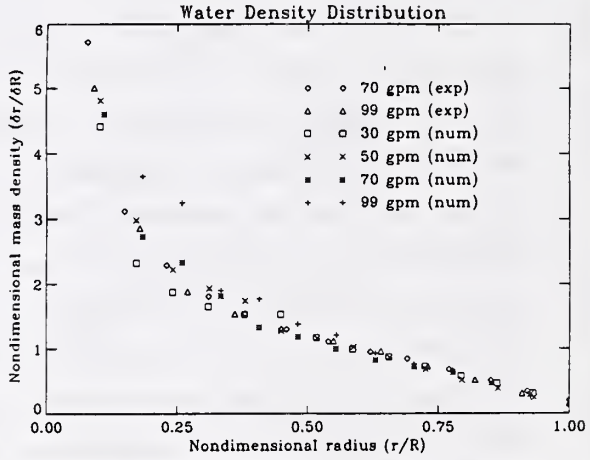

Figure 2. Comparison between numerical simulation and measurement of nondimensionalized water density distribution of sprinkler: measurement for 70 and 99 gpm, ∘ and △ in tbe figure respectively, show remarkable similarity between δ_r/δ_R and r/R. Tbe results obtained by computation also show a good agreement.

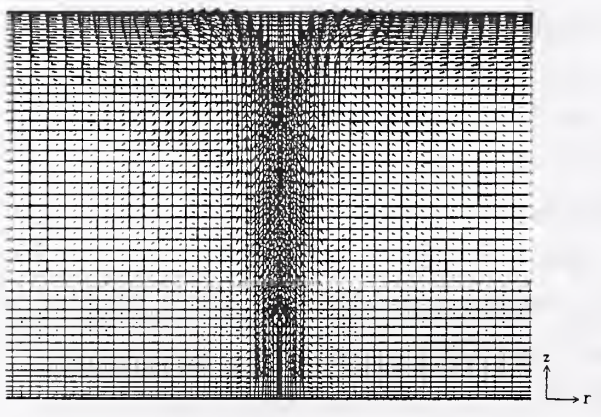

Figure 3. Air flow in the interaction between 500 kW fire and 30 gpm water sprinkler spary.

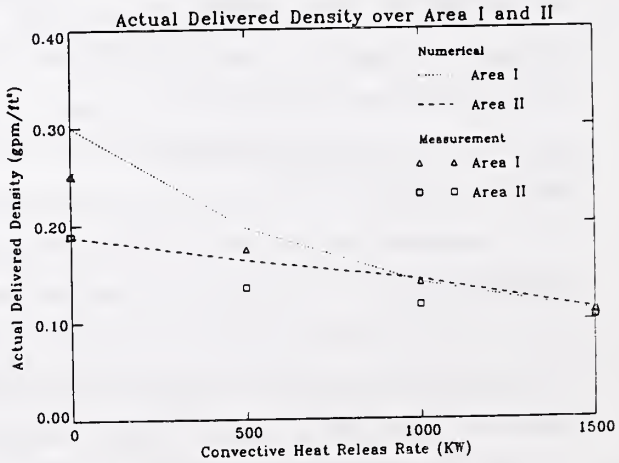

Figure 4. Comparison between numerical simulation and experiment of actual delivered density over Area I and II of the rack-storage-fire-simulator

* Water density reaching the base of a fire

WATER MIST FIRE SUPPRESSION WORKSHOP SUMMARY

Kathy A. Notarianni, P.E.
National Institute of Standards and Technology
Gaithersburg, MD 20899

The imminent lack of availability of halon fire suppressants has sparked worldwide efforts in developing other total-flooding agents. Water mist systems are potential replacements in many industrial uses, as well as in new markets, such as residences and commercial passenger aircraft. To facilitate the process of commercializing water mist systems, a workshop on water mist fire protection was held at the National Institute of Standards and Technology (NIST) in Gaithersburg, MD, March 1 and 2, 1993. The workshop was funded by the Building and Fire Research Laboratory (BFRL) and the Advanced Technology Program (ATP) at NIST.

The Advanced Technology Program, which is administered by NIST, funds advanced technologies that have a significant potential for improving the competitiveness of U.S. businesses. The ATP is a federal assistance program and awards are based on merit as determined through a full and open competition.

To facilitate the process of commercializing water mist systems, the workshop brought together a diverse group of people from industrial, academic, governmental, and approval organizations to discuss the issues impeding the commercialization of water mist technology. The workshop included representatives from system suppliers, end users (consumers), researchers, insurance, and approval laboratories. The workshop united the industrial effort by assessing the value of such systems, and identifying the areas of concern for all groups that could form the basis of future ATP projects.

The Director of the ATP presented an overview of the program and information on application for an ATP award. Speakers presented state-of-the-art papers on the incentives of using misting sprays, the advances in spray drop size measurement, and the engineering criteria for water mist fire suppression systems. Three papers discussed projects demonstrating the use of water mist systems in aircraft, marine, and telecommunications applications.

With this common background, the speakers and attendees were prepared to participate in the panel discussions. Participants were divided into three panels: Research Needs; End Use Criteria; Marketing. Each panel was composed of representatives from various technical and industrial backgrounds or interests. The panel themes were identified prior to the workshop and attendees were asked to identify discussion items within each panel. This list of discussion items was provided to the panel chairs prior to the workshop, and also inserted into the information packet received by each attendee at workshop registration. The sole purpose of the list was to provide discussion points within each panel. After three to four hours of discussion, each panel chair summarized the conclusions of their panel to all participants. Participants voted on each panel recommendation, and a prioritized list was developed. Each participant could cast a total of from one to five votes for the priorities within each panel. It is possible that the results of the voting would be different if there had been more time to vote.

The Research Needs Panel identified 17 topic areas to be addressed. The End-Use Criteria Panel identified 39 user needs which they broke down into three categories: Research and Development Needs, Information Affecting the System Selection, Standards Development Needs. Research and Development was further subdivided into Research-Oriented Needs and Development-Oriented Needs. The Marketing Panel identified 7 impediments to commercialization of water mist systems.

In the Research Needs Panel, the top four of the 17 needs identified received nearly 50% of the votes. They are: 1) full-scale tests where drop size, concentration, and jet momentum would be characterized; 2) determination of relationships among drop size, application rate, fire size, and room geometry; 3) development of at least one application to the point where standards/requirements can be set for that application; and 4) tests to determine the effects of water mist on all types of energized and de-energized electrical equipment.

In the End-Use Criteria Panel, standards development needs received the majority, 46%, of the votes including development of NFPA standards, development of standardized fire tests, third party testing, and listing of equipment. Receiving an additional 30% of the votes was information affecting system selection.

In the Marketing Panel, 46% of the votes were for issues relating to the fact that water mist is a "new technology." Another 26% of the votes related to system reliability and effectiveness.

The following topics concerned more than one panel:

- water mist and electrical equipment
- standards development
- drop size/system optimization
- additives
- confidence in design criteria/system reliability
- cost
- acceptability by authorities having jurisdiction
- water quantity and/or quality

The above topics reflect areas where the workshop participants felt work could be done that would aid in the commercialization of water mist systems. With the availability of ATP funding to sponsor such work, it is hoped that industry will generate proposals for developing and implementing water mist fire suppression systems.

CHEMICAL ENHANCEMENT OF COMBUSTION DURING FIRE SUPPRESSION BY WATER

ARVIND ATREYA, TODD CROMPTON AND SANJAY AGRAWAL

Combustion and Heat Transfer Laboratory
Department of Mechanical Engineering and Applied Mechanics
The University of Michigan, Ann Arbor, MI 48109-2125

(Supported by NIST)

Suppression of fire results from *chemical* and/or *physical* effect of the suppression agent on the burning process. *Physical* suppression mechanisms act by either cooling the condensed-phase to inhibit fuel pyrolysis (e.g. water application) or by quenching the gas-phase combustion reactions. The gas-phase quenching may be accomplished by simply blowing-off the flame (i.e. by increasing the strain rate) or by diluting the fuel and/or the oxidizer streams with inerts such as H_2O, CO_2, and N_2 (effect of heat capacity, heat of vaporization or heat of decomposition) or by separating the reactants by mechanical or other means (blanketing). Clearly, combined extinguishment actions are also possible and in-fact desirable. These may occur naturally, as in the case of water application, where in addition to condensed-phase cooling, the pyrolyzed fuel is also diluted by evaporated water vapor. The *chemical* suppression mechanisms, on the other hand, are believed to interfere with the critical reaction steps responsible for maintaining the flame[1].

Water, the most widely used suppression agent, is thought to be chemically inert in a fire and is believed to have a *physical* effect. However, there is little information on the magnitude of these effects during fire suppression[1]. Thus, initially experiments were done with water as the extinguishing agent applied to a burning PMMA sample in the stagnation-point flow configuration. This was done to establish a standard for comparison of suppression effectiveness of other agents. However, the experimental results for PMMA revealed some unexpected and very interesting phenomena. Two simultaneous effects were found as a result of water application: (i) chemical enhancement of burning rate (which is important only when the flames become sooty; Note: most fires are sooty), and (ii) physical cooling of the solid via water evaporation and the resulting dilution of combustible vapor. The chemical enhancement effect is new and has not been previously reported. This is probably because water is usually applied in large quantities and in this domain the physical cooling effect dominates. To separate the chemical and physical effects of water application, PMMA was replaced by a porous ceramic gas burner. Thus, physical cooling effect was eliminated leaving only dilution and chemical enhancement effects.

Results of the gas experiments conducted in both stagnation-point flow and counterflow diffusion flame configurations are described in this paper along with the results of numerical calculations performed to help identify the chemical mechanisms. Methane was chosen as the fuel and the methane flow rate, the oxidizer flow rate and external radiation were held constant. Experiments were conducted for different O_2 concentrations (to change the soot volume fraction) and for different constant water application rates. The overall transient species composition measurements in the exhaust gases of the stagnation-point flow apparatus were used to calculate the effect of water droplets (or other suppression agents) on the overall heat release rate. Clearly, an increase in the CO_2 production rate and O_2 depletion rate corresponds to an increase in the burning rate and vice versa. Representative results for three different oxygen concentrations are presented here: (i) 12% O_2 which produced a blue flame, (ii) 15% O_2 which produced a sooty yellow flame, and (iii) 30% O_2 which produced a high temperature bright and sooty flame.

Blue CH_4 flame (12% O_2)

As a result of fuel dilution due to water evaporation: CO_2 & CO production rates and O_2 depletion rates were decreased. Less hydrocarbons were burned and hydrocarbon percentage increased until extinguishment was obtained.

---

[1] Physical cooling of porous and non-porous solids by water droplets was investigated extensively earlier by Dr. diMarzo[2] and the present author[3]. Both these are quantitative studies, but were conducted on hot solids in the absence of a diffusion flame. Current results are obtained in the presence of a diffusion flame. At the time of these earlier studies, physical cooling by water droplets and reactant dilution were believed to be the only fire suppression mechanisms of water.

Chemical enhancement was not observed in any of our experiments with non-sooty (blue) flames. CO_2 production rates for a blue methane flame are presented in Fig.1 for various water application rates (applied during 300 to 1200 sec). Absence of chemical enhancement of the burning rate may be because of low flame temperatures. It is also possible that water reacts more easily with intermediate products of soot formation. Flame structure measurements are being performed to resolve these questions.

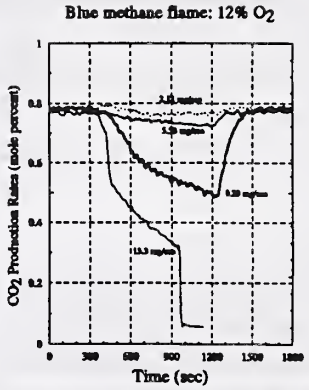

Fig. 1: CO_2 production rates for various water application rates

Sooty CH_4 flame (15% O_2)

As the water application rate was increased, first the O_2 depletion rate and CO & CO_2 production rates were observed to increase. This implies an increase in the heat release rate (i.e. more efficient combustion). With further increase in the water application rate, CO production rate continued to increase even after CO_2 production rate stopped increasing. Thus, there was not enough O_2 available to oxidize CO to CO_2. Eventually, with further increase in water application rate, dilution effects become dominant and the flame was extinguished. Also, unburned hydrocarbon concentration increased throughout -first due to reduction in soot formation and later due to dilution effects. O_2 depletion measurements for various water application rates are shown in Fig.2. It is interesting to note that CO production rate increased for all cases of the yellow flame, whereas it decreased for all cases of the blue flame.

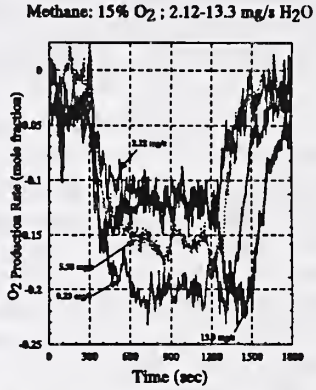

Fig. 2: O_2 depletion rates for various water application rates

Bright sooty flame (30% O_2)

Further increase in the oxygen concentration makes the flame more sooty and bright yellow. Also, for the same flow rates of fuel and oxidizer, the flame moves closer to the porous ceramic surface. Since the flame temperature is significantly increased, water addition is expected to be more effective. Results of such an experiment are shown in Fig.3 for 13.3 mg/sec water application rate. Note that both CO and unburned hydrocarbons are oxidized to CO_2. This clearly shows chemical enhancement of the burning rate due to water application. Similar experiments conducted with 40% dilute solution of HBr show a reduction in the burning rate.

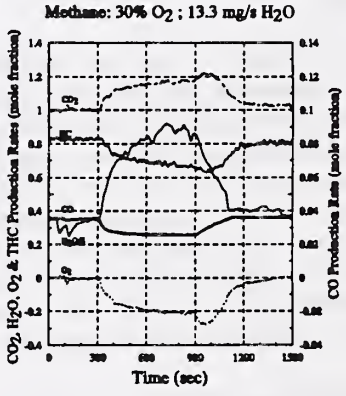

Figure 3

These results are consistent with the experiments conducted in sooty (fuel-rich) methane counterflow diffusion flames[4]. Here detailed flame structure measurements were made. It was found that by reducing the O_2 concentration while maintaining the flame temperature by preheating the reactants (thus reducing the H_2O concentration in the reaction zone) led to an early soot inception and increased soot volume fraction. However, direct addition of only 3.6% H_2O (while holding all other conditions constant) resulted in delayed soot nucleation and a significant reduction in the soot volume fraction. These observations can be consistently explained by the mechanism of OH interference with soot inception. An increase in the H_2O concentration (brought about either by an increase in the O_2 concentration or by direct addition) results in an increase in the OH concentration provided the flame temperature is high enough. This reduces the PAH and C_2H_2 concentrations (the corresponding reduction in total hydrocarbons and CO was observed in the stagnation-point flow diffusion flame) and delays soot inception. This substantially decreases the ultimate soot loading and increases the combustion efficiency and hence the burning rate.

A model based upon the SANDIA CHEMKIN code is being used to help understand the changes in the flame structure caused by water addition. Comparison of the model results with experiments and possible suppression mechanisms are also presented.

REFERENCES

[1] Pitts, W. M., Nyden, M. R., Gann, R. G., Mallard, W. G., and Tsang, W., "Construction of an Exploratory List of Chemicals to Initiate the Search for Halon Alternatives," *NIST Technical Note 1279*, National Institute of Standards and Technology, Gaithersburg, MD, 1990.

[2] Abu-Zaid, M., and Atreya, A., "Transient Cooling of Hot Porous and Non-Porous Ceramic Solids by Droplet Evaporation," Presented in the Poster Session of the 22nd. Symposium (International) on Combustion and accepted for publication in the ASME J. Heat Transfer, being revised, 1992.

[3] diMarzo, M.; Liao, Y.; Tartarini, P.; Evans, D. D.; Baum, H. R.; "Dropwise Evaporative Cooling of a Low Thermal Conductivity Solid," *IAFSS*, 3rd International Symposium, 1991.

[4] Zhang, C., Atreya, A. and Lee, K., "Sooting Structure of Methane Counterflow Diffusion Flames with Preheated Reactants and Dilution by Products of Combustion," *Twenty-Fourth Symposium (International) on Combustion*, The Combustion Institute, 1992, in press.

SIMULATING DISCHARGE OF FIRE SUPPRESSION AGENTS FROM A PRESSURIZED VESSEL AND ESTABLISHING INITIAL/BOUNDARY CONDITIONS FOR THE PROBLEM OF AGENT DISPERSION IN A PROTECTED SPACE*

Leonard Y. Cooper
Building and Fire Research Laboratory
National Institute of Standards and Technology
Gaithersburg, MD 20899

Introduction. This work reports on part of an effort to study the dispersion and extinguishment effectiveness of Halon and Halon-alternative fire extinguishment agents discharged from N_2-pressurized vessels through a simple, nozzle/orifice-like exit. The systems under consideration involve vessel volumes of the order of $10^{-3}m^3$, with required discharge times of the order of $10^{-2}s$. To achieve such rapid discharge times, the pre-pressurization levels must typically be of the order of several tens of atmospheres. Prior to discharge, the contents of the vessel involve liquid agent below, with some dissolved N_2, and a mixture of gaseous agent and N_2 above.

The overall objective is to predict the dispersion of a discharging agent throughout a protected space. Time-dependent agent concentrations associated with a particular agent discharge and threat scenario would be used as a basis for estimating extinguishment effectiveness. The strategy to predict agent dispersion characteristics involves two basic mathematical model components: 1) a model to simulate the time-dependent discharge of the agent from the high-pressure discharge vessel; and 2) a model to simulate the development and dispersal of the ensuing, mixed, air/two-phase-agent jet.

A critical element in exercising any component-2 model is to establish a set of initial/boundary conditions for the jet. This must be at a location of the jet axis near the exit section of the discharge vessel. The initial/boundary conditions would be derived from the predictions of the component-1 model. The purpose of this work is 1) to develop a component-1 model to simulate agent discharge [1] and 2) to establish a method of using the predictions of the model to estimate the initial/boundary conditions for the problem of agent dispersion throughout the protected space [2].

The Model of Agent Discharge from a Pressurized Discharge. The developed mathematical model and associated computer program solves initial value problems involving field-deployed and laboratory agent delivery systems depicted in Fig. 1.

The field-deployed system, which forms the basis of example calculations, involves a half-liter cylindrical discharge vessel with a circular discharge nozzle/orifice of diameter 0.019m. The vessel is half-filled with liquid Freon 22 at 294K and is pressurized with N_2 to 600psi. Vessel discharge is initiated by actuation of an explosive cap over the nozzle/orifice.

The simulating experimental configuration involves a modified field-deployed system. A diaphragm with nominal 600psi rupture pressure (actual values between 550psi and 650psi) replaces the explosive cap. The system is equipped with a high-pressure N_2 holding tank connected to the discharge vessel *via* an orifice. An experimental run begins with the onset of through-orifice N_2 flow from the holding tank. The vessel is pressurized to the point of diaphragm rupture and this is immediately followed by vessel discharge.

The model is used to simulate discharge of the field-deployed system and pressurization/discharge of the experimental system. Simulations of the experimental system involve holding tank volumes of $2.5(10^{-3})m^3$ or $2.5(10^{-5})m^3$; orifice diameters of 0.005m, 0.001m, or 0.0005m; and initial vessel pressures of 136psi (the saturation pressure of Freon 22 at 294K) and 500psi.

From the calculations it was determined that the $2.5(10^{-3})$m3 holding tank with the 0.0005m orifice could be used to accurately simulate the discharge of the field-deployed system and that it is reasonable to expect that this experimental design would give good simulations even when extended to a range of parameters and agent materials well beyond the scope of the present calculations. Calculations also indicated that use of the $2.5(10^{-5})m^3$ holding tank and/or the 0.005m orifice would not be consistent with an acceptable experimental design.

Establishing Initial Boundary Conditions for the Problem of Agent Disresal in the Protected Space. As the agent exits the pressure vessel, thermodynamic and fluid-dynamic instabilities lead to flashing and break-up of the agent into a two-phase droplet/gaseous jet mixture. This occurs in a transition region which starts at the vessel exit and ends at a section of the two-phase jet where thermodynamic and fluid dynamic instabilities have ceased. Thus it is conjectured that downstream of this latter section, called the *initial section*, the agent there begins to develop a mixed, two-phase, agent/air jet where thermodynamic

*Sponsored by the U.S. Air Force Wright Patterson Laboratory

equilibrium is maintained and where droplet collision and agglomeration will not play an important role in the ensuing jet dynamics and in the dispersal of the agent though the protected space.

Figure 2 depicts the transition region when conditions inside the vessel are such that the liquid agent initially penetrates the ambient space as a metastable superheated liquid column. This has been observed experimentally at NIST. Another possibility, that may have been observed toward the end of liquid agent discharge experiments at NIST, is that the liquid agent (in the vessel) is absolutely unstable (thermodynamically) as it penetrates the outside ambient-pressure environment and that it flashes explosively, within a distance of the order of a single nozzle/orifice diameter, upon emerging from the vessel exit.

The above discharge model simulates the time-dependent discharge of the agent from the pressure vessel. Using the output of this model and thermodynamic and fluid-dynamic considerations of the phenomena in the transition section, a method was developed for determining a set of initial/boundary conditions at the initial section of the jet, downstream of the transition region. These initial/boundary conditions are in a form that can be used to formulate and solve the problem of the development and dispersal of the ensuing air/two-phase-agent jet.

The developed methodology was applied in example cases of agent discharge from the above-referenced half-liter cylindrical discharge vessel. The simulations involve discharge of the vessel when it is half-filled with either Freon 22 or Halon 1301 and then pressurized with N_2 to 600psi.

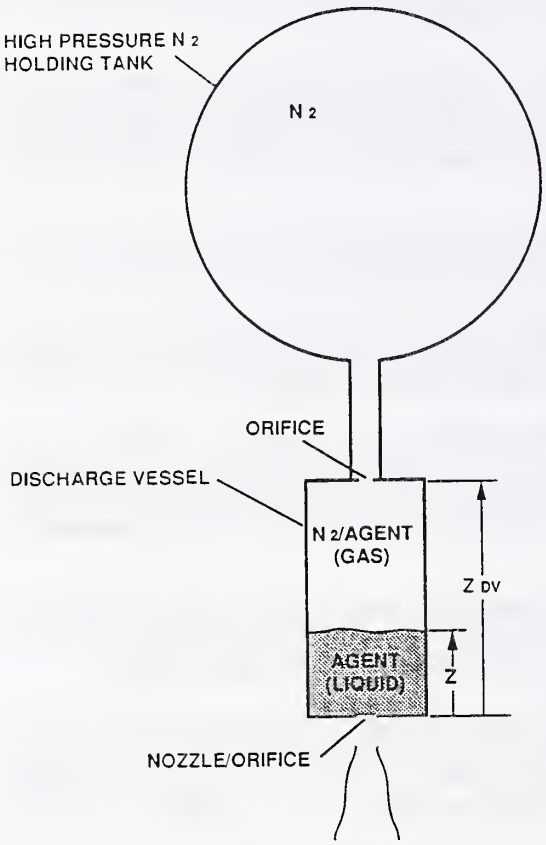

Fig. 1. The generic agent delivery system.

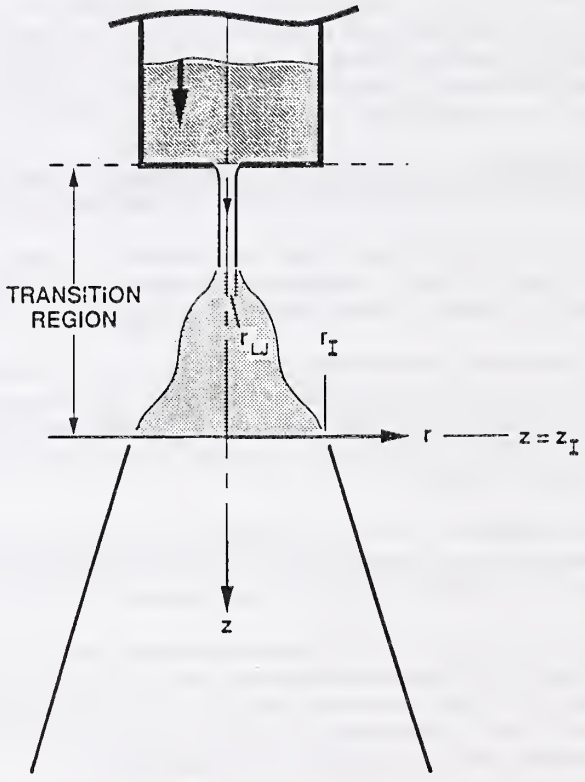

Fig. 2. Sketch of the discharging agent, the transition section, and the initial section at $z = z_I$.

References

1. Cooper, L.Y., Discharge of Fire Suppression Agents from a Pressurized Vessel: A Mathematical Model and Its Application to Experimental Design, NISTIR 5181, NIST, Gaithersburg MD, 1993.
2. Cooper, L.Y., The Dispersion of Fire Suppression Agent Discharged From High-Pressure Vessels: Establishing Initial/Boundary Conditions for the Flow Outside the Vessel, to appear as a NISTIR, NIST, Gaithersburg MD.

SUPPRESSION OF HIGH-SPEED TURBULENT FLAMES BY HALON-ALTERNATIVE EXTINGUISHING AGENTS*

G.W. GMURCZYK and W.L. GROSSHANDLER

Building and Fire Research Laboratory
National Institute of Standards and Technology
Gaithersburg, MD 20899
(301) 975-2301

ABSTRACT

Fast turbulent flames may occur when the composition of a combustible mixture falls in an appropriate range and the geometric conditions promote the turbulent mixing process. In such circumstance the flame may accelerate dramatically, reaching a supersonic regime of flow which is inherently associated with the presence of shock waves. There are three scenarios possible in this situation. First, the flame is coupled with the shock wave but its velocity is below the speed of sound in the combustion products, yielding a high-speed turbulent flame. Second, the flame is coupled with the shock wave but its velocity is above the speed of sound in the combustion products and yet below the Chapman-Jouguet velocity, producing a so-called quasi-detonation flame. Third, the accelerating flame follows the generated shock wave at a distance but it is not coupled directly with it, which is called an explosion. Although there exists extensive literature on these mechanisms, the knowledge and understanding of the suppression process under these conditions is sparse. The importance of the problem may be emphasized by the fact that even a slight variation in concentration of a combustible mixture near the limit of different combustion modes may cause a change in flame velocity of an order of magnitude. The resulting pressure waves propagating in a free space or within an installation or compartment may be totally destructive for material structures and human beings. The process is especially dangerous because of its exceptionally high speed, and consequently increased difficulty of intervention. This is one of the reasons that the phenomena associated with supersonic speeds need to be abstracted into a separate field of fire safety science and engineering.

The suppression effectiveness of halon alternative extinguishing agents has been studied in a detonation tube specially designed at NIST for that purpose. The tube consists of two sections separated by a high-vacuum gate valve. Both sections are filled with spiral-shaped obstructions that have been inserted into the tubes. The pitch of the spirals is equal to the inner diameter of the tubes and the blockage ratio of the obstacles is 44%. The purpose of the obstacles is to generate turbulence in

* Sponsored by Wright Laboratory - U.S. Air Force

the propagating flame, thus enhancing dramatically the flame velocity.

The first section of the tube, called the driver section, is 5 meters long. It is equipped at one end with a spark plug for igniting the combustible mixture. The ignition energy is delivered in a microexplosion of a tin droplet short-circuiting the tips of nichrome electrodes connected via a transformer with an AC power supply. The driver section is filled with a combustible mixture. The other section of the tube, called the test section, is 2.5 meters long. It is filled with the combustible mixture of the same composition as the driver section, plus the extinguishing agent. During the filling process the two sections of the tube are separated by a manually operated gate valve. The compositions of the mixtures are established with the method of partial pressures. The partial pressures are adjusted in such a way as to keep equal the total pressure in both sections of the tube. That routine allows one to avoid unwanted motion of the mixture through the valve, which is opened just before ignition, due to a pressure difference. After the filling process both mixtures in the two sections are circulated separately with the use of a two-sectional, spark-free circulating pump. The purpose of the circulation is to homogenize the mixtures so the flame produced in the tube is of a pre-mixed type.

The flame propagating in the driver section reaches the high-speed turbulent regime associated with the occurrence of shock waves. After passing the gate valve the flame coupled with the shock wave enters the test section, encountering the same combustible mixture and a certain amount of the agent. Depending on the concentration of the agent, the flame is decelerated. As a result of this effect the pressure wave supported by the flame is simultaneously attenuated. The velocity of the pressure wave and its pressure ratio are determined by means of a set of piezoelectric pressure transducers located at the end of the test section, giving one the opportunity to establish the suppression effectiveness of the halon-alternative extinguishing agents.

Ethene and air are mixed in the system at an equivalence ratio of 0.75, which implies a composition of 5% by volume of ethene in the ethene/air mixture. This lean composition falls within the high-speed turbulent combustion regime for the mixture. The impact of the following factors on the performance of the setup and its suitability for suppression research is under investigation: the percentage of the agent present in the test section, the initial pressure of the mixture, the voltage of the ignition system, the mixing time of the components before ignition, the speed of opening of the valve before ignition as well as the presence of the valve itself, and the presence of the spirals.

The ranking of the agents will be based on the minimum concentration necessary to substantially retard the flame velocity and pressure increase.

ASSESSMENT OF HALON ALTERNATIVES FOR SUPPRESSION OF TURBULENT SPRAY FLAMES[1]

William Grosshandler, William Rinkinen and Darren Lowe
Building and Fire Research Laboratory
and
Cary Presser
Chemical Science and Technology Laboratory
National Institute of Standards and Technology
Technology Administration, U.S. Department of Commerce
Gaithersburg, MD 20899

ABSTRACT

A coaxial turbulent jet burner has been built to evaluate the relative effectiveness of alternative extinguishing agents for suppressing engine nacelle fires. Jet fuel is injected on the centerline of the 50 mm diameter burner using an oil burner pressure jet nozzle at a mass flow rate of 0.5 g/s. Air is brought in parallel to the fuel in an annular region at nominal velocities of 5 m/s to 30 m/s, producing overall stoichiometric ratios between 0.15 and 0.6. The flame is stabilized in the wake formed behind a 35 mm diameter disc surrounding the fuel nozzle. The temperature of the air is maintained between ambient and 422 K.

Eleven different fluoro-chloro-hydrocarbons have been evaluated in the NIST study. Prior to a test, the agent is transferred as a gas to an evacuated one liter chamber and maintained at an elevated pressure. At the desired moment, a computer controlled solenoid valve is opened for 65 ms and the agent is injected impulsively into the air stream. The amount of agent is controlled by varying the initial pressure in the chamber. Uniform dispersion across the combustion chamber is achieved by passing the agent/air mixture through mixing screens before it encounters the fuel spray.

The influence of air velocity, air temperature and injection period on the amount of a N_2 needed to extinguish a turbulent JP-8 spray flame has been studied. A signifcant reduction in the mass of nitrogen required occurs when the gas is injected over the shortest period of time (6 ms). The average extinction concentration is considerably below the values found in cup burner experiments.

An injection period of 50 ms was chosen to evaluate the relative performance of the eleven proposed agents. This is about ten times longer than the estimated residence time in the laboratory spray flame and about ten times shorter than what is typical for existing halon 1301 systems installed in engine nacelles. The attached table summarizes the results. On a mass basis, nitrogen is the most effective material, requiring only 0.58 grams to extinguish the flame.

---

[1]Sponsored by Wright Patterson AFB, OH, Flight Dynamics Laboratory

This translates to an average mass fraction of 0.18, as compared to 0.28 in the cup burner. HFC-22 is the most effective of the other chemicals being considered; FC-31-10 is the least effective on the same basis. Using mole fraction (hence, volume) as a measure of effectiveness, nitrogen is the least desirable and FC-31-10 is the most. Generally speaking, however, the variations in effectiveness among the chlor-fluoro-hydrocarbons is much less than the difference between halon 1301 and any of the proposed alternatives.

Table. Results for jet burner experiments.

Designation	Formula	Spray Flame Extinction Mass, g	Extinction Volume @ 101 kPa, 298 K, l	Spray Flame Mass Fraction	Cup Burner Mass Fraction[2]	OFDF High Strain-rate Mass Fraction[3]
	N_2	0.58	0.510	0.18	0.28	0.046
FC-116	C_2F_6	0.75	0.183	0.22	0.28	
Halon 1301	CF_3Br	0.44	0.080	0.15	0.14	0.021
HFC-32/HFC-125 azeo	CH_2F_2/C_2F_5H	0.71	0.260	0.22	0.30	
HFC-125	C_2F_5H	0.28	0.149	0.22	0.28	
HFC-227	C_3F_7H	0.70	0.115	0.24	0.28	0.074
HFC-22	$CClF_2H$	0.89	0.183	0.20	0.28	0.061
FC-218	C_3F_8	0.89	0.149	0.20	0.29	
HFC-134A	$C_2F_4H_2$	0.76	0.183	0.24	0.28	0.096
HCFC-124	C_2ClF_4H	0.74	0.132	0.22	0.28	0.062
FC-318	C_4F_8	0.97	0.149	0.20	0.31	
FC-31-10	C_4F_{10}	1.00	0.103	0.20	0.30	
HFC-236FA	$C_3F_6H_2$	0.78	0.126	0.23		

[2]Hamins, A., personal communication, 1993.

[3]Seshadri, K., personal communication, 1993.

Mixing Behavior of Halon 1301 Alternatives Released from Pressurized Bottles[1]

W. M. Pitts, J. C. Yang, B. D. Breuel, W. Cleveland, and G. Gmurczyk

Building and Fire Research Laboratory
National Institute of Standards and Technology
Gaithersburg, MD 20899 USA

1. INTRODUCTION

Halon 1301 has been widely employed on military and commercial aircraft for fire fighting purposes. Unfortunately, due to the deleterious effects of chlorine and bromine on stratospheric ozone, the manufacture of halon 1301 will be phased out by the end of 1993. The National Institute of Standards and Technology has been tasked to recommend which of eleven potential halon replacements [1] should be tested at full scale for firefighting on aircraft. The work reported in this paper is part of this task.

The rate at which an agent is released from a storage vessel as well as its dispersion within the volume containing the fire are two critical factors in fire extinguishing capability. An experimental system has been developed to characterize the following processes: 1) agent behavior during release from a pressurized vessel, 2) rate of agent release, 3) qualitative behavior of the agent following release, 4) velocity of the downstream edge of the released agent, and 5) rate of vaporization of agent. This talk focuses on the mixing behavior of the agents following release from the vessel, (i.e. processes 3 to 5).

2. EXPERIMENTAL

The agent to be studied is placed in a 500 ml vessel equipped with a 19 mm rupture disk designed to burst at a nominal pressure of 4.1 MPa (600 psig). An experiment is initiated by slowly pressurizing the vessel with nitrogen. Instrumentation for characterizing the released agent outside of the vessel includes five helium-neon lasers and detectors aligned such that their beams pass perpendicularly through the centerline of the release, two dynamic pressure transducers (one placed near the exit of the vessel and one downstream centered in the flow), an aspirated hot-film positioned at the same location as the downstream pressure transducer, and two high speed (3000 and 500 frames/s) cameras.

3. EXPERIMENTAL RESULTS

Measurements have been made for each of the agents with a variety of release directions (e.g, vertically upwards and downwards). In this talk results for downward releases of two of the eleven agents--HCFC 22 (CHF_2Cl, boiling point = -41 °C) and FC 31-10 (C_4F_{10}, boiling point = -2 °C) will be emphasized. These two agents cover a range of physical properties typical of the eleven compounds.

High-speed films show that the mixing behavior of the agents is very complex. When HCFC 22 is released a very rapid expansion (flashing) of the agent is evident near the vessel exit immediately following the disk bursting. Shortly afterwards, a liquid flow develops near the exit with flashing occurring further downstream. Near the conclusion of the liquid release a second, extremely strong flash is observed at the exit. FC 31-10 has a different behavior. The initial flash is much less intense, while a second more intense flash (relative to the first flash, not to HCFC 22) is observed near the end of the liquid release.

Figure 1 shows examples of external pressure traces observed during releases of HCFC 22 and FC 31-10 for the pressure transducer located near the vessel exit. The effects of the two "flashes" observed in motion pictures of the release are evident for the HCFC 22. As expected, based on the films, only one much weaker flash is detected for the FC 31-10. The downstream pressure transducer records a very high transient pressure (not shown) when the FC 31-10 arrives, while the HCFC 22 generates a much smaller pressure rise. This behavior is attributed to the relative degree of vaporization of the two agents.

Time records for the lasers are shown in Figure 2 for a release of FC 31-10. Sharp extinctions are observed when the released agent reaches a laser beam. Average velocities were determined from laser

[1]Sponsored by USAF Wright Patterson Laboratory

extinction times for the downstream edges of the two-phase flows. Different behaviors are found for the two agents. For HCFC 22 the highest velocities are recorded near the vessel exit with lower velocities further downstream. The reverse is true for the FC 31-10 where the highest velocities are measured for positions far removed from the vessel exit.

Both the hot-film measurements and downstream dynamic pressure measurements indicate that a much larger fraction of the higher boiling agent (FC 31-10) remains as a liquid for the furthest downstream measurement station than for HCFC 22.

4. DISCUSSION

Observed behaviors for all of the releases are consistent with nonboiling liquid being forced from the vessel by the high pressure gas above it. As the agents exit the pressurized vessel as liquids they become superheated (i.e, the vapor pressure of the liquid is greater than atmospheric pressure). Superheated liquids boil very rapidly leading to rapid volume expansion. This process is known as flashing. Flashing results in a rapidly expanding two-phase flow. The period required for a superheated fluid to flash decreases with increased superheating (higher boiling liquids require longer periods to flash). All of the measurements discussed above can be understood in terms of differences in boiling points between HCFC 22 and FC 31-10.

The findings suggest that room temperature release rates of the various agents from the vessel will not vary greatly. However, the vaporization and mixing behaviors of the released agents outside of the vessels do depend dramatically on the agents' properties. Such variations in vaporization and mixing behavior affect the ability of an agent to suppress a fire. Criteria need to be developed to characterize such effects.

[1] D. M. Zallen, "Halon Replacement Study," Report Prepared for Aeronautical Systems Division, Wright-Patterson AFB, OH.

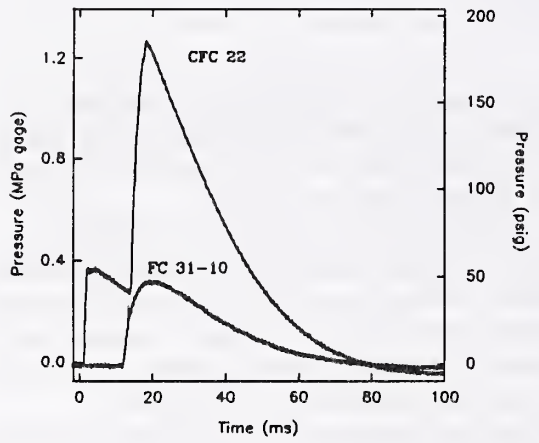

Figure 1. Pressure traces detected near vessel exit for releases of HCFC 22 and FC 31-10.

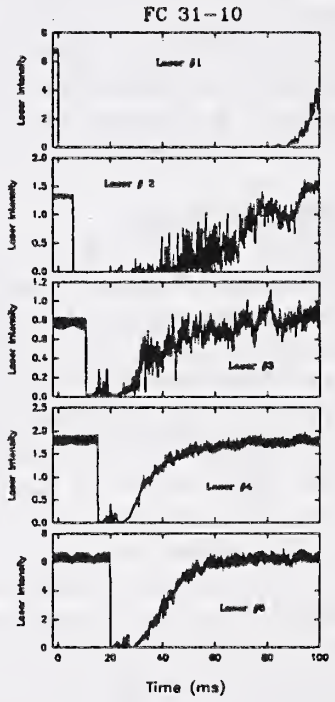

Figure 2. Extinction of laser beams located 0, 32.0, 65.5, 96.0, and 130.0 cm from vessel exit by a release of FC 31-10.

Experimental Studies on the Extinction of Diffusion Flames Using Halon Substitutes

by

K. Seshadri and D. Trees
Center for Energy and Combustion Research
Department of Applied Mechanics and Engineering Sciences
The University of California, San Diego
La Jolla, California - 92093

ABSTRACT

An experimental study was conducted to characterize the relative influence of various inhibiting agents in extinguishing diffusion flames burning liquid fuels. The liquid fuels used were heptane and JP-8, and the agents tested were C_3HF_7 (HFC-227), CHF_2Cl (HCFC-22), CH_2FCF_3 (HFC-134a), C_2F_6 (FC-116), $CHFClCF_3$ (HCFC-124), CHF_2CF_3 (HFC-125), C_3F_8 (FC-218), C_4F_{10} (FC-31-10), cyclo-C_4F_8 (FC-318) and CH_2F_2/CHF_2CF_3 (azeotrope) (HFC-32/HFC-125). Since, these agents are considered as possible substitutes for Halon 1301 (CF_3Br), the effectiveness of these agents in extinguishing diffusion flames were compared with that of CF_3Br. The experimental configuration employed in the study, was the diffusion flame stabilized in the mixing layer produced by directing an oxidizing gas stream downward on to the burning surface of the liquid fuel. This configuration is referred to in the literature as the counterflow configuration and is a convenient geometry for detailed fundamental studies of the structure and mechanisms of extinction of diffusion flames. The oxidizing gas used in the experiments was a mixture of air and the inhibiting agent.

Critical conditions of extinction of the flame, in terms of the composition of the oxidizing stream as a function its volumetric flow-rate at extinction, were measured over a wide parametric range. The injection velocity of the oxidizing stream was presumed to be equal to the ratio of the volumetric flow rate of the oxidizing gas mixture to the cross-sectional area of the duct. The strain rate, which is a measure of the characteristic flow time τ_f was calculated from the injection velocity of the oxidizing gas stream and the characteristic length of the system which is taken to be the distance between the exit of the gas duct and the surface of the liquid pool. In Figs. 1 and 2 the strain rate is plotted as a function of the mole fraction of the inhibiting agent at extinction for diffusion flames burning heptane and JP-8 respectively. For comparison Figs. 1 and 2 also shows the amount of N_2 which must be added to the air stream to extinguish the flame in absence of the inhibitor. At a given value of the strain rate the mole fraction of CF_3Br required to extinguish the flame is lower than the mole fraction of all other agents and N_2. Therefore, when compared to all the agents tested here, CF_3Br is most effective in extinguishing the flame. The results shown in Figs. 1 and 2 are a rough measure of the effectiveness of various agents in extinguishing these flames. The experimental data was interpreted by examining the value of the Damkohler number at extinction.

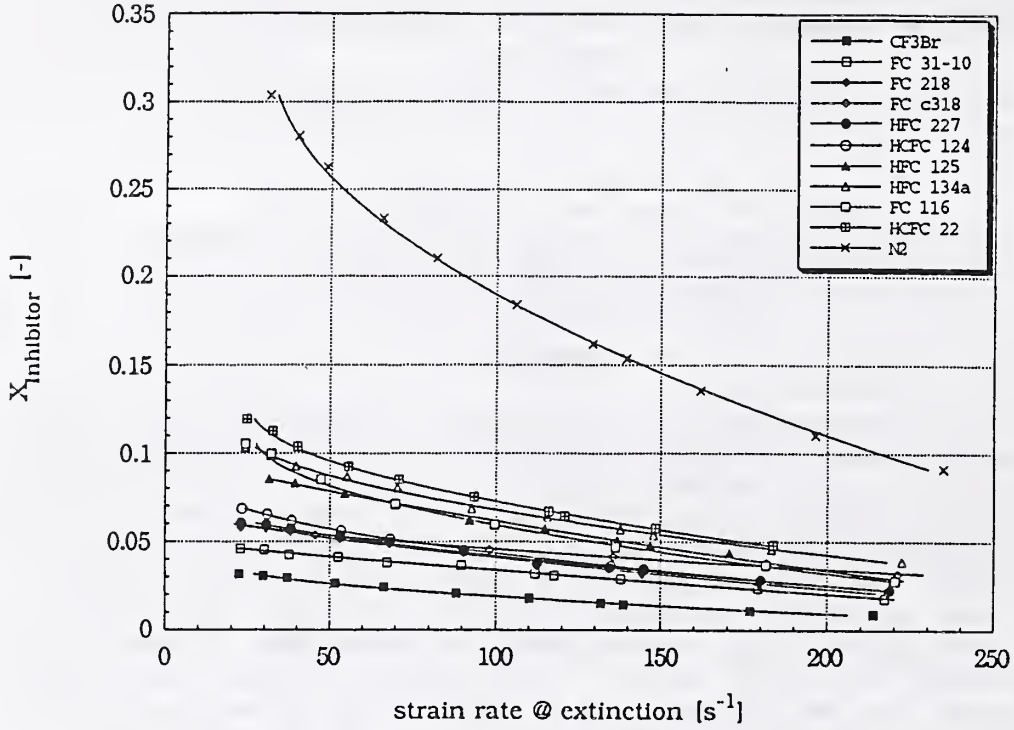

Figure 1. The strain rate as a function of the mole fraction of the inhibiting agent in the oxidizer gas stream at extinction of diffusion flames burning heptane.

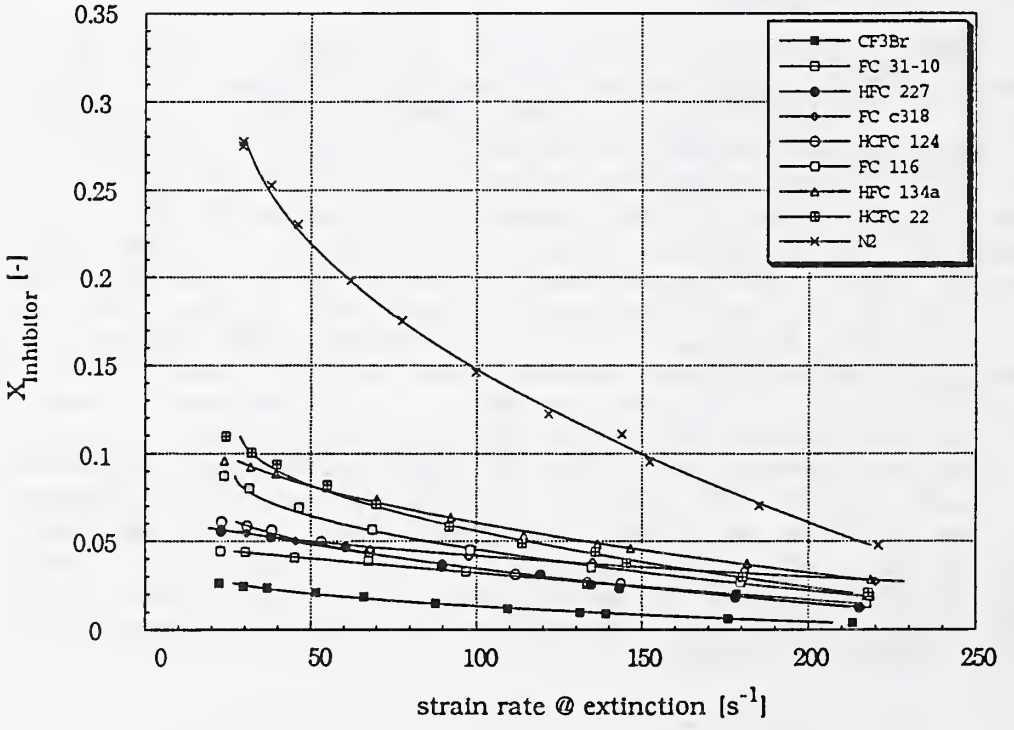

Figure 2. The strain rate as a function of the mole fraction of the inhibiting agent in the oxidizer gas stream at extinction of diffusion flames burning JP-8.

HALON REPLACEMENTS TESTED IN A CUP BURNER

A.Hamins, R.G. Rehwoldt, T. Cleary, and M. Nyden
Building and Fire Research Laboratory
National Institute of Standards and Technology
Gaithersburg, MD 20899

The results from a series of flame extinction measurements are described which seek to find a suitable replacement for the ozone-depleting fire suppressant, CF_3Br, for in-flight fire protection. Gases, liquids and solid powder agents were tested in a cup burner to determine the relative suppression effectiveness of the agents. The critical agent concentration in the oxidizer stream at extinction in a cup burner flame was measured. The agents tested included inert gases, gaseous and liquid halogenated agents, and sodium bicarbonate powder. Fuels tested included pure liquids and gases as well as multi-component liquids.

In order to perform the measurements using $NaHCO_3$, a motor driven screw feed powder delivery system was developed. Wire mesh screens were used to reduce turbulence. Powder concentration inside of the chimney of the cup burner was monitored using a HeNe laser and detector. Quantification of the powder flow was achieved by vacuum sampling into a funnel/filter assembly for 60 sec. The powder was washed from the assembly into a pyrex flask which was subsequently baked and the powder weighed. Because a number of previous studies have denoted the importance of particle size in flame extinction, several powder size fractions were utilized. Powder, exiting the burner chimney was collected and characterized by optical microscopy.

On a mass basis, $NaHCO_3$ was one of the most effective agents, more effective than Halon 1301, which is in agreement with work by previous investigators. Fluorinated and partially chlorinated agents exhibited practically the same suppression effectiveness as inert nitrogen, while the partially brominated agents were much more effective. On a volumetric basis, the most effective agents contained bromine. The most effective fluorinated agents were those that contained a large number of fluorine atoms. A simple heat capacity model was applied in order to differentiate between physical and chemical suppression action of the agents.

Results from extinction measurements in an opposed-flow diffusion flame will be compared to the cup burner results. It is suggested that the results determined in these different experimental configurations are related through the critical Damkohler Number (D_e) at extinction, where D_e is the ratio of a characteristic flow time to a characteristic chemical reaction time.

ACID GAS FORMATION IN INHIBITED FLAMES

G.T. Linteris, Y.E. Hsin, A. Liu, R. Harris

Building and Fire Research Laboratory
National Institute of Standards and Technology
Gaithersburg MD 20899

Introduction: Although the corrosiveness and toxicity of candidate fire suppressants have always been recognized as important, it has also been observed that since the most effective flame suppressants are not chemically inert the properties of their decomposition by-products are also important. Halogenated hydrocarbons (halons) are widely used and effective flame suppressants; however, their production will be discontinued in January 1994. The proposed alternatives to halon 1301 (CF_3Br), primarily fluorinated and chlorinated hydrocarbons, appear to be required in much higher concentrations than 1301. Consequently, they have the potential to have correspondingly higher concentrations of decomposition by-products. Since most hydrocarbon-based compounds at flame temperatures typically undergo both thermal decomposition and decomposition by radical attack, the formation of products other than the inhibitor itself is highly probable. The acid gases hydrofluoric (HF) and hydrochloric acid (HCl) are believed to be the most corrosive products. The concentrations of HF and HBr in the burned gases of premixed flames inhibited by CH_3Br and by CF_3Br have been reported[1,2]. While several small and large scale tests of the acid gas formation in suppressed fires have been conducted[3,4,5,6,7], there have been few attempts to understand the relationship between fuel and inhibitor type, flame characteristics, and the concentrations of by-products formed. The formation of toxic and corrosive by-products in flames suppressed by halons may be controlled by transport rates of the agent into the flame, chemical kinetic rates, or equilibrium thermodynamics.

Experimental Approach: A cup burner[8,9] is used for the measurements. The burner consists of a 28 mm diameter pyrex cup positioned concentrically in a 120 mm diameter 450 mm tall chimney at about 150 mm from the base. The cup is filled with a liquid fuel which is maintained at a constant level and an over-ventilated co-flow diffusion flame is established in the chimney with overall equivalence ratios of 0.1 to 0.25 for propane and 0.4 to 0.9 for JP-8. For gaseous fuels, the cup is filled with 1 mm diameter glass beads and covered with a stainless steel screen. The inhibitor is added to the air stream. Gas flows are measured with calibrated rotameters; the liquid fuel flow rate is determined by timing and weighing the liquid fuel supplied from a reservoir. A wet chemistry technique is used to measure the HF and HCl concentrations in the exhaust gases from the cup burner. A quartz probe extracts a measured fraction of the product gases (approximately 0.5 %), and directs the gases through polyethylene sample lines to polyethylene impingers filled with water which traps the acid gases. The sample flow is continued for a total collection time of sixty seconds. The quartz probe and sample lines are washed with water which is returned to the impinger. The sample is tested for F^- and Cl^- using ion-selective electrodes. It should be noted that since COF_2 is know to rapidly hydrolyze in the presence of water, this technique for acid gas measurement includes F^- from both HF and COF_2.

Analytic Model: A first estimate of the amount of HF or HCl present in the product gases can be made by assuming: 1.) complete reaction of the inhibitor molecule with fuel and air to the most stable products; 2.) equal rates of transport for oxygen and the inhibitor to the flame sheet; 3.) the inhibitor in the air stream which by-passes the flame sheet does not decompose through interaction with the post-combustion product gases.

Results: Table 1 lists the concentration of inhibitor in the air stream (corresponding to a concentration of about 50% of the amount required to extinguish the flame) for propane flames, and lists the measured concentration of HF in the product stream and the concentration estimated as described above for the inhibitors tested. As the table indicates, even with this very simple model, reasonable agreement is obtained between the estimated and measured HF concentrations. Continuing work will determine the importance of kinetic limitations and variations in diffusion rates.

Table 1 - Estimated and measured HF concentration (in percent) in product gases of propane cup burner flames in air.

	Propane		
Inhibitor	[Inhib]	$[HF]_{est}$	$[HF]_{meas}$
C_2F_6	4.7	4.2	2.1
C_2HF_4Cl	4.3	2.8	1.9
C_2HF_5	5.1	4.1	3.6
$C_2H_2F_4$	5.2	4.3	2.8
C_3F_8	3.6	4.1	2.6
CHF_2Cl	7.1	2.2	1.7
C_3HF_7	3.1	5.0	3.6
C_4F_8	3.9	4.3	4.4
C_4F_{10}	3.3	4.8	2.7
CH_2F_2/C_2HF_5	9.5	6.9	4.2

References

1. Wilson, W.E., Jr., "Structure, kinetics, and mechanisms of a methane-oxygen flame inhibited with methyl bromide," *Tenth Symposium (International) on Combustion*, The Combustion Institute, Pittsburgh PA, 47-54, (1965).

2. Biordi,J.C., Lazzara, C.P., Papp, J.F., "Flame-structure studies of CF_3Br-inhibited methane flames," *Fourteenth Symposium (International) on Combustion*, The Combustion Institute, Pittsburgh PA, 367-381, (1973).

3. Sheinson, R.S., Musick, J.K., and Carhart, H.W., "HF and HBr production from full scale CF_3Br (Halon 1301) fire suppression tests," Journal of Fire and Flammability, **12**, 229-235, (1981).

4. Sheinson, R.S. and Alexander, J.I., "HF and HBr from Halon 1301 extinguished pan fires," Fall Meeting, Eastern States Section Meeting/The Combustion Institute, Pittsburgh PA, Paper 62, (1982).

5. Sheinson, R.S., Penner-Hahn, J.E., and Indritz, D., "The physical and chemical action of fire suppressants," Fire Safety Journal, **15**, 437-450, (1989).

6. Ferreira, M.J., Hanauska, C.P., and Pike, M.T., "Thermal decomposition product results utilizing PFC-410," Halon Alternatives Technical Working Conference, New Mexico Engineering Research Institute, Albuquerque, NM, May, (1992).

7. Ferreira, M.J., Hanauska, C.P., and Pike, M.T., "An update on thermal decomposition product results utilizing PFC-410," Halon Alternatives Technical Working Conference, New Mexico Engineering Research Institute, Albuquerque, NM, Oct., (1992).

8. Booth, K., Melina, B.J., Hirst, R., "Critical concentration measurements for flame extinction of diffusion flames using a laboratory 'cup burner' apparatus," Imperial Chemical Industries Limited, Mond Division, Cheshire, UK 31 August, (1973).

9. Balpai, S.N., J. Fire and Flammability, **5**, 255, (1974).

Carbon Monoxide Production in Compartment Fires by Wood Pyrolysis

William M. Pitts, Erik L. Johnsson, Nelson P. Bryner
Building and Fire Research Laboratory
National Institute of Standards and Technology
Gaithersburg, MD 20899 301-975-3083

Introduction

Nearly 4000 fire deaths occur each year in the United States. [1] Roughly two thirds of these deaths can be attributed to carbon monoxide. [2,3] Carbon monoxide is known to be the dominant toxicant in smoke. [4] Yet, despite its importance, the production mechanisms for CO are poorly understood, and it is not possible to predict levels generated in an enclosure fire. A long-term program (Carbon Monoxide Production and Prediction Priority Project) at the Building and Fire Research Laboratory (BFRL) of the National Institute of Standards and Technology (NIST) is seeking to develop an understanding of and predictive capability for the generation of CO in compartment fires. [5]

Victims in many fires have extremely high levels of carboxyhemoglobin in their bloodstreams. This is evidence for the generation of very potent concentrations of CO. A 1987 townhouse fire in Sharon, PA killed three people. The fire was isolated in the kitchen which had a very heavy fuel loading of wood. One of the victims was found to have an extremely high carboxyhemoglobin level. [6] This fire prompted BFRL investigators to conduct an experimental simulation of the fire at the NIST full-scale fire facility. CO concentrations (dry volume) as high as 8.5% downstairs and 5% in upstairs rooms were measured. [6] The observation of CO levels this high in this fire test, as well as others, prompted speculation as to mechanisms of CO production which can account for them.

Research on wood pyrolysis has shown that 30% of the mass of fuel pyrolyzed at 1100 K is converted to CO. [7] The potential for this to boost CO production in compartment fires prompted an investigation of wood pyrolysis as a possible source of high CO. The existing Reduced Scale Enclosure (RSE) test facility [8] at NIST was used. The RSE was modified to include wood in the upper layer, and twelve experiments were performed with various levels of natural gas piloting. Temperatures and CO, CO_2, and O_2 concentrations inside the RSE were measured for each test.

Experimental

The RSE is described in detail elsewhere [8]. It is a 2/5 scale ISO/ASTM standard room [9,10] constructed of a steel frame, sheet metal walls, and lined on the inside with 2 layers of 1.27 cm $CaSiO_2$ board. The RSE has been extensively tested using natural gas as fuel. The instrumentation consists of thermocouple trees and sampling probes in the front and rear upper layer of the fire. Sample gases are analyzed for CO, CO_2, and O_2 concentrations. Data was recorded every ten seconds, and each fire was videotaped as a visual record.

The ceiling and the upper 35.6 cm of the walls of the RSE were lined with a layer of 0.64 cm fir plywood. Natural gas fires from 45 to 600 kW, assuming complete combustion, were used to pilot the wood and/or establish a vitiated upper layer of combustion product gases. For fires of heat release rate greater than 200 kW from natural gas, pyrolysis of the wood and its involvement in the fire occurred nearly instantaneously. For natural gas heat release rates less than 200 kW, a delay was observed before the wood became involved in the fire. Two tests were performed with the natural gas shut off upon the ignition of the wood. The duration of each test was governed by the time for ignition, complete burning of the wood from the upper layer, and substantially complete burning of the wood coals on the floor of the enclosure.

Results and Discussion

Figure 1 shows a plot of CO concentration versus time for two 400 kW natural gas fires, one of which had an added fuel loading of plywood in the upper layer. For the gas/wood fire, the wood became involved immediately after the natural gas was ignited (120 seconds). The CO levels observed in the rear of the upper layer while the wood remained in the upper layer were greater than 14%. In the front, the CO concentration increased to about 6%. At about 350 seconds, pieces of wood began to fall from the walls and ceiling. By 500 seconds, significant amounts of wood were burning on the floor. The two-layer flow structure in the room was disrupted for a time by the fallen wood. After the wood fell, the CO levels returned to those characteristic

of a 400 kW natural gas fire, 2% in the rear and 3% in the front. The subsequent burning of the wood on the floor did not generate any more CO than is typical of a strictly natural gas fire.

Figure 2 shows a plot of CO concentration versus time for two 50 kW natural gas fires, one of which had the wood lining. The fire was ignited at 120 seconds. The delay in the appearance of the CO to 240 seconds shows that a two minute period was required for the wood to become involved. CO concentrations observed once the wood became involved are similar to those for the 400 kW gas/wood fire. After the wood fell, however, the CO returned to the very low level associated with the 50 kW natural gas fire.

The wood fires for which the natural gas was shut off after the wood ignited also showed similar behavior to the other wood fires until the wood fell to the floor. After that time, the burning and then smoldering coals produced almost no CO. All of the wood fires produced similar CO concentrations up to the point of the wood falling.

Conclusions

The results of twelve fires in the RSE lined with wood in the upper layer confirm an important new mechanism of CO formation in enclosure fires. Pyrolysis of wood in high temperature, vitiated environments, such as the upper layer of a flashed-over, underventilated enclosure fire, directly generates large quantities of CO. Experimental observations of CO concentrations upwards of 14% help to explain similarly high levels observed in such disastrous fires as that in Sharon, PA, where there was a considerable wood loading.

REFERENCES

1. Karter, Jr., M. J. Fire Losses in the U.S. During 1991. *NFPA Journal*. 86(5):32-43; Sept./Oct.
2. Harland, W. A.; Anderson, R. A. Causes for Death in Fires. Proceedings, Smoke and Toxic Gases from Burning Plastics; pp. 15/1-15/19; Jan. 6-7, 1982, London, England.
3. Harwood, B.; Hall, J. R. What Kills in Fires: Smoke Inhalation or Burns?. *Fire Journal* 83(3):29-34; 1989 May/June.
4. Babrauskus, V.; Levin, B. C.; Gann, R. G.; Paabo, M.; Harris, Jr., R. H.; Peacock, R. D.; Yusa, S. Toxic Potency Measurement for Fire Hazard Analysis. National Institute of Standards and Technology Special Publication 827; December 1991. 107 p.
5. Pitts, W. M. Long Range Plan for a Research Project on Carbon Monoxide Production and Prediction. National Institute of Standards and Technology Internal Report NISTIR 89-4185; 1989 October; 40 p.
6. Levine, R. S.; Nelson, H. E. Full Scale Simulation of a Fatal Fire and Comparison of Results with Two Multiroom Models. National Institute of Standards and Technology Internal Report NISTIR 90-4268; August 1990. 101 p.
7. Arpiainen, V.; Lappi, M. Products from the Flash Pyrolysis of Peat and Pine Bark. *Journal of Analytical and Applied Pyrolysis* 16(4):355-376; 1989.
8. Bryner, N. P.; Johnsson, E. L.; Pitts, W. M. Carbon Monoxide Production in Compartment Fires - Reduced-Scale Enclosure Test Facility. NISTIR to be published.
9. Fire Tests - Full Scale Room Test for Surface Products. Draft International Standard ISO/DIS 9705. International Organization for Standardization. 1990; 41 p.

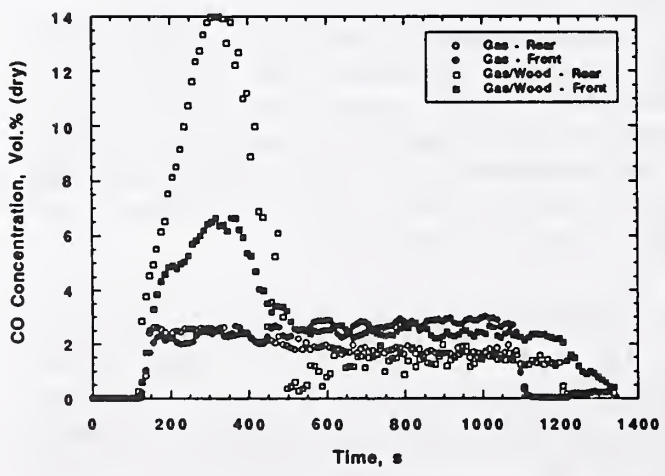

Figure 1: Carbon monoxide concentration versus time. Results for 400 kW natural gas fires in RSE with and without wood lining the upper layer.

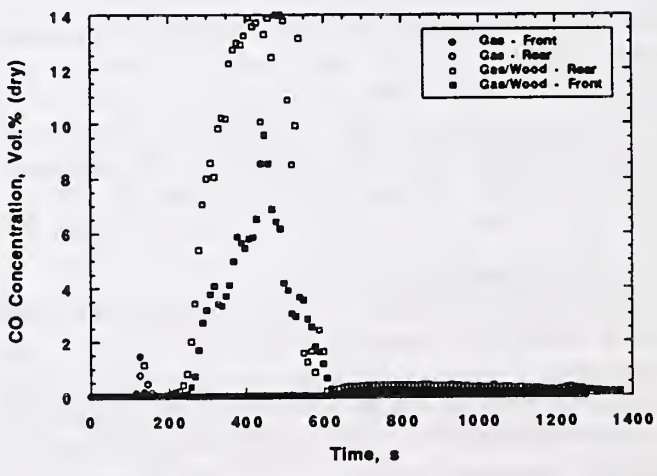

Figure 2: Carbon monoxide concentration versus time. Results for 50 kW natural gas fires in RSE with and without wood lining the upper layer.

CO and Smoke Signatures for Smoldering Coal Combustion

by J. C. Edwards, M. R. Egan, and J. Corry

U.S. Department of the Interior, Bureau of Mines
Pittsburgh Research Center, P.O. Box 18070
Pittsburgh, Pennsylvania 15236

ABSTRACT

Smoldering coal combustion experiments were conducted in the Pittsburgh Research Center's 0.8-m-square intermediate scale fire tunnel in order to characterize the predominant incipient fire signatures of smoke and CO for fire detection in a mine (1). This information is useful for mine fire location and miner rescue. For the first three experiments a 14 kg mass of Pittsburgh seam coal particles with diameters less than 4 cm was heated by an embedded 0.1 m diameter cylindrical heater which produced 1.1 kW of thermal energy. The cylindrical heater simulated an overheated roller on a mine conveyor belt drive. Smoke particle mass and number concentration were determined independently with a condensation nuclei monitor (CNM), a tapered-element oscillating microbalance (TEOM), and a submicron particulate detector (SMPD). A three wavelength optical detector was used to determine optical density and particle size over an optical path of 0.68 m. The tunnel is instrumented to measure CO, CO_2, SO_2, H_2S, and NO. An array of eight thermocouples was used to monitor the coal temperature during heating. Results of three experiments for linear airflow rates of 0.76 and 2.48 m/s in which the smoldering combustion leads to flaming combustion have shown that the CO concentration reaches 5 ppm and the optical density (OD) reaches 0.044 m^{-1}, corresponding to a 10 pct obscuration over a 1 m optical path length, within 10 min of each other for one experiment, and within 2 min of each other for the other two experiments. CO alarm thresholds less than 5 ppm are not practical. It was observed that during smoldering the ratio of smoke mass concentration to CO mass concentration (R_3) reached a quasi-steady state value of 0.6 to 1.1. Application of a mathematical buoyancy driven thermal model to the experimental configuration predicted the onset of CO production for two of the experiments, and predicted the coal temperature 3 cm above the heating prior to flaming for the three experiments. In addition to the embedded cylindrical heat source experiments, experiments were conducted with electrical stripheaters embedded at the bottom of a mass of coal particles.

Two experiments were conducted with heater strips embedded in 10 kg of coal particles prepared as for the above referenced experiments. In each experiment linear airflow of 0.5 m/s was maintained over the coal pile, with 0.5 kW power supplied in one experiment, which resulted in a smoldering steady-state, and 1.1 kW in the other. The heater temperature reached a steady-state of 610° C and the CO production rate reached a constant 0.01 $mg/m^3/s$, without flaming combustion, for the 0.5 kW heater source, whereas the 1.1 kW heat source drove the coal to flaming combustion when the strip temperature reached 560° C. Larger smoke particles as determined from the optically measured volume-to-surface diameter using Mie scattering theory were associated with the lower temperature regime. For the 0.5 kW heater source the optically measured smoke particle diameter decreased asymptotically from 0.55 μm to 0.35 μm over the smoldering period; for the 1.1 kW heat source the smoke particle diameter decreased from 0.4 μm to 0.35 μm over the smoldering period. Maximum values of R_3 were 0.45 and 0.9 for the 0.5 kW heat source and the 1.1 kW heat source respectively. A difficulty in the interpretation of R_3 is the partial clogging of the TEOM filter during the experiment.

As expected, there was a decrease in the time spread, from 28 min to 2 min, between the CO reaching 5 ppm and the OD reaching 0.044 m^{-1} as the heating rate was

increased from 0.5 kW to 1.1 kW. A commercially available ionization smoke detectors was used in both experiments. An increase in the heating rate from 0.5 kw to 1.1 kw resulted in a decrease in the CO level at alarm from 10 ppm to 3 ppm. The associated heater temperatures were 350° C and 230 ° C. The characterization of CO levels and CO growth rates relative to a fixed smoke detector alarm is useful for characterizing the extent of an embedded fire in mined coal.

The 0.5 kW smoldering heating experiment was forced into flaming combustion by increasing the power input to 0.8 kW. The smoke particulate number concentration, which had been relatively constant during the smoldering stage, rapidly increased by a factor of 3, while the smoke mass concentration decreased. This latter effect is associated with a decrease in the smoke particulate diameter from 0.35 μm to 0.20 μm. The optical transmission of the average of the 0.45 μm and 0.63 μm wavelength in the visible regime decreased from 60% to 30%. A comparison is made between measured volume-to-surface, mean mass, and number mean smoke particulate diameter as determined from measurements with the optical detector, CNM, TEOM, and SMPD.

REFERENCE

1. Edwards, J. C. and M. R. Egan. Smoldering Combustion of Coal-Measurement and Prediction. Central and Eastern States Meeting of the Combustion Institute, New Orleans, LA, March 15-17, 1993, pp. 425-428.

ASYMPTOTIC LIMIT OF SMOKE GENERATION EFFICIENCY AND EFFECTS OF STRUCTURE FOR HYDROCARBON FUELS

By
A.Tewarson
Factory Mutual Research Corporation
Norwood, MA 02062

Generation of smoke in fires has been investigated in many studies from the fundamental and applied research point of view. Numerous measurement techniques have been developed. For example, Notarianni *et al* [1] have used flux (mass deposition), carbon ratio, and light extinction methods to quantify smoke generation in well-ventilated crude oil fires in: 1) small pools (0.085 m diameter), 2) intermediate pools (0.6 m diameter), 3) large pools (2.0 m diameter), and 4) very large pools (7 to 17 m effective diameter). The three methods give similar results. Smoke yield increases with fire diameter [1], as shown in Fig. 1, where smoke generation efficiency is plotted against the fire diameter. Smoke generation efficiency, η_s is the smoke yield normalized by the maximum stoichiometric yield of carbon (fraction of vaporized fuel carbon converted to carbon particulate and emitted from the flame). The η_s value appears to reach an asymptotic limit of about 0.17. The increase in η_s values with fire diameter is suggested to be due to decrease in mixing of entrained air with fuel in the flame [1].

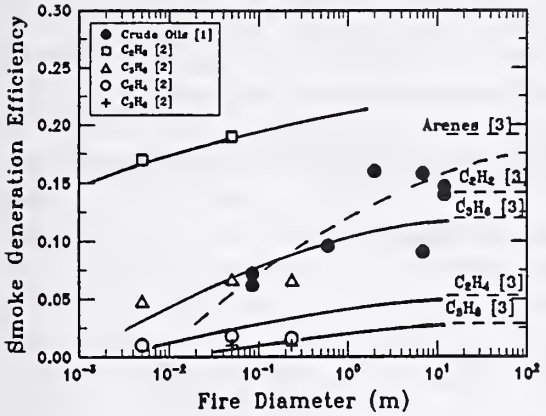

Figure 1. Smoke Generation Efficiency Versus Fire Diameter.

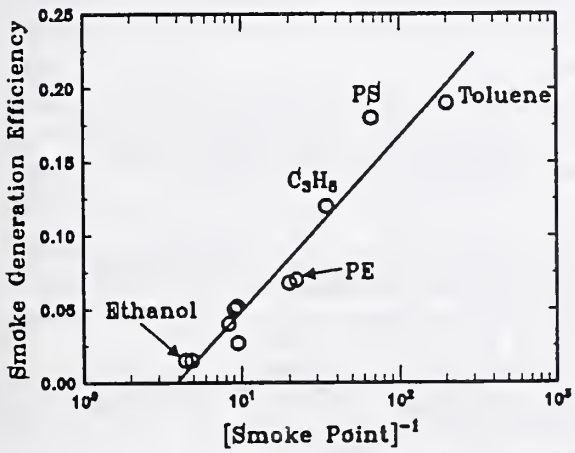

Figure 2. Smoke Generation Efficiency Versus Inverse of Smoke Point.

The η_s values for turbulent acetylene, propylene, ethylene, and propane diffusion flames, burning in still air, have been quantified by Sivathanu and Faeth [2], using light extinction method Their data, plotted in Fig. 1, also show that η_s values increase with fire diameter. The increase in η_s values is suggested to be due to increase in heat release rate (residence time in the flame) relative to smoke point heat release (smoke point residence time) [2].

We have also measured η_s values for variety of fuels in buoyant turbulent diffusion flames, using flux (mass deposition) and light extinction methods [3]. The η_s values for arenes, acetylene, propylene, ethylene, and propane, measured in our laboratory, are indicated by the dashed lines in Fig. 1. Our η_s values appear to represent the asymptotic limit for each fuel. The η_s value for acetylene, however, shows deviation. The value measured by us is 0.14, whereas the values reported by Sivathanu and Faeth [2] are higher than the value for arenes, which is not expected. The asymptotic η_s value for the crude oils appears to be between the values for arenes and acetylene.

We have also correlated η_s and smoke point values, measured in our laboratory, as shown in Fig. 2. The correlation suggests the following relationship:

$$\eta_s = 0.0514 * LN(1/L_s) - 0.070 \qquad (1)$$

where L_s is the smoke point in m measured in our laboratory. From correlations between L_s values

from our and other laboratories, η_s values for variety of fuels have been calculated from Eq. (1). The calculated η_s values, assumed to represent asymptotic values, are tabulated in Ref 3.

Koylu and Faeth [4] have quantified η_s values for liquid fuels using fuel soaked wicks. Table 1 compares their values with our values.

Table 1. Smoke Generation Efficiencies for Liquid Fuels

Fuels	Smoke Generation Efficiency	
	Koylu & Faeth [4]	This Study[a]
Toluene	0.16	0.20
Benzene	0.15	0.19
n-Heptane	0.0032	0.04
Isopropanol	0.00	0.02
Methanol	0.00	<0.003

[a]: asymptotic value

The η_s values for aliphatic fuels (propane, propylene, ethylene, heptane, isopropanol, and methanol), listed in Table 1 and in Fig. 1, appear to be more sensitive to fire scale than the values for aromatic fuels (toluene and benzene). It thus appears that smoke formation is less sensitive to fire scale for fuels with high smoke formation propensity, but is quite sensitive for fuels with low smoke formation propensity. The smoke formation propensity depends on the unsaturation and aromaticity of the chemical bonds in the fuels, as indicated by the data in Table 2. The data show that η_s values are sensitive to number of carbon atoms only for the low molecular weight hydrocarbons and increase with unsaturation and aromaticity of the chemical bonds. Based on this analysis, the data for crude oils in Fig. 1 suggest distillation of unsaturated and aromatic hydrocarbons as precursors for smoke formation during burning.

Table 2. Asymptotic Values of Smoke Generation Efficiency for Hydrocarbon Fuels

Fuel	Structure	No. of Carbon Atoms	η_s
n-Alkanes	C_nH_{2n+2}	n = 2-5	0.010-0.038
		n = 6-16	0.046-0.050
n-Alkenes	C_nH_{2n}	n = 2	0.052
		n =3 & 4	0.12-0.14
		n = 5-18	0.063-0.087
n-Alkynes	C_nH_{2n-2}	n = 2-12	0.10-0.14
Arenes	RC_6H_5	n = 6-21	0.18-0.20

Our study suggests that asymptotic values of η_s for fuels with carbon atoms greater than 6 would be desirable for use in smoke formation modeling in large-scale fires of hydrocarbon based liquid and solid polymers. These polymers gasify as oligomers rather than as monomers.

REFERENCES

1. Notarianni, K.A., Evans, D.D., Walton, W.D., Madrzykowski, D., Lawson, J.R., and Koseki, H., *Proceedings of the Sixth International Fire Conference, Interflame* 93, p.111-119, Interscience Communications Ltd., London, U.K., 1993.
2. Sivathanu, Y.R., and Faeth, G.M., *Combustion and Flame,* **81**: 133-149, 1990.
3. Tewarson, A., "Prediction of Fire Properties of Materials Part 1: Aliphatic and Aromatic Hydrocarbons and Related Polymers", Technical Report NBS-GCR-86-521, National Bureau of Standards, Center for Fire Research, Gaithersburgh, MD., 1986.
4. Koylu, U.O., and Faeth, G.M., *Combustion and Flame*, **87**: 61-76, 1991.

QUANTITATIVE BACKDRAFT EXPERIMENTS

C. M. Fleischmann, P. J. Pagni and R. B. Williamson

University of California, Berkeley, CA 94720

This paper extends our pervious results to provide a quantitative study of backdraft phenomena. Backdraft has been defined as a rapid deflagration following the introduction of oxygen into a compartment filled with accumulated excess pyrolyzates. There are many scenarios which can lead to backdrafts fitting this definition but the physical and chemical fundamentals underlying these phenomena are not well understood. This presentation divides backdrafts into several categories: rich backdrafts with early, middle and late ignition and lean backdrafts. For the rich case sudden compartment venting is required in order for a backdraft to occur. In the less common lean case the compartment upper layer approaches the flammable limit from the lean side with an ignition source constantly present so that sudden venting is not required. Videotapes and data illustrating each category will be presented.

A half-scale apparatus[1] was used to obtain data from 52 backdraft experiments. The primary focus of this study was the rich backdraft case where experiments included 40 with early, 5 with middle, and 3 with late ignition. Four experiments were also conducted for the lean case. Experimental parameters measured include species concentrations, (HC, CO, CO_2, O_2), layer temperatures, layer height, vent flow, compartment pressure, leakage rate, and fuel flow rate. A gas burner supplied a range (70 - 180 kW) of methane fires in a 1.2 m high, 1.2 m wide, 2.4 m long compartment with two different opening geometries: a centered horizontal slot 0.4 m high by 1.1 m wide and a centered window 0.4 high, by 0.4 m wide, as shown Fig. 1. In the rich case, significant unburned fuel (18% to 35% by volume) accumulates in the compartment after the oxygen concentration drops below ~ 10% as shown in Fig. 2. At a predetermined time, a hatch covering the front opening was released, simulating a window breaking due to thermal stresses or entry by fire service personnel. Once the compartment is open, a gravity current of cold oxygen rich air enters through the new opening and propagates across the compartment. This gravity current carries a flammable mixed layer to an existing spark located near the burner on the opposite wall (early ignition). Upon ignition, a rapid deflagration moves through the compartment culminating in a large exterior fire ball. Compartment pressure >70 Pa were recorded in these experiments. Middle ignitions were obtained by delaying the spark onset by 4 to 12 s to allow the reflected gravity current to generate a larger mixed region. Late ignitions, with 60 to 600 s delays, occurred in unburnt fuel trapped by the soffit. These rich backdraft scenarios are known to cause firefighter injuries. The lean case is more of an explosion than a backdraft. The upper oxygen concentration remains high (> 15%) and the aggregated flammable species (HC and CO) increase to the lower flammable limit. To investigate this scenario, the gas burner was shrouded with a fine mesh screen that acted to quench the flame and inhibit the combustion efficiency. The upper layer was ignited by a pilot flame left burning in the center of the compartment at the same height as the burner. A large mushroom shaped flame erupted within the compartment causing significant overpressure, as high as 350 Pa, before the pressure relief panel operated. Additional salt water model experiments of backdraft gravity currents have been compared with NIST computations by McGratten[2]

---

[1]Fleischmann, C.M., Pagni, P.J., and Williamson, R.B., "Exploratory Backdraft Experiments", Fire Technology, In Press.

[2]Fleischmann, C.M. and McGratten, K., "Modeling Compartment Gravity Currents", Submitted to Fire Safety Journal.

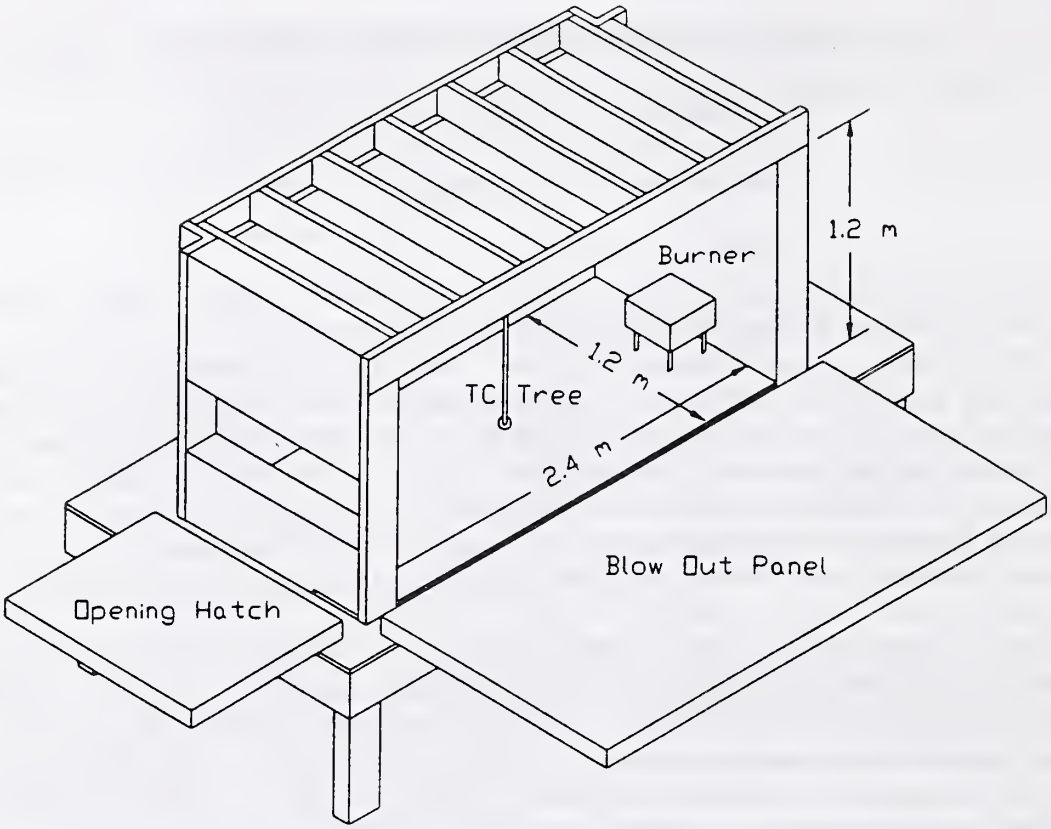

Fig. 1 Schematic of the half-scale backdraft apparatus with original slot opening.

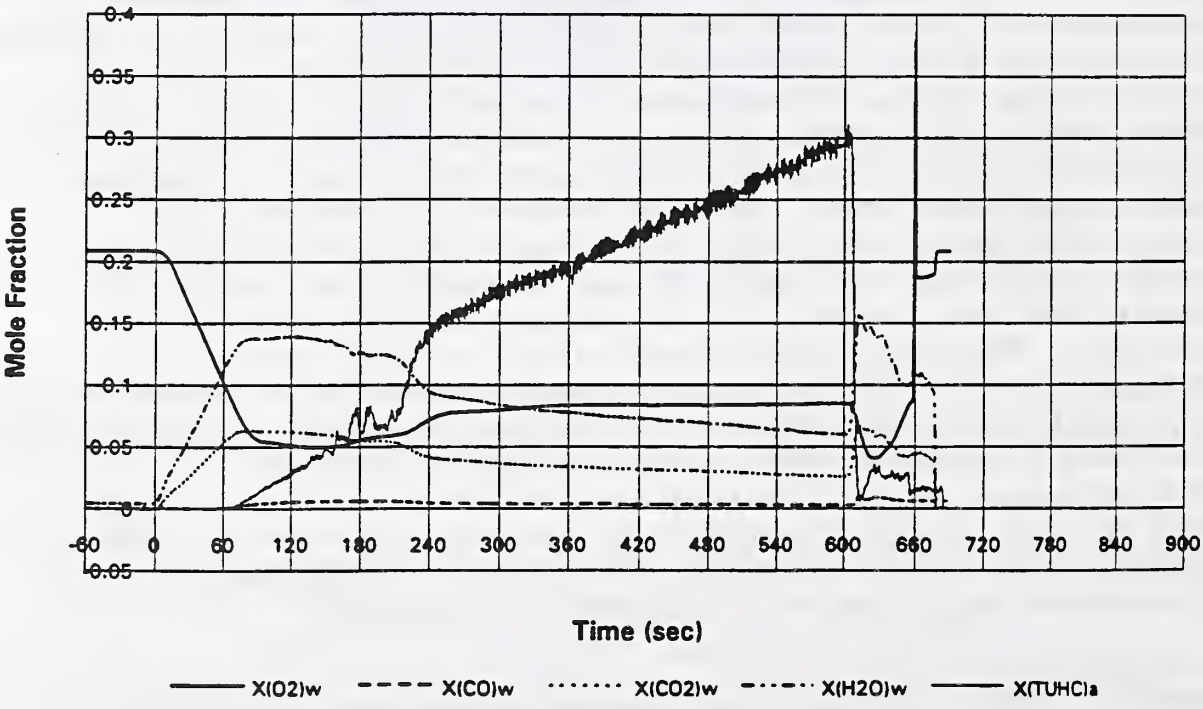

Figure 2 Typical measured upper layer gas species (O_2, CO, CO_2, H_2O, and HC) histories prior to the rich early ignition backdraft at 604 s.

Using Modeling, Research, and Professional Judgment to Analyze Fire Risk in Federally Occupied Space: The General Services Administration Program

David W. Stroup, P.E.
Fire Protection Engineer
U.S. General Services Administration

The General Services Administration (GSA) is the business agent for the United States Government. It is responsible for the acquisition and management of everything from pencils to buildings. GSA is divided into four services: the Federal Supply Service, the Federal Property Resources Service, the Information Resources Management Service, and the Public Buildings Service. The Public Buildings Service (PBS) is the Federal government's real property manager. In this capacity, PBS is responsible for the acquisition, design, construction, and operation and management of various types of space for Federal agencies. Currently, the inventory of space includes 1700 Government owned buildings and 5100 leased locations. This represents approximately 230 million square feet of space.

A number of historic buildings are included in the multitude of buildings controlled by GSA. A recent survey of buildings indicated the oldest building in the inventory was 180 years old. GSA real estate leasing policy gives preferential treatment to historical buildings.

As part of its responsibility, the GSA must ensure the safety of employees and visitors, protect Federal real and personal property, ensure continuity of Federal tenant mission, and safeguard emergency forces responding to an incident. The Fire Protection Engineering Branch within the Public Buildings Service of GSA is responsible for developing the policies and procedures used for evaluating the fire safety of government occupied buildings and coordinating implementation by the GSA regional offices throughout the nation.

GSA seeks to provide safety with cost effectiveness. Simple code compliance does not ensure an acceptable level of safety. The continual search for code compliance is not sufficient justification for resource allocation. In many cases, code requirements can conflict with each other or violate other laws (e.g., historic preservation). To ensure adequate levels of safety, the relationship between expenditures on fire safety and the actual impact of these expenditures is examined.

Most building and fire safety codes contain equivalency clauses. These clauses allow for the use of alternative methods and materials when their equivalency can be proven to the *authority having jurisdiction*. The United States Congress included an equivalency option in the Federal Fire Safety Act of 1992 (Public Law 102-522). This Act requires sprinklers or an *equivalent level of safety* in specific types of Government owned or leased high rise office buildings and Federally assisted housing.

In the past, the determination of equivalency has been based primarily on subjective judgment. Continuing research into fire phenomena has made it possible to perform an engineering analysis of the fire safety performance of a building. This building could differ widely from current perceptions of a code conforming building. Using these analytical engineering tools, the development and impact of fire in a building can be assessed. Improvement recommendations can be prioritized based on their predicted impact on the risks associated with potential fire exposure.

GSA professional staff have been involved in the development of various methods of analyzing fire safety, e.g., system concepts and NFPA 101M (*Alternative Approaches to Lifesafety*), for over 25 years. Using science-based methods, technical analysis is conducted to assess building fire safety risks and develop necessary solutions. GSA has devoted significant resources to the development, enhancement, and implementation of these building fire safety assessment methodologies.

In the last six years, GSA has spent over $2 million on research into fire phenomena. The development of *FPETool* was a significant result of this research. Using this package of analytical engineering tools, the development and impact of fire in a building can be assessed. GSA has integrated the use of *FPETool* into its design review and facility assessment processes to evaluate fire risk to occupants of GSA controlled space and improve effective allocation of resources.

Other research results have included methodologies for evaluating the response of detection and suppression systems and the effectiveness of various strategies for protecting disabled persons. Currently, efforts are underway to develop corridor flow and second room models. These models will allow for evaluation of fire impact on corridors and adjoining rooms that are adjacent to but not yet involved in the fire. Heat release rate data is vital to the successful application of most fire models. Work on a catalog of heat release rates for typical office furnishings is being initiated. Finally, validation of models and subcomponents is a continuing effort.

Various elements of modeling, research, and professional judgment are being integrated into a process for facility fire safety assessment. With the previously mentioned GSA objectives in mind, professional staff develop performance-based goals for each building, e.g., allowable damage to building, mission down time, etc. Each building in the GSA inventory is surveyed every five years by a professional staff including a fire protection engineer and an industrial hygienist. Based on data obtained during the building survey, preliminary analysis is conducted using the Fire Safety Evaluation System (FSES) contained in Chapter 7 of NFPA 101M. More detailed analysis of fire impact in these facilities is conducted using computer fire models. Actual risk conditions in each building are identified and corrective actions recommended. As necessary, resources are allocated to abate significant risks and satisfy the identified goals.

The evaluation of fire impact is the most significant step in the building fire safety assessment process. Full and bench scale tests of fuel packages, analysis of fire loss statistics, and professional judgment are used to establish design fires. Heat release rate data for design fires is contained in an expanding database. Using the design fires and building characteristics, potential fire scenarios are modeled to determine the effects on life safety, property, and mission. *FPETool* is typically used for the analysis. However, other models are employed if conditions require additional study. Finally, modeling is used to evaluate the impact of various protection schemes on the identified safety risks.

The methodology has been used to evaluate a number of buildings. The Danville Post Office-Courthouse, the Klingle Mansion, the Department of Commerce Headquarters Building, and the Department of Interior Building are examples of several historical buildings which have been examined using the assessment process. A variation of the analysis was a vital component in determining the feasibility of using staging areas to protect mobility impaired persons in Federal buildings. From applications of the methodology, necessary changes in the process and additional research are identified and implemented.

Fire Risk Assessment: A Systematic Approach for Telecommunications Facilities

Edward K. Budnick, Hughes Associates, Inc., Columbia, MD
Brian D. Kushler, Bellcore, Morristown, NJ
John M. Watts, Jr., Fire Safety Institute, Middlebury, VT

Regulatory requirements for fire safety in telecommunications facilities appropriately place emphasis on life safety and facility preservation. However, fire experience indicates that conformance with these requirements does not adequately address the fire risk to equipment or to service continuity.

Initial evaluation of this problem revealed significant conflict among demands for technical accuracy, ease of use, and implementation costs. As a result, a unique method was developed which utilizes the strengths of numerical grading systems developed in Europe and the U.S., but with significant advancements necessary to address risk factors associated with service continuity. Key elements of the methodology include a risk framework that is not linked to a regulation or fire safety code, a focus on thermal and nonthermal impact on equipment performance, and independent assessments of life safety and network integrity fire risk. In addition, limited deterministic analysis of known incident scenarios is implicit in the numerical assignments for risk impact, and provisions were made for the introduction of appropriate analytical methods as they become available.

The approach uses a point system to produce a weighted sum of the potential contributions to fire risk from individual fire safety parameters of a facility space. Weights for these parameters are developed systematically from fire safety policy, objectives, and strategies. Individual weights for each parameter are then multiplied by an intensity grade for that parameter as determined by on-site survey. The sum of these products for all parameters represents a relative measure of the fire risk to network integrity.

Parameter Weights

Components of fire hazard and fire safety in a facility space were modeled as hierarchical categories of fire risk. Five levels were defined: policy, objectives, strategies, parameters, and survey items. Each level represents a set that was partitioned into elements comprising the next lower level.

The fourth level in the hierarchy consists of the individual features of a facility that represent measurable components of the fire risk. Each feature, referred to as a fire safety parameter, contributes to achievement of the fire safety strategies, objectives, and policy. Four groups of fire safety parameters were identified: (1) facility, (2) contents, (3) fire protection, and (4) occupants. Seventeen parameters were selected to provide measures of those features within a particular space that influence the level of fire risk. These fire safety parameters are defined as components of fire risk that are quantitatively determinable by direct or indirect measurement or estimation. They are intended to represent factors that account for an acceptably large portion of the total fire risk in a facility space.

For the first four levels, a modified Delphi technique was employed to assess the relative importance of the elements comprising each level to the elements at the next higher level. The resulting matrices were combined to produce numerical weights of each of 17 fire safety parameters indicating its relative importance to the fire safety policy for network integrity.

This result can be used with any survey in which a degree of compliance or intensity is determined for each parameter. The next step involved a methodology for numerical association of survey items, the fifth hierarchical level, with the fire safety parameters to produce parameter grades.

Parameter Grades

An essential feature of fire risk assessment of a telecommunications facility is the grading of the fire safety parameters. Each identified parameter has a determined relative importance that is generalized for all cases. Individual facilities will vary in the degree to which parameters exist and impact fire risk in a space. The parameter grades are a measure of these levels of danger or security. In most cases, they are not directly measurable. This is especially true under conditions of surveying existing buildings with limited information readily available.

To simplify grading of parameters, they were partitioned into measurable constituent parts, i.e., survey items. For a number of parameters, there are also subparameters. These are defined as intermediate components of a parameter with a grade or assignment based on one or more survey items. Thus, the time determination of parameter grades is dependent on those characteristics of a room or space identified specifically as survey items.

Decision tables were used to develop the logic for translating survey items into parameter grades. Decision tables are structured forms for enumerating the possible outcomes of combinations of conditions. Each of the seventeen fire safety parameters has at least one associated decision table, utilizing appropriate survey items. For each parameter, the final outcome of a decision table is the parameter grade.

The parameter grade is defined as a relative measure of fire risk for that parameter in a specific situation. The grade is assigned from a scale of 0-5, where 0 is a theoretical optimum equivalent to zero risk, and 5 is a worst feasible case. If subparameters are involved, they are either input to another decision table or combined with subparameter weights. The resulting outputs are the parameter grades.

The scalar product of these grades with the parameter weights produces the fire risk assessment. This value can be used as an indication of the level of relative fire risk in a telecommunications facility space. In addition, when considering fire safety improvements, the relative change in risk can be evaluated for each improvement and used in conjunction with cost data to provide a benefit/cost basis for decision making.

Risk Analysis for the Fire Safety of Airline Passengers[1]

Richard L. Smith
Building and Fire Research Laboratory
National Institute of Standards and Technology
Gaithersburg, MD 20899

Introduction. The objective of this project is to develop the generic methodology and an intelligent computer program that will compute the fire risk for passengers of airlines. The program can determine the risk assuming the implementation of various fire safety regulations. The emphasis is on assisting the decision-maker gain greater understanding of the decision to be made rather than furnishing a "correct" conclusion. This report will describe the progress to date.

Airline fire safety is important for the airline passengers and for the potential flying public that needs to be assured of the safety of flying. The public has demonstrated a willingness to pay for flight safety when it is cost effective. Therefore, it is critical that fire safety regulations provide demonstrable safety improvement at an acceptable cost.

One approach to evaluating the merit of a fire safety system is to do a cost benefit analysis based on an analysis of past accidents using classical statistical techniques. We note that injuries or deaths due to airplane fires are rare events. Also, each crash is studied so that changes can be made in procedures or equipment to reduce the likelihood of a similar accident occurring. Therefore, the evidence available is inappropriate for the applications of classical statistical techniques in the fire risk analysis for the fire safety of airline passengers.
In the last decade considerable progress has been made in Artificial Intelligence in dealing with reasoning with uncertainty or vague knowledge. Some advances have used such approaches as Bayesian probability theory [Pearl], influence diagrams [Holtzman], and expert systems [Henrion]. Also, probability theory has been impacted significantly by developments in Bayesian Probability Theory and new applications of the Maximum Entropy theory [Loredo]. This project applies some of these advances to the risk analysis for the fire safety of airline passengers.

Discussion. The software to be developed for this project is required to be able to incorporate state-of-the-art safety analysis technology, the historical data on fire losses in airplanes, the results of experiments and tests, the predictions of physical science models, and experts' opinions. Also the program will have the ability to report the source of each piece of knowledge or assumption made that is used in a particular analysis. The system will allow various safety features to be analyzed independently or collectively.

---

[1]*This research was supported by the Department of Transporation's FAA Technical Center under contract number DTFA03-92-Z-00018.*

We will develop three progressively refined risk models: pilot, prototype, and production [Howard]. For each of these we will first do the basic development which includes determining the alternatives, collecting the available information, and determining the decision maker's preferences. The second major step consists of developing the deterministic structures of the model. This is followed by the probabilistic evaluation which includes the use of probability distributions instead of unique values. Then the basic appraisal is done which includes sensitivity analysis, value of information analysis, value of control analysis, and a review of the decision maker's preferences. At this point the model is either complete or we start over and iterate the process until the decision maker is satisfied.

The selected approach utilizes influence diagrams rather than decision trees. Besides providing a clear and simpler representation of the problem, influence diagrams grow linearly with the size of the problem while decision trees grow exponentially [Holtzman]. Some principal components of influence diagrams are: 1. Decision variables which are quantities over which the decision maker exercises direct control; 2. Value parameters which represent aspects of the preferences of the decision maker; and 3. Chance variables which are quantities which represent properties of states of the world.

We are reporting on the pilot version of the risk model for which we are using a beta version of a commercial software program. A pilot model is an extremely simplified representation of the problem. Its main use is for determining the most important relationships. As far as these have been determined, they will be presented. For this version the only decision is whether or not to add a water mist system to the airplane and the only preference variable is the number of deaths. The model determines the expected number of deaths with and without the water mist system. The model uses a subset of FAA's incapacitation model which addresses the effects of temperature, carbon monoxide, carbon dioxide, oxygen depletion, and hydrogen cyanide.

References:

Henrion, M., J. S. Breese, and E. J. Horvitz, *Decision Analysis and Expert Systems*, AI Magazine, Winter 1991, pp64--91

Holtzman, Samuel, **Intelligent Decision Systems**, Addison-Wesley Publishing Co.,Inc. 1989

Howard, R. A., **Influence Diagrams**, in The Principles and Applications of Decision Analysis, Vol 2 editors R. Howard and J. Matheson 1989

Loredo, T. J., *From Laplace to Supernova SN1987A: Bayesian Inference in Astrophysics* in **Maximum Entropy and Bayesian Methods**, P. F. Fougere, Editor, Kluwer Academic Publishers, 1990

Pearl, J., **Probabilistic Reasoning in Intelligent Systems: Networks of Plausible Inference**

DEVELOPMENT OF POWER-GROWTH FORMULAS FOR ACTUAL FIRE INCIDENTS

Bert M. Cohn, PE
President, Bert Cohn Associates, Inc.

The Fire Simulator in FPETOOL, version 2.06, was used to model fire incidents that occurred in an industrial building, a health club, a residence and a school. In each case, only limited witness information was available. All of the fires occurred at night. In only one case were there a few people in the building.

While the objective of the fire modeling differed in each instance, a commonality was the need to develop fire growth equations that would be close to the actual fire development, as reconstructed from the evidence.

An unexpected result was that in three of the four incidents the fires developed much more slowly than would be anticipated from the "traditional" growth rates included in the MAKEFIRE routines of Fire Simulator. Labeled as Slow, Moderate, Fast and Ultrafast, the t^2 power-growth rates included as guides for actual fire development use alpha values of .00293, .0117, .0469 and .1874, respectively.

In only the school incident did the fire appear to follow a t^2 fire development curve for a "fast" fire and then only for about 8 minutes; a "slow" decay for about 22 minutes followed. For the other incidents, the formula fire development had to be slowed down considerably below the cited examples in order to match the facts that were known in each instance. In the case of the industrial building, a t^2 fire with an alpha value of .002035, resulting in a 1 kW fire at 12 minutes, produced a fire development curve that closely matched the time frame that witnesses were able to provide for the pre-flashover stage.

For the initial stages of the residential fire, a growth rate at $t^{1.85}$ and an alpha of .002 appeared to match the very slow fire progression, producing flashover in the room of origin about 19 minutes after the start of active flaming. Fire continued to spread slowly through the property without intervention, until finally extinguished more than two hours later.

Three fire development rates were combined to simulate the fire incident in the health club. Initial t^2 fire growth was very slow (α=.002), followed by a slow period (α=.00293), and finally, very moderate growth (α=.005) as the fire involved more of the building. It took about 2 hours for the fire to reach its peak, and about 65% of the combustibles were estimated to have burned.

It was possible in each incident to calculate the approximate amount of fuel that was consumed in the course of the fire. The approximate duration of burning also was known. This provided a test for the validity of possible fire development curves that might be applicable. Burning at traditional growth rates consumes available fuel more rapidly than was indicated by the descriptions furnished by witnesses on the scene and by other time-related events.

In dramatic contrast to the slow fire development found in actual fires is the growth rate in some standardized fire tests. This was discovered while developing formulas to match the furnace fires at Underwriters Laboratories so as to be able to predict outcomes when changing some variables. In the case of the 350-pound wood crib ignited by an n-heptane spray in UL Standard 199, the extremely rapid fire development was characterized by t^3 growth with α=.480, reaching t_c in 13 seconds.

Proposed for Presentation at
The Annual Conference on Fire Research
Rockville. MD., October 18-22, 1993
SAND 93-1381A

Use of Simplified Deterministic Fire Models to Estimate Object Response for Probabilistic Fire Safety Assessments*

Louis A. Gritzo, Jaime L. Moya and Vernon F. Nicolette
Thermal and Fluid Engineering Department 1513
Sandia National Laboratories
Albuquerque, NM

A large number of fire scenarios must be considered to thoroughly assess the fire survivability of engineered systems. Many of these scenarios include an engulfing pool fire which occurs, for example, as a result of a facility fire or transportation accident. In many cases, accurate prediction of the thermal response of an object subjected to the extreme thermal environment of an engulfing pool fire requires an advanced, detailed, fire physics model. Such models are presently under development by numerous research organizations, including a collaborative effort being established between Sandia National Laboratories (SNL) and the Norwegian Institute of Technology (NTH)/SINTEF. Furthermore, even if such a model existed, applying it to *each* engulfing fire scenario would quickly become intractable due to time and computer-use constraints. Probabilistic fire safety assessments, therefore, historically have relied on statistical methods. These techniques use existing fire data to develop object heat flux and temperature frequency distributions. As data typically is restricted to a limited set of test conditions (such as wind speed, object size, shape, location, etc.), significant uncertainty is inherent when applying these distributions to a broader range of conditions. The broader range of conditions are required to evaluate all potential hypothetical accident scenarios.

Recent efforts at SNL have been focused on developing simplified deterministic models which reduce this uncertainty. These models incorporate a simplified deterministic formulation of the dominant heat transfer mechanisms. Using this approach, it is possible to estimate object response trends over an expanded range of conditions since the dominant mechanisms associated with varying fire conditions are modeled.

The development of these simplified models has provided SNL with a suite of tools which are well-suited for probabilistic fire safety assessments. Models have been developed for geometries including a vertical flat plate, an inverted flat plate (i.e. a plate oriented such that the surface is horizontal and is subjected to impinging flames), and a cylinder in cross flow. All of the simplified models include radiative heat transfer between a gray-diffuse surface and a gray-gas, and advection of energy by the buoyant gas plume. Radiative heat transfer is considered only in a direction normal to the object surface. Scattering of radiative energy is neglected, since these models have been tailored primarily for hydrocarbon pool fires. Flow fields are modeled using solutions from potential flow theory and correlations are included to model convective effects. These models have successfully illustrated the coupled responses between the object and the fire environment which have been observed in experimental data[1]. When coupled with a conduction code to model the object thermal response, these simplified models have been used to identify a regime specified by nondimensional parame-

---

1. Nicolette, V. F. and Larson, D. W. "The Influence of Large Cold Objects on Engulfing Fire Environments," Heat and Mass Transfer in Fires. J. G. Quintiere and L. Y. Cooper (eds), ASME HTD Vol. 141, pp. 63-70.

* This work was performed at Sandia National Laboratories, Albuquerque, NM and supported by the U.S. Department of Energy under Contract DE-AC04-76DP00789.

ters for which the fire can reasonably be treated as a blackbody radiant heat source[1]. Outside of this regime, differences in heat fluxes of up to 65% were observed between the gray gas treatment used in the simplified models and the blackbody treatment. Since deterministic modeling has been limited to the dominant physics, computational requirements to exercise the model remain sufficiently low. The computational efficiency of these models is required to realistically perform probabilistic fire safety assessments, since these models must be exercised on the order of thousands of times to cover a broad range of scenarios.

These simplified deterministic models require a set of input parameters consisting of the freestream gas temperature distribution, the freestream gas velocity, the effective gas absorption coefficient, a, and effective volumetric energy generation rate, S'''. Presently, experimental data is used to quantify these input parameters. This data can be applied to the problem in three different fashions: 1) through statistical use of a fire database, 2) by identifying general trends from the fire data, and 3) by performing specific tests designed to measure certain parameters. The freestream gas temperature distributions are extracted from a fire temperature database. The current fire temperature database is for free pool fires (i.e. fires without objects) over a limited range of fire conditions (i.e., wind speed and pool size). Since several tests are available for similar conditions, limited statistical analysis of the data is possible. The freestream gas velocity is determined in accordance with general trends identified from pool fire data. Typically, the freestream gas velocity is assumed to be about 5 m/s. The effective parameters a and S''' are being determined from specific tests designed to calibrate the models. In these cases, the model is employed to perform inverse calculations which use experimental data (which consists of temperature distributions and heat fluxes) as input. Recently, tests were performed to identify effective parameters for cases in which a vertical flat plate, or a cylinder in crossflow, was engulfed in a large pool fire. Although the experimental data available for calibrating these models is limited, the model can be expected to yield reasonable results outside of the region of available data since the influence of the changing conditions is accounted for by modeling the dominant heat transfer mechanisms. The error associated with applying the model outside the range of available data can be decreased, at the expense of increased computational requirements, by increasing the degree of fidelity by which the model accounts for the dominant chemical and physical processes. The use of simplified deterministic models is, therefore, a trade-off between the degree of fidelity associated with detailed models, and the computation time required to adequately perform a probabilistic fire safety assessment. The methodology being followed by SNL is to use the simplified deterministic fire models to perform preliminary scenario evaluation. The detailed fire physics models are then applied to a smaller number of scenarios which have been identified from screening the results from the simplified deterministic fire models.

Improvements in simplified deterministic models can be obtained through reducing the number of input parameters, improving the accuracy of input parameter estimates, or improving the speed of the deterministic calculations. To release the restriction of using a freestream temperature distribution, the development of a simplified partially-deterministic combustion submodel is being considered. It is expected that scoping calculations performed using a benchmarked, advanced fire physics model will allow trends in combustion and effective properties to be identified. The matrix of advanced model runs can be supported by specific test for conditions which can not yet be addressed by advanced models. The ability to accurately quantify input parameters is influenced, to a certain extent, by the ability to obtain high fidelity data. Therefore, future efforts are also being focused on developing improved measurement techniques and gaining an improved understanding of existing data. The development of an advanced radiation heat transfer model has been initiated at SNL and is expected to contribute to providing an improved understanding of fire measurements. The exploitation of the massively parallel computing environment in conjunction with improved algorithm development is also viewed as an opportunity for improving simplified, deterministic models.

---

1. Gritzo, L. A. and Nicolette, V. F. "Coupled Object Response of Objects and Participating Media in Fires and Large Combustion Systems," presented at the Symposium on Fires and Combustion Systems, 1993 National Heat Transfer Conference, Atlanta, Ga.

Coordinated Qualitative/Quantitative Risk Analysis Promoting Flexible Design and Operability

John A. Noronha, Engineering Associate & Consultant,
Fire & Explosion Protection Engineering Unit
Architectural & Engineering Services Division
Eastman Kodak Company
Rochester, NY

Chairman, Symposium on Risk Analysis and Process Safety Management
AIChE National Meeting
Atlanta, GA, April 1994

Abstract

Fire and explosion prevention and protection are significant and integral parts of chemical plant design. Hence, the risk and hazard analysis used in chemical plant design should incorporate the fire and explosion risks. This paper is an attempt to present a "coordinated" risk approach for the chemical industry, and to illustrate the highlights of the fire and explosion risk analyses and designs.

Many practicing engineers and management representatives are concerned about the growing use of a variety of risk analysis which might be invalid in certain cases.

We discussed 4 types of risk analysis, QL/L, QN/L, QL/C, and QN/C. "QL" stands for qualitative or judgmental approach to estimate risk. "QN" stands for quantitative or a computational and/or experimental approach. "L" stands for the likelihood of an event; while "C" stands for consequences of a risk event.

There is a common use of a variety of definitions of some risk terms which appear similar but can be quite different. This can be very confusing; so we will discuss them.

We will propose what we call a "coordinated" risk approach which is primarily based on qualitative judgment augmented, where feasible, with quantification estimation.

Next, we will discuss the flexibility of the use of alternate preventive and protective measures that may be used to achieve a certain level of risk which might be acceptable. Some examples of fire and explosion designs will be illustrated.

Judgment is a key criteria in a risk assessment; so we will discuss the qualifications required for such judgment.

We do expect some barriers of acceptance of this coordinated approach by extreme proponents of each type of risk analysis. We will discuss how we intend to promote this coordinated position.

Finally, we will discuss the need for guidelines of what we describe as "non-credible" cases. Basically, there are several codes, guides, and other sources of recommendations as to what needs to be considered in risk analysis and safety designs. However, there is a need for a "cut-off" point at which we feel adequate preventive and protective measures have been taken.

PROBABILITY-BASED DESIGN OF A BUILDING FOR FIRE SAFETY

Dr. G. Ramachandran,* Consultant, Risk Evaluation and Insurance

Mathematical models and associated computer packages have been developed for analysing quantitatively the risk posed by materials or products in building fires and the response of passive and active fire protection measures to these fires. These tools currently available to fire protection engineers are being continuously improved with increasing scientific knowledge about fire and combustion products and data provided by experiments. Some of these techniques also include the behaviour of building occupants at the time of a fire, response to fire alarms, use of portable extinguishers, travel through smoke and use of escape routes.

The historical development of deterministic models mentioned above has been in the treatment of patterns of fire growth and human behaviour as though the implied relationships based on scientific theories and experimental results were exactly fulfilled in real fires. This is tantamount to ignoring uncertainties involved in the evacuation behaviour of building occupants and in the development of fire, smoke and toxic gases. In the latter case, apart from environmental factors, the uncertainties are due to multiple interactions, at different times, among physical and chemical processes evolved by a variety of burning materials arranged in different ways. Reliability of active fire protection systems, if installed, is another source of uncertainty. Deterministic models are rarely validated in the light of statistics provided by real fires.

Probabilistic models, on the other hand, offer rational methods for dealing with the randomness of risk posed by fire and combustion products, behaviour of occupants and effectiveness of safety measures. These methods, well developed for structural reliability (Ref.1) and property protection (Refs.2,3), can be extended for evaluating life safety from fire, combining the movement of occupants and the spread of combustion products. In this probabilistic framework, which is time-based, the total performance of a building and fire protection measures is assessed in terms of probability of death or fatality rate per fire. Non-fatal injury rate per fire can also be included in this risk evaluation procedure. Statistics of real fires, particularly those available in the United Kingdom, provide some information for evaluating the total performance of passive and active fire protection measures.

An acceptable level specified for the total performance will provide design values for means of escape facilities, fire resistance and sizes of compartments and other passive measures constituting the design of a building. The design can be altered depending on the presence or absence of smoke control systems and other active fire protection devices. Individual fire protection measures or combinations of measures satisfying the target level prescribed for total performance can be considered in the design process. Among these alternative designs providing equivalent safety level, a property owner may select one which minimizes the total cost composed of fire loss (material and consequential), cost of fire protection and fire insurance premiums. Under the design scheme described above, an overall acceptable level of life safety from fire can only be assured in probabilistic terms for any type of building. Absolute safety is realistically unattainable or prohibitively expensive.

The basic features of the probabilistic framework suggested are as follows. A target (maximum) value, acceptable to the community, will be specified for the probability of occurrence of an undesirable event with due regard to

*Retired, Head of Operational Research Section, Fire Research Station, U.K.
Currently, Visiting Professor, Glasgow Caledonian University.

consequences in terms of life loss, fatal and non-fatal. Such events would include fire spreading beyond the room of origin, destruction of the structural barriers of a fire resistant compartment, visual obscuration due to smoke on the escape routes and incapacitation caused by toxic gases. A "large" magnitude of area damaged with "low" probability of occurrence can also be considered as an undesirable event. Casualty rate per fire is regarded as the product of two components - probability of occurrence of an undesirable event if a fire breaks out in the building and the "conditional" probability of becoming a casualty if the undesirable event occurs. The probability of fire starting during, say, a year is not considered although this component of fire risk is required for assessing the economic benefits due to safety measures on an annual basis.

The probability of fire spreading beyond a compartment by the destruction of structural barriers (not by convection) is the product of probability of flashover and the probability of compartment destruction given flashover. The latter probability depends on the probability distributions of the fire resistance of the compartment and the fire severity attained in a post-flashover fire. Design values for fire resistance can be estimated according to a safety index corresponding to the level specified for the probability of compartment destruction. Sprinklers reduce the probability of flashover. Hence, for a compartment equipped with sprinklers, the probability of compartment destruction can be increased, by lowering the fire resistance, subject to the condition that the probability of spreading beyond the compartment does not exceed the level specified.

While fire is a major threat to occupants in its immediate vicinity, it is generally smoke and toxic gases which pose the greatest threat to occupants who are remote from the fire. Smoke is likely to be the first threat appearing on an escape route followed by heat and narcotic gases. Hence, visual obscuration due to smoke would be experienced first by an occupant or group of occupants in a chain of events leading subsequently to sensory irritation and incapacitation due to burns and narcotics.

According to the scenario described above an occupant may become a casualty if the total time (since the start of ignition) taken by him/her to reach a safe place exceeds the time taken by smoke to travel from the place of fire origin and produce visual obscuration of specified magnitude on an escape route. Both the time components, movement of occupant and movement of smoke, are random variables with probability distribtutions. Based on these distributions, the probability of an occupant encountering smoke can be evaluated. An acceptable level specified for this probability would provide a design value for the evacuation time used in determining maximum travel distance and number and widths of escape routes.

The "design evacuation time" mentioned above is one of three components consituting "the total evacuation time". Discovery time and "recognition time" are the other two components. For a building equipped with sprinklers or detectors the design evacuation time can be increased up to a limit such that the level specified for the "encounter probability" is not exceeded. Smoke control systems would enable the occupants to move faster on escape routes.

References

1. Design Guide: Structural Fire Safety. Report of CIB W14 Workshop. Fire Safety Journal, 10, 2, 1986, 77-137.
2. Ramachandran, G. Probabilistic Approach to Fire Risk Evaluation. Fire Technology, 24, 1988, 204-226.
3. Ramachandran, G. Probability-based Fire Safety Code. Journal of Fire Protection Engineering, 2(3), 1990, 75-91.

Analysis of Critical Information Flows and Decision Making Priorities in Fire Safety Codes within the European Community.

A.Kilpatrick, L.Campbell, Glasgow Caledonian University, Scotland.

Introduction

Code harmonisation in the European Community

The statutory requirements for the design and construction of buildings vary between different countries in both their content and method of implementation(1,2,8). The focus of national fire safety requirements is on the protection of occupants achieved primarily through a framework of prescriptive rules for active and passive fire protection. The levels of performance specified in these rules have been determined, and are modified, largely on the basis of experience(11,12). There is little published information on the regulatory systems and building regulations of the member states in the European Community (EC) although a study commissioned by the Department of the Environment of the United Kingdom is due for publication in 1993(4,5,7). Current work in the EC is directed at the differences between fire tests in national codes and standards and progress is being made on the technical detail these contain (3,6,9,10,13,15). One of the primary aims of the work is to remove technical barriers to trade within the EC. The impact of this work on the functioning of the regulatory system for fire safety in each EC member state has not been established. However it is probable that variations will continue to occur in the interpretation and detail of the building regulations at regional and local level(14,15) as will differences in the determination of 'fire safety equivalence' for new products, for innovative designs or for refurbishment projects where strict compliance with fire safety codes cannot be demonstrated.

Research programme

In 1992 a research programme to evaluate the effect of variations between the fire safety codes of different EC member states began at Glasgow Caledonian University. The aims of the programme are to identify the critical information flows and decision making priorities and to determine their impact on design and construction outcomes.

The first phase of the research programme is focusing on the fire safety codes of Belgium, France and the United Kingdom and on high rise commercial buildings, retail complexes and hotels. The project is is being supported in France by Centre Scientifique et Technique du Batiment, and in Belgium by the Ministry of the Interior and Gent University. The sample of countries and building types will be extended in 1994.

Processes contributing to code harmonisation

Within the EC four processes can be identified as contributing to the convergence of fire safety standards.

Direct harmonisation work by the European Community

The European Commission has focused its funding and activity on establishing correlations between the results of the different national fire tests. Based on a test-classification-regulation view of regulatory systems this approach aims to avoid direct reference to the different national building regulations. Progress to date includes identification of the critical performance criteria and the extent to which the national standard fire tests yield comparable information, but has not produced a common basis for the exchange and use of test data.

Incorporation of new standards in national building regulations

The incorporation of an international, or another countries', standard for a construction material, product or element in the building regulations contributes towards harmonisation. As with the incorporation of updated standard tests and codes cases have been identified where the context of the host building regulations makes interpretation difficult.

Use of fire engineering techniques

For innovative design and construction concepts and for refurbishment projects, strict compliance with regulations is seldom possible. The procedures for assessment for fire safety vary between countries but generally involve the use of fire engineering techniques to demonstrate equivalence with the requirements of the codes. The basis for the development of these techniques is international and therefore contributes to harmonisation of design and construction practice.

Use of statistical analysis

The potential of probability-based analysis of overall fire safety requirements for life and property is recognised within the EC but statistical techniques are not as yet used to assess equivalence of proposals with code requirements.

Fire safety requirements in Belgium, France and United Kingdom

Form and technical content

Fire codes in general attempt to ensure life safety through prescriptive requirements aimed at providing a combination of structural fire protection, means of escape and fire fighting facilities. The detail of the requirements is dependant on factors which are indirectly correlated with the risk to people in the event of a disaster and on the likelihood of a disaster occurring (e.g. building use, number of occupants and height of the building). While this is common to countries in the EC, within the study group the approach to classifying buildings varies and has a significant effect on the performance requirements for the building types examined. In addition there are differences in detail such as requirements for fire resistance of materials and elements and for travel distances along escape routes. The similarities and differences are summarised as information flows and decision points for each country in the study.

Interpretation and application

The context of the fire safety codes within the legislative framework differs between countries with particular impact on the location of responsibility for interpretation and application. The roles of the local authority inspectorate (public sector) and approved private sector inspectorate in relation to the fire service are summarised for each country.

References

1. Anchor, Malhotra, Purkiss : Design of Structures Against Fire (1986), Aston University : Elsevier Applied Science.
2. Atkinson : "Building Regulations - The International Scene" - Building Research and Practice (Sept/Oct 1973), UDC 69.009.182 (047.1).
3. Burry : "Fire Detection Standards : A Case Study" - Fire Surveyor (1987), Vol 16, Part 2, pp 4-8.
4. CIB &Byggdok : A Survey of Building Regulations Worldwide ; 3rd Edition (1989), Working Commission W57.
5. Construction Industry Research & Information Association : Special Publications 66 (1989), 67 (1989), 68 (1990).
6. Commission of the European Communities : Interpretative Document : Safety in the Case of Fire, Draft Document TC2/022, (1991).
7. Grimwood : Fog Attack, (1992), FMJ Publications, Surrey.
8. Mathez, Moye : "Introduction to the French Fire Safety Regulations" - Centre Scientifique et Technique du Batiment., France, (1988), Paper 2268.
9. Malhotra : "The EEC Proposals for achieving common standards of structural fire protection." - Fire (1988), Vol 90, Part 992, pp25-33.
10. Malhotra : "Towards European Standards in the Manufacture of Construction Products by 1992 and beyond" - Fire Prevention, (1988), Part 215, pp18-19.
11. Ramachandran : "Probabilistic Approach to Fire Risk Evaluation" - Fire Technology (1988), No. 24, pp 204 -226.
12. Ramachandran : "Probability -Based Fire Safety Code" - Journal of Fire Protection Engineers, (1990), No2, pp 75-91.
13. Robinson : "Fire Safety Regulations in Europe" - Fire Surveyor (1984), Vol 13, Part 5, pp21 - 25.
14. Twilt & Witteveen : "Trends in Fire Safety Design" - Heron (1987), Vol 32, Part4, pp95-114.
15. Blachere : Report on a Comparative Study on Reaction-to-Fire Tests in the EC : Seminar on Fires in Buildings, (1988), pp 252 -260.

EXIT89 - An Evacuation Model for High-Rise Buildings

Rita F. Fahy
National Fire Protection Association
1 Batterymarch Park
Quincy, Massachusetts 02269-9101

Introduction

EXIT89 is an evacuation model designed to simulate the evacuation of a large population of individuals from a high-rise building or other complex space. It has the ability to track the location of individuals as they move through the building so that the output from this model can be used as input to a toxicity model that will accumulate occupant exposures to combustion products. EXIT89 uses occupant densities in building spaces to compute each occupant's walking speed. In this way, queueing effects are modeled. Ongoing development work on the model is being funded by a grant from NIST.

EXIT89 was developed to meet the need for an evacuation model that could track large populations of individuals in high-rise buildings. The need for a model that can handle behavioral aspects of the evacuation of a high-rise building became obvious during some other project work being done at NFPA using Hazard I, a general fire hazard analysis model whose evacuation module has only behavioral features. Hazard I calculates toxic doses and other fire exposure by occupant, so it needs to track individuals along their routes out of the building. EXIT89 was specifically designed to track individuals and address all key evacuation phenomena in high-rise buildings with large occupant populations.

Overview of EXIT89

EXIT89 requires as input a network description of the building, geometric data for each room and for openings between rooms, and smoke data if the effect of smoke blockages is to be considered. The user has the option of having the model calculate shortest routes to a location of safety, or setting the path occupants will take from each location in the building. The model moves people along the calculated or specified routes until a location is blocked by smoke. Affected exit routes are recalculated and people movement continues until the next blockage occurs or until everyone who can escape has reached the outside. Evacuation can begin for all occupants at time 0 or can be delayed to reflect externally calculated delays in alerting or responding. Smoke data can be used to predict when the activation of a smoke detector would occur and evacuation will begin then or after some user-defined delay beyond that time.

The model calculates walking speeds based on occupant densities. When escape routes are blocked by smoke, only the routes on the affected floor need to be recalculated. When the smoke blockage occurs in a stairwell, only the floors immediately above and below the blockage will be recalculated.

The model uses Predtechenskii and Milinskii's work that involved the calculation of average body sizes for Russian subjects in different types of dress. Subsequent work by Ezel Kendik using Austrian subjects found significant differences in the results. The Austrian data and available American data have been added to the model.

From Predtechenskii and Milinskii's work, a value of 0.113 m^2 (adults in mid-season street dress) is used. The Russian value used compares to the Austrian result for subjects between the ages of 10 and 15 years without coats. The value for Austrian subjects between ages 15 and 30 without coats was 0.1458 m^2. The value for adults over age 30 without coats was 0.1740 m^2. The lower value is used in the model. From a table of mean body dimensions representative of U.S. male and female workers between 18 and 45 years of age, mean values for shoulder breadth and chest depth were obtained. In order to add the additional bulk of clothing, both dimensions were increased by 0.02 meters. The resulting value was 0.0906 m^2, far smaller than that calculated for Soviet or Austrian subjects.

The choice between these three sets of data is an input option set by the user. As part of the continuing work on the model, the differing results in EXIT89 will be examined.

Other Ongoing Work

Under the grant, the program was changed to give the user the option of either printing the full output listing or restricting the output to summary measures only. The summary measures added to the program are floor clearing times and stairway clearing times. The program prints out the time to complete evacuation, and the total number of occupants trapped or reaching safety. The model output has also been enhanced by adding a summary section showing the number of people who used each exit out of the building and at what time the last person passed through.

When people exit a building, even under emergency conditions, they will often take their most familiar route. The capability for occupants to travel along those paths has been added to EXIT89 in order for it to be able to model that behavior. As each node is described, the user specifies the adjacent node to which an occupant will move. If routes on a floor need to be recalculated due to smoke blockages, the specified routes are overridden by the calculated shortest routes.

Detailed results from building evacuations in the U.K. have been made available and are being used to compare the results generated by the model. One of the data sources included the effects of disabled occupants on occupant evacuation. Comparisons from the observations from these evacuations and from the model's output are being evaluated. The data on the impact of disabled occupants on the overall building evacuation will be used to add the presence of disabled adults to the model.

Other modifications planned include the use of CFAST output for smoke input, the addition of reverse flows in stairwells to simulate the effect of fire department operations in stairwells and the inclusion of additional human behavior data, such as delays in beginning evacuation and delays in the course of evacuating a building.

Conclusion

The goal for the current phase of development of EXIT89 is to have a model ready for peer review and ultimately for use as an enhancement of the Hazard I package for high-rise buildings. It will incorporate available human behavior data to the extent possible. It will be tested using data from actual evacuations under either emergency or non-emergency conditions and it will include user options to allow a greater degree of flexibility and ease of use.

Background to the Draft British Standard Code of Practice on: The Application of Fire Engineering Principles to Fire Safety in Buildings

John Barnfield

Introduction

A Draft British Standard Code of Practice regarding the application of fire engineering principles to building design is currently being completed. The main objectives of the code are to:

provide a rational framework for the application of fire engineering principles to the achievement of fire safety in buildings;

to provide a common basis for the design and approval of buildings which do not comply with existing prescriptive codes of practice.

The draft encompasses both deterministic and probabilistic approaches to design and sets out a basic methodology and format for a fire safety engineering study that may be accepted by regulatory bodies.

The basic methodology involves:

Setting design objectives and criteria

Qualitative Assessment (by hazard assessment team)
- hazard identification
- problem simplification
- identification of alternative fire protection strategies
- determination of depth and scope of quantification required

Engineering Analysis

Evaluation of consequences
- deterministically or
- probabilistically

Comparison of results against design criteria

Documentation of procedures and assumptions for statutory approval.

Scope of the code

The purpose of this British Standard is to provide a rational approach, by the application of fire engineering principles, to achieving fire safety in buildings against clearly defined design objectives. It provides a background to the various methodologies and their appropriateness to the design process.

This British Standard code of practice provides guidance in designing or assessing the adequacy of fire safety measures intended to protect people from the effects of fire in buildings, and reduce the potential for loss of load-bearing capacity and fire spread due to loss of separation provided by the structural barriers. It provides an alternative to existing British Standard codes for means of escape, and allows the effects of departures from more prescriptive codes to be evaluated.

This code addresses the objectives of designing for fire safety and recognises that these may be achieved by a range of alternative strategies.

The code takes into account human factors, construction, means of escape, smoke management, detection, alarm, and fire suppression methods and their contribution to the achievement of the fire safety objectives.

The basic principles may be applied to all types of buildings and their use but this code does not deal specifically with buildings used for the storage or processing of flammable liquids or explosive materials. The intrinsic risks associated with such buildings necessitate special consideration beyond the scope of this document.

It is intended that the code, when used by a suitably qualified and experienced fire safety engineer, will provide a means of establishing acceptable levels of fire safety, economically and without imposing unnecessary constraints on other aspects of building design.

Contents of the code:

U.S. COAST GUARD CUTTER FIRE SAFETY ANALYSIS USING THE SHIP FIRE SAFETY ENGINEERING METHODOLOGY

LT Brian L. Dolph

Marine Fire and Safety Research Branch
USCG Research and Development Center, Groton, CT

Mr. Chester M. Sprague, P.E., Mr. Herbert A. Holmstedt

CompuCon, Haddam, CT

The **Ship Fire Safety Engineering Methodology** (SFSEM) is a probabilistic-based risk analysis methodology. It is useful to conduct a structured and comprehensive analysis of the performance of all types of surface ships as a fire system. The SFSEM provides an integrated framework for analyzing fires on ships in comparison to established fire safety objectives. The methodology accounts for relevant aspects of fire safety; the growth and spread of fire, the effectiveness of passive design features such as barriers, active fire protection features such as fixed fire extinguishing, and manual suppression systems.

The **Ship Applied Fire Engineering** (SAFE) computer programs implement the SFSEM and evaluates the probability of spaces and barriers limiting a fire. The evaluation is conducted on a compartment-by-compartment basis. SAFE calculates the probable paths of fire spread for specified time durations. SFSEM/SAFE has been used successfully in a design application and in retrofit situations.

The USCG R&D Center's **Small Cutter Fire Protection Project** is a comprehensive effort to analyze the fire protection levels of nine classes of U.S. Coast Guard Patrol Boats, Tugboats, and Buoy Tenders between 65' and 110' in length. The fire safety analysis was conducted using the SFSEM and SAFE to evaluate existing and alternative fire protection procedures and equipment on these cutters. The results of these analyses are being used to develop specific fire protection doctrines for these small cutters.

Results of the detailed fire safety analyses show that the majority of shipboard compartments meet fire safety objectives with their existing passive and active fire protection features in effect, even without the manual suppression features contributing. In addition, the SFSEM was shown to be a valuable analytical tool to evaluate alternative fire protection features and quantify their effectiveness. The study clearly demonstrates that it is feasible to reduce reliance on manual firefighting in small cutters by enhancing selective passive and automatic fire protection features.

Fire safety analysis results of the existing conditions on the nine cutters will be presented along with discussions of specific problems encountered during the data collection and processing efforts. Proposed alternative fire protection features will be shown, with analysis results, illustrating the capability of the SFSEM and SAFE to readily evaluate the fire safety levels of modified fire protection features. These alternative protection features are compared using cost-benefit analysis to determine which is the most desirable to accomplish. Also discussed will be many of the questions raised during the analyses and specific full room involvement time algorithm validation testing conducted at the Coast Guard's full-scale Fire and Safety Test Detachment (F&STD) in Mobile, Alabama. The specific testing was for compartments with thermally thin barriers typical of shipboard construction.

Beyond the in-house analysis of the Coast Guard's own fleet, it is anticipated that the SFSEM and SAFE may be used to aid the Coast Guard in developing more precise means of evaluating requests for equivalency submitted by commercial shipbuilders. The Coast Guard is responsible for approving shipboard fire protection features in accordance with the Code of Federal Regulations (CFR). The CFR allows equivalency determinations to be made with respect to proposed alternative fire protection features as long as they afford the same level of fire safety required by code. Without a performance-based fire safety analysis method, such as the SFSEM, merely identifying the existing levels of fire safety provided by the codes is extremely difficult.

Proposed future areas of development for the SFSEM and SAFE include additional modules such as Smoke Movement and People Movement. These two areas must be integrated into the method's framework to allow life safety issues to be adequately evaluated. Other improvement areas include quantification of fire safety objectives, developing barrier performance curves, and streamlining SAFE computer programs.

Toxicity Assessment of Combustion Gases and Development of a Survival Model

Louise C. Speitel
Federal Aviation Administration Technical Center

Summary

A new Combined Hazard Survival Model was created using selected regression equations to be used as a predictive tool to gauge human survivability in full-scale aircraft cabin fire tests.

This new model uses incapacitation data to obtain a fractional effective dose for incapacitation (FED_I) and lethality data to obtain a fractional effective dose for lethality (FED_L). The time when either FED reaches one determines the exposure time available to escape from an aircraft cabin fire and to survive post exposure.

Time to incapacitation is the best measure of the ability to escape and survive exposure to the narcotic gases such as CO, CO_2, HCN, and low oxygen. The incapacitation concentration is less than the LC_{50} for these gases. If a passenger were incapacitated, one can assume that subsequent death will occur by rapidly spreading fire or toxic gases. The FED_Is for each hazard are added to give the total FED_I as a function of time.

LC_{50}s are the best measure of the ability to escape and survive exposure to the irritant gases such as HF, HCl, HBr, NO_2, and SO_2. An LC_{50} is the concentration for a given exposure duration which results in the death or subsequent death of 50 percent of the animals. Exposure to high concentrations of these gases may not prevent escape, but may result in subsequent death due to respiratory system damage. The LC_{50}s are less than the incapacitation concentrations for these gases.

The new FED_I model has become an important tool for analyzing full-scale fire tests conducted at the FAA Technical Center Fire Test Facility, where concentrations of toxic gases, smoke, and temperature are monitored at various locations in the fuselage as a function of time.

Method

An extensive literature search was conducted for animal exposure data for each of the above gases as well as heat exposures. Regression equations giving the best fit to the concentration time data were derived from those studies. The studies include human, monkey, baboon, rat and mouse exposures.

Figures 1-5 present the predicted times to effect for CO, HCN, HCl, CO_2, and temperature obtained from the literature for various species at different activity levels. Hydrogen Fluoride, HBr, NO_2, SO_2, and oxygen depletion are also included in the survival model. A regression equation which was judged to best model the human escaping from an aircraft cabin was selected for each gas and utilized in the survival model.

The effect of CO_2 on increasing the uptake of other gases was factored into the concentration term in the FED equation for each gas. Higher respiratory minute volumes due to CO_2 exposure was found to be an important factor in predicting the time to incapacitation or death.

Figure 6 illustrates a typical survival curve for a wide body fuselage initiated by an external fuel fire. The contribution of each hazard to the total FED_I is shown, illustrating their relative importance in the predicted time of incapacitation.

Figure 1. Comparison of Predicted Times to Effect for CO

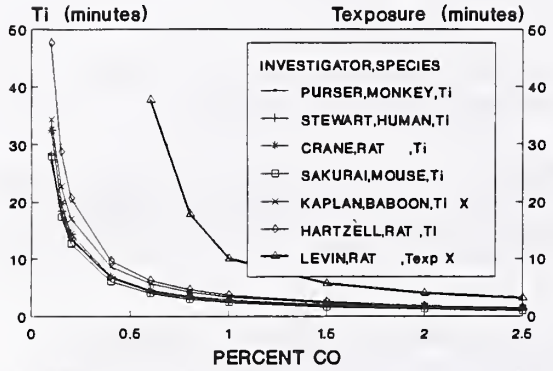

X Selected for the Survivel Model

Figure 2. Comparison of Predicted Times to Effect for HCN

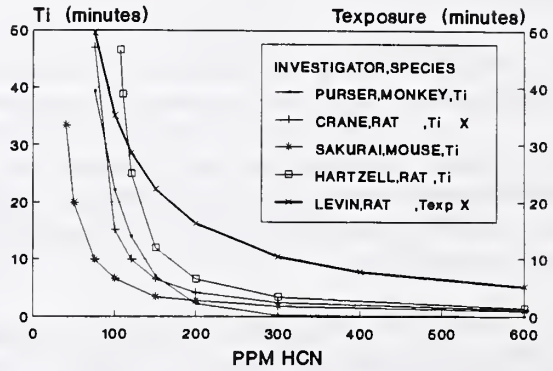

X Selected for the Survival Model

Figure 3. Comparison of Predicted Times to Effect for HCl

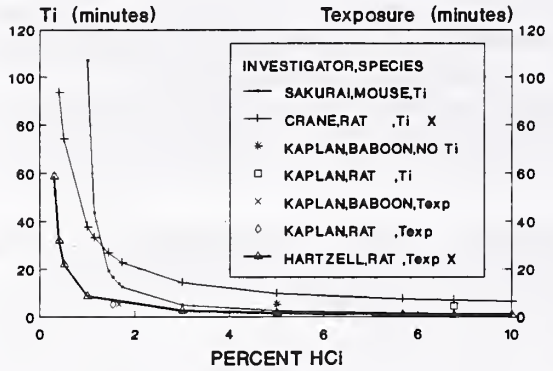

X Selected for the Survival Model

Figure 4. Comparison of Predicted Times to Incapacitation for CO2

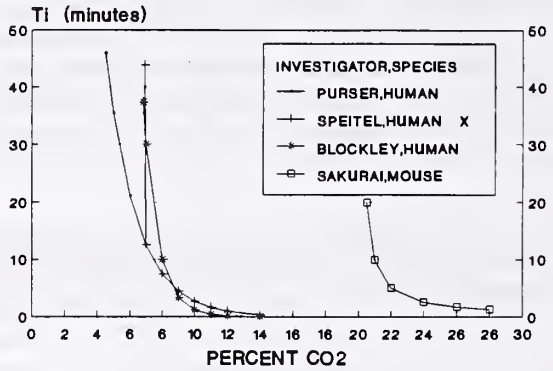

X Selected for the Survival Model

Figure 5. Comparison of Predicted Times to Incapacitation for Heat

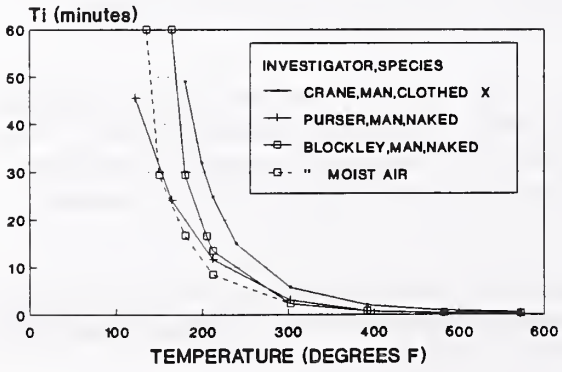

X SELECTED FOR THE SURVIVAL MODEL

Figure 6. Typical Survival Curve for a Wide Body Fuselage

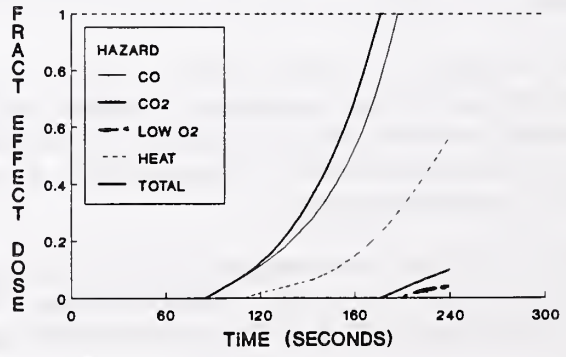

FED = 1 AT 196 SECONDS

Laser Extinction, Scattering and Fluorescence Imaging of the Soot Region in Time-Varying and Steady-State Diffusion Flames.

Joel E. Harrington, Christopher R. Shaddix and Kermit C. Smyth

Fire Science Division
National Institute of Standards and Technology
Gaithersburg, Md 20899

When a time-varying velocity perturbation is applied to the fuel flow of a non-smoking, steady-state ethylene/air diffusion flame, smoke breaks out the top. Methane/air flames of similar height on the same burner never smoke, but the character of the in-flame soot changes dramatically with acoustic forcing of the fuel flow. Why is soot production sensitive to time-varying fuel perturbations when the mean flows remain constant?

Combustion reactions are strongly coupled to fluid mechanical mixing of the reacting medium through chemical heat release. An unsteady flame may provide residence times, temperature histories, local stoichiometries, strains and scalar dissipation rate unavailable in a corresponding steady flame. If the sets of conditions in steady and unsteady flames are sufficiently disjoint and the processes of interest sufficiently sensitive, data from steady flames cannot be mapped onto laminar flamelet models of unsteady flames. Data from conveniently periodic time-varying flames could expand the sampled range of conditions for application to more general, even turbulent conditions.

In steady, co-flowing diffusion flames, pre-particle soot inception chemistry is relatively slow [1]; the earliest soot particles form near the high-temperature, primary reaction zone and a majority are transported to richer and cooler regions by convection and thermophoretic forces [2]. As a consequence, soot inception, growth and oxidation occur sequentially [3]. Chemistry-flowfield interactions are likely to lead to different time-temperature histories and thus have a strong impact upon soot formation in diffusion flames.

Experiment

The laminar co-flowing methane/air and ethylene/air diffusion flames were stabilized on a coannular burner with a loudspeaker attached to its plenum below a 1.1 cm diameter fuel tube. Laser-sheet scattering images of the soot region in a time-varying methane flame, whose fuel flow is modulated at a frequency matching the 10.13 Hz laser repetition rate, show a factor of eight enhancement in peak scattering intensity when compared with images of a steady-state flame with the same mean fuel and and air co-flows (Figures 1 and 2). No enhancement appears in a comparison between the peak values of what is commonly interpreted as soot volume fraction, obtained through tomographic reconstruction of HeNe (Figure 3) and Ar ion extinction measurements. Further complicating interpretation, the radial profiles of the 454.5 nm Ar ion reconstructions exhibit much stronger extinction near the center of the axi-symmetric flames than do the 632.8 nm HeNe data, for profiles taken closer to the burner. Higher in the flames, radial profiles from both wavelength extinction measurements agree. Differences in spatial extent of the 454.5 and 632.8 nm extinction profiles are compared to images of fluorescence attributed to polycyclic aromatic hydrocarbons (PAH).

Surprisingly, ethylene flames show very little change in peak laser scattering signal when the loudspeaker forces the fuel flow, even though the flame starts smoking. Clearly, dramatic changes in the soot field occur when the fuel is periodically forced for both flames studied. However, a meaningful quantitative comparison between the soot fields in our steady-state and time-varying flames requires answers to fundamental questions about soot and its interaction with light: What is an appropriate operational distinction between soot and large PAH? How do scattering/absorption properties and refractive indices change with size and structure of growing soot particles? Properly quantified soot data combined with accurate temperature and velocity profiles of the time-varying flames promises insights into the influence of time-temperature histories, strain and stoichiometry on in-flame soot formation and smoke emissions.

[1]Santoro, R.J., Yeh, T.T., Horvath, J.J. and Semerjian, H.G., *Combustion Science and Technology* **53**: 89 (1987).
[2]Dobbins, R.A., Santoro, R.J. and Semerjian, H.G., *Twenty-third Symposium (international) on Combustion*, The Combustion Institute, Pittsburgh, 1990, p. 1525.
[3]Glassman, I., *Twenty-second Symposium (international) on Combustion*, The Combustion Institute, Pittsburgh, 1988, p. 295 and references therein.

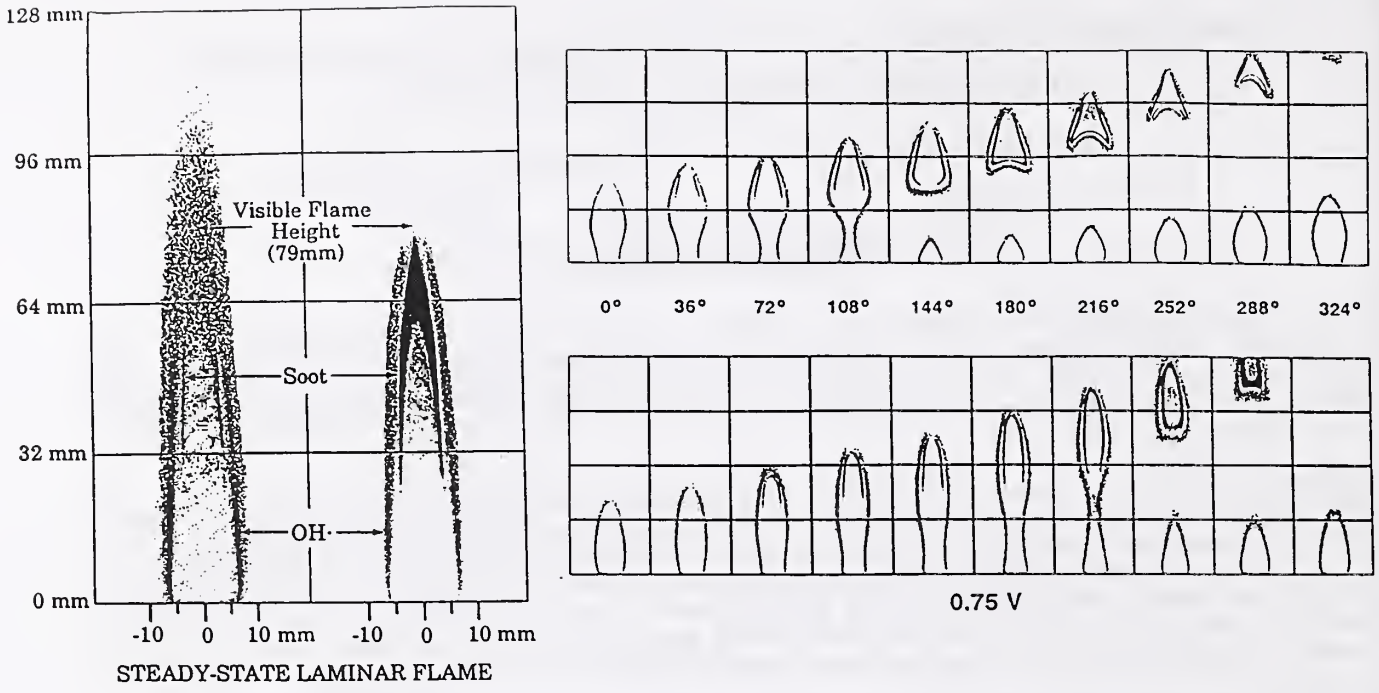

Figure 1. OH· laser-induced fluorescence and soot scattering images in a steady-state laminar CH_4/air diffusion flame using horizontally polarized light (left) and vertically polarized light (right). Note that the gain on the CCD camera was reduced for the latter series, making the OH· fluorescence signals appear weaker. The wavelength of the UV light is 283.55 nm, and the visible flame height is 79 mm above the fuel tube exit, which is located 1 mm above the bottom of the first frame.

Figure 2. OH· laser-induced fluorescence and soot scattering images in a time-varying laminar CH_4/air diffusion flame using horizontally polarized light at 283.55 nm. Ten phase angles are shown, corresponding to a time interval of 10 ms. The excitation voltage on the loudspeaker is 1.5 V peak-to-peak (top) and 0.75 V (bottom). At each phase angle, four separate single-shot images have been recorded at different heights above the burner. The zero phase angle for each series is arbitrary.

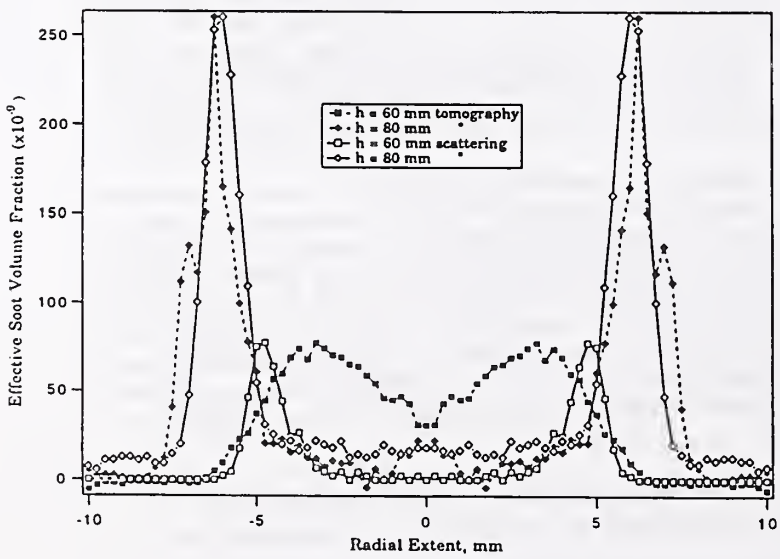

Figure 3. Comparison of 283.55 nm scattering profiles (solid lines) with tomographic reconstructions of 632.8 nm extinction data (dotted lines) at two heights above the burner in a forced, time-varying, axisymmetric methane/air diffusion flame. Peak scattering values are scaled to match the peak extinction for each height. Note that the lower extinction profile fills in towards the flame center relative to the scattering profile.

Thermodynamic Properties and Solubitities of Nitrogen and Freon-23 in Alternative Agents[1]

J. C. Yang, B. D. Breuel, and W. L. Grosshandler

Building & Fire Research Laboratory
National Institute of Standards & Technology
Gaithersburg, MD 20899 U.S.A.

ABSTRACT

This study constitutes a part of a U.S. Air Force sponsored program, currently being conducted at NIST, to identify alternatives to halon 1301 for in-flight aircraft fire protection. Eleven agents have been proposed as potential candidates for replacement. They are: HFC-236, FC-31-10, FC-318, HCFC-124, HFC-227, HFC-134a, FC-218, HCFC-22, HFC-125,HFC-125/HFC-32 azeotrope, and FC-116.

Depending upon their applications, existing halon 1301 bottles are normally filled to about half of the bottle volume, and the bottle is then pressurized with nitrogen to 4.1 MPa (600 psig) at room temperature. The purpose of using the pressurization gas is to expedite the discharge of the agent and to increase the penetration distance of the agent during discharge. However, this driving force, i.e., the total pressure, will change depending on the ambient temperature because the vapor pressure of the agent and the solubility of the pressurization gas in the liquid agent vary with temperature. In order to use existing halon 1301 bottles for "drop-in" replacement agents or to provide safety guidelines on bottle design for the alternative agents, an important task is to find out what the final pressure of the vessel will be when the charged vessel is exposed to different ambient temperatures.

The first part of this study involved measurements of the thermodynamic properties of the agents. In particular, the objective was to determine the final pressure of the vessel when the vessel, filled with either a pre-determined amount of pure agent or with agent and pressurization gas, was exposed to different ambient temperatures (from -60°C to 150°C). Because nitrogen or Freon-23 (HFC-23) was being proposed as a pressurization gas, these two gases were used in the study.

Since the initial amount of nitrogen or Freon-23 required to pressurize the vessel plays a major role in the determination of the final pressure of the vessel, the second part of this study was to determine the solubilities of the pressurization gases in the agents at room temperature.

For measurements of the thermodynamic properties of the agent, the experimental apparatus consisted of a 53.9 cm^3 stainless steel vessel equipped with a thermocouple, a pressure transducer, and a pressure relief valve to prevent any accidental pressure overshoot at elevated ambient temperature. The experimental procedure was as follows. The set-up was evacuated

---

[1] sponsored by USAF Wright-Patterson Laboratory

for at least 5 minutes, and the vessel was then filled with a pre-determined amount of agent. By immersing the vessel in dry ice, liquid agent was dispensed into the vessel by condensing gaseous agent from the supply bottle. No attempt was made to remove noncondensible gases, if there were any, in the liquid agents. In the case of agent charged with pressurization gas, the vessel was pressurized with nitrogen or Freon-23 to 4.1 MPa (600 psig). In the case of pure agent, no pressurization gas was used. The vessel was then immersed in a temperature-controlled bath. The final internal pressure of the vessel was recorded from the pressure transducer read-out when the internal temperature of the vessel had reached thermal equilibrium with the temperature of the bath.

For solubility measurements, the experimental set-up was very similar to that used in the measurements of thermodynamic properties, except the removal of the pressure relief valve. The experimental procedure was as follows. After the vessel was evacuated, filled with liquid agent, and charged with pressurization gas to 4.1 MPa (600 psig) at room temperature, the amount of pressurization gas was determined by weighing the apparatus. This amount corresponded to the sum of the mass of the pressurization gas in the vapor phase as well as that dissolved in the liquid agent.

The total amount of agent used in all the experiments was approximately equal to the amount required to fill one-third of the vessel volume with liquid. The one-third fill capacity was used to ensure that a liquid-filled condition would not be encountered when the vessel was exposed to elevated ambient temperatures.

For all the agents evaluated so far, the final pressure was found to be less than 12.4 MPa (1800 psig) at 150°C for pure agents. For agents charged with nitrogen, the final pressure was found to be less than 15.1 MPa (2200 psig) at 150°C. Preliminary results for two agents (HCFC-22 and HFC-32/HFC-125 azeotrope) charged with Freon-23 showed that pressures greater than 13.7 MPa (2000 psig) were observed at temperatures less than 60°C.

The total amount of nitrogen required to pressurize the vessel to 4.1 MPa (600 psig) was less than 8% of the total mass of the agent. The amount of nitrogen dissolved in the liquid agent was calculated to be less than 25% of the total amount of nitrogen added. The amount of Freon-23 needed to pressurize the vessel was found to be as much as or greater than that of the agent in the vessel, implying that the solubility of Freon-23 in the liquid agent was much greater than that of nitrogen.

Because the amount of Freon-23 was found to be significant and very high pressure in the vessel would result at elevated temperatures, extreme care should be taken in the design of the bottle for the replacement agents if Freon-23 were to be selected as the pressurization gas.

KINETICS OF CELLULOSE PYROLYSIS - EFFECTS OF SAMPLE DENSITY AND HEATING RATE

Ivan Milosavljevic and Eric M. Suuberg
Division of Engineering, Brown University
Providence, RI 02912

There is significant interest in studying the kinetics of cellulose pyrolysis from the standpoint of fire research, since the products of pyrolysis are directly involved in flaming combustion and, therefore, the kinetics of decomposition determines the rate of volatiles supply to the flame. There have been many previous studies of the kinetics of pyrolysis. Here, the focus is on obtaining reliable kinetics of relevance to high heat flux burning of bulk solids. The experiments were carried out in a thermogravimetric analyzer (TGA), differential scanning calorimeter (DSC) under conditions simulating fire conditions. Whatman cellulose powder CF11 (ash content 0.009%) with 200 μm medium fiber length and with fiber diameter 12-15 μm was studied. The samples for TGA and DSC were made by cutting cubes with sides of 3 mm (TGA), or discs of 5 mm in diameter and 1 mm in thickness (DSC) out of powder pressed to densities of 0.956 g/cm^3, 0.658 g/cm^3 and 0.476 g/cm^3. The DSC and TGA were continuously purged by a flow of nitrogen. The heating rates for TGA and DSC were chosen so as to simulate the conditions on the front surface (60 K/min), in the middle (15 K/min) and on the back surface (6 K/min) of a pyrolyzing cellulose sample of 10 mm in thickness, under the radiative heat flux of 40 kW/m^2. Gas analyses were performed by FTIR for the case in which the effect of initial sample density was explored.

Figure 1 shows a DSC scan at 60 K/min for the 0.956 g/cm^3 sample (Figure 1a) and TGA scans (also at 60 K/min) for three different density samples (Figure 1b). There is only one DSC scan shown due to the great similarity in results for all three different density samples. It can be seen that the TGA curves are slightly shifted toward higher temperatures when the initial sample density increases. Careful examination of the starting point for mass loss reveals very small differences in temperatures. If the starting point is defined as a point at which the mass loss curve shows the first deviation from an initial steady mass, then for 0.956 g/cm^3 sample this occurs at 300°C, for 0.658 g/cm^3 sample it occurs at 296°C and for 0.476 g/cm^3 sample it occurs at 292°C. Although these differences cannot be termed large, they are measurable. Furthermore, it can be seen from Figure 1b, that the slopes in the middle portion of pyrolysis are slightly different. This is evidence of a very small external heat transfer limitations.

The ultimate char yields increase with increase in initial sample density (8.0% for 0.956 g/cm^3, 6.5% for 0.658 g/cm^3 and 5.8 for 0.476 g/cm^3). It was postulated that this is due to the mass transport limitations. The higher initial sample density leads to higher char density and higher resistance to the outward flow of volatiles, which can then undergo secondary reactions to produce more char and more cracking gases (as confirmed by gas analysis).

Kinetic parameters were calculated from the data of Figure 1b, by considering first order Arrhenius type kinetics: $dM_p/dt = - A M_p \exp(-E/RT)$, where M_p is the remaining pyrolyzable mass of cellulose (defined as current mass less the mass of the char left), t is the time, A is the frequency factor, E is the activation energy, R is the gas constant and T is the temperature. The calculations were performed for the entire set of data and the activation energies for samples of initial densities 0.956 g/cm^3, 0.658 g/cm^3 and 0.476 g/cm^3 were 37.0 kcal/mole, 36.4 kcal/mole and 36.4 kcal/mole, respectively. Their respective frequency factors were: 1.68×10^{10} s^{-1}, 1.36×10^{10} s^{-1} and 5.19×10^{10} s^{-1}. Therefore, it was shown that the initial sample density does not significantly affect the apparent kinetics of pyrolysis, in spite of the small difference in heat transfer conditions (the heat sink in the particles is almost twice as large in the case of 0.956 g/cm^3 as in the case of 0.476 g/cm^3). These values are in fair agreement with those reported previously (1).

The effects of heating rate on kinetics, at a constant density of 0.956 g/cm^3 are shown in Figure 2 (TGA scans for 6 K/min, 15 K/min and 60 K/min). As expected, both the mass loss curve and the pyrolytic endotherm (from DSC results not shown) are shifted to higher temperatures for higher heating rates. For a heating rate of 60 K/min the endotherm is 314.2 J/g (as shown in Figure 1a), for a heating rate of 15 K/min the endotherm is 249.4 J/g and for a heating rate of 6 K/min the endotherm is 187.3 J/g, using consistent integration methods (note that the significant shift in baseline is due to a change in heat capacity with mass loss). These data suggest that if cellulose is heated more slowly there is less energy required for its decomposition. Kinetic parameters were calculated from the TGA data shown in Figure 2.

The data for 60 K/min are the same as those shown in Figure 1b and the kinetic parameters are given above. For a heating rate of 15 K/min the apparent activation energy was 47.9 kcal/mole and the frequency factor was 1.80×10^{14} s^{-1}. For a heating rate of 6 K/min the activation energy was 60.1 kcal/mole and the frequency factor was 2.59×10^{18} s^{-1}. These data suggest that cellulose decomposition is "path dependent". In support for this hypothesis, an experiment was performed in which the sample was held isothermally for one hour at 300°C, after 6 K/min heating. If the frequency factor is assumed as above for 6 K/min, 2.59×10^{18} s^{-1}, then the calculated activation energy is 58.2 kcal/mole, which is in fair agreement with the above value of 60.1 kcal/mole. The sample was further heated at 60 K/min after the isothermal period, up to 550°C, and for that step the kinetic parameters were: 2.57×10^{15} s^{-1} for the frequency factor and 47.7 kcal/mole for the activation energy. Earlier, we had concluded that heating rate had little effect on pyrolysis kinetics in the range from 5 K/min to 1000 K/min (1). A small discrepancy at the lowest heating rates (5 K/min) was, however, noted. We believe that the evidence now supports a difference in kinetics in this low heating rate regime.

The conclusions derived from this work are that the kinetics of cellulose pyrolysis is not influenced by the initial sample density but that the kinetics of cellulose pyrolysis depend upon heating rate. This might help explain why, in the literature, there continue to be reports of higher activation energies.

References:

1. Suuberg, E. M. and Dalal, V. F. Proc. Eastern States Section, Combustion Institute, 65-1 to 65-4, November, 1987

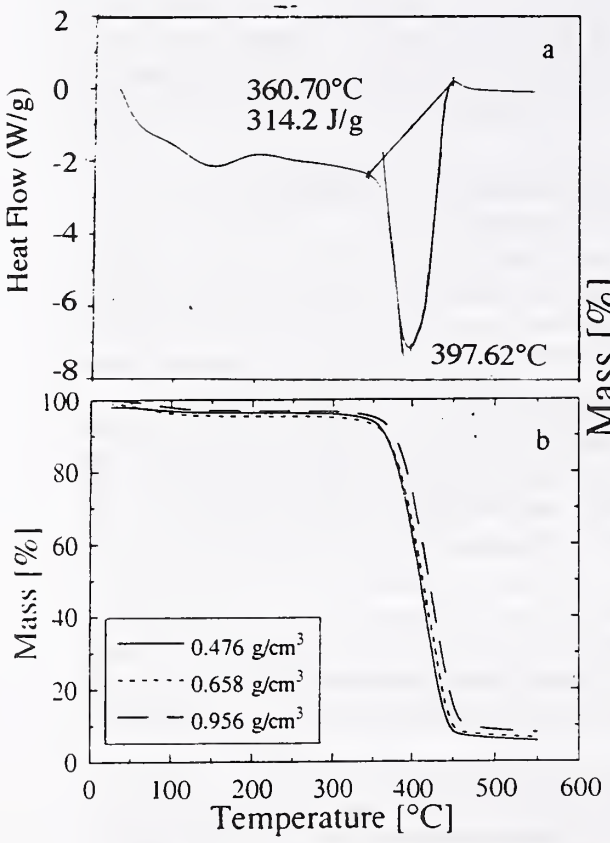

Figure 1: (a) DSC for a sample of density 0.956 g/cm^3; (b) mass loss for samples of densities 0.956 g/cm^3, 0.658 g/cm^3 and 0.476 g/cm^3 (heating rate 60 K/min in all cases)

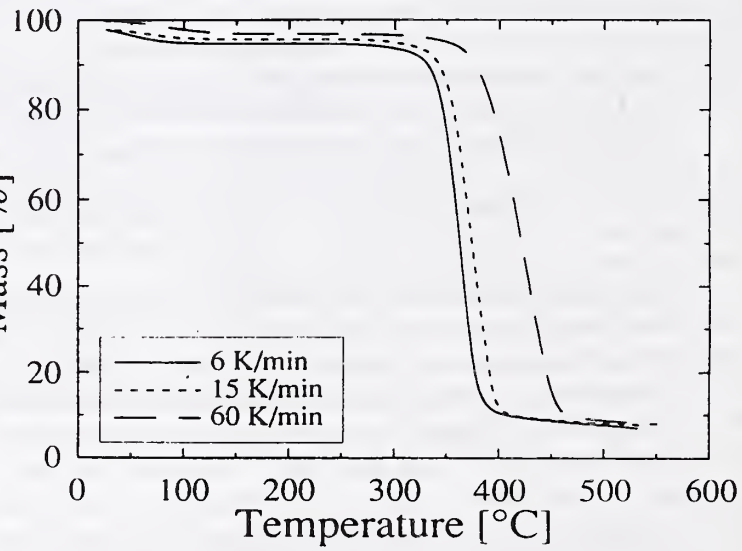

Figure 2: Mass loss for sample of density 0.956 g/cm^3 at heating rates of 6 K/min, 15 K/min and 60 K/min

A Correction to de Ris Formula for Creeping Flame Spread Over Thermally Thin Material

Subrata Bhattacharjee
Steve Dockter
Department of Mechanical Engineering
San Diego State University, San Diego, CA 92182-0191

The numerical solution (Bhattacharjee, 1993) of the well known de Ris (1969) problem of flame spread over thin condensed fuel in opposed-flow environment was not in complete agreement with the analytical solution (Delichatsios, 1986). It was hypothesized(Bhattacharjee, 1993) that the neglect of the overhang of the flame in front of the eigen location in the analytical solution is the reason for this discrepancy. Later, doubts were raised (Delichatsios, 1993) about the accuracy of the numerical results.

In this paper, the effect of the overhang distance on de Ris flame is further analyzed through numerical case studies. It is shown that the discrepancy between the numerical results and de Ris formula, which can be as high as 60% in extreme situations, can be correlated with the overhang distance. For favorable values of the controlling parameters, as the overhang distance tends toward zero, the discrepancy also vanishes. The hang distance, an unknown in de Ris problem, is correlated to the controlling parameters and a correction to de Ris formula due to the overhang phenomenon is proposed.

de Ris problem for flame spread over thermally thin materials can be formulated in terms of four non-dimensional parameters, $\beta_1 \equiv \frac{m_{O,\infty}}{s}$, $\beta_2 \equiv \frac{\Delta \hat{H}_c}{\hat{C}\hat{T}_\infty}$, $\beta_3 \equiv \frac{\hat{T}_v}{\hat{T}_\infty}$ and $\beta_4 \equiv \frac{\hat{L}_v^o}{\hat{C}\hat{T}_\infty}$, retaining all the assumptions of the original theory. The exact solution for the de Ris spread rate (Delichatsios, 1984), assuming the overhang distance to be zero can be expressed as:

$\beta_{dR} \equiv \hat{V}_f \frac{\hat{\rho}_s \hat{\tau} \hat{C}_s}{\hat{\lambda}_g} = \frac{\pi}{4} F$ where, $F \equiv \frac{T_f - \beta_3}{\beta_3 - 1}$, and T_f, the adiabatic flame temperature for the linearized de Ris model is $T_f = 1 + \beta_1\beta_2 - \beta_1\beta_4 \frac{B}{\ln(1+B)}$, where $B \equiv \frac{1}{\beta_4}(1 - \beta_3 + \beta_1\beta_2)$. This widely used relation is actually exact for large value of F. In the limit of small F the exact de Ris solution is, $\beta_{dR} = F$ (Delichatsios, 1986).

In the numerical solution of the de Ris problem (Bhattacharjee, 1993), the exact solution of Delichatsios could not be reproduced. The discrepancy between the results, for a particular baseline case ($\beta_1 = 0.45$, $\beta_2 = 26.94$, $\beta_3 = 2.18$, $\beta_4 = 0.844$) is 45%. After extensive testing of the calculations the author attributed this discrepancy to the overhang of the flame leading edge. This hang-distance, l, defined as the separation (non-dimensionalized with the thermal length) between the flame leading edge and the eigen location was implicitly assumed to be zero in the solution of de Ris and Delichatsios.

In this study, the controlling parameters are varied over a wide range, ($\beta_1 = 0.35, 0.45, 1.41$; $\beta_2 = 16.17, 26.94, 53.9$; $\beta_3 = 1.50, 2.18, 3.50$; $\beta_4 = .025, 0.844, 6.94$) ; the resulting 81 cases cover every realistic situation for the de Ris problem and β computed for each case is shown in Fig. 1 along with the prediction from the analytical solution. It is clear from this figure that the

discrepancy prevails, reaching as high as 60% in some cases with no apparent trend. It is interesting to note that, in all cases, the computed spread rate is higher than the de Ris spread rate.

If the discrepancy is truly because of the hang-distance, as proposed earlier (Bhattacharjee, 1993), it should correlate with the hang distance. The percent difference between the spread rates are plotted against the hang-distance obtained from the numerical results in Fig. 2, where a strong correlation is evident. As the hang distance approaches zero, the numerical solution reproduces the exact solution (Delichatsios, 1986).

The hang distance, l, can be shown to scale with $\alpha \equiv \dfrac{\beta_1}{\ln(1+B)}$, where B, the mass transfer driving force, has been already defined in terms of the controlling parameters. As Fig. 3 testifies, the hang distance can be accurately predicted from the correlation $l = 1.36e^{-7.463\alpha}$, A correction factor for the de Ris formula can, therefore, be developed using the correlations of Figs. 2 and 3, yielding: $\beta = C_{h.d.}\beta_{dR}$, where $C_{h.d.} \equiv 1.0 + 1.324l - 0.684l^2$. This modified formula for spread rate matches computational spread rate within 1% thus extending the validity of de Ris formula to situations with non-zero hang distance.

References:

Bhattacharjee, S., *Combust. and Flamee* ,, in press.

de Ris, J.N., *Twelfth Symposium (International) on Combustion*, Pittsburgh, 1969, pp. 241-252.

Delichatsios, M.A., *Combust. Sci. Technol.*, 44:257-267 (1986).

Delichatsios, M.A., *Combust. and Flamee* , in press.

Acknowledgement:
This work was supported by NASA through Contract NCC3-221. Suggestions from Sandra Olson, Robert Altenkirch and Michael Delichatsios are gratefully acknowledged.

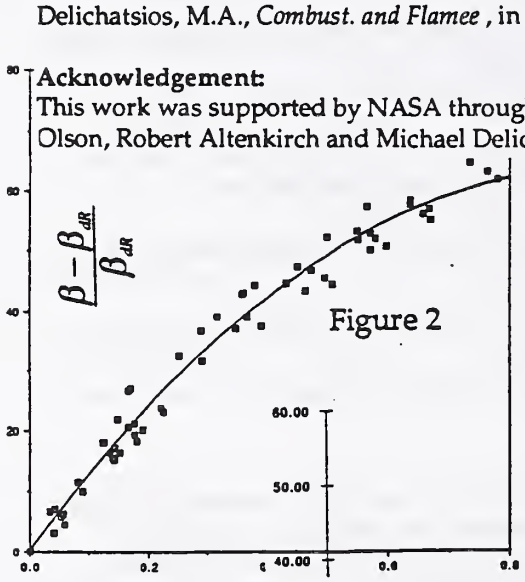

Figure 2

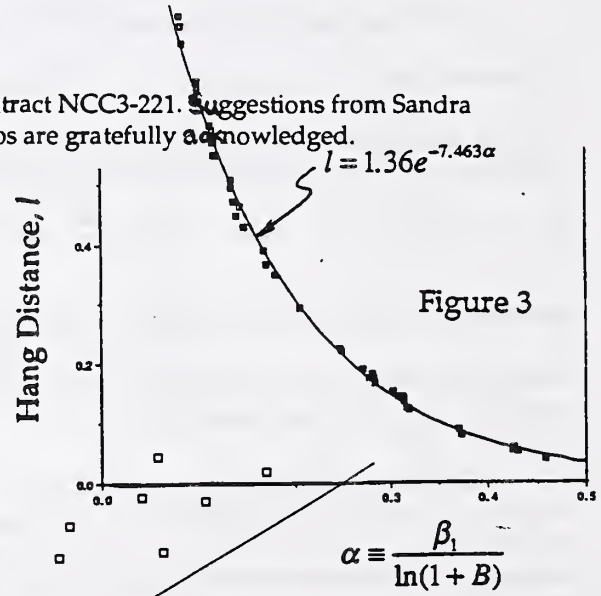

Figure 3

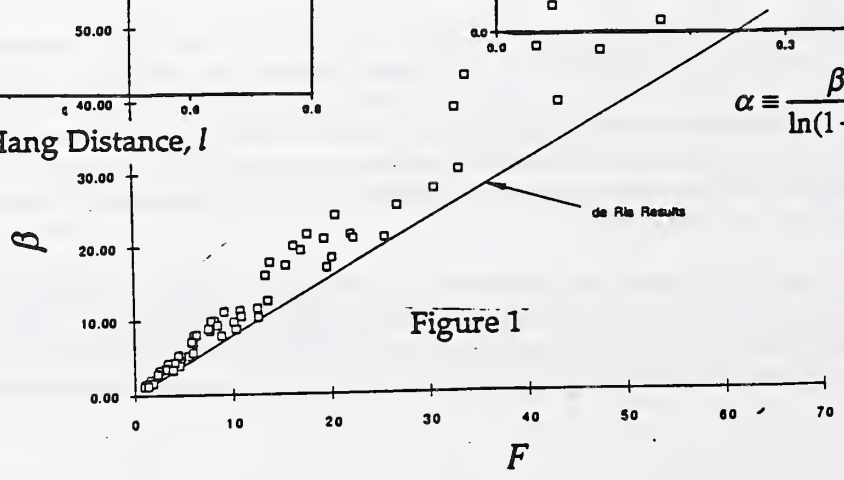

Figure 1

COUPLED RADIATION AND SOOT KINETICS CALCULATIONS IN LAMINAR ACETYLENE/AIR DIFFUSION FLAMES

Y. R. Sivathanu and J. P. Gore
School of Mechanical Engineering
Purdue University
West Lafayette, IN 47907-1003

Introduction- Soot kinetics calculations in laminar and turbulent diffusion flames have assumed constant radiative heat loss allowing the use of temperature state relationships [1-3]. However, in strongly radiating flames, there is substantial variation in the local radiaitve fractions [4]. This causes a strong coupling between the local radiative heat transfer and the chemical processes in these flames. Based on this observation, the objective of the present investigation is to study this coupling between radiation and soot kinetics in acetylene/air and acetylene+methane/air diffusion flames.

Theoretical and experimental methods- Transport equations for mass, momentum, gas phase mixture fraction, enthalpy (sensible + chemical), soot mass fraction, and soot number density are solved using a modified Genmix program. A simplified soot kinetics model [3] incorporating nucleation, growth, oxidation, and agglomeration processes is used. The reaction rates in the simplified kinetics model depend on the temperature and the local concentrations of acetylene and oxygen. The major gas species concentrations are obtained from state relationships. The local temperature is obtained by solving the energy equation taking radiation loss and gain and the energy exchanges associated with soot formation and oxidation into consideration. The radiative source/sink term in the energy equation is obtained using a multi-ray method [4]. Since these flames radiate a substantial part of their energy, the kinetic rates associated with soot processes are strongly coupled to the energy equation. In addition, the local mass fraction of soot reaches around 0.4 necessitating the consideration of two phase effects. The calculations are evaluated by comparing the predictions with measurements of mixture fraction and soot volume fractions for four different flames. Two acetylene and two acetylene+methane fueled laminar jet diffusion flames stabilized in a coflow of air were considered. The details of the burner configurations and operating conditions are provided by Gore [5] and Gore and Skinner [6]. The experimental studies involved measurements of soot volume fractions using laser extinction and tomography, and mixture fractions using sampling and gas chromatography, at different positions in these flames. Therefore, a direct comparison of the model predictions with the experimental data is possible.

Results and Discussion

Figure 1 shows the measurements as well as the predictions of the coupled and three sets of uncoupled calculations with X_R = constant (35%, 50% and 60%). Global measurements of radiative loss fraction have yielded values close to 60% prompting this choice [5]. However, as seen in Fig. 1., this leads to two orders of magnitude lower soot volume fractions than those observed in the experiments. A decrease in 10% in the global radiative loss fraction leads to a factor of 20 increase in the peak soot volume fraction. However, the predictions are still significantly (by factor of five) lower than the data. A relatively low radiative fraction of 35% has to be used to achieve a peak soot volume fraction of 45 PPM. As seen in Fig. 5, this choice predicts reasonably rapid growth to the experimentally observed peak. However, the low value of X_R also leads to higher temperatures in the oxidation region and corresponding lower (by a factor of 2) predictions of soot volume fractions near 80 mm height. These results show that it is crucial to calculate local radiative fractions when modeling soot kinetics in strongly radiating flames. Figure 2 shows a comparison between measured and predicted soot volume fractions as a function of equivalence ratios at three axial locations for the two acetylene/air diffusion flames. The experimental data as well as the calculations show the effects of lack of diffusivity of soot. The predictions of soot volume fractions match the experimental data reasonably well. The peak soot volume fraction is underpredicted at the highest location for both the flames due to an overestimation of the oxidation rates. The current model neglects gas band radiation which is important close to the stochiometric regions where oxygen is present.

Another limitation of the oxidation model is the neglect of oxidation by OH radicals [7]. There is some disagreement between the predictions and measurements of the position of the peak soot volume fraction at the highest position for the Re=88 acetylene/air diffusion flame. This result is due to the underprediction of mixture fraction at that particular location. However, the trends in the relationship between equivalence ratio and soot volume fraction with axial position are captured reasonably well by the model predictions. Figure 3 shows the measurements [6] and predictions of peak soot volume fractions for flames burning mixtures of acetylene and methane in air. The close agreement between the predictions and measurements highlights the effectiveness of the coupled radiation/soot kinetics model.

References

1. Moss, J. B., Stewart, C. D., and Syed K. J., *Twenty-Second Symposium (International) on Combustion,* The Combustion Institute, Pittsburgh, 1988, p. 413.
2. Kennedy, I. M., Kollmann, W., and Chen, J. Y., *Combust. Flame* **81**:73-85 (1990).
3. Leung, K. M., Lindstedt, R. P., and Jones, W. P., *Combust. Flame* **87**:289-305 (1991).
4. Gore, J. P, Ip, U. S., and Sivathanu, Y. R., *J. of Heat Transf.* **114**:487-493 (1992).
5. Gore J. P., Ph. D. thesis, The Pennsylvania State University, University Park, PA, 1986.
6. Gore, J. P., and Skinner M., *Combust. Flame* **87**:357-364 (1991).
7. Puri, R., Moser, M., Santoro, R. J., and Smyth, K. C., *Twenty-Fourth Symposium (International) on Combustion,* The Combustion Institute, Pittsburgh, 1992, p. 1015.

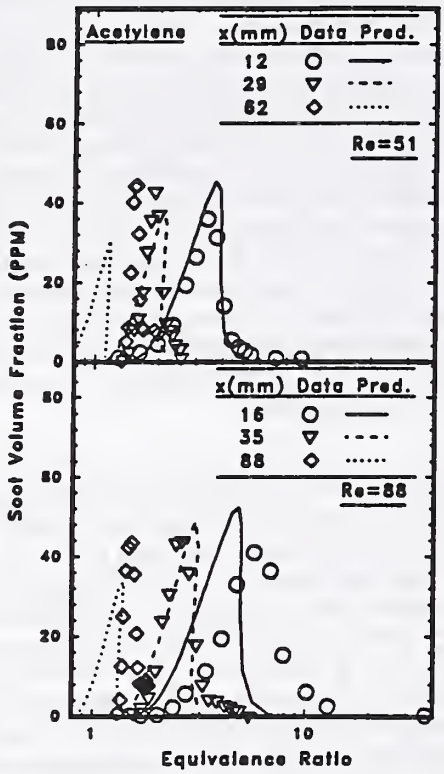

Fig. 2. Soot volume fractions as a function of equivalence ratio in at three axial locations in acetylene/air diffusion flames.

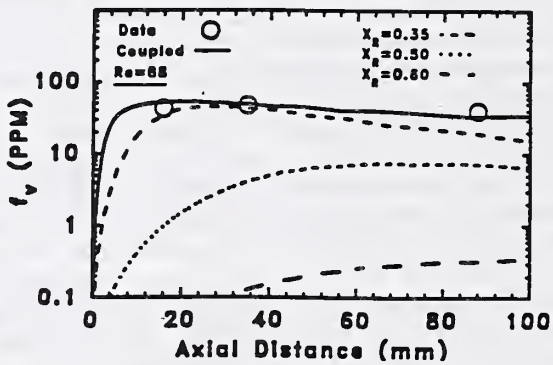

Fig. 1. Axial variation of peak soot volume fraction in an Acetylene/Air diffusion flame.

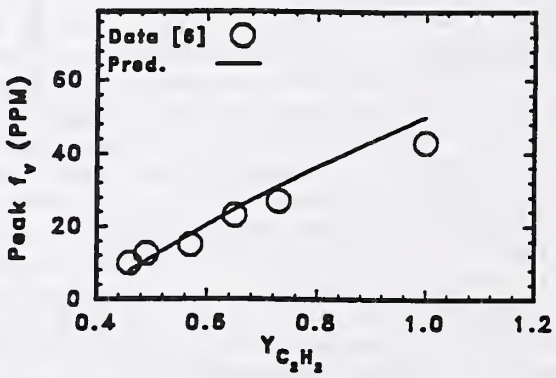

Fig. 3. Predictions and measurements of peak soot volume fraction for different mixtures of acetylene-methane/air diffusion flames.

Flame Height and Radiation Properties of High Liquid Loading Two Phase Spray Fires

P. Dutta and J. P. Gore
School of Mechanical Engineering
Purdue University, West Lafayette, IN 47907

Two phase spray fires with high liquid loading may result from accidental pressurized-liquid pipe leaks, storage tank breakage, and oil well blowouts. Most of the past research has focussed on fires with the fuel supplied as a gas or vapor. The present abstract summarizes the results of flame-height, radiant fraction and emission/absorption measurements for crude oil (80 to 95 % by mass) + methane fueled turbulent jet flames stabilized on an effervescent atomizer burner in stagnant air.

The heights of seven flames were measured using a video record by averaging over 10 frames. The resulting data are plotted as a function of heat release rate in Fig. 1. The data show that for a fixed heat release rate, the flames with the highest liquid loading (95%) are 25 % taller than those with the lowest liquid loading (85%). Figure 1 also shows the estimates of flame height obtained from the correlation of Hustad and Sonju as dark symbols. The velocity and density of the material exiting the burner were calculated from the two phase density and the total mass flow rate. Hence the "two-phase correction" was not used. In any event, if this correction was used, the differences between the measurements and predictions increase. The highest liquid loading (95%) flame is estimated by the correlation to be 15% shorter than the lowest loading (85%) flame for a fixed heat release rate of 14 kW. This is contradictory to the experimental data. The correlation suggests that the flame heights would be independent of heat release rate for fixed liquid loading (95%). However, measurements show that the flame height increases with liquid loading as seen from the open triangular symbols in Fig. 1. It is apparent from these results that two phase effects in spray fires need to be considered.

The radiation heat loss fractions (X_R) varied from 10 to 20% with increasing liquid loading for a fixed heat release rate of 14 kW. These values are low indicating a highly forced jet flame. The flame height correlations indicate a forced flame regime as well. However, the measurements show increasing flame height with heat release rate, perhaps due to two-phase rather than buoyancy effects. The reasons for the relatively low radiant heat loss were examined using path integrated measurements of emission and absorption by the flames at several axial locations. Figure 2 shows the emission temperatures and transmittances as a function of axial distance for liquid loadings of 95, 90 and 86%. The data show that the combustion efficiency of all three flames is relatively high. The transmittance for the low liquid loading flame is always high indicating low soot loading and resulting radiation. The transmittance for the highest liquid loading flame stays above 0.6 resulting in relatively low radiative heat loss and smoke emission to surroundings.

Acknowledgement: The work is partially supported by NIST Grant 60NANB1D1172 with Dr. Evans serving as Scientific Officer.

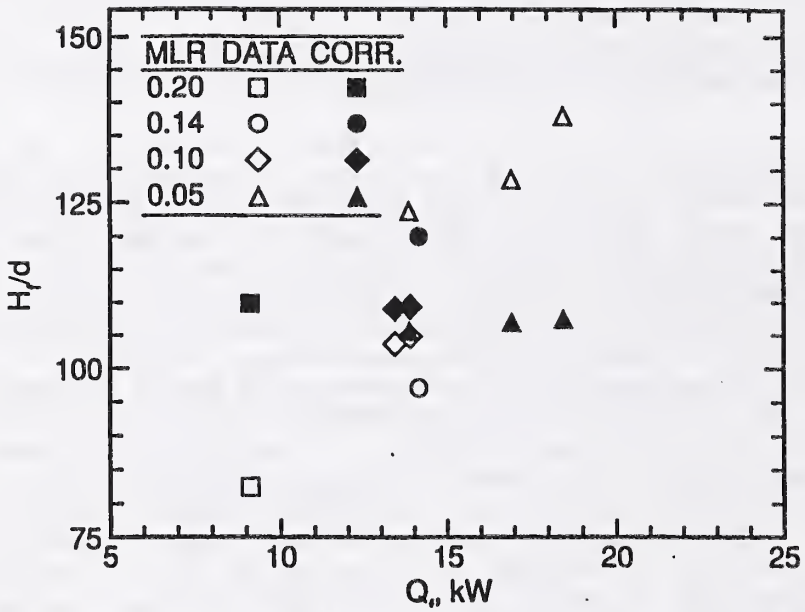

Fig. 1 Measurements of flame heights and results of an existing correlation for two phase spray flames.

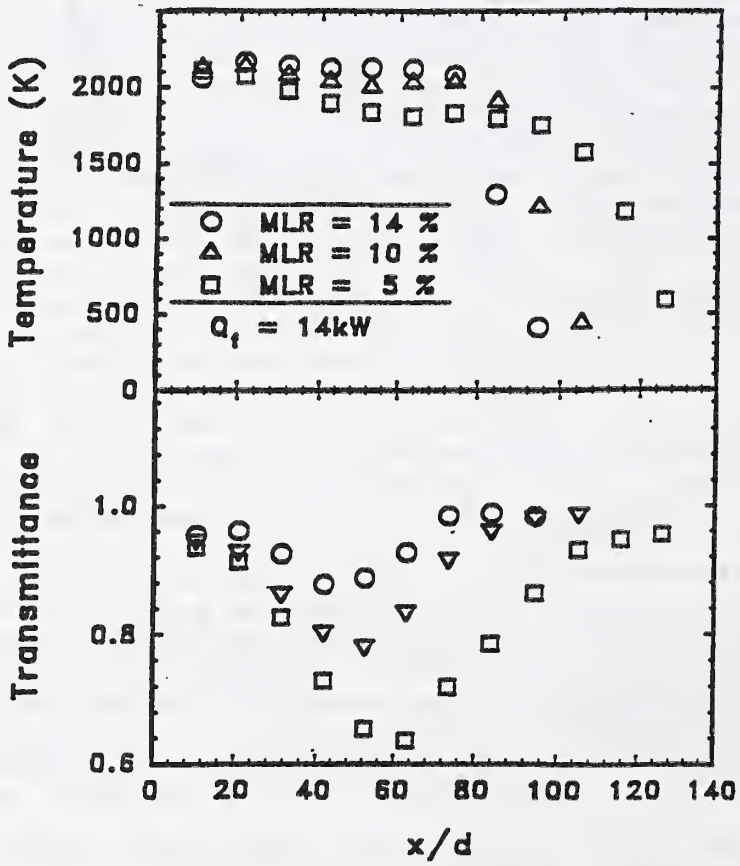

Fig. 2 Axial variation of emission temperatures and transmittance for 14 kW two phase spray flames for three liquid loadings.

"Using Fire Protection Systems and Hazards Analysis for Fire Protection Systems Selection and Design"

Dale Merrick, P.E.
Longhurst International

The purpose of this presentation is to present the use of Fire Protection Systems and Hazards Analysis (FHA) for the selection and design of fire protection systems. With the increasing problems in the determination, selection and justification of fire protection systems, additional support and guidance is now needed. The methodology of FPSHA is based on standard fire protection engineering practices combined with additional new techniques. FPSHA was created as an additional method to provide the greater level of information and data than normally developed during the use of existing code and regulations. While FPSHA was originally developed as a means to provide additional information and supporting data in the design and selection of fire protection systems for projects having special and/or unusual problems or where standard fire protection engineering practices it can also be used for other more standard applications. Presently, there are no specific guidelines and methodologies available in many fire codes to determine the type, level, and design constraints of the fire protection systems. This problem is especially evident when the application of performance based fire codes and systems design. Another area of concern that has greatly increased in the last five years is the issue of litigation. In the future, the selection and design of fire protection systems based solely on a broad based and undocumented interpretation of the fire and building codes will not be accepted. Additional information will be required to support the selection of specific fire protection systems. This information will then possible be subject to a detailed overview and interpretation, if there is not adequate technical and scientific data to justify the selection of the fire protection systems.

The basic concept for FPSHA is the Fire Protection Design Analysis (FPDA) approach presently already used by the Department of Energy. The key to FPSHA is the application of the Fire Effects and Responses Analysis (FERA). Applied as the level of detail requires, the use of FERA approach requires the use of Design Model Fires (DMFs) and Model Fire Scenarios (MFSs) to provide a basis for the analysis of the fire protection systems. These then employ Computer Fire Modeling, Cost/Benefit Studies and other analytical methods to provide a special level of detail and information on the fire protection systems and project design that would otherwise not be available. This also includes the concept of following the Fire Losses As Low As Reasonable (FLALAR) concept of the overall reduction of fire losses and fire protection costs.

Based on the "Systems Approach," an FPSHA report broadly reviews the project design including such diverse areas as HVAC system interface, passive fire protection, contents/process analysis, fire signature, occupant characteristics, and facility operation modes. This information is then integrated into FERA for development of the final systems selection. Other special areas that an FPSHA is designed to review includes: life safety; occupational and health safety; security; and environmental protection.

An example of the changing face of fire protection will be the requirement in the near future to include such special analytical areas as the Occupant Injury Index (OJI), Occupant Expected Response Scenario (OERS), and Fire Smoke Signature Analysis (FSSA) which have not been conducted, or even considerations in the past. These and many other special areas are assuming an increasing importance in the field of fire protection as performance based fire codes are being implemented. These areas must be included in the consideration of future fire protection systems due to the impact of new government involvement in fire protection systems. An example of this new type of regulation is the involvement of the Environmental Protection Agency in the recent review and acceptance of halon alternatives not only from a pure environmental standpoint, but health and safety aspects as well. This type of special governmental review will continue to grow in the future necessitating even more detailed fire protection reviews and analyses. It was with these types of challenges and the others already mentioned that the FPSHA methodology was developed.

While still in the early stages of application and in only very limited use FPSHA has already laid the groundwork for a number of special activities. Included is the initiation of the development of a special fire modeling program using finite element analysis (FEA), and the development of an actual FPSHA program using existing fire modeling codes.

SELF-PRESERVING ROUND TURBULENT PLUMES

Z. Dai, L.-K. Tseng and G.M. Faeth
Department of Aerospace Engineering
The University of Michigan
Ann Arbor, Michigan 48109-2140

Introduction. The structure of round turbulent plumes is an important fundamental problem, relevant to flows found in fire environments and exhaust plumes, that has attracted significant attention since the classical study of Rouse et al. [1]. Conditions within the self-preserving portion of plumes, where both mean and fluctuating properties exhibit similarly when variables are scaled appropriately, generally have been sought in past studies, in order to simplify the interpretation of measurements. In particular, the self-preserving region of plumes represents a quasi-stationary dynamic state that highlights interactions between buoyancy and turbulence without the intrusion of disturbances from the source that generally are hard to characterize. Thus, flow properties within self-preserving plumes are important for developing and evaluating models of buoyant turbulent flows, see Pivovarov et al. [2] and references cited therein. Unfortunately, there are considerable differences among existing measurements of mean and turbulent properties stated to be within the self-preserving portion of round turbulent plumes [1-14]. A possible reason for the difficulty is that although existing results reached conditions where buoyancy dominates effects of source momentum, according to the criterion of Morton [15], the measurements involved relatively small streamwise distances in comparison to values required for self-preserving conditions in nonbuoyant jets [16,17]. Thus, the objectives of the present study were to complete measurements of mean and fluctuating velocities and scalar properties in round turbulent plumes in order to assess conditions required for self-preserving flow. More details about the study may be found in Dai et al. [18].

Experimental Methods. Plume conditions were simulated using dense gases (carbon dioxide and sulfur hexafluoride) in still air, within a screened enclosure to control effects of room disturbances. Mean and fluctuating velocities were measured using laser velocimetry. Scalar properties were represented by the mixture fraction (the mass fraction of source gas in a sample) using state relationships for isothermal mixing to find other scalar properties. Mixture fractions are measured by seeding the source flow with iodine vapor and using two-point laser-induced iodine fluorescence (LIF).

Results and Discussion. Figures 1 and 2 illustrate the evolution of mean and fluctuating mixture fractions, $\bar{f}$ and $\bar{f}'$, with distances from the virtual origin $x\text{-}x_0$, where Fr_0 is the source Froude number, ρ_0 and ρ_∞ are the source and ambient densities, d is the source diameter, r is radial distance and the subscript c denotes conditions at the flow axis. The variables in these figures are scaled according to the requirements of self-preserving round turbulent plumes [15-17]. The results show a progressive narrowing of the flow with increasing distance until self-preserving conditions are reached for $(x\text{-}x_0)/d \geq 87$; this region is more than 12 Morton length scales from the source, indicating that effects of buoyancy are dominant [15,17], with plume Reynolds numbers of 2500-4200 which are reasonably high for unconfined turbulent flows [17-19]. The present self-preserving plumes are narrower, with higher scaled values at the axis, than past results which appear to be in the transitional portion of the flow [1-14], which helps explain difficulties using established turbulence models to predict their properties assuming self-preserving flow [2].

The plots of mixture fraction fluctuations in Fig. 2 highlight effects of buoyancy on the properties of turbulent plumes. In particular the results near the source exhibit a dip near the axis, similar to nonbuoyant jets [16,17]. The dip, however, disappears completely in the self-preserving region, yielding values of maximum mixture fraction fluctuations in plumes roughly twice those observed in nonbuoyant jets. This behavior can be attributed to turbulence production near the axis of plumes due to buoyant instability in the streamwise direction. Another interesting effect of buoyancy/turbulence interactions in plumes is that conventional -5/3 power decay of temporal power spectra, associated with the inertial subrange of turbulence, is followed by a prominent -3 power subrange not seen in nonbuoyant turbulence—called the inertial-diffusive subrange where the local dissipation of turbulent fluctuations is caused by buoyancy-generated inertial forces rather than viscous forces [12].

Acknowledgments. This research was supported by the United States Department of Commerce, National Institute of Standards and Technology, Grant No. 60NANB1D1175, with H. R. Baum of the Building and Fire Research Laboratory serving as Scientific Officer.

References

1. H. Rouse, C.S. Yih and H.W. Humphreys, Tellus 4:201-210 (1952).
2. M.A. Pivovarov, H. Zhang, D.E. Ramaker, P.A. Tatem and F.W. Williams, Combust. Flame 92:308-319 (1992).
3. G. Abraham, ASCE J. Hyd. Div. 86:1-13 (1960).
4. W.K. George, Jr., R.L. Alpert and F. Tamanini, Int. J. Heat Mass Trans. 20:1145-1154 (1977).
5. A. Shabbir and W.K. George, Jr., NASA Tech. Memo. 105955, 1992.
6. V.D. Zimin and P.G. Frik, Izv. Akad. Nauk. SSSR, Mekh. Zhid. Gaza 2:199-203 (1977).
7. T. Mizushima, F. Ogino, H. Veda and S. Komori, Proc. Roy. Soc. London A366:63-79 (1979).
8. F. Ogino, H. Takeuchi, I. Kudo and T. Mizushima, Int. J. Heat Mass Trans. 23:1581-1588 (1980).
9. E.J. List, Ann. Rev. Fluid Mech. 14:189-212 (1982).
10. N.E.Kotsovinos, Int. J. Heat Mass. Trans. 28:771-777 (1985).
11. P.N. Papanicolaou and E.J. List, Int. J. Heat Mass Trans. 30:2059-2071 (1987).
12. P.N. Papanicolaou and E.J. List, J. Fluid Mech. 195:341-391 (1988).
13. D. Papantoniou and E.J. List, J. Fluid Mech. 209:151-190 (1989).
14. J. Peterson and Y. Bayazitoglu, J. Heat Trans. 114:135-142 (1992).
15. B.R. Morton, J. Fluid Mech. 5:151-163 (1959).
16. J.O. Hinze, *Turbulence*, 2nd ed., McGraw-Hill, New York, 175-319, 1975.
17. H. Tennekes and J.L. Lumley, *A First Course in Turbulence*, M.I.T. Press, Cambridge, 1972.
18. Z. Dai, L.-K. Tseng and G.M. Faeth, J. Heat Trans. in press.

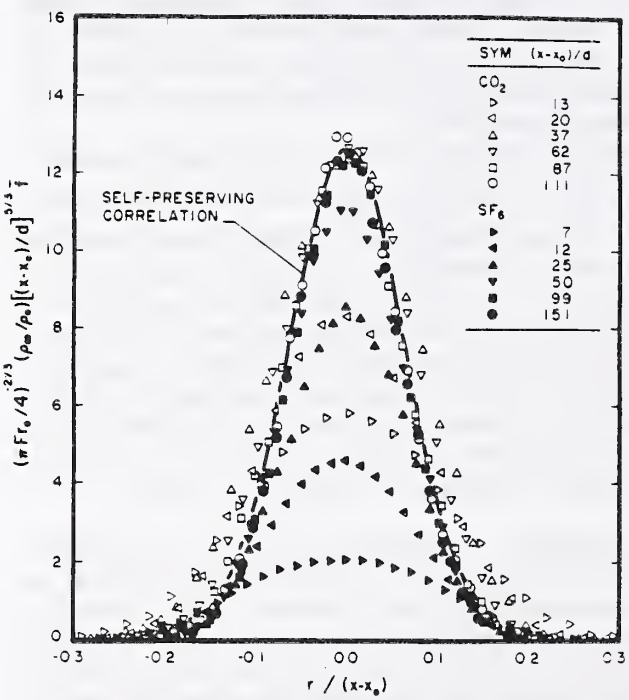

Fig. 1 Mean mixture fractions.

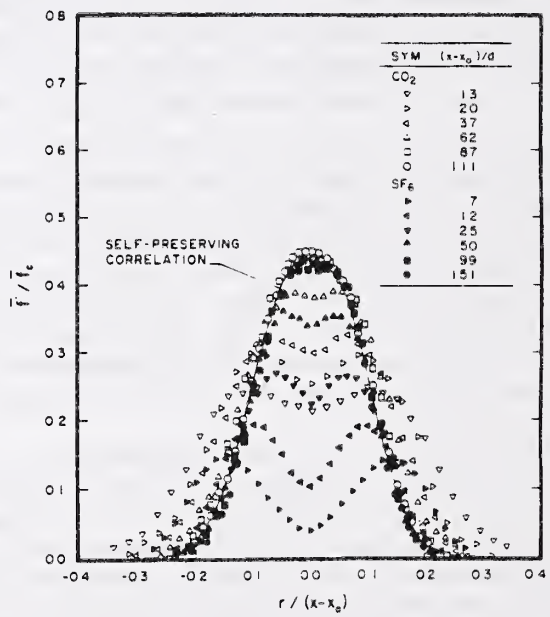

Fig. 2 Mixture fraction fluctuations.

OPTICAL PROPERTIES OF SOOT IN DIFFUSION FLAMES

Ü.Ö. Köylü and G.M. Faeth
Department of Aerospace Engineering
The University of Michigan
Ann Arbor, Michigan 48109-2140

Introduction. Both predictions of continuum radiation from flames, and nonintrusive laser-based measurements of soot structure and concentrations, require an understanding of the optical properties of soot. Soot optical properties are a challenging problem, however, due to the complexities of soot structure. In particular, soot consists of small spherical primary particles that collect into open structured aggregates having a broad distribution of sizes [1]. Thus, various models of soot optical properties have been proposed, including Rayleigh scattering, Mie scattering for an equivalent sphere and Rayleigh-Debye-Gans scattering for polydisperse fractal aggregates (denoted RDG-PFA theory in the following) [2]. RDG-PFA theory appears to be the most promising approach [3-8]. In particular, recent measurements of both soot structure and scattering properties for soot aggregates found in the overfire region of buoyant turbulent diffusion flames exhibited good agreement between measurements and predictions based on RDG-PFA theory [7]. However, these overfire soot aggregates were too large for practical scattering measurements in the small-angle (Guinier) regime where use of the RDG scattering approximation is least reliable [2]. Thus, the objective of the present investigation was to carry out a similar study for soot aggregates in the fuel-rich (underfire) region of buoyant laminar diffusion flames, where smaller aggregate sizes provide improved access to the Guinier regime.

Experimental Methods. The test apparatus consisted of round laminar jet diffusion flames directed upward in coflowing air. Several positions along the axis of ethylene and acetylene flames were considered. Soot structure was measured using thermophoretic sampling and analysis by transmission electron microscopy (TEM). Soot scattering was measured using the 514.5 nm line of an argon-ion laser with collecting optics capable of observing scattering at angles in the range 20-160° for various polarization orientations. Absolute scattering levels were found, based on calibrations using Rayleigh scattering from nitrogen.

Theoretical Methods. Predictions of soot optical properties were based on RDG-fractal aggregate methods described in Refs. [1,4,6] for a single aggregate, however, attention was focused on the RDG-PFA theory of Köylü and Faeth [7]. This approach extends methods of Dobbins and Megaridis [6] for polydisperse fractal aggregates to provide an improved treatment of the large-angle (power-law) regime. Soot structure was prescribed in two ways: (1) directly from the TEM structure measurements, and (2) with the higher moments of the aggregate size distribution functions selected to best fit the scattering measurements, because experimental uncertainties of these moments are rather large (ca. 40%).

Results and Discussion. The soot structure measurements indicated aggregate fractal dimensions of 1.73-1.77, which are comparable to a variety of earlier measurements of soot in flame environments, see Ref. [2] and references cited therein. Other structure properties varied with the fuel and the position within the flame, yielding the following ranges: primary particle diameters of 21-54 nm, mean number of primary particles per aggregate, $\overline{N}$, of 31-83, and $\overline{N}^2/\overline{N}$ of 70-154—the last indicating the broad size range typical of soot aggregates.

Present predictions of differential soot scattering cross-sections based on measured soot structure properties were in good agreement with measurements: discrepancies for ethylene aggregates were negligible while those for acetylene aggregates were less than 37%—well within uncertainties anticipated due to the uncertainties of $\overline{N}^2/\overline{N}$. Some typical measured and predicted scattering patterns are illustrated in Figs. 1 and 2 with predictions based on fitted higher moments. Figure 1 is for relatively small soot aggregates in the underfire region of the laminar ethylene flame, which is dominated by the Guinier regime: this exhibits behavior somewhat beyond Rayleigh scattering behavior with forward scattering roughly three times larger than back scattering. Figure 2 is for relatively large soot aggregates in the overfire region of a large buoyant turbulent acetylene flame from Ref. [7], which is dominated by the power-law regime: this exhibits behavior well beyond Rayleigh scattering behavior with forward scattering more than one hundred times larger than back scattering. The comparison between predictions and measurements is seen to be quite good over the broad range of scattering conditions illustrated in Figs. 1 and 2.

Acknowledgments. This research was supported by the United States Department of Commerce, National Institute of Standards and Technology, Grant No., 60NANB1D1175, with H. R. Baum of the Building and Fire Research Laboratory serving as Scientific Officer.

References

1. R. Jullian and R. Botet, *Aggregation and Fractal Aggregates*, World Scientific Publishing Co., Singapore, 45-60, 1987.
2. Ü.Ö. Köylü and G.M. Faeth, J. Heat Trans. 115:409-417 (1993).
3. T. Freltoft, J.K. Kelms and S.K. Sinha, Phys. Rev. B 33:269-275 (1986).
4. J.E. Martin and A.J. Hurd, J. Appl. Cryst. 20:61-78 (1987).
5. M.Y. Lin, H.M. Lindsay, D.A. Weitz, R.C. Ball, R. Klein and P. Meakin, Proc. Roy. Soc. London A423, 71-87 (1989).
6. R.A. Dobbins and C.M. Megaridis, Appl. Optics 30:4747-4754 (1991).
7. Ü.Ö. Köylü and G.M. Faeth, J. Heat Trans., in press.
8. Ü.Ö. Köylü and G.M. Faeth, J. Heat Trans., submitted.

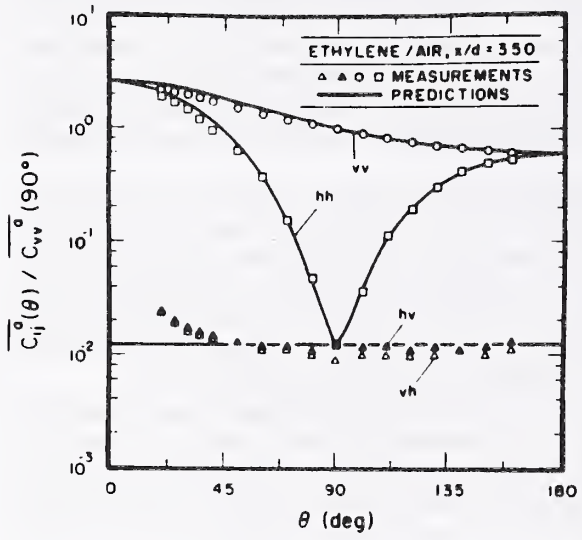

Fig. 1

Typical scattering pattern of underfire soot.

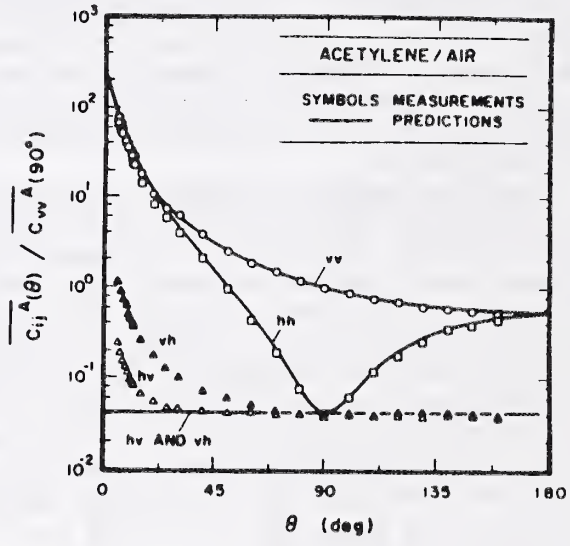

Fig. 2

Typical scattering pattern of overfire soot.

CORROSIVITY TEST METHODS FOR POLYMERIC MATERIALS PART 5 - A COMPARISON OF FOUR TEST METHODS

STEPHEN L. KESSEL
Quantum Chemical Corporation, USI Division

CHARLES E. ROGERS
Union Carbide Corporation

JAMES G. BENNETT, JR.
GE Plastics

ABSTRACT

The effects of smoke and corrosive gases released in a fire are gaining increased attention. Several recent fires have revealed that significant damage to equipment occurs from gas corrosion rather than from direct flame exposure. Corrosion is particularly important with fires around electronic equipment such as computers and telecommunications equipment. The concern over corrosive gas release extends to building structures, as structural components can be damaged and weakened in a fire. Concerns about corrosion underscore the need for standardized tests that measure smoke corrosivity.

This is the fifth in a series of papers on corrosivity test methods published by the Polyolefins Fire Performance Council, a unit of the Society of the Plastics Industry, Inc. In this paper, four test methods are compared for their ability to evaluate smoke corrosivity of polymeric materials; 1) the proposed ASTM E05.21.70 radiant combustion/exposure standard test method, 2) the CNET corrosivity test standard being reviewed by ISO (DIS 11907-2), 3) the DIN 57 472 acid gas test standard, and 4) the proposed ASTM D09.21.04 cone corrosimeter standard test method.

The ASTM E05.21.70, CNET and ASTM D09.21.04 test methods directly determine the corrosive effects of combustion gases, as they measure the resistance changes in copper circuit targets exposed to the gases. The ASTM tests report the resistance change in terms of metal loss and the CNET test reports the resistance change in terms of % corrosivity factor. The DIN test standard determines the conductivity and pH changes of aqueous solutions through which combustion gases are passed. Each method is discussed in detail.

Twenty-four polymeric materials were evaluated for smoke corrosivity by these four test methods, so that the test methods could be reliably compared based on results from many types of polymeric materials. The polymeric materials evaluated are commercially available and they cover a broad range of compositions used for wire and cable insulation and jacketing. Included are non-halogenated filled polyolefins, polyolefins containing halogenated flame retardants, halogenated polymers, high temperature thermoplastics, polyolefin and nylon base resins and a Douglas fir reference material.

The ASTM E05.21.70, CNET, DIN and ASTM D09.21.04 tests are evaluated based on several criteria. Each test is evaluated on the basis of precision, or whether the test is repeatable, and accuracy, or whether the test differentiates corrosive potentials consistent with the expectations based on the known chemistry of the material compositions. To also determine accuracy, the ASTM E05.21.70, CNET and D09.21.04 test methods are compared to the DIN 57 472 test method, as this test and similar acid gas tests are accepted standards that have been historically used to measure corrosive potential. The methods are also compared in terms of equipment cost and availability and the convenience of operation.

The results show that no one test method satisfies all criteria for measuring corrosive potential. Each of the four test methods ranked the corrosive potentials differently, indicating that numerical results from different methods or results from different targets within one method cannot be used interchangeably.

The proposed ASTM E05.21.70 standard test method differentiated the corrosive potentials consistent with expectations based on the known chemistry of the material compositions. The ASTM E05.21.70 results are generally consistent with the DIN 57 472 conductivity and pH results.

The CNET test standard did not differentiate the corrosive potentials in a manner consistent with the expectations based on the known chemistry of the material compositions. The CNET results are generally not consistent with the DIN 57 472 conductivity and pH changes.

Of the four test methods, the DIN 57 472 acid gas test standard gave the greatest differentiation of corrosive potentials with the most repeatable results. The DIN 57 472 test standard does not directly measure the corrosive potential, as it measures conductivity and pH changes.

The proposed ASTM D09.21.04 standard test method provided limited differentiation of corrosive potentials when run at 50 kW/m^2 with 45,000 Å targets. The 45,000 Å target results are generally consistent with both the expectations based on the known chemistry of the material compositions and the DIN 57 472 conductivity and pH results.

When 2500 Å targets were used in the D09.21.04 test, specimens for many materials exceeded the target span, making it difficult to differentiate materials and to compare metal loss results to DIN 57 472 conductivity and pH results. Some of the 2500 Å target results are not consistent with the expectations based on the known chemistry of the material compositions.

The proposed ASTM E05.21.70 standard test method gave numerical corrosion results consistently lower than the proposed ASTM D09.21.04 standard test method, when 2500 Å targets were used in both tests.

Chemistry of Fluorinated Species in Hydrocarbon Flames

D. Burgess, Jr., W. Tsang, P.R. Westmoreland, and M. R. Zachariah
Chemical Science and Technology Laboratory
National Institute of Standards & Technology
Gaithersburg, MD 20899

Abstract

A comprehensive list of thermochemistry for halogenated hydrocarbons was compiled with an emphasis on fluorinated compounds. This compilation includes substituted methanes, ethanes, ethylenes, and their radicals and experimental, theoretical, or estimated values. From these data, group additivity values were determined in order to estimate thermochemistry for other compounds. A comprehensive list of kinetic rate constants for reactions involving the fluorinated hydrocarbons was also compiled. For hydrogen abstraction reactions, a simple exponential relationship between the heat of reaction and activation energy for the reaction was determined. For important reactions where no kinetic data were available, rate constants were estimated by analogy to other similar reactions. This reaction set was then combined with a validated hydrocarbon/air mechanism and used under a variety of conditions (assuming plug flow) to simulate the fluorocarbon chemistry. From this work a preliminary reaction mechanism (involving a subset of the species and reactions in the complete reaction set) was determined. This mechanism is being extended to a premixed flame calculations and eventually a diffusion flame system.

Surface Mount Technology - Can Miniaturization Lead To Safety Problems ?

Flammability Evaluation Of Surface Mount Adhesives

Peter J. Boden - Engineering Research, Underwriters Laboratories Inc.

Advances in the electronics industry have lead to new design, assembly, and manufacturing techniques to miniaturize electronic components and circuitry. One such advancement is called surface mount technology (SMT). SMT involves using miniaturized electronic components called surface mount devices (SMD). SMDs have electrodes or specialized leads rather than through-hole leads for electrical connection to the circuit of a printed wiring board (PWB). The electrodes of the SMD are soldered directly to the pads of a trace on the surface of the PWB. Figure 1 shows 1) a through-hole assembly, 2) a surface mount assembly with a common gull-wing lead and surface mount adhesive, and 3) the approximate proportion between the two assemblies.

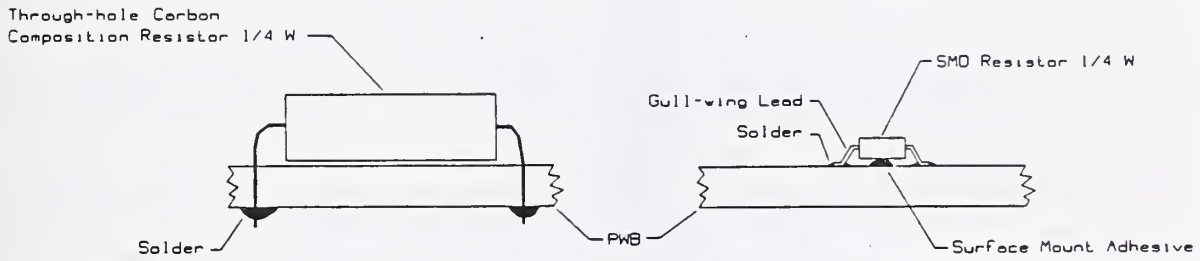

Fig. 1 - Through-hole and Surface Mount Assemblies. SMDs are mounted directly to the surface of a printed wiring board (PWB) rather than inserting component leads through a PWB as in through-hole design.

Surface mount adhesives are used to affix a SMD onto the surface of a PWB prior to the soldering process. The main function of the adhesive is to prevent component loss from the board until soldering has taken place. The purpose of this original work, which was sponsored by the Electronic Industries Association (EIA), was to acquire data on the effect that adhesives have on the flammability classification of a PWB.

Three generic classes of adhesives are used in SMT. These classes are epoxies, acrylics, and epoxy acrylates. Within these classes, 16 different adhesives were provided by EIA member companies for this original work. The adhesives included six epoxies, four acrylics, and six epoxy acrylates.

The vertical burning test for classifying materials was conducted in accordance with the Standard for Safety, *Tests For Flammability Of Plastic Materials, UL 94*, Third Edition on the surface mount adhesives. Identical 5 X 1/2 X 1/16 inch thick UL/ANSI type CEM-1 laminate boards were used for all test and control samples. The boards consisted of epoxy resin with a base material of continuous filament glass fabric surface and a cellulose paper core.

Two rounds of vertical burning tests were conducted.

Round 1

The vertical burning test was conducted on 16 different adhesives to determine the effect on the flammability classification of the CEM-1 laminate board. Ten board samples were tested for the control and ten for each of the 16 adhesives. Each unique adhesive was applied in a uniform thickness to one entire surface of ten CEM-1 boards. The adhesives were then cured either by IR or a combination of IR and UV. The control samples were as-received uncoated boards. The results were used to categorize the effect of each adhesive on the overall flammability classification of the CEM-1 board.

The results showed that of the 16 adhesives tested, ten did not qualify for a flammability classification and four complied with the requirements for a 94V-1 classification. Two types of adhesives complied with the requirements for the higher, 94V-0 classification, the same classification as the uncoated CEM-1 control board.

Round 2

The vertical burning test was conducted on the CEM-1 test boards with the adhesive from each generic class that had the longest total burn times in Round 1. Ten board samples were tested for each of the three adhesives. Each unique adhesive was applied to one side of a test board in a dot matrix pattern. The pattern, shown in Figure 2, represented a dot density considered greater than found in actual production practices. The dot size, however, was typical of an actual production size. The adhesives were cured using the same methods as in Round 1.

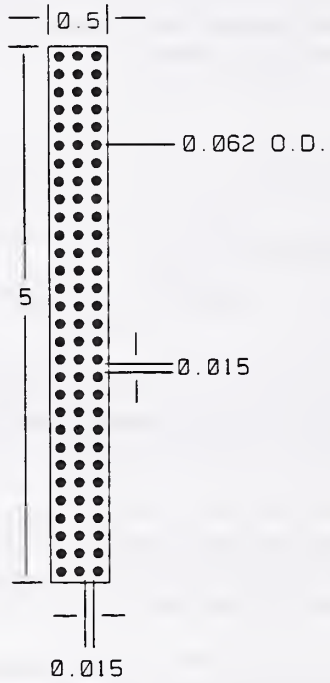

Fig. 2 - Dot Matrix Pattern. All dimensions are in inches.

The results of the vertical burning test conducted on adhesives applied to the test boards in a dot matrix pattern showed that all three adhesives complied with the requirements for a 94V-O flame class. This flame class is the same as the CEM-1 control board.

The results suggest that surface mount adhesives do not adversely affect the flammability classification of a PWB, at least for the test design and sample configurations within this work. As a result of this original work, UL does not require additional end-product flammability based testing of PWBs employing surface mount adhesives, such as those used in the radio and TV industries. This outcome results in a long-term cost-effective benefit to the electronics industry.

LEGAL AND ECONOMIC CRITERIA FOR THE REGULATORY USE OF COMPUTERIZED FIRE MODELS: REGULATORY EFFECTIVENESS ANALYSIS

Vincent Brannigan J.D.
Professor
Department of Fire Protection Engineering
University of Maryland College Park
College Park Md. 20742
301-405-6667vb15@umail .umd.edu

Carol Meeks Ph. D.
Professor and Head
Department of Housing and Consumer Economics
University of Georgia, Athens Georgia

The regulation of fire safety has an ancient history. In each generation new hazards and new responses are developed and integrated into the social response to fire. There is a constant tension between the desire to use new technology and design to build structures and the social need for protection from fire. One of the most important recent developments in the fire safety field has been the use of computerized mathematical models of fires and fire risk. It has been proposed that these models be used in the determination of acceptability of various technologies for fire safety regulation.

The primary rationale for the use of these models is that construction costs will be reduced without reduction in the life safety requirements of buildings. The models may also permit the construction and use of types of structures which were not available under traditional codes. However, the introduction of such models also causes concern, since they may not be supported by the widespread base of technical experience with existing building construction techniques which underlies the existing regulatory structure. Before the widespread use of such models can be approved, it is necessary to analyze the suitability of such models under existing or possible building regulatory systems. Regulatory Effectiveness Analysis is a tool for examining the social control of technological hazards.

REGULATORY EFFECTIVENESS ANALYSIS (REA) is a method for evaluating the compliance of a technological system with an existing or proposed regulatory program. REA is designed to measure separately and together three key components of a technical regulatory system:

The first component in the REA is the set of PUBLIC POLICIES which might be accomplished. Public policy is a narrative statement of the goals to be achieved by the regulatory program. These statements can be either concrete or abstract. For example, some authors claim that the socially acceptable level of building safety is embodied in buildings built in compliance with current codes. A mathematical model which generates an equivalent level of safety would arguably satisfy the public policy standard. However, it can be equally argued that a building can comply with current codes, yet fall below the socially desired level of safety. Societies often change their codes in response to greater

understanding of hazards and control techniques. The greater knowledge of hazards generated by a mathematical model might even be the catalyst for such change.

Public policy can be thought of as a combination of economic efficiency and distributional equity. For example, how much fire protection should we expect the owner to build into a building, and how much should be provided by the Government? In addition, users of buildings, especially ordinary consumers, expect a certain level of government protection. Several new technologies, which lower costs to builders, have been shown to increase life cycle costs to consumers. Effective articualtion of the public policies is critical to analysis of the acceptability of the models.

The second component in the REA is the set of LEGAL STRUCTURES used to implement the public policy. Regulation requires a mechanism to enforce the social will on individuals or firms who would not otherwise comply. Legal structures are the formal requirements imposed by the society. For convenience, in the area of building regulation we can consider both the code and the enforcement mechanism to be legal structures. Questions usually arise over ambiguities or inadequacies in the code itself, and the probability at any time of actual enforcement of the code.

The third component in the REA is the set of TECHNICAL TOOLS available for regulation. Every technology has a distinct and often limited set of technical tools available. Technical tools are not limited to machines or laboratories; statistical quality assurance and post fire investigations are all technical tools. In this paper the technical tools to be analyzed are mathematical models of the performance of buildings in fires. These models show all of the characteristics of mathematical models used in other fields of endeavor. It is necessary to examine the underlying assumptions of the models, and to test them by determining their precision, accuracy, robustness, level of resolution, and calibration. It is also necessary to show that the mathematical model has been properly transformed into a computer program, by validation and verification of the software.

The theory of Regulatory Effectiveness Analysis is that all three of these components must be properly designed to achieve a working regulatory system. Public policies must be coherent, legal structures must contain all necessary elements, and technical tools must be available and produce the needed results. Further, the components interact. Public policy, legal structures and technical tools have interlocking sets of requirements and capabilities. REQUIREMENTS are the preconditions which must be satisfied by other components before a given component can function. CAPABILITIES reflect the ability of a tool to satisfy a requirement of another component. For example, a given public policy tool requires certain capabilities in the legal structure. Similarly, a legal structure has capabilities that can satisfy the needs of public policy. If a component is ill defined or there is no match between policy goals, structure and tools a "**discontinuity**" exists. Public policy, legal structures and technical tools must be matched to one another to produce a functioning regulatory program. The relationship among these characteristics is shown in the diagram below:

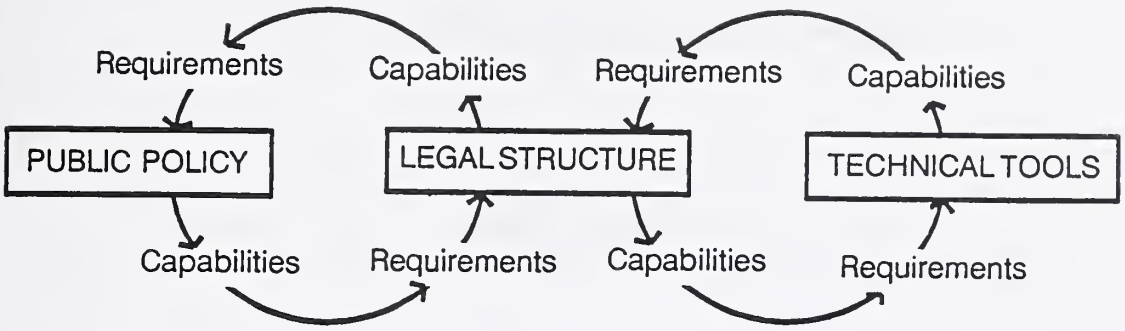

To examine the suitability of computerized fire models for regulatory use, it will be necessary to construct a matrix which compares the requirements and capabilities of the mathematical model, and compares it to both existing and possible legal structures. For example, a given computerized fire model assumes the continued existence of a particular level of municipal fire protection. REA analyses whether the legal system has the capability of making sure that the level of fire protection continues in place, and queries whether the model describes adequately the consequences of such failures. The matrix provides a series of questions to be posed to the users and developers of such models, and indicates the importance of such questions to the regulators. These question include:

What is the protection against interdependence of the variables?
What is the proof that all relevant variables are included?
Has the entire model been published?
How was the model validated?
What are the assumptions used in the model?
What are the assumptions used in the data?
What is the confidence structure built into the model?
What is the reliability of the data?
Describe the sensitivity analysis used to check the model.
Describe with particularity the code provisions which lead to different scores between buildings.
Describe with particularity the physical or behavioral assumptions which lead to differences between buildings.

While adequate answers to these questions do not necessarily indicate that a model is valid, failure to properly answer them would indicate that the model is not yet well enough defined to meet the requirements of the regulators. The regulatory use of computerized risk assessment models depends on the ability of the modeler to properly specify the model, obtain data suitable to the model, and carry out appropriate validation and verification tests of the model. It is the job of the regulator to ensure that the model reflects the appropriate public policy and legal structures. The regulator must be especially on guard that technical decisions are not masquerades for substituting private technical judgements for public safety decisions. Otherwise this potentially very useful technique will not achieve its potential in fire safety regulation.

Incorporating Heat Conduction into a Zone Fire Model

William F. Moss
Clemson University
Department of Mathematical Sciences

Abstract

Heat conduction through the ceilings, walls, and floors of the rooms in a zone fire model can be modeled by an initial-boundary value problem for the 1-D or 2-D heat equation. Using the method of lines (MOL), this problem can be reduced to a differential-algebraic equation (DAE) system. This DAE system, together with the ordinary differential equations for pressure, layer height, and upper and lower layers temperatures in a room, make up the full model which is a large DAE system. The bulk of the solution variables and the CPU time is attributable to the heat conduction submodel.

A domain decomposition method has been developed for splitting this large DAE system into a main system and a secondary one. The main system is solved for pressure, layer height, upper layer temperature, lower layer temperature, and the temperatures at ceiling, wall, and floor surfaces. The secondary system is used to model heat conduction. The main and secondary systems are coupled through heat flux boundary conditions at ceiling, wall, and floor surfaces (heat flux in equals heat flux out). Time discretization for the secondary system is done using the backward Euler method. The time stepsize used for the secondary system is the stepsize chosen by DASSL, the DAE solver used for the main DAE system. This method has proved to be both efficient and accurate.

An Instrument for Characterization of the Thermal and Optical Properties of Charring Polymeric Materials

Michael A. Serio, David S. Pines, Anthony S. Bonanno, and Peter R. Solomon
Advanced Fuel Research, 87 Church Street, East Hartford, CT 06108

Abstract

A test instrument is under development which will be used to characterize the changes in thermal and optical properties of charring polymeric materials when exposed to radiative heat fluxes. The system is based on a bench top emissometer apparatus which was developed at AFR to simultaneously measure the surface temperature and spectral properties of a material. The advantage of using a modified emissometer is that the front surface temperature is measured accurately with a thermocouple since these are affected by the radiant heat source. Time resolved measurements of the front surface temperature, along with thermocouple measurements of the back surface temperature provide information on the changes in thermal conductivity and thermal diffusivity with the extent of charring. These data can be used for characterization of polymeric materials or as inputs into a model of a charring polymer surface. In addition, this apparatus measures the changes in the material's spectral emissivity and functional group composition as it chars. Data will be presented for experiments on two different samples of 1/8" thick polyurethane, heated using black body source temperatures from 600°C to 850°C.

Tunable Diode Laser Diagnostics of Ethylene/Air Axially Symmetric Diffusion Flames

R. Reed Skaggs and J.Houston Miller
Department of Chemistry
The George Washington University
Washington, D.C. 20052

We report here *in situ* measurements of carbon monoxide concentration and local flame temperature in a series of ethylene/air axially symmetric laminar diffusion flames. These measurements will allow for further insight into the dynamics of thermal loss from soot radiation, soot oxidation, and carbon monoxide emission processes that occur in "sooting" flames. For these studies we have matched experimental conditions for three fuel flow rates conditions given by Santoro et. al. [1] referred to as non-sooting (NS), incipient sooting (IS), and sooting (S) flames. These authors studied soot formation in these flames using a thermocouple to measure the local flame temperature and laser light scattering and extinction to measure local soot properties. Their results have shown qualitatively how temperature at the flame tip decreases with fuel flow rate due to increased radiative heat transfer at higher soot loadings. Our measurements compliment these earlier ones by adding carbon monoxide concentrations to the data available at the flame tip and providing a check of the thermocouple temperature measurements.

The use of tunable diode laser absorption spectroscopy (TDLAS) for *in situ* diagnostics in axisymmetric laminar hydrocarbon diffusion flames is developing into a useful tool for combustion diagnostics. High sensitivities are available using wavelength modulation techniques which is critical in short beam length regions such as that at the tip of these diffusion flames. During the past year, our TDLAS research has involved the study of two axisymmetric laminar hydrocarbon diffusion flames, methane/air and ethylene/air. Both flames have been previously studied by Santoro et. al. using probe, thermocouple, and optical techniques [1,2]. Probe and thermocouple are intrusive and difficult to employ in highly sooting environments (because of probe clogging and soot deposition), but infrared absorption is applicable in studies of particle-laden flows because of the relative insensitivity to scattering and extinction at long wavelengths.

Our studies of a methane/air flame allowed for the development of a reliable experimental technique that was extended to ethylene/air flames with flow rates near the sooting limit. In our experiments with the three ethylene/air flames described above, second harmonic spectra of the (CO) lines, R(15) & R(7), were collected every 0.5 mm at a height of approximately 55 mm HAB (Height Above Burner). For measurements at a height of 10 mm HAB, the (CO) lines, R(11) & R(19), were collected using a direct absorption technique. Because TDLAS is a line-of-sight technique, it is necessary to employ tomographic reconstruction to obtain radial data from the collected projection data, which is the convolution of the incremental absorptions from each spatial location in the flame traversing the length of the laser beam. We use a three point Abel inversion algorithm [3] for tomographic reconstruction of spectra for each radial location. The reconstructed spectra is then individually fit to the functional form of the second harmonic signal of a Lorentzian line shape [4]. This technique, as suggested by Varghese et al. [5], should lead to the most accurate measurements of temperature and concentration using TDLAS.

Soot particles have a graphitic morphology. Because aromatic oxidation produces copious quantities of CO, we anticipate an increase in carbon monoxide concentrations at the flame tip as the quantity of soot is increased. Puri et al. have found that increased amounts of soot result in larger concentrations of CO in higher regions of flames as well as depleted hydroxyl radical species [6] in a series of methane flames which are either undiluted or diluted with butane or butene. The temperature profiles are qualitatively similar to those of previous studies using thermocouples [1] and coherent anti-

Stokes Raman spectroscopy (CARS) [7]. Santoro has shown that particle formation tends to occur in the fuel rich region, and the maximum temperatures occur at radial positions just outside of this zone [1] at low flame heights. Peak temperatures observed higher in these flames are lower due to radiative cooling by soot particles. Our profile data agree with these earlier observations.

Our data also indicate that the concentration of CO has a dependence on soot volume fractions which has been observed previously by other workers [6,8]. Low in these flames, the peak in the carbon monoxide concentration profile occurs near the same radius as the peak in the soot volume fraction. Higher in all three flames the peak CO concentration occurs at the burner centerline. For the non-sooting flame, the peak CO concentration observed at 55 mm HAB is substantially lower than the peak concentration at 10 mm HAB. However, for the flames with higher soot loadings, the peak CO concentrations at 55 mm HAB are comparable to those seen lower. These results suggest the important role that soot particle oxidation may play on CO levels.

References:

1. R.J. Santoro, T.T. Yeh, J.J. Horvath, and H.G. Semerjian: "The Transport and Growth of Soot Particles in Laminar Diffusion Flames," *Combust. Sci. and Tech.*, **53**, 89-115 (1987).
2. R.J. Santoro, H.G. Semerjian, and R.A. Dobbins: *Combust. and Flame*, **51**, 203-218 (1983).
3. C.J. Dasch: *Appl. Optics* , **31**, 1146 (1992).
4. R. Arndt: J. *Appl. Phys.*, **17**, 2477 (1965).
5. X. Quyang, P.L. Varghese: *Appl. Optics*, **29**, 4884-4890 (1990).
6. R. Puri, R.J. Santoro: *Fire Safety Science, Proceedings of Third International Symposium*, 595-504.
7.. L.R. Boedeker, G.M. Dobbs: *Combust. Sci. and Tech.*, **46**, 301-323 (1986).
8. U.O. Koylu, G.M. Faeth, *Combust. and Flame*, **87**, 61-76 (1991).

The Validation of Conserved Scalar Relationships In Laminar Methane / Air Diffusion Flames

M. A. T. Marro and J. H. Miller
Department of Chemistry
The George Washington University
Washington, DC. 20052

In general, to compute the structure of a laminar diffusion flame requires the simultaneous solution of the energy, momentum, and species conservation equations. The latter can be written in the Shvab-Zeldovich form as [1]:

$$L(Y_i) \equiv \rho u_k \cdot \left[\frac{\partial Y_i}{\partial x_k} \right] - \frac{\partial \left[\rho D_i \cdot \left[\frac{\partial Y_i}{\partial x_k} \right] \right]}{\partial x_k} = w_i \qquad (1)$$

where Y_i is the mass fraction of species i, w_i is its chemical production rate of species i, ρ is the gas density and u_k is the component of velocity in the x_k coordinate.

Chemical elements (such as C, H, and O) are conserved during chemical reaction ($L(Z_i) = 0$) and linear combinations of elemental abundances, such as the mixture fraction, ξ, will also be conserved [2]. Here we adopt Bilger's definition for mixture fraction:

$$\xi = \frac{\beta - \beta_{ox}}{\beta_{fu} - \beta_{ox}} \qquad (2)$$

with

$$\beta = 2 \cdot \frac{Z_C}{W_C} + \frac{1}{2} \cdot \frac{Z_H}{W_H} - \frac{Z_O}{W_O} \qquad (3)$$

where fu and ox refer to the fuel and oxidant streams, and Z_i and W_i are the mass fractions and atomic masses for carbon, oxygen and hydrogen.

It has been noted that the concentrations of many flame species are only a function of mixture fraction, $Y_i = f(\xi)$ [1]. For these species, since

$$\rho u_k \cdot \left[\frac{\partial \xi}{\partial x_k} \right] - \frac{\partial \left[\rho D \cdot \left[\frac{\partial \xi}{\partial x_k} \right] \right]}{\partial x_k} = 0 \qquad (4)$$

it follows that the chemical rate is given by

$$w_i = -\left[\frac{1}{2}\right] \cdot \rho\chi \cdot \left[\frac{d^2 Y_i}{d\xi^2}\right] \tag{5}$$

with the instantaneous scalar dissipation rate, χ, defined as:

$$\chi = 2D \cdot \left[\frac{\partial \xi}{\partial x_k}\right]^2 \tag{6}$$

Despite the widespread acceptance that the conserved scalar description of diffusion flame structure has found in the combustion community, there has been surprisingly little effort expended to a detailed evaluation of how well it actually works [refs. 3 and 4 and references therein]. Turbulent combustion environments can not provide the level of flame structure detail necessary to perform this validation. We report here an evaluation of conserved scalars in laminar flame systems, where considerably more experimental data is available and detailed calculations have been performed.

Using eighty-three reactions, with twenty-six reactant species from four elements (H, O, C, and N), as well as the conservation equations of mass, momentum, chemical species and energy, M. Smooke [3] has calculated temperatures, mixture fractions, ξ, scalar dissipation rates, χ, and concentrations at a series of radial positions and heights for a model CH_4/Air axi-symmetric co-flow flame. Because of the detail provided by these results, we can evaluate the magnitude of the net rate of chemical transformation, w_i, in two ways. First, we can develop a chemical kinetic rate expression for each species from the mechanism. We can then compare this with w_i calculated from Eq. 5. The agreement between these two calculations in effect provides a test of the conserved scalar concept.

In our poster, we will perform this calculation for a number of locations in Smooke's axially symmetric flame and draw some comparisons with recent experimental work performed using Tunable Diode Lasers in our laboratory to measure species concentrations.

References:

1. Bilger, R.W.: *Combust. Flame 30*, 277 (1977).
2. Bilger, R.W.: *Ann. Rev. Fluid Mech. 21*, 101 (1989).
3. T.S. Norton, K.C. Smyth, J.H. Miller, and M.D. Smooke: *Combust. Sci. and Tech.* 89, pp. 1-34 (1993).
4. M.D. Smooke (ed.): Reduced Kinetic Mechanisms and Asymptotic Approximations for Methane-Air Flames *Lecture Notes in Physics* Vol. 384 Springer-Verlag : New York (1991).

HASL: Hazard Analysis of Smoke Leakage, A New Module for **FPEtool**

Scot Deal
BFRL/NIST
Gaithersburg, MD

HASL is a mathematical smoke movement simulation; it is the newest addition to **FPEtool**, which is a collection of mathematical fire-safety simulations that run on a personal computer. HASL allows one to simulate smoke movement from one room to another. In post-flashover fires a hallway (exposing space) will typically be filled with smoke and some of this smoke will leak into rooms off of the corridor (target rooms). HASL simulates this smoke movement, calculates the resulting temperature and toxicant concentrations in the room, and predicts if an occupant will die from a lethal exposure. While several other programs are capable of conducting this type of analysis, the virtue of adding **HASL** to **FPEtool** is the speed and simplicity in obtaining results. Obviously there are tradeoffs for this speed and simplicity and these tradeoffs are manifest in the limitations of the model. However, **HASL** accomplishes what it intends, and that is to estimate smoke conditions and lethality in a target room for the design professional and safety engineer.

The **HASL** model is three part: data input, program execution, and data output. The data input section has the ability to create new scenarios, edit existing scenarios, store scenarios as data files, edit previous data files, and print out existing data files. The input parameters include the initial conditions for the air and or smoke in the exposing space, the target room and the outside environment. Geometrical descriptions of the target room and the leakage area are required. Thermophysical properties of the target are necessary for heat transfer. The user has the ability to define the run length and adjust the numerical time step of the mathematical simulation.

The **HASL** model is a simplified approach to smoke movement and the resulting speed was achieved at a cost to applicability and analytical accuracy. The following items are limitations associated with HASL: steady-state conditions in the exposing space, one leakage area between the exposing space and the target room, numerical instability for large time steps, no entrainment of smoke leakage into the target room, no steel--only thermally thick target room walls, smoke emissivity is independent of fuel, radiation to an object located under the smoke layer assumes that person is in the center of the room, convection and radiation heat transfer assume exposed skin, lethality analysis analyzes each layer independently: there are no behavioral rules for determining which layer a person is in contact with.

HASL is the third in a series of modules within **FPEtool.** This series begins with a fire in the room of origin. This fire is simulated with **FIRE SIMULATOR**. The post-flashover regime is also modeled by **FIRE SIMULATOR** but the resulting smoke flow can be traced down a straight hallway with **CORRIDOR.** From the output values of **CORRIDOR** the user can obtain input values necessary to run **HASL.** The intent of **HASL** is to provide an analysis of the time to lethality in room of refuge.

HASL will be available at the end of October through the Fire Research Information Services library or the Building and Fire Research computer Bulletin Board System, both of which are located at NIST in Gaithersburg, MD. The number for FRIS is (301) 975 6862, the number for BFRBBS is (301) 990 2272.

Tunable Diode Laser Absorption Detection of Polyatomic Species in Hydrocarbon Diffusion Flames: Some Cautions and Measurement Strategies

Michael Tolocka and J. Houston Miller
Department of Chemistry
The George Washington University
Washington, DC 20052

Over the past few years we have demonstrated the application of tunable diode laser absorption spectroscopy (TDLAS) for the measurement of concentration and temperature in hydrocarbon diffusion flames. These studies have focussed on absorptions of carbon monoxide near 2150 cm^{-1}. The great promise of the mid infrared region is that almost every molecule of interest absorbs light here. We report here some considerations for application of TDLAS to some of these species and report some preliminary data for methane and acetylene concentrations.

The fractional absorption of infrared laser light is given by

$$\ln\left(\frac{I^o}{I}\right) = S(T)\cdot g(\nu-\nu^o)\cdot p_j\cdot l$$

where I^o is the incident beam intensity, I is the transmitted beam intensity, g is the line shape factor (in our work assumed to be Lorentzian), p_j is the partial pressure of the absorbing species, and l is the path length through the absorbing medium.

The line strength at flame temperatures is given by:

$$S(T) = S(296)\cdot\frac{Q_{296}}{Q_T}\cdot R\cdot\exp\left[\frac{hc}{k}\cdot E''\cdot\frac{(T-296)}{(T\cdot 296)}\right]$$

with

$$R = \frac{1-\exp\left[-\frac{hc}{k}\cdot\frac{(E'-E'')}{T}\right]}{1-\exp\left[-\frac{hc}{k}\cdot\frac{(E'-E'')}{296}\right]}$$

Here the Q's refer to partition functions, and E' and E" refer to the upper and lower state energies, respectively. The ratio of partition functions is a steep function of temperatures for polyatomic molecules and this factor may hamper application of TDLAS for analysis of large molecules at flame temperatures. Further, the density of lines in the infrared is quite high in many spectral regions which also may limit our ability to detect species of interest here.

This poster will discuss these limitations in detail, and will present some results for the detection of both methane and acetylene is small, laboratory scale flames. We will also discuss the potential benefits and limitations of the application of TDLAS for larger scale combustion systems.

CIGARET, a Mathematical Model of a Smoldering Cigarette

Henri E. Mitler

BFRL/NIST

ABSTRACT

This paper describes the computer model CIGARET. CIGARET solves the equations describing the physics and chemistry of the heating and ignition process numerically; it calculates the temperature, gas velocity, and oxygen concentration throughout a cylindrical volume which simulates a cigarette. The cigarette is assumed to be cylindrically symmetric; the medium is modeled as being homogeneous and solid but porous. It is a time-dependent model, which incorporates diffusion and (radial) convection of gases, the kinetics of char oxidation, and the three-dimensional transfer of heat *via* conduction and radiation. The temperature-dependence of some of the thermophysical "constants" are taken into account. For the default run, a quasi-steady smolder wave develops after a two-minute transient, upon ignition. It yields a remarkably constant and physically realistic velocity. This model permits investigation of the consequences of changing one or more of the input variables, such as the permeability of the paper wrapping, the density of the tobacco column, etc. Some of the results are displayed.

CEdit 2.0 - An Object-Oriented User Interface for the CFAST Fire Model

Rebecca W. Portier, Walter W. Jones,
Richard D. Peacock, and Paul A. Reneke

Building and Fire Research Laboratory
National Institute of Standards and Technology
Gaithersburg, MD 20899

CEdit is an interactive program used to generate data files for input to the CFAST model. CEdit 2.0 is a new generation of the input editor which utilizes graphical objects to represent the structure, the flow relationships between compartments, placement of fires, and other phenomena. This editor is a first step in the ongoing development toward a CAD-type input editor.

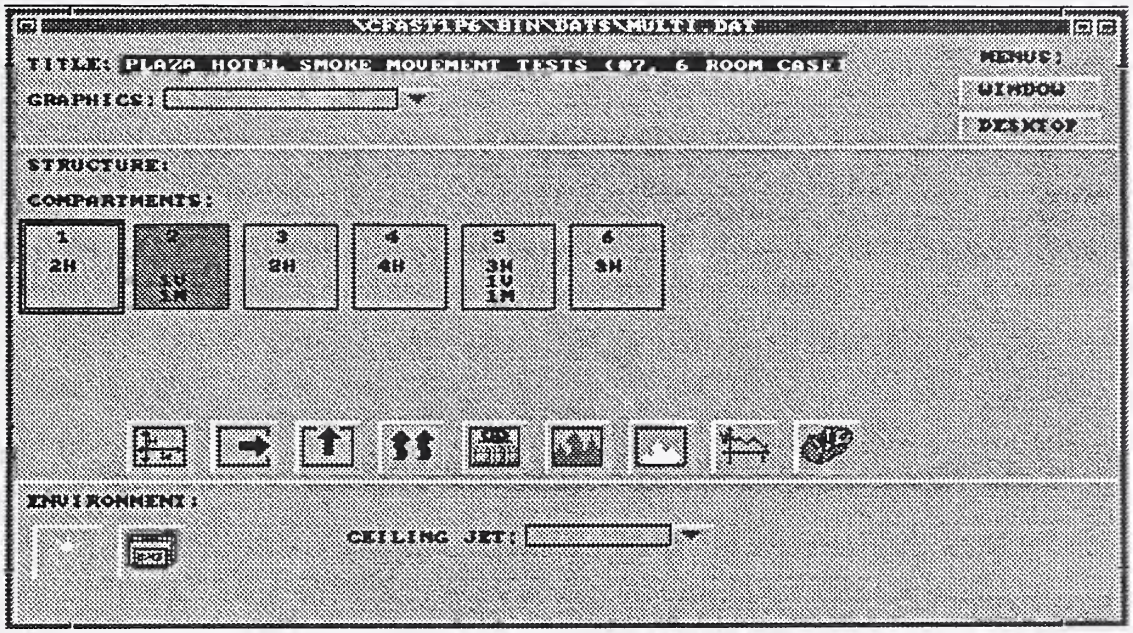

CEdit 2.0 Overview Screen

Structure overview allows user to know at a glance:

- number of compartments
- number of horizontal and vertical flow openings in each compartment
- number of HVAC openings in each compartment
- "main" fire compartment and "other" objects compartments

Context sensitive icon buttons imply outcome dependent on current compartment:

- geometry
- horizontal and vertical flow to other compartments
- HVAC connections
- main fire definition
- "other" objects
- time-dependent events

Horizontal and vertical flow selection screens allow user to know at a glance:

- All compartments with flow from current compartment, and the number of vents for each compartment pair
- Compartments which cannot be connected because of positioning
- Compartments which could be connected but are not currently

HVAC system overview allows user to know at a glance:

- Which compartments are connected by HVAC ducts and fans, and the topology of the connection path
- Direction of flow through fans
- Which nodes are "external" and which are "internal"

Additional advantages:

- Compartment and node numbering handled by the editor
- "From" and "to" specifications are context-based
- Possibility of defining the same item twice, especially in HVAC, is limited
- Able to view structure and HVAC side by side
- Quick access to all options and configuration information without paging
- Finite "choice" sets handled as pull-down menus

New features:

- FIREFORM estimation routines
- Sprinklers and detectors

Demonstrations of the features of CEdit 2.0 as they exist at this time will be offered during the poster sessions.

References

[1] Peacock, R.D., Jones, W.W., Forney, G.P., Reneke, P., Portier, R., CFAST, the Consolidated Model of Fire and Smoke Transport, National Institute of Standards and Technology, Technical Note 1299 (1992)

[2] Portier, R.W., Reneke, P.A., Jones, W.W., and Peacock, R.D., A User's Guide for CFAST, Version 1.6, National Institute of Standards and Technology, NISTIR 4985 (1992).

[3] Shneiderman, B., *Designing the User Interface: Strategies for Effective Human-Computer Interaction*, Addison-Wesley Publishing Company, Reading, MA, (1987).

NIST-114
(REV. 6-93)
ADMAN 4.09

U.S. DEPARTMENT OF COMMERCE
NATIONAL INSTITUTE OF STANDARDS AND TECHNOLOGY

MANUSCRIPT REVIEW AND APPROVAL

(ERB USE ONLY)
ERB CONTROL NUMBER | DIVISION
PUBLICATION REPORT NUMBER: NISTIR 5280 | CATEGORY CODE

INSTRUCTIONS: ATTACH ORIGINAL OF THIS FORM TO ONE (1) COPY OF MANUSCRIPT AND SEND TO THE SECRETARY, APPROPRIATE EDITORIAL REVIEW BOARD.

PUBLICATION DATE: October 1993 | NUMBER PRINTED PAGES

TITLE AND SUBTITLE (CITE IN FULL)

1993 Annual Conference on Fire Research: Book of Abstracts

CONTRACT OR GRANT NUMBER | TYPE OF REPORT AND/OR PERIOD COVERED

AUTHOR(S) (LAST NAME, FIRST INITIAL, SECOND INITIAL)

Wanda J. Duffin, Editor

PERFORMING ORGANIZATION (CHECK (X) ONE BOX)
- [X] NIST/GAITHERSBURG
- [ ] NIST/BOULDER
- [ ] JILA/BOULDER

LABORATORY AND DIVISION NAMES (FIRST NIST AUTHOR ONLY)

Building & Fire Research Laboratory/Fire Safety Engineering Division

SPONSORING ORGANIZATION NAME AND COMPLETE ADDRESS (STREET, CITY, STATE, ZIP)

PROPOSED FOR NIST PUBLICATION

- [ ] JOURNAL OF RESEARCH (NIST JRES)
- [ ] J. PHYS. & CHEM. REF. DATA (JPCRD)
- [ ] HANDBOOK (NIST HB)
- [ ] SPECIAL PUBLICATION (NIST SP)
- [ ] TECHNICAL NOTE (NIST TN)
- [ ] MONOGRAPH (NIST MN)
- [ ] NATL. STD. REF. DATA SERIES (NIST NSRDS)
- [ ] FEDERAL INF. PROCESS. STDS. (NIST FIPS)
- [ ] LIST OF PUBLICATIONS (NIST LP)
- [X] NIST INTERAGENCY/INTERNAL REPORT (NISTIR)
- [ ] LETTER CIRCULAR
- [ ] BUILDING SCIENCE SERIES
- [ ] PRODUCT STANDARDS
- [ ] OTHER _____

PROPOSED FOR NON-NIST PUBLICATION (CITE FULLY) [ ] U.S. [ ] FOREIGN

PUBLISHING MEDIUM
- [ ] PAPER
- [ ] CD-ROM
- [ ] DISKETTE (SPECIFY) _____
- [ ] OTHER (SPECIFY)

SUPPLEMENTARY NOTES

ABSTRACT (A 2000-CHARACTER OR LESS FACTUAL SUMMARY OF MOST SIGNIFICANT INFORMATION. IF DOCUMENT INCLUDES A SIGNIFICANT BIBLIOGRAPHY OR LITERATURE SURVEY, CITE IT HERE. SPELL OUT ACRONYMS ON FIRST REFERENCE.) (CONTINUE ON SEPARATE PAGE, IF NECESSARY.)

The NIST Annual Conference on Fire Research has long been a prime forum for presentation and discussion of the latest advances in fire science and engineering. The conference includes mostly fire research performed within Federal laboratories, or sponsored by Federal agencies. However, some private sector and foreign fire research is also included.

KEY WORDS (MAXIMUM OF 9; 28 CHARACTERS AND SPACES EACH; SEPARATE WITH SEMICOLONS; ALPHABETIC ORDER; CAPITALIZE ONLY PROPER NAMES)

Burning rate; fire detection; fire hazard analysis; fire modeling; fire risk; fire tests; flame spread; halon; large fires; plumes; suppression; smoke production; water

AVAILABILITY
- [X] UNLIMITED
- [ ] FOR OFFICIAL DISTRIBUTION - DO NOT RELEASE TO NTIS
- [ ] ORDER FROM SUPERINTENDENT OF DOCUMENTS, U.S. GPO, WASHINGTON, DC 20402
- [X] ORDER FROM NTIS, SPRINGFIELD, VA 22161

NOTE TO AUTHOR(S): IF YOU DO NOT WISH THIS MANUSCRIPT ANNOUNCED BEFORE PUBLICATION, PLEASE CHECK HERE. [ ]

ELECTRONIC FORM